

**Molecular Control of Extracellular DNA Release and
Degradation in *Shewanella oneidensis* MR-1 Biofilms:
The Role of Phages and Nucleases**

Dissertation

zur Erlangung des Doktorgrades
der Naturwissenschaften
(Dr. rer. nat.)

dem
Fachbereich Biologie
der Philipps-Universität Marburg
vorgelegt von

Lucas Binnenkade

aus Aachen

Marburg (Lahn), 2015

Die Untersuchungen zur vorliegenden Arbeit wurden von Mai 2011 bis März 2015 am **Max-Planck-Institut für terrestrische Mikrobiologie** und am **Institut für Molekularbiologie und Mikrobiologie an der Justus-Liebig-Universität Gießen** unter der Leitung von Prof. Dr. Kai Thormann durchgeführt.

Vom Fachbereich Biologie der Philipps-Universität Marburg (HKZ: 1180)
als Dissertation angenommen am: 27.04.2025

Erstgutachter: Prof. Dr. Kai Thormann
Zweitgutachter: Prof. Dr. Martin Thanbichler

Tag der mündlichen Prüfung: 13.05.2015

Die während der Promotion erzielten Ergebnisse sind zum Teil in folgenden Originalpublikationen veröffentlicht:

1. **Binnenkade L, Teichmann L, Thormann KM.** 2014. Iron triggers λ So prophage induction and release of extracellular DNA in *Shewanella oneidensis* MR-1 biofilms. Appl Environ Microbiol **80**:5304-5316.
(‘AEM Spotlight Article’ - veröffentlicht als Publikation von besonderer Signifikanz in der Kategorie ‘Physiology’)
2. **Gödeke J, Binnenkade L, Thormann KM.** 2012. Transcriptome analysis of early surface-associated growth of *Shewanella oneidensis* MR-1. PloS One **7**:e42160.
3. **Heun M#, Binnenkade L#, Kreienbaum M, Thormann KM.** 2012. Functional specificity of extracellular nucleases of *Shewanella oneidensis* MR-1. Appl Environ Microbiol **78**:4400-4411.

Ergebnisse aus Projekten, die in dieser Dissertation nicht erwähnt wurden, sind in folgenden Originalpublikationen veröffentlicht:

4. **Binnenkade L#, Lassak J#, Thormann KM.** 2011. Analysis of the BarA/UvrY two-component system in *Shewanella oneidensis* MR-1. PloS One **6**:e23440.
5. **Lassak J, Henche AL, Binnenkade L, Thormann KM.** 2010. ArcS, the cognate sensor kinase in an atypical Arc system of *Shewanella oneidensis* MR-1. Appl Environ Microbiol **76**:3263-3274.

diese Autoren wirkten gleichberechtigt an der Publikation mit

Ich versichere, dass ich meine Dissertation:

**“Molecular Control of Extracellular DNA Release and
Degradation in *Shewanella oneidensis* MR-1 Biofilms:
The Role of Phages and Nucleases”**

selbstständig, ohne unerlaubte Hilfe angefertigt und mich dabei keiner anderen als der von mir ausdrücklich bezeichneten Quellen und Hilfen bedient habe. Die Dissertation wurde in der jetzigen oder einer ähnlichen Form noch bei keiner anderen Hochschule eingereicht und hat noch keinen sonstigen Prüfungszwecken gedient.

Marburg (Lahn), den 22.3.2015

Lucas Binnenkade

“In wine there is wisdom, in beer there is freedom, in water there is bacteria.”

Benjamin Franklin

To my parents

ABSTRACT

Under natural conditions, most bacteria tend to form surface-associated multicellular communities that are commonly referred to as biofilms. Biofilm formation is a complex and highly regulated process that enables bacteria to colonize almost every kind of surface and to resist diverse physical stresses, starvation, and antibiotics. Moreover, surface-associated growth increases virulence in many pathogenic bacteria and allows environmental bacteria to exploit surfaces as nutrient and energy reservoir. Accordingly, bacterial biofilm formation has been shown to be of great medical, ecological, and economical relevance. An essential component of biofilms is the extracellular polymeric matrix that commonly consists of a complex mixture of exopolysaccharides, proteins, and extracellular DNA (eDNA). The significance of eDNA in biofilms has long been disregarded, but a high number of studies has now demonstrated that it is required for structural biofilm formation in most bacteria, including *Shewanella oneidensis* MR-1. However, mechanisms that regulate and mediate eDNA release on the one hand, and those that control eDNA modulation and degradation (e.g. to induce biofilm dispersal or to exploit eDNA as source of nutrients) on the other hand, are still incompletely understood.

In our lab, it has been demonstrated that prophage-induced lysis (particularly mediated by prophage λ So) is required for eDNA release and normal biofilm formation in *S. oneidensis* MR-1. In this study, I investigated molecular mechanisms that regulate prophage λ So spatiotemporal induction and eDNA release in *S. oneidensis* MR-1 biofilms. To this end, a functional fluorescence fusion was utilized to monitor λ So activation in various mutant backgrounds and in response to different physiological conditions. λ So induction mainly occurred in a subpopulation of filamentous cells in a strictly RecA-dependent manner, implicating oxidative stress-induced DNA damage as the major trigger. Accordingly, mutants affected in the oxidative stress response ($\Delta oxyR$) or iron homeostasis (Δfur) displayed drastically increased levels of phage induction and abnormal biofilm formation, while planktonic cells were not, or only marginally, affected. To further investigate the role of oxidative stress, I performed a mutant screen and identified two independent amino acid substitutions in OxyR (T104N and L197P) that suppress induction of λ So by hydrogen peroxide (H_2O_2). However, λ So induction was not suppressed in biofilms formed by both mutants, suggesting a minor role of intracellular H_2O_2 in this process. In contrast, addition of iron to biofilms strongly enhanced λ So induction and eDNA release while both processes were significantly suppressed at low iron levels. Analogous observations were made for biofilms formed by the mutants that suppress induction of λ So by H_2O_2 , strongly indicating that iron and not H_2O_2 is the limiting factor. I conclude that uptake of iron during biofilm formation triggers λ So prophage-mediated lysis of a subpopulation of cells, likely by an increase in iron-mediated DNA damage that is sensed by RecA. Further, I propose that colonization of surfaces implies a conflict between high requirements for iron, iron-mediated DNA stress, prophage-induced lysis, and release of biofilm promoting factors such as eDNA, and that tight regulation of these partially antagonistic factors is required for successful biofilm formation.

Extracellular nucleases degrade eDNA both in biofilms and planktonic cultures and have been shown to exhibit diverse functions, including induction of biofilm dispersal, structural modulation of the biofilm matrix, utilization of DNA as nutrient source, control of horizontal gene transfer, and escape from neutrophil extracellular traps. To date, three extracellular nucleases, ExeM

(SO_1066), ExeS (SO_1844) and EndA (SO_0833), have been identified in *S. oneidensis* MR-1. Earlier studies demonstrated that EndA is required for growth on DNA as nutrient source under planktonic conditions, whereas ExeM is required under biofilm conditions to prevent excessive accumulation of eDNA to abnormal levels. In this study, a combination of bioinformatic, biochemical, and genetic analyses was utilized to characterize the molecular and physiological roles of both extracellular nucleases in *S. oneidensis* MR-1. The results indicate that both enzymes are sugar-unspecific endonucleases that require either Mg^{2+} or Mn^{2+} for function, whereas ExeM additionally requires Ca^{2+} as second cofactor. EndA seems to be a highly active and planktonic growth-specific secreted nuclease that is strongly induced in exponential phase. Exogenous addition of purified EndA to biofilms or endogenous induction of *endA* did not result in dispersal, suggesting a minor role under biofilm conditions. In contrast, *in vitro* analyses of ExeM demonstrated only weak nucleolytic activity; however, addition of purified MBP-ExeM strongly inhibited biofilm formation, further indicating that it is a biofilm-specific nuclease. Finally, immunoblot analyses of truncated variants and specific substitution mutants of ExeM in different cellular fractions confirmed that ExeM localizes transiently to the inner membrane and that a specific Gly-Gly-CTerm motif is involved in processing and transport of ExeM across the cell envelope. The results suggest functional specificity of both enzymes and represent a first basis for the decryption of structure-function relationships in extracellular nucleases.

ZUSAMMENFASSUNG

Bakterien bilden unter natürlichen Bedingungen häufig oberflächen-assoziierte multizelluläre Gemeinschaften, welche allgemein als Biofilme bezeichnet werden. Die Bildung von Biofilmen ist ein komplexer und präzise regulierter Prozess, der es Bakterien ermöglicht, beinahe jede Art von Oberfläche zu besiedeln und dadurch physikalischen Stressfaktoren, Nährstoffmangel und Antibiotika standzuhalten. Des Weiteren kann oberflächenassoziiertes Wachstum die Virulenz von pathogenen Bakterien erhöhen und Umweltkeimen die Erschließung von Oberflächen als Nährstoff- und Energiequelle ermöglichen. Aus diesem Grund hat sich gezeigt, dass bakterielle Biofilmbildung von großer medizinischer, ökologischer und ökonomischer Relevanz ist. Ein wichtiger Bestandteil von Biofilmen ist die extrazelluläre polymere Matrix welche sich typischerweise aus Exopolysacchariden, Proteinen und extrazellulärer DNA (eDNA) zusammensetzt. Die Bedeutung der eDNA für Biofilme war lange unklar, jedoch konnte durch eine Reihe von Studien gezeigt werden, dass eDNA für die meisten Bakterienspezies, darunter *Shewanella oneidensis* MR-1, von essentieller Bedeutung für die strukturelle Entwicklung der Biofilme ist. Vielfach unbekannt sind jedoch Mechanismen, welche die Freisetzung von eDNA regulieren bzw. ausführen und solche, die an der Modulation und am Abbau (z.B. zur endogen induzierten Auflösung von Biofilmen oder zur Erschließung von eDNA als Nährstoffquelle) beteiligt sind.

In unserem Labor durchgeführte Studien konnten belegen, dass die durch Prophagen induzierte Lyse (vor allem vermittelt durch Prophage λ So) eine Voraussetzung für die Freisetzung von eDNA und normale Biofilmbildung ist. Im Rahmen der vorliegenden Studie wurden molekulare Mechanismen erforscht, welche die raumzeitliche Induktion des Prophagen λ So und die daraus resultierende Freisetzung von eDNA in *S. oneidensis* MR-1 Biofilmen regulieren. Für diesen Zweck wurde eine funktionale Fluoreszenzfusion als Sensor für die Aktivierung des Prophagen in einer Reihe von spezifischen Mutanten und unter verschiedenen physiologischen Bedingungen verwendet. Die Induktion von λ So war primär in einer aus filamentösen Zellen bestehenden Subpopulation zu beobachten und erfolgte in strikter Abhängigkeit von RecA. Basierend auf diesen Ergebnissen wurden DNA-Schädigungen, die durch oxidativen Stress entstanden sein könnten, als möglichen Auslöser in Betracht gezogen. Der Hypothese entsprechend konnte gezeigt werden, dass Mutanten, die entweder im Schutzmechanismus gegen oxidativen Stress ($\Delta oxyR$) oder in der Regulation der Eisen-Homöostase (Δfur) beeinträchtigt sind, drastisch erhöhte Spiegel an Prophagen-Induktion und abnormale Biofilmbildung zeigten, während kein Effekt auf planktonische Zellen zu beobachten war. Um die Bedeutung von oxidativem Stress genauer zu untersuchen, wurde ein Mutanten-Screening durchgeführt, welches zur Identifizierung von zwei unabhängigen Aminosäuresubstitutionen in OxyR (T104N und L197P) verhalf, die jeweils eine Induktion des Prophagen durch Wasserstoffperoxid (H_2O_2) verhindern. Unter Biofilmbedingungen wurde die Induktion von λ So dennoch nicht in den Mutanten unterdrückt, was auf eine unwesentliche Rolle von H_2O_2 in diesem Prozess hinweist. Im Gegensatz dazu konnte in Biofilmen die Induktion des Prophagen und die Freisetzung von eDNA durch Zugabe von Eisen stark erhöht, und durch Herabsetzung des Eisenspiegels deutlich verringert werden. Entsprechendes wurde in Biofilmen beobachtet, die von denjenigen Mutanten gebildet wurden, welche eine Induktion von λ So durch H_2O_2 unterdrücken. Demzufolge scheint Eisen und nicht H_2O_2 der limitierende Faktor zu sein. Aus den Ergebnissen kann geschlossen werden, dass die Aufnahme von Eisen während der Biofilmbildung höchstwahrscheinlich DNA-Schäden verursacht, welche von RecA erkannt werden

und in einer Subpopulation filamentöser Zellen die λ So Prophagen-vermittelte Lyse auslösen. Generell scheint die Besiedlung von Oberflächen einen Konflikt zwischen dem hohen Bedarf an Eisen, eiseninduzierten DNA-Schäden, prophageninduzierter Lyse und der Freisetzung von Faktoren, welche die Biofilmbildung unterstützen (wie z.B. eDNA), mit sich zu ziehen. Es ist zu erwarten, dass diese zum Teil antagonistischen Faktoren einen hohen Grad an Regulation erfordern, um die erfolgreiche Bildung von Biofilmen zu gewährleisten.

Extrazelluläre Nukleasen sind am Abbau von eDNA in Biofilmen und planktonischen Kulturen beteiligt und wurden mit diversen Funktionen in Zusammenhang gebracht, darunter die Auflösung von Biofilmen, die strukturelle Modulation der Biofilmmatrix, die Erschließung von eDNA als Nährstoffquelle, die Überwachung von horizontalem Gentransfer und das Entkommen aus neutrophilen extrazellulären Fallen. Bisher wurden drei extrazelluläre Nukleasen in *S. oneidensis* MR-1 identifiziert, ExeM (SO_1066), ExeS (SO_1844) und EndA (SO_0833). Frühere Studien konnten belegen, dass die Fähigkeit zum Wachstum auf DNA primär auf EndA zurückzuführen ist, während ExeM eine übermäßige Akkumulation von eDNA in Biofilmen verhindert. Für die vorliegende Studie wurde eine Kombination an bioinformatischen, biochemischen und genetischen Analysen durchgeführt um die Funktion der beiden Nukleasen in *S. oneidensis* MR-1 auf molekularer und physiologischer Ebene zu charakterisieren. Die Ergebnisse zeigen, dass es sich bei beiden Enzymen um zuckerunspezifische Endonukleasen handelt, die entweder Mg^{2+} oder Mn^{2+} als spezifischen Kofaktor benötigen, wobei ExeM zusätzlich Ca^{2+} als zweiten Kofaktor benötigt. EndA weist im Vergleich eine hohe nukleolytische Aktivität auf, ist funktionell von besonderer Relevanz für planktonisches Wachstum und stark induziert während der exponentiellen Wachstumsphase. Die exogene Zugabe von aufgereinigtem EndA-Protein zu Biofilmen hatte keinen Effekt, was ebenfalls auf eine untergeordnete Rolle für die Biofilmbildung hinweist. Im Gegensatz dazu zeigten *in vitro* Analysen von ExeM einen wesentlich geringeren nukleolytischen Wirkungsgrad. Die Zugabe von aufgereinigtem ExeM-Protein verhinderte jedoch weitgehend die Bildung von Biofilmen, was ebenfalls darauf hinweist, dass ExeM eine biofilmspezifische Funktion zugewiesen werden kann. Ferner zeigten Immunoblot-Analysen von verkürzten Varianten von ExeM und einer Substitutionsmutante, dass ExeM transient in der inneren Membran lokalisiert und ein spezifisches Gly-Gly-CTerm-Motiv die Prozessierung und den Transport von ExeM über die Zellhülle beeinflusst. Die Ergebnisse weisen auf eine funktionelle Spezifität der beiden Enzyme hin und bilden eine Grundlage für die weitere Entschlüsselung von Zusammenhängen zwischen Struktur und Funktion extrazellulärer Nukleasen.

CONTENT

Abstract	1
Zusammenfassung	3
Introduction	9
1.1 Bacterial biofilms	9
1.1.1 Biofilm development.....	9
1.1.2 The biofilm matrix.....	15
1.1.3 Release mechanisms of eDNA in biofilms	22
1.1.4 The role of extracellular nucleases in biofilms	27
1.2 <i>Shewanella oneidensis</i> MR-1	29
1.2.1 Biofilm formation of <i>S. oneidensis</i> MR-1	30
1.3 Scope.....	33
Results	35
1.4 Analyses of λ So prophage induction in biofilms	35
1.4.1 λ So prophage-mediated lysis is required for normal biofilm formation	35
1.4.2 Biofilm conditions trigger λ So prophage induction	38
1.4.3 RecA controls λ So prophage induction and eDNA release.....	42
1.4.4 Regulation by OxyR and Fur affects λ So prophage induction.....	43
1.4.5 λ So induction in biofilms cannot be suppressed by an increase in	
cellular H ₂ O ₂ turnover	46
1.4.6 Availability of iron controls timing and level of λ So prophage induction	
and eDNA release.....	49
1.5 Functional specificity of extracellular nuclease EndA	55
1.5.1 Purification and <i>in vitro</i> analyses of EndA	55
1.5.2 PhoA is not essential for growth on DNA as sole source of phosphorus	56
1.5.3 EndA is a planktonic growth-specific nuclease.....	57
1.6 Molecular characterization of ExeM nuclease activity and transport.....	61
1.6.1 <i>In silico</i> analyses of ExeM	61
1.6.2 Purification of ExeM.....	64
1.6.3 <i>In vitro</i> analyses of ExeM.....	65
1.6.4 Processing and transport of ExeM	66
1.6.5 Effect of ExeM on biofilm formation.....	68
Discussion	71
1.7 Analyses of λ So prophage induction in biofilms	71
1.7.1 RecA-mediated induction of prophage λ So in biofilms	71
1.7.2 Filamentous cells in biofilms.....	72
1.7.3 The role of iron	74
1.7.4 Iron-mediated oxidative stress.....	77
1.8 Functional specificity of extracellular nuclease EndA	81
1.8.1 <i>In vitro</i> analyses of EndA.....	81
1.8.2 Regulation of EndA-mediated extracellular nucleolytic activity.....	82

1.8.3	EndA is a planktonic growth-specific nuclease	83
1.9	Molecular characterization of ExeM	85
1.9.1	<i>In silico</i> analyses of ExeM	85
1.9.2	<i>In vitro</i> analyses of ExeM	86
1.9.3	Processing and transport of ExeM	88
1.9.4	Effect of ExeM on biofilm formation	91
Material and Methods		93
1.10	Materials	93
1.10.1	Reagents and Enzymes	93
1.10.2	Buffers and solutions	93
1.10.3	Media	93
1.10.4	Kits	95
1.10.5	Laboratory equipment and software	96
1.10.6	Oligonucleotides	96
1.10.7	Strains and plasmids	100
1.11	Microbiological methods	103
1.11.1	Cultivation of <i>E. coli</i>	103
1.11.2	Cultivation of <i>S. oneidensis</i> MR-1	103
1.11.3	Storage of bacteria	103
1.11.4	Cultivation of biofilms under static conditions	104
1.11.5	Cultivation of biofilms in flow cells	104
1.11.6	Cultivation of biofilms in the cell harvesting system	106
1.11.7	β -galactosidase activity in culture supernatants	107
1.11.8	Time-lapse analysis of phage-induced lysis	108
1.11.9	Determination of cell length	108
1.11.10	Isolation of H ₂ O ₂ -resistant mutants	108
1.12	Molecular biological methods	108
1.12.1	Isolation of DNA	109
1.12.2	Polymerase chain reaction (PCR)	109
1.12.3	Restriction enzyme digests	110
1.12.4	Ligation of DNA	110
1.12.5	Agarose gel electrophoresis	111
1.12.6	DNA sequencing	111
1.12.7	Plasmid construction	111
1.12.8	Preparation and transformation of chemically competent <i>E. coli</i> cells	113
1.12.9	Conjugation of <i>S. oneidensis</i> MR-1 cells	113
1.12.10	Total-RNA extraction and reverse transcriptase PCR (RT-PCR)	114
1.12.11	Quantitative real-time RT-PCR (qPCR)	114
1.12.12	Chromosome staining	115
1.13	Biochemical methods	115
1.13.1	SDS-PAGE	115
1.13.2	Immunoblot assays	116
1.13.3	Heterologous production and purification of MBP-EndA	117
1.13.4	EndA nuclease assays	117
1.13.5	Determination of eDNA concentration in planktonic cultures	118

1.13.6	Quantification of eDNA in static biofilms	119
1.13.7	Heterologous production and purification of MBP-ExeM.....	119
1.13.8	ExeM nuclease assays.....	120
1.13.9	Fractionation of inner and outer membrane of <i>S. oneidensis</i> MR-1	120
1.14	Microscopic methods	121
1.14.1	Fluorescence microscopy and image acquisition	121
1.14.2	Confocal laser scanning microscopy (CLSM) and image acquisition.....	121
1.15	Bioinformatic methods	122
Appendix.....		125
1.16	Figures	125
1.17	Tables.....	129
Abbreviations		131
Acknowledgement		133
Curriculum Vitae		135
References.....		137

INTRODUCTION

1.1 Bacterial biofilms

The predominant lifestyle of most microbes in nature is assumed to be within surface-associated communities which are commonly referred to as biofilms. Microbial biofilms can be seen as the most successful form of life on earth as its total mass exceeds that of all other organisms [1, 2]. Moreover, microbial biofilms can be found in almost every habitat and probably represent the most ancient form of life. Costerton and coworkers defined bacterial biofilms as structured communities of cells enclosed in a self-produced hydrated polymeric matrix adherent to an inert or living surface [3]. Biofilms provide microorganisms important advantages in comparison to the planktonic lifestyle. The availability of nutrients is mostly higher in proximity to abiotic surfaces, high cell densities enhance genetic exchange (horizontal gene transfer) and biofilms are often more tolerant against antimicrobial agents, biocides and immune responses of host organisms [4-7]. Furthermore, biofilms possess an increased tolerance against environmental perturbations and physical stress such as UV-light, pH-gradients, drought and oxidative stress [8-12]. Under natural conditions most bacteria live in heterogenic biofilms, consisting of different species [9]. A single species can coaggregate with multiple partners, which in turn aggregate with other partners, forming a dense bacterial plaque. Based on the particular microenvironment or symbiotic relationships, each species resides at its most advantageous microenvironment within the mixed-culture biofilm [13-15]. The integrity and stability of biofilms is based both on cell-cell and cell-surface interactions and on the extracellular matrix which holds the cells together and helps to form large three-dimensional structures such as microcolonies.

1.1.1 Biofilm development

In the past decades it has been increasingly appreciated that most bacteria follow a defined developmental sequence during biofilm formation. The application of sophisticated molecular and imaging techniques helped to identify many of the mechanisms that are involved in biofilm development [16]. Especially the application of flow-cell systems in conjunction with confocal laser scanning microscopes (CLSM) radically altered the perception of biofilm formation, structure and function [17]. Today, biofilm development of most bacteria is subdivided into four major developmental phases: Initial attachment, microcolony formation, maturation, and dispersal (Figure 1).

1.1.1.1 Initial attachment

Biofilm formation is often initiated through specific environmental stimuli, including osmolarity, pH, availability of nutrients and terminal electron acceptors, oxygen concentrations, and temperature [18-20]. Initially, a bacterial cell approaches and attaches to an appropriate surface (substratum). Adherence to a surface can involve active motility or can be the cause of random contacts. Accordingly, cell appendages such as flagella and pili are often required to direct initial

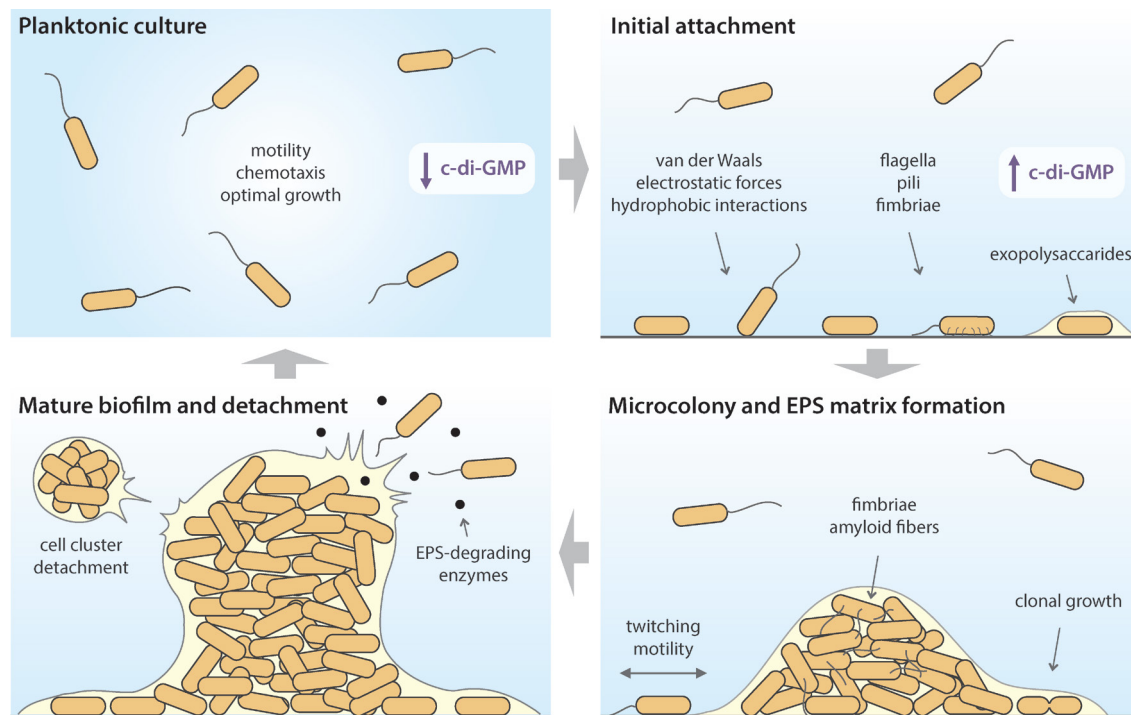


Figure 1. Biofilm development of *Pseudomonas aeruginosa* under hydrodynamic conditions. Schematic illustration of the different biofilm developmental phases. Under planktonic growth conditions cells are mostly motile. During the initial attachment a subpopulation of cells adheres reversibly to the surface, losing motility and starting the biofilm developmental program. Microcolonies are formed by twitching motility and clonal growth, and stabilized by production of an EPS matrix and cellular appendages. Finally, the mature biofilm develops, characterized by mushroom-like three-dimensional structures, accompanied by partial detachment. Low and high *c-di-GMP* levels during the motile to the sessile lifestyle are indicated by downwards and upwards facing arrows, respectively.

attachment [20–24]. Indirect transport of bacteria to a surface can be the cause of Brownian motion, sedimentation, or physical transport towards the surface by the movement of the bulk fluid [25].

The most accepted theory on the attachment of bacteria to a solid surface consists of a two-step process [26, 27]. The first step is reversible and involves van der Waals forces, electrostatic forces, and hydrophobic interactions [28–30]. At this stage, bacteria can still be released from the surface by fluid shear forces, Brownian motion, or active detachment [27]. If the environmental conditions and surface characteristics stimulate biofilm formation, the cells will initiate the second step, which is the irreversible attachment to the surface and the start of the biofilm developmental program. Cell surface appendages such as flagella, type IV pili, or fimbriae play important roles for the irreversible attachment of many bacteria [20–24, 31]. Additionally, cell surface adhesins, such as the LapA protein in *Pseudomonas fluorescens*, the holdfast polysaccharide complex in *Caulobacter crescentus*, or proteinaceous amyloid curli fibers in *Escherichia coli* and *Salmonella spp.*, can help to establish a tight and durable connection to the surface [32–35]. Moreover, extracellular polymeric substances that can also constitute the biofilm matrix during later phases (section 1.1.2), contribute already to early biofilm formation [32, 36–39]. The transition time from reversible to irreversible has been shown to be considerably fast, in the order of seconds or minutes. *Streptococcus thermophilus* and *Bacillus cereus* were shown to attach to stainless steel in less than 60 seconds and similar results were obtained for organic surfaces [40, 41].

Both steps of the initial attachment, the reversible and the irreversible, are influenced by a multitude of physical surface characteristics including surface charge, hydrophobicity, microtopography, and conditioning [25]. Conditioning is the absorption of organic and inorganic molecules by surfaces from the bulk flow that can increase nutrient concentrations at the surface and thereby attract microbial attachment [42, 43]. However, surface conditioning has been shown to be molecule and species-specific and can also inhibit biofilm formation [44, 45]. In addition to physical absorption of molecules by the surface, conditioning can also be the cause of surface-associated microbial growth itself. Under natural conditions, coaggregation is an important process by which surface colonization of one species (primary colonizer) can provide conditions that promote biofilm formation of other species, *e.g.* by the release of extracellular polymeric substances (EPS) [46].

The decision between the planktonic state and biofilm-associated growth can be made prior or upon surface contact of a bacterium, and a complex network of signal transduction systems can impact the final outcome. In recent years, it has emerged that c-di-GMP (bis-(3'-5')-cyclic dimeric guanosine monophosphate) is probably the most important second messenger for the initiation of the biofilm developmental program [47, 48]. C-di-GMP is ubiquitous in bacteria, controlling primarily the transition from the motile to the sessile lifestyle by regulating transcription, enzyme activities and large cellular structures. Moreover, c-di-GMP has been shown to regulate virulence, cell-cycle progression, production of antibiotics, and diverse other cellular functions [47, 48]. Generally, an increase in c-di-GMP levels by the enzymatic action of diguanylate cyclases that produce one c-di-GMP molecule from two GTP monomers shifts the bacterium's lifestyle to the sessile state. In contrast, the motile state is maintained at low c-di-GMP levels due to the action of specific phosphodiesterases that convert c-di-GMP into pGpG (5'-phosphoguanylyl-(3'-5')-guanosine) and subsequently into two GMP molecules. Cyclic-di-GMP can play a role during all phases of biofilm development, including the formation of three-dimensional structures in mature biofilms (section 1.1.1.3) and biofilm dispersal (section 1.1.1.4), but can also play an essential role during the initial attachment. In enteric bacteria such as *E. coli* and *Salmonella enterica*, c-di-GMP seems to indirectly control flagella rotation and thereby impact surface adhesion and initial attachment [49-51]. In *Pseudomonas aeruginosa* and *C. crescentus*, the non-motile lifestyle is induced by down-regulation of flagella expression and assembly, respectively [52-54]. Another common c-di-GMP-triggered mechanism to switch to the biofilm lifestyle is the formation of fimbriae, cell-surface adhesins, and matrix exopolysaccharides [55-57].

Furthermore, two-component systems and regulatory small RNAs play important regulatory roles in the transition to the surface-associated lifestyle by controlling extracellular appendages or exopolysaccharides [58]. One important example is the Gac/Rsm signal transduction pathway that is conserved in gammaproteobacteria, consisting of the GacS/GacA (BarA/UvrY in *E. coli*) two-component system, the sRNA sequestering protein RsmA (CsrA), and regulatory small RNAs RsmY and RsmZ (CsrB and CsrC) [59]. The final output of the Gac/Rsm signal transduction system may vary among species. However, a common scheme is the antagonistic control of motility and processes required for the irreversible attachment. To stimulate biofilm formation, the Gac/Rsm system has been shown to repress flagella genes on the one hand [60], and to (post-) transcriptionally induce adhesion and exopolysaccharide production on the other hand [61, 62].

1.1.1.2 Microcolony formation

Once the cells have irreversibly attached to the surface and the biofilm developmental program is initiated, clonal growth of attached cells results in formation of microcolonies [63]. At this stage, the monolayer biofilm has usually developed into a thin but multilayered biofilm [9]. The formation of microcolonies is limited by the availability of nutrients on the surface or in the media, and the perfusion of those nutrients to cells [39]. Furthermore, biofilm development into complex structures is often limited by the removal of waste or toxic metabolic by-products [1]. Although hydrodynamic flow of the medium increases nutrient availability and removal of waste, an optimal flow rate exists that favors growth and perfusion rather than erosion of the outer cell layers [30]. Other factors that control biofilm maturation include internal pH, oxygen concentration, nature and concentration of carbon source, and osmolarity [19, 30]. Another important issue during this developmental phase and also during later phases is the production and release of EPS to form the biofilm matrix. This subject will be introduced separately in section 1.1.2.

Aside from environmental conditions and EPS, direct cell-cell interactions mediated by cellular appendages play an essential role in the formation and stabilization of surface-attached microcolonies. O'Toole and Kolter analyzed microcolony formation of *P. aeruginosa* using time-lapse microscopy. The results suggest that microcolonies are formed by aggregation of cells present in the monolayer after initial attachment. Characterization of a type IV pilin-deficient mutant showed that this strain was not able to form microcolonies, suggesting that these cell appendages play an important role during this biofilm developmental phase [22]. Klausen and coworkers observed type IV pilin-dependent twitching motility of *P. aeruginosa* across the surface during early phases of biofilm formation [63]. However, type IV pili were not required for the initial attachment as deletion mutant strains are still able to form monolayer biofilms [22]. It was concluded that twitching motility is required for the transition of a monolayer biofilm into microcolonies in *P. aeruginosa* biofilms (Figure 1) [9]. Important roles in the formation of microcolonies have also been attributed to fimbriae that seem to mediate and strengthen direct cell-to-cell interactions [64–66]. The roles of the CupB and CupC fimbriae in *P. aeruginosa* have been attributed especially to cell clustering that is essential for microcolony formation [65]. Fibrillar amyloid adhesins such as curli fibers in *E. coli* and *Salmonella spp.* are not only important for the irreversible attachment to surfaces as mentioned above (section 1.1.1.1), but also for aggregation and the formation of complex biofilm structures [35].

Surface-associated growth within microcolonies appears to require specific metabolic adaptations. Global transcriptomic and proteomic approaches performed on *P. aeruginosa* microcolonies indicated activation of stress response mechanisms and anaerobic and fermentative processes [67]. Petrova and coworkers suggest that microcolony formation is associated with stressful, oxygen-limiting but electron-rich conditions, and seems to require pyruvate and pyruvate fermentation as a specific adaption to this biofilm-developmental phase [67]. Relatively little is known regarding similar metabolic adaptations in other organisms. Nevertheless, nutritional conditions seem to ubiquitously impact biofilm maturation and differentiation of microcolony biofilms into mature biofilms with complex architectures [63, 68].

1.1.1.3 Maturation of the biofilm

Highly regulated social behavior that proceeds through different developmental phases resulting in complexly structured communities was seen for a long time as an unusual feature of myxobacteria

[16, 69]. However, in the last decades biofilm developmental sequences that produce complex community structures have been described for a great number of species, including *P. aeruginosa*, *E. coli*, and *Vibrio cholera* [1, 23, 70]. In-depth characterization of developmental cycles and biofilm structures of model organisms such as *P. aeruginosa* might give the impression that it is a feature of the motile Gram-negative proteobacteria or enteric bacteria [16]. However, analogous dynamic processes including the movement over surfaces, formation of complex biofilm structures, detachment and reattachment, can also be observed for non-motile Gram-positive species such as *Staphylococcus aureus* and *Mycobacterium* [71, 72]. As exemplified by *P. aeruginosa* and generally viewed as typical feature for mature microbial biofilms, microcolonies develop into large cell clusters that are often recognized as towering structures or three-dimensional biofilm architectures (Figure 1). Maturation into such complex structures is often associated with the production of EPS, as described in more detail in section 1.1.2. Mature *P. aeruginosa* biofilms are penetrated by characteristic channels through which the medium can freely flow, allowing access to nutrients and removal of waste products [1]. Watnick and Kolter described analogous three-dimensional structures consisting of pillars of bacteria with characteristic water channels for *V. cholera* biofilms cultured under static conditions [23]. Similar observations were also made for *E. coli* biofilms cultured under hydrodynamic conditions. Reisner and coworkers observed tulip-shaped pillars of cells with sizes up to 100 μm , separated by medium-filled channels where cells were free to move [70]. For simplicity, such pillars of cells of mature biofilms will be termed biofilm macrocolonies henceforth. The shapes, cell densities and sizes of biofilm macrocolonies are largely dependent on environmental conditions. For example, shear forces under hydrodynamic conditions strongly impact macrocolony architecture by removal of loosely attached cells, resulting in densely packed colonies with shapes that resist the flow rates of the medium [68, 73]. At some point, the biofilm reaches a dynamic equilibrium at which the outer cell layers of macrocolonies and cells in close proximity to the surface generate planktonic cells. Furthermore, entire cell clusters are often detached and transported away by the medium flow (Figure 1). These cells may escape the biofilm and colonize other habitats. At very late stages, cells can become quiescent or die from starvation, decreased pH, pO_2 , or an accumulation of toxic metabolic by-products [39, 74]. The appearance of complex structures of biofilm communities is accompanied by highly diverse physiological microconditions, depending on the spacial location of single cells within the biofilm. Accordingly, in a single biofilm community cells exist in a wide range of physiological states. Both, diverse genotypes and phenotypes that express distinct metabolic pathways, stress responses and other specific biological activities are juxtaposed [75]. One important phenotypic variant that may emerge in mature biofilms are persister cells. Persister cells commonly represent subpopulations of biofilm cells that have enhanced tolerance to antibiotics [76]. These cells can be in a metabolically dormant (non-dividing) state against which most antibiotics are less effective. If antibiotic treatment continues, rapidly growing metabolically active cells are eradicated whereas dormant cells can survive and repopulate the biofilm after the treatment [77]. However, unlike antibiotic resistance, antibiotic tolerance by dormant persister cells is a transient and reversible physiological state in a small subpopulation of genetically identical cells [78]. Nevertheless, genetic factors constrain the behavioral options available to the bacteria, and determine responses to chemical or environmental signals [79]. Gene expression of bacterial cells living in biofilms differs significantly from that of free-living cells [80-82]. In recent years, it has become increasingly clear that in numerous species this may be mediated by quorum sensing [83-85].

Quorum sensing can coordinate the switch to the biofilm lifestyle when the cell density of a planktonic population reaches a critical level. However, it has been demonstrated for a high number

of bacterial species that activation of quorum sensing occurs in already established biofilm communities and activates the maturation of the biofilm in a coordinate manner [86]. In addition to the contribution to biofilm formation, it has become clear that many bacterial species use quorum sensing to coordinate the detachment of cells from the mature biofilm [86]. Biofilm dispersion is essential when nutrients and other resources become limited and/or waste products accumulate, and allows bacteria to colonize new habitats and to re-initiate the biofilm life cycle. There are different strategies to accomplish biofilm dispersion that will be discussed in the next section.

1.1.1.4 Biofilm dispersal

Biofilm formation is a dynamic process during which the biofilm partially grows and dissolves. Cells or cell aggregates that detach from the biofilm may move away and colonize new habitats [16, 87, 88]. A drastic change of the environmental conditions can result in a simultaneous release of a great number of cells. Environmental stimuli that induce disassembly of mature biofilms include alterations in the availability of nutrients, high or low levels of iron, oxygen depletion, alterations in the fluid shear, low levels of nitric oxide (NO), changes in temperature, and a variety of bacterially derived signals [89-91] [92].

Regarding the availability of nutrients as environmental signal, both nutrient-induced and starvation-induced dispersal of mature biofilms has been observed. For example, *Pseudomonas putida* shows increased detachment levels in response to carbon starvation. To achieve detachment, a protease (LapG), that is derepressed by low c-di-GMP levels in response to starvation, degrades the adhesin LapA which is essential for the integrity of the biofilm matrix [93]. By contrast, *Acinetobacter* sp. Str. GJ12 biofilms become more tightly packed when starved and *P. aeruginosa* biofilms disperse in response to increasing carbon concentrations [94, 95]. Similarly opposing results were found with regard to iron levels. Both high and low levels of iron seem to trigger biofilm dispersal in *P. aeruginosa* and *E. coli* biofilms [96-98]. In *S. oneidensis* MR-1, oxygen depletion by a stop of the medium flow was shown to induce rapid detachment [99]. In *P. aeruginosa*, a phosphodiesterase (RdbA) controls biofilm dispersal in response to oxygen depletion by decreasing c-di-GMP levels. This in turn induces motility and rhamnolipid synthesis and inhibits exopolysaccharide synthesis, factors that are required for biofilm formation [100]. Furthermore, NO signaling was shown to impact c-di-GMP levels and thereby controlling biofilm dispersal in *P. aeruginosa* and *S. oneidensis* MR-1 [101, 102]. Low concentrations of nitric oxide were also found to induce dispersal in other species, including *E. coli*, *V. cholera*, *S. aureus*, *Bacillus licheniformes*, *Serratia marcescens*, *Bacillus subtilis*, *Legionella pneumophila*, *Nitrosomonas europaea* or *Neisseria gonorrhoeae* [103-106]. The release, perception, and transduction of bacterially derived signals play also important roles in the regulation of biofilm detachment and dispersal. Cell-to-cell signaling by quorum sensing has been primarily linked to biofilm formation (section 1.1.1.3), but it has also been shown to play a role in the dispersal process. For example, artificial induction of the *agr* quorum sensing system in *S. aureus* or addition of the autoinducing peptide causes dispersal of the biofilm, probably by protease-mediated degradation of the EPS matrix [107]. Furthermore, the D-amino acids D-leucine, D-methionine, D-tyrosine, and D-tryptophan seem to act as biofilm dispersal-inducing factors in *B. subtilis*, *S. aureus*, and *P. aeruginosa* [108]. D-amino acids seem to accumulate in late phases of biofilm formation and can be incorporated into the bacterial cell wall to release amyloid fibers that

are anchored into the cell wall. Kolodkin-Gal, Leiman and coworkers propose that D-amino acids represent a widespread signal for biofilm disassembly [108, 109].

To accomplish biofilm dispersion, bacteria must sever existing biofilm bonds and structures and actively or passively escape from the biofilm community. A variety of strategies has been identified, including endogenous enzymatic degradation of the biofilm matrix, stopping the synthesis of biofilm matrix compounds, disrupting non-covalent interactions between matrix components, or the release of EPS or surface-binding proteins [16, 86, 110-113] [114]. Specific extracellular enzymes including polysaccharide-degrading enzymes, chitinases, proteases and nucleases often execute matrix dissolution and cell release [107, 115-118]. The role of extracellular nucleases for biofilm formation and dispersal is described separately in section 1.1.4. To escape from existing biofilm structures, three distinct strategies have been described: ‘swarming/seeding dispersal’, in which single cells are either actively or passively liberated from mature biofilm structures into the surrounding medium or substratum; ‘clumping dispersal’, in which complete aggregates of cells are released; and ‘surface dispersal’, in which biofilm structures move across the surface, for example by twitching or gliding motility [16].

Active dispersal from biofilms is often accompanied by localized death and lysis of cells in the center of mature biofilm structures, a phenomenon that is well known from *P. aeruginosa* biofilms [119, 120]. Due to the heterogeneity of the cells in the mature biofilm, only a subpopulation of cells will undergo lysis, providing nutrients for the bacteria that will differentiate into dispersal cells. Coordinated dispersal of cells can lead to the characteristic hollowing of biofilm structures that is observed during late phases of biofilm formation of many bacteria [92]. Molecular mechanisms that regulate and execute cell lysis in biofilms are described separately in section 1.1.3.

1.1.2 The biofilm matrix

Extracellular polymeric substances (EPS) are commonly a complex mixture of exopolysaccharides, proteins and extracellular DNA, and (along with water) constitute the biofilm matrix. [121-124]. Additionally, the matrix can contain lipids and other biopolymers such as humic substances. The proportion of EPS in biofilms generally ranges between 50 and 90 % of the total biomass [125]. Biofilms matrices are highly hydrated, thus water constitutes by far the largest proportion of the total mass (>90 %). Furthermore, extracellular appendages, otherwise required for motility and biofilm formation, can also stabilize the matrix. These may include flagella, pili, and fimbriae [124]. Membrane vesicles of Gram-negative bacteria can form another component of biofilm matrices. It has been suggested that these vesicles act as carriers for DNA fragments or specific enzymes that may be involved in EPS modification [126, 127]. Membrane vesicles of *P. aeruginosa* were shown to exhibit bacteriolytic effects on other bacteria including pathogens [128].

The characteristics of a given EPS matrix strongly impacts the mode of life of the biofilm community, and is itself determined by the entity of the individual matrix components. The abundance, cohesion, charge, sorption capacity, specificity and structure of the individual components impacts the nature of the entire EPS matrix. The architecture of the matrix is both influenced by the biofilm’s innate biological activity such as localized cell death and enzymatic activity, and by physical forces of the environment such as shear stress. Thus, the outcome can vary

Table 1. Functions of biofilm matrix components

Function	Matrix component(s)	Relevance for biofilms
Adhesion	Polysaccharides, proteins, DNA and amphiphilic molecules	Initial attachment of planktonic cells to biotic or abiotic surfaces, and durable attachment of whole biofilms
Aggregation	Polysaccharides, proteins, DNA	Bridging between cells; temporary immobilization bacterial populations; development of high cell densities; cell-cell recognition
Cohesion of biofilms	Neutral and charged polysaccharides, proteins (such as amyloids and lectins), DNA	Determining the biofilm architecture through EPS structures (capsule, slime or sheath) by forming a complex hydrated polymer network often in conjunction with multivalent cations
Retention of water	Hydrophilic polysaccharides and proteins	Maintaining a highly hydrated microenvironment around biofilm cells; tolerance of desiccation during drought stress
Protective barrier	Polysaccharides, proteins, DNA	Conferring resistance against host defenses during infection; tolerance to antimicrobial agents and environmental stresses
Sorption of organic compounds	Charged or hydrophobic polysaccharides and proteins	Accumulating nutrients from the environment and xenobiotics (environmental detoxification)
Sorption of inorganic ions	Charged polysaccharides and proteins, including inorganic substituents such as phosphate and sulfate	Promoting polysaccharide gel formation, ion exchange, mineral formation, sorption of toxic metal ions (environmental detoxification)
Enzymatic activity	Proteins	Digestion of endogenous macromolecules for nutrient acquisition; degradation of structural EPS for cell detachment and biofilm dispersal
Nutrient source	Potentially all matrix components	Providing a source of carbon, nitrogen, and phosphorus for the biofilm cells under nutrient-limited conditions
Exchange of genetic information	DNA	Facilitating horizontal gene transfer between biofilm cells; increasing fitness and adaptability
Electron donor or acceptor	Proteins (pili, nanowires) and electron shuttles (humic substances, riboflavins)	Redox activity between biofilm cells and redox active substrata and the biofilm matrix
Export of cell compounds	Membrane vesicles containing nucleic acids, enzymes, lipopolysaccharides and phospholipids	Release of cellular material for metabolic turnover or exchange in the biofilm environment
Sink for excess energy	Polysaccharides	Storage of excess carbon under unbalanced carbon to nitrogen ratios
Binding of enzymes	Polysaccharides	Accumulation, retention and stabilization of enzymes through their interactions with polysaccharides

Adapted from Flemming and Wingender, 2010 [124]

strongly between species and habitats resulting in diverse matrix phenotypes with respect to thickness, density, and characteristic features such dense areas, pores and channels. Obviously, the nature of the EPS matrix impacts biofilm morphologies that can be smooth, flat, fluffy, filamentous, and helps to build macrocolonies with different sizes, forms and abundances [124]. However, despite the diversity of matrix compositions and structures, common or representative features have been observed and extensive research has contributed to a better understanding in this important field of biofilm research. An overview over common functions of matrix components is given in Table 1.

Exopolysaccharides

Probably the best-characterized matrix components are extracellular polysaccharides (exopolysaccharides), representing a highly abundant and often essential structural element in biofilm matrices. Exopolysaccharides can be linear or branched and form complex networks within the matrix, often interacting with the cell surface (capsules), the substratum or other EPS components [129-131]. Polysaccharides can be both homo- and heteropolymers. Homopolysaccharides include the glucans and fructans secreted by oral streptococci biofilms and cellulose produced *e.g.* by *Rhizobium* spp., *Agrobacterium tumefaciens* and members of the Enterobacteriaceae and Pseudomonadaceae [132-137]. Heteropolysaccharides consist of a mixture of neutral and charged sugar residues and can contain both organic and inorganic side groups. Examples of well-studied heteropolysaccharides are alginates produced by *Pseudomonas* and *Azotobacter*, xanthan produced by *Xanthomonas*, and colonic acid commonly produced by members of the Enterobacteriaceae [138-140]. Alginate has been extensively studied in the past, revealing that it is a high-molecular-mass unbranched polymer consisting of homopolymeric and heteropolymeric mannuronate and gluronate blocks that are linked by linked by 1,4-linked uronic acid residues [124]. Alginate was found to affect biofilm development and architecture of mostly mucoid *P. aeruginosa*, but it is not essential for biofilm formation [141]. Along with alginate, *P. aeruginosa* produces two other well-studied exopolysaccharides, Psl (Polysaccharide synthesis locus) and Pel (Pellicle formation). Both polysaccharides are involved in biofilm formation of mostly non-mucoid strains that do not overproduce alginate and seem to have partly redundant functions [142, 143]. However, Psl has also been shown to contribute to biofilm formation of mucoid strains [144]. Psl is important for the initial attachment at solid surfaces and biofilm architecture at later stages of biofilm formation [145]. Interestingly, a very recent report by Wang and coworkers demonstrates direct interactions of Psl with eDNA within the *P. aeruginosa* biofilm matrix [146]. Pel's function has mainly been attributed to pellicle formation at liquid-air-interfaces but it can also serve a structural and protective role in solid surface biofilms, apparently at early and late stages of biofilm formation [147, 148]. In *E. coli*, cellulose, colonic acid, and propylene glycol alginate (PGA) seem to be the major polysaccharides that play a role in biofilm formation. Cellulose modulates biofilm formation by counteracting curli-mediated colonization of solid surfaces and might promote resistance to environmental stresses rather than structural integrity of the biofilm [149]. Investigating the role of colonic acid for the development of *E. coli* biofilms, Danese and coworkers found that colanic acid production is not required for surface attachment but is critical for the formation of complex three-dimensional biofilm architectures [150]. PGA serves as an adhesin that is attached to the cell envelope, promoting abiotic surface binding and intercellular adhesion [151]. In *V. cholerae* biofilms, one major component of the biofilm matrix is VPS (*Vibrio* polysaccharide) that seems to be bound to a yet unidentified component, which gives it high viscosity [152, 153]. VPS has been shown to be required for the formation of mature biofilm structures and virulence of *V. cholerae* [154].

Conclusively, exopolysaccharides are indispensable for biofilm formation in many bacteria, and mutants lacking exopolysaccharides synthesis genes are often strongly impaired in surface adherence and/or development of complex biofilm architectures [23, 150, 155]. However, exopolysaccharide-deficient bacteria may commensalistically exist with exopolysaccharide-forming bacteria in mixed-species biofilms by taking advantage of the non-innate matrix polymers [121, 124]. Thus, phenotypes observed for single-species biofilms under laboratory conditions may not necessarily reflect the species' ability to form biofilm under natural conditions.

Proteins

Proteins represent important components of most biofilm matrices and their content can vary among species and habitats. In some cases, the total biomass of matrix proteins can even exceed that of polysaccharides [156, 157]. Matrix proteins can have enzymatic activity to fulfill specific catalytic functions in the extracellular space of the biofilm, or they can function as structural elements to strengthen the matrix or to modulate biofilm architecture.

An important role of enzymatically active matrix proteins is the degradation of other matrix components, including water-soluble polymers such as polysaccharides, proteins, and nucleic acids, and water-insoluble compounds such as cellulose, chitin, and lipids. These biopolymers are fragmented to low-molecular-mass compounds that can be assimilated by biofilm cells and recycled as carbon or energy source. Common enzymes that degrade matrix components to exploit those as nutrient reservoir include glucosidases, cellulases, N-acetyl-glucosamidases, chitinases, proteases, nucleases, phosphatases, lipases, and esterases [124]. It has been suggested that extracellular enzymes can become immobilized within the matrix by interaction with specific EPS components. For example, molecular modeling of lipase LipA indicated attachment of the enzyme to the polysaccharide alginate [158]. Such interactions may reduce “washing-out” of extracellular enzymes under hydrodynamic conditions. Moreover, immobilization at surrounding EPS may retain extracellular enzymes in close proximity to the cells, thereby keeping diffusion distances of enzymatic products relatively short to increase assimilation [124]. Another goal of EPS degradation can also involve the detachment of cells from the community or complete biofilm dispersal (described separately in section 1.1.1.4).

Structural proteins represent another group of extracellular matrix proteins without enzymatic activity. These can be surface-associated or secreted into the extracellular space. Examples of surface-associated proteins are Bap (Biofilm-associated protein) proteins that are known from *S. aureus*, but are also found in several other species. These cell-surface proteins have high molecular masses and play important roles during early adherence, intercellular adhesion, biofilm formation, and infection [159, 160]. One common class of secreted proteins that specifically bind carbohydrates are lectins, such as the glucan-binding proteins in oral *S. mutants* biofilms, or the galactose-specific lectin LecA and the fructose-specific lectin LecB of *P. aeruginosa* [161-163]. Another example for exopolysaccharide binding proteins is CdrA that binds Psl in *P. aeruginosa* biofilms, probably to strengthen the matrix by interconnecting Psl molecules and to attach biofilm cells to the exopolysaccharide [164].

Importantly, proteinaceous matrix components do not only exist as single protein units, but also as long polymers that form complex fibrous networks within the biofilm matrix. Commonly, these are cellular appendages such as pili, fimbriae and flagella. The relevance of each individual component may vary between species, but important functions have been attributed to all of these structures and to all phases of biofilm development. Moreover, proteinaceous fibers have been shown to interact with other components including DNA and possibly polysaccharides [135, 165].

Finally, amyloid fibers represent a ubiquitous and important class of fibrous matrix proteins that have been identified initially in *E. coli*, but have later been shown to exist as well in distantly related model organisms such *B. subtilis* [166, 167]. Amyloid fibers are conserved both in prokaryotes and eukaryotes and have been associated with several human diseases [168]. In *B. subtilis* biofilms, TasA

was found to constitute the major proteinaceous matrix component and was later shown to form amyloid fibers, important for cell-cell interactions, biofilm integrity, and pellicle formation [167].

Extracellular DNA (eDNA)

Significant concentrations of DNA have been identified in the extracellular space of microbial communities in activated sludge, long before DNA was appreciated as an important structural matrix component in bacterial biofilms [156]. Extracellular DNA can be ubiquitously found in the presence of surface-associated bacterial growth, both in terrestrial and aquatic habitats [169]. However, its concentration can vary greatly, ranging from 2 $\mu\text{g g}^{-1}$ dry weight in soil, to 20 mg g^{-1} dry weight in activated sludge [170, 171]. Concentrations of DNA in deep-sea sediments have been shown to be surprisingly high. Dell'Anno and Danovaro determined a concentration of approximately 0.31 g of total DNA/ m^2 in the top centimeter (of which over 90 % accounts for eDNA) of deep-sea sediments and a total mass of approximately 0.45 gigatons of eDNA worldwide [172]. Obviously, such enormous amounts of organic material do not remain unused in microbial ecosystems. Bacteria can utilize DNA as a source of carbon, nitrogen, and phosphorus [173, 174]. Accordingly, turnover rates of eDNA in marine sediments are fairly high, although DNA is normally a stable molecule and can remain intact for thousand of years in a protected environment [169, 172, 175, 176]. DNA represents a central phosphorus source for deep-sea microorganisms. Accounting for 13 % of the total organic phosphorus flux in the deep sea, eDNA plays a key role in the marine phosphorus cycle and deep-sea ecosystem functioning [172]. In addition to its importance as a nutrient reservoir, eDNA represents an important source for the intra- and interspecies exchange of genetic information, referred to as horizontal gene transfer [87].

Despite its ubiquitous abundance and widely accepted relevance in microbial ecosystems, eDNA has long been viewed solely as residual cell debris and not as a key component of the biofilm matrix in addition to polysaccharides and proteins. However, early observations already indicated that eDNA contributes to cellular aggregation and surface colonization. In the 1950's, Catlin and Cunningham described DNase-sensitive viscous slime surrounding *S. aureus* cells that promotes pellicle formation in broth cultures [177, 178]. Twenty years later, Arko and coworkers reported that eDNA contributes to cell clumping in *Neisseria gonorrhoeae* cultures [179]. However, not until 2002 it was demonstrated that eDNA is required for bacterial biofilm formation on solid surfaces. Whitchurch and coworkers showed for the first time that eDNA is an essential component of the *P. aeruginosa* biofilm matrix by addition of DNase I to flow-chamber grown biofilms, resulting in significant release of biofilm biomass from established biofilms and prevention of biofilm formation when DNase I was added continuously [180]. The results indicated that eDNA is a structural component of bacterial matrices, required for the structural integrity and stability of the biofilm community. Double-stranded DNA of high molecular weight is a physically strong and chemically stable polymer that provides a viscous environment when concentrated. These properties seem to make eDNA ideally suited to immobilize and protect microbial cells. Furthermore, when bound to bacterial cells, eDNA can promote adhesion to hydrophobic surfaces [181]. In recent years, a multitude of eDNA degradation assays and phenotypic mutant analyses were performed to investigate whether eDNA plays also a structural role in single or multispecies biofilms of other species than *P. aeruginosa*. The results confirm that eDNA is an important structural matrix component both of Gram-negative bacteria including *E. coli*, *N. gonorrhoeae*,

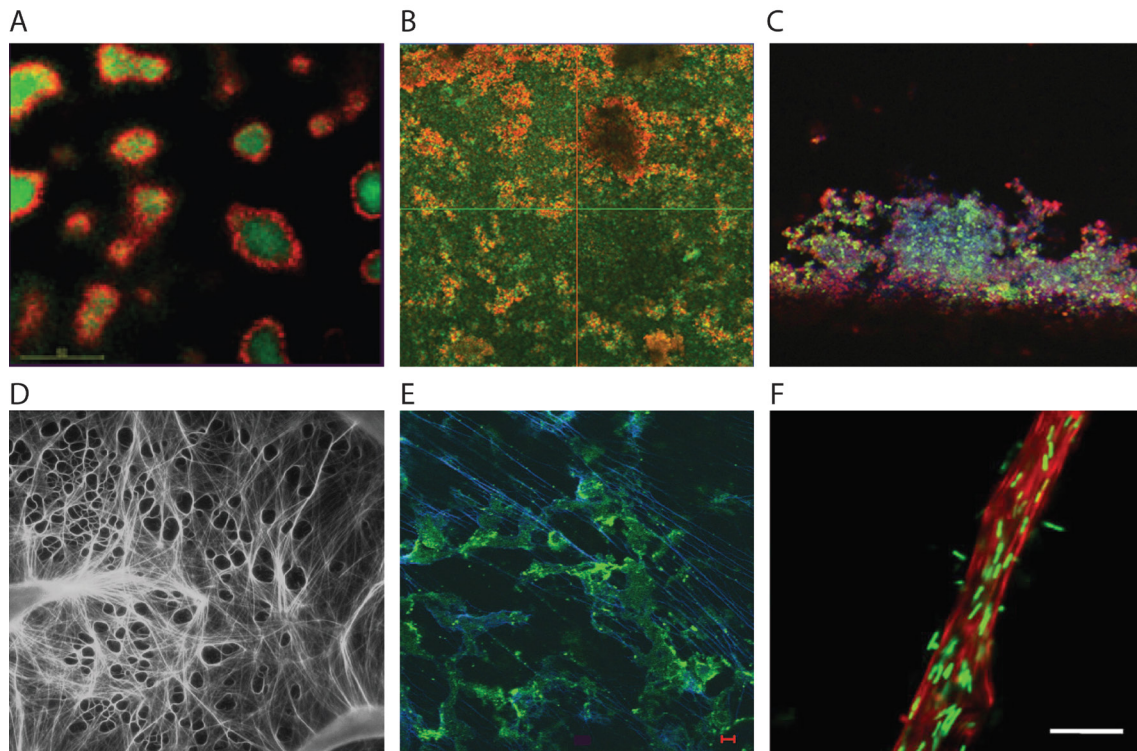


Figure 2. Localization and structural conformation of eDNA in biofilms. (A) CLSM micrograph of DDAO-stained eDNA (red) in a GFP-tagged *P. aeruginosa* PAO1 biofilm (green) grown for two days in a flow chamber. The micrograph is a horizontal optical section in the region of the stalk of mushroom-shaped macrocolonies. The bar equals 20 μ m. Adapted from Allesen-Holm and coworkers, 2006 [182] (B) CLSM micrograph of PI-stained eDNA (orange) in a *S. aureus* UAMS-1 biofilm (green) grown for 24 hours in a flow chamber. The micrograph is a top-down view of all z-stacks. The orthogonal view is shown at $\times 100$ magnification with a Plan-Apochromat $\times 10/0.45$ objective lens. Adapted from Rice and coworkers, 2007 [183] (C) CLSM micrograph of DAPI-labelled eDNA (blue) in a GFP-tagged *N. gonorrhoeae* biofilm (green) grown in flow chambers for three days. The biofilms were additionally stained with 2C3, a mouse MAb to outer membrane protein H.8 (red). The authors did not present a size standard. Adapted from Steichen and coworkers, 2011 [184] (D) Epifluorescence micrograph of filamentous network of strain F8 and eDNA after staining with SYTO9 in a 4-day-old biofilm grown on an isopore filter. The bar equals 50 μ m. Adapted from Böckelmann and coworkers, 2006. [185] (E) Immunofluorescent micrograph of a *H. influenzae* biofilm labelled with rabbit anti-soluble recombinant PilA and AlexaFluor 488 goat anti-rabbit (green) and grown for four days *in vivo* in a animal model (chinchilla). Filamentous eDNA strands were stained with DAPI. The bar equals 5 μ m. Adpated from Jurcisek and Bakaletz, 2007 [186] (F) CLSM micrograph of SYTOX-orange-stained eDNA trail (red) and attached cells in a *M. xanthus* fruiting body grown for three days and stained with SYTO9 (green). The bar equals 20 μ m. Adpated from Hu and coworkers, 2012 [131].

S. oneidensis, *Acidovorax temperans*, *Haemophilus influenzae*, and *Myxococcus xanthus*; and Gram-positive bacteria including *S. aureus*, *Streptococcus sanguinis* and *Streptococcus gordonii*, *Enterococcus faecalis*, and *B. cereus* [38, 131, 183, 184, 186-193]. For most species, degradation of eDNA by addition of eDNA-degrading enzymes or inhibition of eDNA release was shown to result in inhibition of biofilm formation or biofilm dispersal of existing biofilms. However, only little insights in the localization, structural arrangement, and interaction of eDNA with cells or other matrix components exist up to date. In *P. aeruginosa*, eDNA staining in conjunction with CLSM analyses suggested that the eDNA is located primarily in outer parts of the stalks of mushroom-shaped macrocolonies, forming a border between the stalk-forming bacteria and the cap-forming bacteria (Figure 2A). PCR and Southern hybridization analyses demonstrated that the sequence and size of the *P. aeruginosa* eDNA corresponds to chromosomal DNA [182]. Similar results were obtained for

several other organisms, indicating that biofilm eDNA represents mostly high-molecular-weight genomic DNA fragments of random sequences or entire chromosomes [194]. The localization of eDNA can differ significantly between species. In many species eDNA seems to be evenly distributed within the biofilm, surrounding the cells in proximity to the surface or as aggregated cell clusters and macrocolonies. Mostly, eDNA concentrations positively correlate with the density of cells in such biofilm structures. For example, eDNA concentrations in *E. faecalis* biofilms seem to be highest in macrocolonies similar to *P. aeruginosa* biofilms, but the eDNA is evenly distributed within the entire cell cluster and not at a defined localization [187]. Other examples of such localizations are e.g. *S. aureus* or *N. gonorrhoeae* biofilms (Figure 2B,C) [183, 184, 195]. The aquatic isolate F8, which belongs to the gammaproteobacteria, forms a stable filamentous eDNA network in a time-dependent manner. Starting with the accumulation of amorphous material around the cells within the first days, the strain forms microfilaments that were continuously interconnected to result in a complex spacial filamentous structure in 4- to 7-day-old biofilms (Figure 2D). These structures were shown to consist of eDNA with attached cells and cell aggregates [185]. In *H. influenza* biofilms, the eDNA appears to be arranged in a dense interlaced meshwork of fine strands as well as in individual braided filaments that span water channels (Figure 2E) [186]. In *M. xanthus* biofilms (and starvation-induced fruiting bodies), eDNA was shown to strengthen the extracellular matrix by interacting with exopolysaccharides [131]. The eDNA molecules formed well organized structures (such as thick filaments with attached cells) that were similar in appearance to the organization of exopolysaccharides in extracellular matrices (Figure 2F). Extracellular DNA degradation assays demonstrated that *M. xanthus* biofilms exhibited greater physical strength and biological stress resistance in the presence of eDNA.

Although eDNA seems to support biofilm formation in most species, so far one example has been reported where eDNA inhibits biofilm formation of a differentiated cell type. In *C. crescentus* biofilms, eDNA (that has been released by cell lysis into the biofilm matrix) strongly inhibits further settling of motile swarmer cells to the biofilm community by masking the newly synthesized holdfast [196, 197]. Berne and coworkers conclude that this mechanism modulates biofilm development and promotes dispersal without causing a potentially undesirable dissolution of the existing biofilm [196]. Strikingly, the inhibitory effect of eDNA on the attachment of motile cells with a newly synthesized holdfast is species-specific, as only DNA from *Caulobacter*, but not from other genera, suppressed biofilm maturation [197].

In addition to its structural role in biofilm formation of many species, eDNA has been reported to exhibit diverse further functions. For example, it has been demonstrated that eDNA can have antimicrobial activity at physiologically relevant concentrations, causing cell lysis by chelating cations that stabilize lipopolysaccharides and the outer membrane [198]. Furthermore, eDNA has been reported to induce peptide resistance mechanisms at sub-lethal concentrations, possibly to contribute to long-term survival under DNA-rich environments. Binding of divalent metal cations induces the Mg^{2+} -responsive PhoPQ and PmrAB two-component systems that control various genes required for virulence and resisting killing by antimicrobial peptides in *P. aeruginosa* and many other Gram-negative bacteria [199].

Conclusively, eDNA seems to play an important and ubiquitous role in biofilm formation, especially regarding the matrix composition and structural integrity of biofilms. However, the diversity of biofilms in nature is accompanied by diverse species-specific and habitat-specific functions of eDNA in biofilm formation, maturation, persistence, dispersal, resistance, and

nutrition. Many of such species-specific and habitat-specific adaptations are yet to be discovered and we are probably still scraping the surface in this field of research.

One important question that has been posed in eDNA research in the past years is how eDNA is released into the extracellular space of the biofilm and how it is integrated into the matrix. Another crucial aspect that has been addressed is the role of extracellular nucleases in biofilm formation, or more precisely in eDNA modification and degradation. As this study thesis focuses on the control of extracellular DNA release and degradation in *S. oneidensis* MR-1 biofilms, both topics will be introduced separately in section 1.1.3 and 1.1.4.

1.1.3 Release mechanisms of eDNA in biofilms

The origin of eDNA in biofilms has been a focus of numerous studies in the past years. It has emerged as common sense that three general mechanisms exist which may allow DNA to be released from bacteria and to accumulate in the biofilm environment: **vesiculation** [127, 182, 200, 201], **secretion** [195, 202, 203], and **cell lysis**, which may be the most common source of eDNA in natural environments [183, 187, 204, 205]. Notably, although some species may rely on one of the mechanisms to release eDNA (and other biofilm-promoting factors), others seem to utilize several mechanisms simultaneously or for different purposes. An overview over eDNA release mechanisms in different bacteria is given in Figure 3.

1.1.3.1 Vesicle-mediated eDNA release

Very little is known about vesicle-mediated release of eDNA in biofilms. Still, the existence of membrane vesicles in biofilms is known for a long time and vesicles seem to represent a common element in biofilm matrices [126, 206, 207]. Moreover, vesicle-mediated transport of DNA has been described for planktonic cultures and may therefore occur as well under biofilm conditions [208, 209]. Membrane vesicles are generally defined as multifunctional and chemically heterogeneous bilayered structures that bleb from the outer membranes of Gram-negative bacteria [210]. However, it has recently been shown that membrane vesicles are not exclusive to Gram-negative species but exist also in Gram-positives [211]. First evidence of vesicle-mediated eDNA release in biofilms of a Gram-negative species has been provided for the clinical strain *Acinetobacter baumannii* AHMS 7 [200]. Sahu and coworkers utilized transmission electron microscopy (TEM) and atomic force microscopy (AFM) to visualize the release of eDNA from membrane vesicles of varying diameter (20-200 nm). The containing eDNA was shown to exhibit high similarity to genomic DNA and addition of purified eDNA-containing membrane vesicles significantly augmented biofilm formation in polystyrene microtiter plates [200]. In *P. aeruginosa*, eDNA was shown to be associated with the external surface of biofilm-derived membrane vesicles. However, it remains unclear whether surface-associated DNA differs from internalized DNA or matrix eDNA [127]. A very recent report describes vesicle-mediated release of eDNA from a Gram-positive species as well. Liao and coworkers demonstrate that in addition to eDNA that is released by cell lysis, *Streptococcus mutans* also actively releases eDNA-containing vesicles into the biofilm matrix. Deletion of components of the protein secretion and membrane protein insertion machinery altered the vesicle protein profile and reduced eDNA release. However, levels of membrane vesicle production were not altered, indicating that both machineries are required for vesicle-mediated

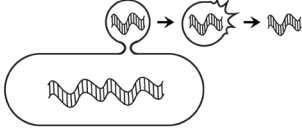
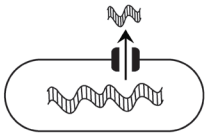
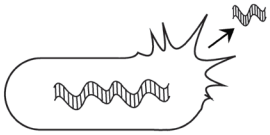
Mechanism of eDNA release	Species	Reference
A 	<i>Pseudomonas aeruginosa</i>	Schooling <i>et al.</i> , 2009
	<i>Acinetobacter baumannii</i>	Sahu <i>et al.</i> , 2012
	<i>Streptococcus mutans</i>	Liao <i>et al.</i> , 2014
B 	<i>Neisseria gonorrhoeae</i>	Hamilton <i>et al.</i> , 2005
	<i>Enterococcus faecalis</i>	Barnes <i>et al.</i> , 2012 Zweig <i>et al.</i> , 2013
C 	S <i>Staphylococcus epidermidis</i>	Heilmann <i>et al.</i> , 1997
	S <i>Staphylococcus aureus</i>	Rice <i>et al.</i> , 2007
	S <i>Pseudomonas aeruginosa</i>	Ma <i>et al.</i> , 2009
	F <i>Bacillus subtilis</i>	González-Pastor <i>et al.</i> , 2003
	F <i>Enterococcus faecalis</i>	Thomas <i>et al.</i> , 2009
	F <i>Streptococcus pneumoniae</i>	Eldholm <i>et al.</i> , 2009
	TA <i>Escherichia coli</i>	Zhao <i>et al.</i> , 2013
	P <i>Staphylococcus aureus</i>	Resch <i>et al.</i> , 2005
	P <i>Pseudomonas aeruginosa</i>	Rice <i>et al.</i> , 2009
	P <i>Streptococcus pneumoniae</i>	Carrolo <i>et al.</i> , 2010
	P <i>Shewanella oneidensis</i>	Gödeke <i>et al.</i> , 2011

Figure 3. Overview of eDNA release mechanisms in bacteria. (A) Vesicle-mediated eDNA release [127, 200, 201] **(B)** Secretion of eDNA [195, 202, 203] **(C)** Release of eDNA by altruistic suicide (S) [155, 183, 212], fratricide killing (F) [213-215], toxin-antitoxin systems (TA) [205], or phage-induced lysis (P) [38, 216-218]. Species that have been reported to access several mechanisms to release eDNA are highlighted in colors.

eDNA release but not for vesicle generation and liberation [201]. Interestingly, the eDNA was shown to be arranged as a structured network of eDNA strands surrounding the cells and mediating cell-cell and cell surface interactions (Figure 4A).

Taken together, the release of membrane vesicles as well as transport and liberation of DNA by membrane vesicles is a ubiquitous phenomenon and recent research indicates that these processes may represent a common strategy to release and embed eDNA into the biofilm matrix. However, very little is understood about molecular mechanisms and regulatory control of vesicle-mediated eDNA release. Furthermore, the exact nature of vesicle-eDNA is unknown for most species and it remains to be elucidated whether internalized and surface-associated DNA molecules differ in sequence and structure or exhibit different functions [127].

1.1.3.2 Secretion of eDNA

To date, active secretion of DNA into the extracellular milieu of biofilms has only rarely been reported and conclusive data is missing for most species. The best-studied model is *N. gonorrhoeae* that has been shown to secrete DNA via an unusual type IV secretion system (Figure 2C) [202]. Most type IV secretion systems require direct cell-cell contacts for function. In contrast, the *N. gonorrhoeae* system secretes chromosomal DNA directly into the extracellular space. Extracellular DNA was shown to exhibit an important structural component of the *N. gonorrhoeae* biofilm matrix and eDNA levels are antagonistically controlled by an extracellular nuclease [184]. Since the type IV secretion system of *N. gonorrhoeae* secretes DNA only in the single-stranded form, Zweig and

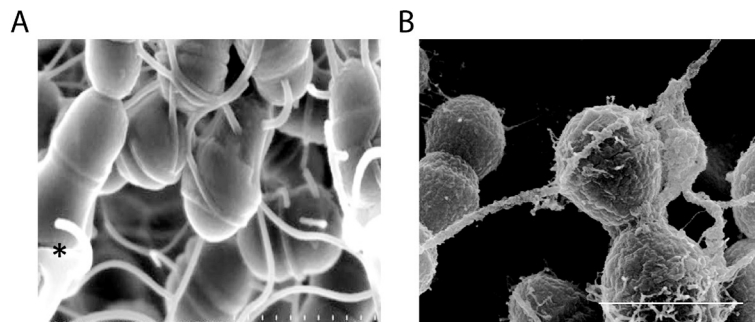


Figure 4. Intercellular strands of eDNA in biofilms. (A) Field emission-scanning electron microscopy (FE-SEM) of intercellular eDNA strands surrounding *S. mutant* cells in biofilms grown on silicon discs for 24 hours. The asterisk indicates DNA of a lysed cell. The image was taken at $\times 50,000$ magnification. Adapted from Liao and coworkers, 2014 [201] (B) Scanning electron micrograph (SEM) of intercellular eDNA strands surrounding *E. faecalis* cells in biofilms grown on Aclar fluoropolymer coupons for 4 hours. Bar equals 1 μm . Adapted from Barnes and coworkers, 2012 [203]

coworkers used a combination of DNA binding proteins, specific nucleases, and fluorescent dyes to investigate the role of both single-stranded and double-stranded DNA in *N. gonorrhoeae* biofilms [195]. Remarkably, single-stranded DNA that is secreted by the type IV secretion system seems to be important during the initial phases, whereas double-stranded DNA accumulates mostly in later phases, probably via an alternative release mechanism. For several other species, observations have been made that indicate release of eDNA by lysis-independent mechanisms; however, the data mostly lacks direct evidence for active secretion. For example, exponential-phase cells of *B. cereus* seem to be decorated with eDNA that might be required for biofilm formation [188]. In *B. subtilis*, DNA fragments that correspond to whole genome DNA are released in late-exponential phase that might be utilized as matrix component under biofilm conditions [219]. Barnes and coworkers utilized cationic dye-based biofilm matrix stabilization techniques with correlative immuno-scanning electron microscopy (SEM) and fluorescent techniques to analyze the eDNA matrix of *E. faecalis* [203]. Similar to the arrangement of eDNA strands in *Streptococcus mutants* biofilms, the eDNA of *E. faecalis* was visualized as long filaments connecting and surrounding the cells (Figure 4B). The authors suggest a release by secretion since eDNA release was observed at the cell poles [203].

Conclusively, due to the lack of data it is unclear whether secretion of eDNA in biofilms represent a rare phenomenon of certain specialists or whether the significance of secretion has been overseen so far.

1.1.3.3 Release of eDNA by cell lysis

Cell lysis of a subpopulation of cells is probably the most common origin of eDNA in biofilms, both of Gram-negative and Gram-positive species [194]. So far, two major strategies have been described of lysis-induced release of eDNA: Autolysis mechanisms and prophage-induced cell lysis.

Autolysis mechanisms

Potential inducers of cell lysis are autolysins that degrade cell wall components. Autolysis systems have been described to promote DNA release in a number of species, including *Staphylococcus*

epidermidis and *E. faecalis* [187, 212, 220, 221]. Autolysins (murein hydrolases) destabilize the bacterial cell wall by degrading essential domains of the peptidoglycan layer and thereby causing cell lysis. Thomas and coworkers established the concept of two modes of autolysis: Suicide and fratricide [222].

Suicidal autolysis resembles a form of altruism and represents a form of self-controlled lysis of single cells within a population. Although altruistic suicide is being used as a generic term, the molecular mechanisms that control it can be quite diverse. For example, in *S. epidermidis* biofilms extracellular DNA is released through AtlE-mediated lysis of a subpopulation of the bacteria [212]. AtlE is an autolysin protein and its expression is controlled by the *agr* quorum sensing system and the SaeRS two-component system [212, 223, 224]. Other strategies to mediate altruistic suicide in bacteria are programmed cell death mechanisms that resemble to some extent those of eukaryotic apoptosis [225, 226]. An example of such a mechanism is the Cid/Lrg system that is conserved in many Gram-negative and Gram-positive species [227]. In *S. aureus*, loss of *cidA* significantly represses cell lysis and eDNA release, resulting in impaired biofilm formation [183]. *cidA* belongs to the *cidABC* operon and shares structural homologies to bacteriophage encoded holins that control timing and induction of bacterial cell lysis whereas Lrg acts as an antiholin to antagonistically control cell lysis [226, 228]. Similar to *S. aureus*, the *cidAB* and *lrgAB* genes of *P. aeruginosa* were shown to have severe effects on biofilm formation by antagonistically controlling cell death and lysis [155].

Recently, toxin-antitoxin systems have been discussed as another mode of programmed cell death in bacteria that might be involved in the release of eDNA under biofilm conditions [205, 229]. Toxin-antitoxin systems are widespread in bacteria with often more than one copy per organism and normally consist of two or more closely associated genes that together encode a ‘poison’ and a corresponding ‘antidote’. Toxin-antitoxin systems have been discussed to be involved in a range of cell physiological processes, including biofilm formation [230]. However, to date there is only one report that implies a toxin-antitoxin system (*hipBA*) in the release of eDNA by toxin-induced cell lysis [205]. Thus, the role of toxin-antitoxin systems remains controversial and further research is required to better understand their impact on biofilm formation and eDNA release.

Fratricide killing is a process similar to eukaryotic necrosis and describes a mechanism by which the induction of autolysis in one cell is controlled by another cell within the population. One fraction of the cells differentiates into attackers and releases factors that induce autolysis in the target cells at which the attackers are simultaneously protected from self-destruction [231]. Fratricidal killing was discovered by Thomas and coworkers in *E. faecalis* and is mediated by GelE, which activates the primary autolysin AtlA in the target cells, whereas the AtlA-modifying protein SprE confers immunity of the attacking cells. Similar mechanisms of fratricidal killing have been identified in other bacteria as well, including *B. subtilis* and *S. pneumoniae* [213, 215].

Prophage-induced cell lysis

Prophages often reside stably in bacterial genomes and constitute substantial amounts of bacterial DNA. About 60 - 70 % of all sequenced genomes contain prophages that can be either functional or cryptic [232]. However, despite this substantial abundance little is known about their implication in host physiology and ecology. The presence of prophages can provide the host with fitness advantages such as increased growth rates, virulence and resistance against antibiotics and

environmental stress factors [233, 234]. In recent years, a number of studies on both Gram-positive and Gram-negative species have demonstrated the impact of prophages on biofilm development and cell lysis-mediated eDNA release [38, 120, 216-218, 235-237].

The most extensively studied system is probably the filamentous phage Pf4 in *P. aeruginosa* [182, 217]. Pf4 is continuously released from host cells, but does not produce plaques and has no effect on the growth of *P. aeruginosa*. However, under biofilm conditions a superinfective form of Pf4 is released that lyses a subpopulation of biofilm-associated cells. The formation of the superinfective form impacts microcolony maturation and stability, biofilm dispersal, and the formation of small colony variants that exhibit a strongly accelerated biofilm development [217, 238]. Petrova and coworkers identified the novel two-component regulator BfmR that controls Pf4-mediated lysis and eDNA release during biofilm development [237]. BfmR targets the promoter of the *phdA* gene, encoding a homolog of the prevent-host-death (Phd) family of proteins that confers resistance to the superinfective form of Pf4. Thus, BfmR seems to regulate biofilm development by fine-tuning bacteriophage-mediated lysis and eDNA release via PhdA [237]. Another example of prophage-induced lysis that enhances biofilm formation by the release of biofilm promoting factors, such as eDNA, as has been described in our lab for *S. oneidensis* MR-1 and will be introduced in more detail in section 1.2.1 as it represents a central topic in this thesis [38].

Notably, the impact of prophage induction/excision on biofilm formation and lysis may vary between species. For example, *E. coli* harbors two prophages, CP4-57 and DLP12, that were identified to be strongly regulated under biofilm conditions [239]. Activation of several (lytic) prophage genes was shown to be controlled by the global transcriptional regulator Hha [240]. Already 4 hours after initial attachment of the host cells, prophage CP4-57 is induced and excises from the *E. coli* genome whereas induction of phage DLP12 occurs both in planktonic and biofilm-associated cells and during all phases of biofilm development [236]. However, deletion of the prophages resulted in enhanced biofilm formation, reduced lysis, and induction of motility genes. Thus, the presence of prophages may have oppositional effects on cell lysis, eDNA release, and, finally, biofilm formation.

Phage induction has also been shown to be critical for biofilm formation of Gram-positive bacteria. Putative phage particles Φ 11, Φ 12 and Φ 13 were detected in *S. aureus* biofilms already 4 hours after initial attachment. Cell lysis was accompanied by a release of nutrients and potential matrix components into the environment, which may affect biofilm development and stability [216]. Similar results were obtained for *S. pneumonia* biofilms [218]. Carrolo and coworkers demonstrated that prophage carriage has a positive impact on pneumococcal biofilm formation through spontaneous induction of the lytic cycle and that the release of eDNA is crucial for the development of robust biofilms [218].

In conclusion, detection of prophage-induced lysis in a variety of species has indicated the relevance for bacterial biofilm formation. Although molecular mechanisms that regulate this process seem to be diverse, prophage-mediated cell lysis and eDNA release appears to be a common beneficial feature for biofilm stability and integrity.

1.1.4 The role of extracellular nucleases in biofilms

Many bacteria possess extracellular nucleases, which are either anchored to the cell wall or secreted into the extracellular space. Extracellular nucleases have been shown to play important roles in biofilm formation, both in Gram-negative and Gram-positive species [118, 184, 241-245]. Degradation of eDNA by extracellular nucleases seems to represent an antagonistic mechanism to the release of eDNA during biofilm development (section 1.1.3). However, the production of extracellular nucleases does not necessarily coincide with a decreased dependence on eDNA for biofilm formation of those species but rather seems to represent a mechanism to balance eDNA levels in the biofilm matrix [246]. Consequently, uncontrolled eDNA accumulation can result in altered biofilm formation.

Two major nuclease-linked biofilm phenotypes have been observed in a range of organisms: Development of thicker biofilms and increased matrix production (mainly eDNA) in nuclease-deficient mutants, and increased biofilm dispersal in response to endogenous overexpression or exogenous addition of the corresponding extracellular nucleases. For example, deletion of thermonuclease gene *nuc* in *S. aureus*, encoding a secreted thermostable nuclease, resulted in 2-fold thicker biofilms with a rougher surface that was covered with high amounts of eDNA, both in the lab strain and in methicillin-resistant strains (MRSA) [118, 243]. Recently it was shown that *S. aureus* harbors a second staphylococcal thermonuclease (Nuc2) that is attached to the cell surface and expressed during infection [245]. Purified Nuc2 prevented biofilm formation *in vitro* and decreased biofilm biomass in dispersal experiments. *N. gonorrhoeae* and *H. influenzae* also express each a thermostable nuclease that has homology to Nuc in *S. aureus* [184, 247]. Accordingly, biofilms formed by the nuclease deletion mutants contained elevated amounts of eDNA, were significantly thicker and of greater biomass, and showed decreased dispersal compared to the parental strains [184, 247]. Analogous results were obtained for the nucleases Dns and Xds in *V. cholerae* [242]. However, enhanced capacities to form biofilms in nuclease mutants under *in vitro* conditions do not necessarily coincide with phenotypes observed *in vivo*. Instead, unbalanced biofilm formation (due to a lack of extracellular nucleolytic activity) has rather been shown to decrease community fitness, virulence, and antibiotic tolerance under natural conditions [242, 244].

Another prominent role that has been attributed to extracellular nucleases is to exploit eDNA as a reservoir of carbon, phosphorus and nitrogen. Growth experiments with *Shewanella* species demonstrated that DNA can be used as a sole source of carbon, nitrogen, and phosphorus [173]. Pinchuk and coworkers suggest that extracellular nucleases and extracellular phosphatases may play a combined role in degradation of eDNA under phosphate-limiting conditions. Accordingly, Mulcahy and coworkers reported that an extracellular nuclease in *P. aeruginosa* is required for utilization of eDNA as nutrient source and that the nuclease gene is induced under phosphate-limiting conditions, or when DNA is supplied as a sole source of phosphate [174].

Further, extracellular nucleases seem to participate in the control of horizontal gene transfer. In *V. cholerae*, the extracellular nucleases Xds and Dns have been shown to reduce uptake of foreign DNA from the environment [248]. The more significant role has been attributed to Dns, which is produced at low cell densities, possibly to provide nutrients for rapid growth, and repressed in high-density populations by the quorum-sensing regulator HapR [249]. *Vibrio vulnificus* expresses a periplasmic nuclease (Vvn) that has also been shown to reduce natural transformation [250]. Notably, nucleases that exhibit significant sequence homologies to Dns and Vvn can be found in many bacteria, including *e.g.* periplasmic endonuclease EndA from *E. coli* [251]. In contrast to the

roles described for Dns and Vvn, nucleases can also contribute to natural transformation. In *S. pneumoniae*, membrane-bound EndA (not homologous to EndA in *E. coli*) nicks one strand of eDNA to provide a single-stranded substrate for the DNA uptake machinery [252].

In pathogenic bacteria, a biofilm-independent but vital function of extracellular nucleases is the escape from neutrophil extracellular traps (NETs). NETs are part of the human immune system and contain antimicrobial proteins, bound to a DNA scaffold. Upon infection, NETs degrade virulence factors and bind and kill microbes extracellularly [253]. Recently it has been shown that in addition to antimicrobial proteins in NETs, DNA itself exhibits antimicrobial activity [254]. Both Gram-negative and Gram-positive species have been shown to escape from NETs by the action of extracellular nucleases, including *P. aeruginosa*, *V. cholerae*, *S. pneumoniae*, and *S. aureus* [253, 255-258].

Another aspect of nuclease research with high medical relevance is the biofilm-mediated colonization of human hosts by pathogenic bacteria such as *P. aeruginosa*. The growing number of studies in this field of research has helped to gain more insights into mechanisms of eDNA turnover and biofilm dispersal. This is of particular importance, since extracellular nucleases may be used to reduce or block infectious biofilms, an approach termed 'biofilm control'. Biofilm control is based on the discovery that nucleolytic degradation of eDNA can prevent formation of or disperse biofilms, or sensitize these to antimicrobials [259]. In the era of multi-resistant germs, new strategies for biofilm control are required to replace or complement the use of antibiotics. One strategy to release biofilm biomass from a surface is exogenous addition of DNase to growing biofilms, as has been shown for the first time by Whitchurch and coworkers in 2002 [180]. A second potential strategy to induce biofilm dispersal is the endogenous induction of extracellular nuclease expression in growing biofilms, since many extracellular nucleases seem to be regulated at the level of transcription [194]. Different regulatory systems have been shown to be involved in transcriptional regulation of extracellular nucleases. Regulation may be achieved through sigma factors such as sigma factor B in *S. aureus*, two-component systems such as VirR/VirS in *Chlostridium perfringens*, or other condition-specific regulators such as the nutrient stress-responsive regulator CodY and peroxide regulator PerR in *Streptococcus pyogenes*, or the quorum-sensing and competence regulator HapR in *V. cholera* [243, 249, 260-262].

Although progress has been made regarding regulatory mechanisms controlling nuclease expression, it is important to point out that more factors might be involved in the regulation of extracellular nuclease activity, including post-transcriptional regulation, post-translational modification, transport, and biochemical conditions altering catalytic kinetics of extracellular nucleases. However, very little is known to date in this field of research. Furthermore, many species produce more than one extracellular nuclease and these nucleases often exhibit diverse characteristics that may be critical under different conditions or to exhibit distinct roles. For example, Nuc of *S. aureus* is a secreted nuclease whereas Nuc2 is anchored to the cell wall [245]. Thus, it would be interesting to understand the individual functions of each nuclease.

Taken together, extracellular nucleases seem to play a central role for the modification and/or degradation of eDNA in microbial biofilms and exhibit diverse functions with medical relevance, such as natural transformation, degradation of DNA in NETs, and induction of biofilm dispersal for biofilm control. However, the underlying molecular and regulatory mechanisms are still poorly understood and remain to be elucidated in more detail.

1.2 *Shewanella oneidensis* MR-1

S. oneidensis MR-1 is a facultative anaerobic, rod-shaped, and motile gammaproteobacterium with a polar flagellum. Natural habitats of *S. oneidensis* comprise the deep-sea bottom, freshwater habitats as well as soil and sediments. *S. oneidensis* MR-1 (formerly *Alteromonas putrefaciens* MR-1) was isolated from Lake Oneida (NY, USA) and received attention for its capacity to utilize insoluble manganese oxide as terminal electron acceptor for anaerobic respiration [263]. After several taxonomic rearrangements within the last century, 5S RNA analyses finally helped to define *Shewanella* as a new genus within the order of *Alteromonadales*, and *Alteromonas putrefaciens* MR-1 was initially designated as *Shewanella putrefaciens* MR-1 and finally corrected to *S. oneidensis* MR-1 [264]. Currently, the genus *Shewanella* counts more than 40 species and more than half of these have been fully sequenced [265]. The genome of *S. oneidensis* MR-1 was sequenced in 2002 and consists of a 4.9 mbp circular chromosome and a 161 kbp plasmid. The genome of *S. oneidensis* MR-1 is characterized by a high number of transposase genes and IS elements, and harbors three prophage genomes, encoding a functional Lambda-like phage (λ So), a cryptic Mu-like phage (MuSo1), and a functional Mu-like phage (MuSo2) [38, 266].

Shewanellae compose a physiological and ecological diverse group of bacteria that are often psychrotolerant and known for their capacity to use a vast array of organic and inorganic terminal electron acceptors, including chlorinated compounds, radionuclides, and other environmental pollutants [267]. The possibility to mobilize and immobilize insoluble and soluble pollutants, respectively, has a high potential for bioremediation purposes and is believed to play an important role in biogeochemical cycling processes. *S. oneidensis* MR-1 is able to reduce soluble and insoluble forms of iron and manganese, organic compounds such as fumarate and dimethyl sulfoxide (DMSO), inorganic compounds such as nitrate, nitrite, thiosulfate and sulfite and a variety of toxic metal ions such as uranium and arsenic [268].

The molecular mechanisms of dissimilatory metabolism that are required to respire solid metal oxide substrates have been intensely studied in the last decade, and *S. oneidensis* MR-1 has emerged as an important model organism in this field. *S. oneidensis* MR-1 encodes 42 putative cytochrome *c* molecules, containing each one or multiple heme groups [269]. The high number of cytochromes is required to exhibit such a versatile respiratory metabolism and has probably evolved as an adaptation to redox-stratified environments. Dissimilatory reduction of solid metal oxides has been shown to require a set of cytochromes that span the cell wall to allow exchange of electrons between the intra- and extracellular space. For the reduction of iron and manganese, *S. oneidensis* MR-1 utilizes inner membrane cytochrome CymA, periplasmic cytochrome MtrA, and outer membrane cytochromes MtrC and OmcA. MtrC and OmcA are lipoproteins associated to the outer membrane and outer membrane protein MtrB [265]. The functions of most other cytochromes have yet to be elucidated. For the transport of electrons to solid electron acceptors other than direct contact, *S. oneidensis* MR-1 utilizes at least two sophisticated strategies: Electron shuttling and nanowires. Under anaerobic conditions, *S. oneidensis* MR-1 secretes riboflavins that act as electron shuttles, accepting electrons from outer membrane cytochromes and carrying them to external acceptors such as iron and manganese oxides [270]. In 2006, Gorby and coworkers observed for the first time electrically conductive cellular appendages that are involved in dissimilatory metal reduction [271]. These nanowires were initially thought to consist of pilus-like structures but were recently shown to comprise cellular extensions of the outer membrane and the periplasm, packed with components of the extracellular electron transport machinery, including

OmcA, MtrA/B/C, and CymA [272]. A potential application of dissimilatory metal-reducing bacteria such as *S. oneidensis* MR-1 is the generation of electric energy in microbial fuel cells [273].

The carbon metabolism of *S. oneidensis* MR-1 is non-fermentative and characterized by the consumption of organic breakdown products such as small organic acids (acetate, pyruvate, lactate), fatty acids, amino acids, peptides, and nucleosides [265, 274]. Complete glycolysis is not possible in *S. oneidensis* MR-1, as it lacks 6-phosphofructokinase, and the only sugar to be efficiently catabolized is *N*-acetylglucosamine [275]. Furthermore, *S. oneidensis* MR-1 and other members of this genus utilize DNA as sole source of carbon, nitrogen, and phosphorus [173].

S. oneidensis exists in diverse and often redox-stratified habitats that are exposed to seasonal changes in temperature, nutrient availability, and oxygen levels. Such diverse and changing growth conditions require a high degree of metabolic plasticity and complex sensory and regulatory systems that allow rapid and efficient adaption. Accordingly, sequence analysis of the *S. oneidensis* MR-1 genome indicates the presence of 47 one-component and at least 211 two-component regulatory systems that are probably involved in sensing a diverse set of environmental stimuli and mediation of adequate transcriptional responses [266]. A similar degree of complexity holds true for post-transcriptional regulatory systems by secondary messengers such as c-di-GMP. Bioinformatic analysis by Fredrickson and coworkers predicted 51 diguanylate cyclases, 27 phosphodiesterases, and 20 hybrid diguanylate cyclase or phosphodiesterase proteins, which represents one of the highest numbers of c-di-GMP signaling proteins that have been described so far [265]. Moreover, *S. oneidensis* MR-1 is predicted to have a more complex chemotaxis system than most other bacteria, consisting of 3 sets of chemotaxis genes and 27 chemoreceptors [265].

Taken together, *S. oneidensis* MR-1 exhibits a striking metabolic and regulatory adaptability and flexibility. In addition to metabolic and regulatory adaptations, living in complex communities provides important advantages that enable bacteria to thrive in diverse habitats and to cope with variable environmental conditions. Accordingly, *S. oneidensis* MR-1 is able to form structured biofilms on diverse surfaces and seems to exhibit a complex biofilm developmental program. Especially the capacity to grow on solid metal oxides and to utilize these surfaces as terminal electron acceptor has made *S. oneidensis* MR-1 a unique model organism for biofilm formation in recent years. Biofilm formation of *S. oneidensis* MR-1 will be introduced in the next section.

1.2.1 Biofilm formation of *S. oneidensis* MR-1

In recent years, *S. oneidensis* MR-1 has attracted notice in the field of biofilm formation, reflected by an increasing number of studies that helped to gain more insights into the complex community behaviors of this organism [24, 38, 90, 99, 241, 276-289].

Biofilm development of *S. oneidensis* MR-1 has been characterized predominantly on the basis of flow cell assays that mimic hydrodynamic conditions. Under these conditions, *S. oneidensis* MR-1 proceeds through a defined series of developmental phases including initial attachment, microcolony formation, formation of complex three-dimensional architectures (including macrocolonies), and detachment of cells (or cell clusters) from mature biofilms [24, 90, 99, 279, 280]. Biofilm formation starts with the initial attachment of planktonic cells, a process that requires a functional mannose-sensitive hemagglutinin type IV pilus and pilus retraction system [24, 282]. Notably, flagella-mediated swimming motility is not required for efficient adhesion but important

for the formation of structured biofilms with large cell clusters [24]. Microarray analyses of biofilm cells demonstrated great transcriptomic variations within the first hour after initial attachment and a high demand for iron during this phase [286]. After complete surface coverage, *S. oneidensis* MR-1 proceeds with extensive vertical growth to form microcolonies within the first day, and more complex cell clusters and macrocolonies within 2 days, depending on nutrient conditions and temperature. Deletion mutant analyses and transposon mutant screens have helped to identify a number of cellular components and environmental factors that are critical for complete biofilm development of *S. oneidensis* MR-1. Two associated proteins have been shown to be of particular importance: AggA and BpfA. The TolC-like agglutination protein AggA is a part of the type I secretion system in *S. oneidensis* MR-1 and was shown to form active channels [278, 290]. BpfA (Biofilm-promoting factor) is a large cell surface protein belonging to the Bap family and RTX-toxin family of proteins. BpfA is secreted to the surface by a type I secretion system and likely dependent on AggA [283]. Deletion of either gene resulted in strongly impaired surface adhesion and defective biofilm formation [278, 283]. During later phases of biofilm formation, a drop in oxygen tension has been reported to induce rapid detachment of cells and cell clusters from the biofilm. The global transcriptional regulators, ArcA and CRP, were shown to be involved in the regulation of cellular detachment [99]. Moreover, c-di-GMP levels control the stability of *S. oneidensis* MR-1 biofilms by shifting the state of a biofilm cell between attachment and detachment in a concentration-dependent manner [90]. The c-di-GMP-forming diguanylate cyclase MxdA and the c-di-GMP-degrading phosphodiesterase PdeB have been shown to play central roles in the control of cellular c-di-GMP levels and biofilm formation, presumably as counteracting partners [90, 288].

Gödeke and coworkers demonstrated that eDNA serves as an essential structural component in all stages of biofilm formation under static and hydrodynamic conditions [38]. Differential gene expression patterns of λ So, MuSo1 and MuSo2 were identified during initial phases of biofilm formation [291]. Analyses of deletion mutants revealed that all three prophages individually contribute to cell lysis. However, only λ So and MuSo2 form infectious phage particles. Deletion of the prophages resulted in significantly less cell lysis and reduced eDNA levels in biofilms. Furthermore, prophage mutants were strongly impaired in biofilm formation through all stages of development. Among the prophages, λ So exhibited the most prominent role in eDNA release and biofilm formation. Gödeke and coworkers suggest that, in *S. oneidensis* MR-1, prophage-mediated lysis results in the release of crucial biofilm-promoting factors, in particular eDNA [38]. Release mechanisms of eDNA other than prophage-induced lysis have not been described so far.

The fact that eDNA constitutes an important structural component of *S. oneidensis* MR-1 biofilms raised the question of eDNA-degrading factors that might be released to control *e.g.* eDNA turnover, horizontal gene transfer, or biofilm dispersal (see section 1.1.4). To date, three extracellular nucleases, ExeM (SO_1066; **extracellular endonuclease, membrane-associated**), ExeS (SO_1844; **extracellular endonuclease, secreted**) and EndA (SO_0833; **endonuclease A**), have been identified in *S. oneidensis* MR-1 [173, 241, 292]. Phenotypic analyses of corresponding deletion mutants indicated nucleolytic activity of all three nucleases in supernatants of planktonic cultures. However, ExeM seems to contribute only marginally to the growth on DNA as sole source of phosphorus, and deletion of *exeS* had no effect [241]. In contrast, deletion of *endA* results in complete stagnation of growth on DNA as sole phosphorus source, suppression of extracellular nucleolytic activity in culture supernatants, and formation of cell clumps in stationary phase [292].

Phenotypic analyses of *exeM* deletion mutants revealed an important role in biofilm formation. Under hydrodynamic conditions, deletion of *exeM* leads to altered biofilms that consist of densely packed structures, which are covered by a thick layer of eDNA. Deletion of *exeS* had no effect under hydrodynamic conditions but resulted in elevated biofilm formation under static conditions, whereas deletion of *exeM* had the opposite effect [241]. Transcriptional analyses indicated induction of *exeM* and *exeS* gene expression under biofilm conditions and in response to phosphate limitation, but no altered expression of *endA* [241, 292]. Interestingly, *endA* is cotranscribed with *phoA* (SO_0830), encoding a putative periplasmic alkaline phosphatase [292]. However, the role of PhoA for the capacity of *S. oneidensis* MR-1 to grow on DNA as sole source of phosphorus has not yet been determined.

Nucleolytic activity of ExeM, ExeS, and EndA has been detected in culture supernatants, suggesting that these nucleases are likely secreted. However, degradation of eDNA may also be conducted by nucleases that are attached to the cell envelope or that have been released by cell lysis. Experimental elucidation is therefore required to determine transport pathways and actual destinations of extracellular nucleases, including periplasm, inner or outer membrane, or the extracellular space. ExeS was initially predicted to be a β -barrel protein located in the outer membrane. However, Pinchuk and coworkers identified ExeS in cell-free culture supernatants by mass spectrometry, indicating that ExeS is secreted to the extracellular space [173]. ExeM contains a putative N-terminal transmembrane domain and has been predicted to remain associated with the cell envelope. Tang and coworkers performed a biotinylation method in conjunction with affinity enrichment to profile the membrane proteome of *S. oneidensis* MR-1, and detected ExeM in the outer membrane fraction [293]. In contrast, Brown and coworkers detected ExeM in the inner membrane fraction by sarkosyl-based fractionation and LC-MS/MS analyses [294]. EndA in *E. coli* is a periplasmic endonuclease and shows high sequence homologies to EndA in *S. oneidensis* MR-1 [295]. Nevertheless, experimental proof for the localization of EndA in *S. oneidensis* MR-1 is still missing.

Taken together, the exact localizations of ExeM, ExeS, and EndA are controversial and molecular mechanisms that regulate and execute secretion across the cell membranes or incorporation into the cell envelope remain to be elucidated. Furthermore, none of these proteins has been characterized *in vitro*. However, biochemical characteristics such as cofactor dependencies may give important insights into physiological aspects of extracellular nuclease activity.

1.3 Scope

Release of eDNA

The impact of prophages on biofilm development and cell lysis-mediated eDNA release was demonstrated in a number of species, including *S. oneidensis* MR-1 [38, 120, 216-218, 235-237]. However, environmental signals and molecular mechanisms that control prophage induction/excision under biofilm conditions remain mostly elusive. Likewise, spatiotemporal patterns of prophage induction and cell lysis during biofilm development are unknown for most species. I propose that elucidating the molecular and physiological principles of prophage-induced lysis in biofilms may help to better understand host-prophage interactions in general and, in particular, under ecologically relevant conditions. Moreover, studying the balance between single cell lysis and community fitness may help to gain more insights into complex community behaviors in bacterial biofilms that may similarly exist in other systems as well.

Accordingly, this study aims to identify molecular mechanisms and biofilm-specific signals that underlie λ So prophage induction and cell lysis in *S. oneidensis* MR-1 biofilms. Prophage λ So has been shown to exhibit the most dominant phenotype in *S. oneidensis* MR-1 biofilms and has therefore been selected as a model system for this study [38]. To monitor the spatiotemporal induction of prophage λ So under hydrodynamic biofilm conditions at the single-cell level, a reporter strain was constructed that harbors a transcriptional fusion of the putative regulator of early λ So gene transcription (Cro) and the yellow-fluorescent protein Venus. Using that strain, λ So prophage induction was characterized in various genetic backgrounds and under different physiological conditions.

Degradation of eDNA

Extracellular nucleases have been shown to impact biofilm formation/dispersal by degrading the structural matrix component eDNA. In addition, diverse other functions have been described, including acquisition of DNA as nutrient reservoir, control of horizontal gene transfer, and escape from neutrophil extracellular traps. Notably, a single bacterial species may produce more than one nuclease and each nuclease may differ in structure, localization, and function. Although a role in biofilm formation and particularly in biofilm dispersal has been demonstrated for a number of nucleases, important aspects, such as transport mechanisms across the cell envelope and biochemical characteristics that determine specific nuclease functions, remain to be elucidated.

The extracellular nuclease EndA in *S. oneidensis* MR-1 was shown to be required for growth on DNA as sole source of phosphorus while ExeM appeared to have only a minor role. In contrast, deletion of *exeM* resulted in altered biofilm formation and strongly elevated eDNA accumulation while the *endA* mutant phenotype was indistinguishable from the wild type. To investigate the functional specificity of these two nucleases, *in vitro* degradation assays were performed to determine specific nucleolytic characteristics. Furthermore, biofilm dispersal was assayed by endogenous nuclease induction and exogenous addition of the purified proteins. Finally, DNA degradation assays and immuno detection of the nuclease proteins in different cell fractions was performed to investigate transport and localization of the nucleases.

RESULTS

1.4 Analyses of λ So prophage induction in biofilms

This chapter focuses on the characterization of λ So prophage induction and eDNA release in *S. oneidensis* MR-1 biofilms. Phenotypic analyses of deletion mutants that lack the λ So prophage lysis operon indicated that cell lysis is the major biofilm-promoting factor provided by prophage λ So (section 1.4.1). A functional transcriptional fluorescence fusion to *venus* (*P_{cro::venus}*) was generated to investigate λ So prophage induction and cell lysis under hydrodynamic biofilm conditions in flow cells. As demonstrated in section 1.4.2, induction and cell lysis occurred mainly in a subpopulation of filamentous cells at the transition phase prior extensive three-dimensional growth. Deletion of *recA* suppressed λ So induction and was accompanied by a reduction of eDNA levels in biofilms. These results suggested that λ So prophage induction and lysis are controlled by RecA, likely by an increase in DNA damage that is sensed by RecA (section 1.4.3). Elevated levels of λ So prophage induction in an *oxyR* deletion mutant indicated a role of oxidative stress in this process (section 1.4.4). To elucidate whether elevated levels of hydrogen peroxide promote oxidative stress and DNA damage by Fenton chemistry under biofilm conditions, a mutant screen was performed to isolate mutants that suppress induction of prophage λ So by hydrogen peroxide. However, fluorescence studies and immunodetection of λ So in biofilms demonstrated that λ So induction couldn't be blocked or reduced by suppression of hydrogen peroxide-mediated oxidative stress (section 1.4.5). Instead, the degree of λ So induction as well as eDNA accumulation in biofilms correlated with environmental ferrous iron levels, both in the wild type and in H₂O₂-resistant mutants (section 1.4.5). Accordingly, deletion of ferric uptake regulator *fur* resulted in drastically increased λ So prophage induction levels in biofilms (section 1.4.4). Taken together, the results presented in this chapter strongly indicate that iron triggers λ So prophage induction and eDNA release in *S. oneidensis* MR-1 biofilms, likely by an increase in iron-mediated DNA damage that is sensed by RecA. The presented data further indicates that this process occurs largely independent of hydrogen peroxide.

Part of the work presented in this chapter was conducted together with Laura Teichmann as part of her Bachelor thesis that was supervised by me [296].

1.4.1 λ So prophage-mediated lysis is required for normal biofilm formation

Earlier it has been demonstrated in our lab that a *S. oneidensis* MR-1 mutant devoid of prophage λ So ($\Delta\lambda$ So) was unable to cover the surface during later phases of biofilm development (24 hours after the initial attachment) and to form distinct three-dimensional structures. Mainly based on studies on $\Delta\lambda$ So mutants, Gödeke and coworkers suggested a correlation between a reduced degree of cell lysis, reduced eDNA levels, and impaired biofilm formation [38]. Cell lysis has been shown to be a common mechanism of many biofilm-forming species to release matrix components such as eDNA (see section 1.1.3.3). However, based on the data presented by Gödeke and coworkers, the deficit of $\Delta\lambda$ So mutants with respect to biofilm formation may not be restricted exclusively to a

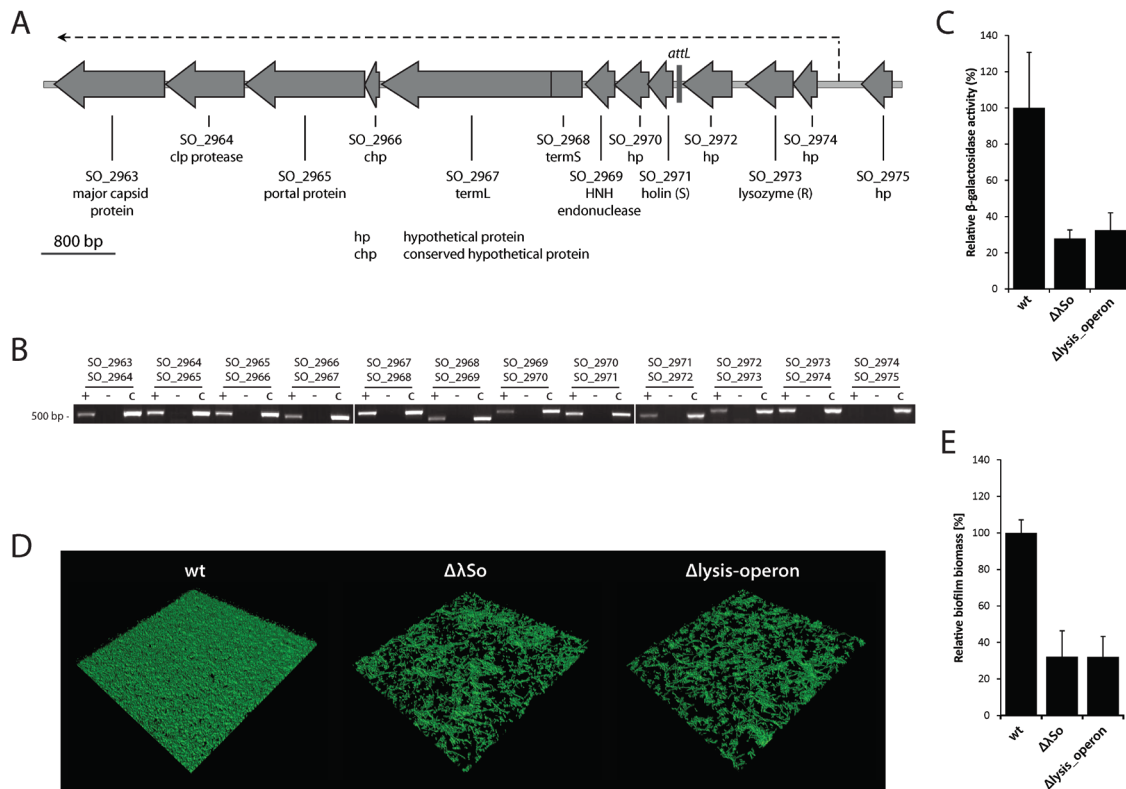


Figure 5. λ So prophage-mediated lysis is required for normal biofilm formation. (A) Genetic and transcriptomic organization of cluster SO_2963 to SO_2975. Predicted genes are indicated as grey arrows. Gene transcription starts at gene SO_2974 and continues at least until gene SO_2963, as indicated by RT-PCR analysis. Bioinformatic predictions are based on NCBI BLASTP (National Library of Medicine) and PFAST [297] analyses. (B) RT-PCR products separated on a 2% agarose gel for operon mapping on genes SO_2963 to SO_2975. cDNA samples (+) were amplified using appropriate primer pairs bracketing the gaps between the genes of interest. Total-RNA (-) served as negative control, and chromosomal DNA (C) served as positive control. (C) Relative extracellular β -galactosidase activity in culture supernatants after mitomycin C treatment of strain S2933 (Δ lysis-operon) and S1387 ($\Delta\lambda$ So) in comparison to the wild type. All strains harbored plasmid pME6031-*P_{motB}-lacZ* for constitutive cytoplasmic expression of β -galactosidase. Black bars represent mean values of biological and technical triplicates with standard deviations. (D) CLSM projections of 24 hours-old biofilms formed by the wild type, the lysis operon deletion mutant (Δ lysis-operon) and the λ So prophage deletion mutant ($\Delta\lambda$ So) under hydrodynamic conditions in flow cells. All strains were tagged with GFP. The lateral edge of each micrograph is 250 μ m. (E) Relative biomass as a measure of total GFP fluorescence compared to the wild type of 24 hours-old biofilms formed by strain $\Delta\lambda$ So and Δ lysis-operon under hydrodynamic conditions in flow cells. Bars represent the mean values (in %) with standard deviations displayed as error bars.

reduction in cell lysis. Instead, other unknown factors encoded by prophage λ So may also impact biofilm formation of *S. oneidensis* MR-1. To determine whether λ So-mediated cell lysis is the predominant biofilm-promoting factor of λ So in biofilm formation of *S. oneidensis* MR-1, the prophage's putative lysis operon was identified and characterized by bioinformatic analyses, RT-PCR, and phenotypic mutant analyses.

Genes SO_2971 and SO_2973 were predicted by NCBI BLAST sequence alignments and PFAST analyses to encode a putative holin and lysozyme protein, respectively (Figure 5A) [297]. The bacteriophage λ holin (commonly designated gene product 'S') and endolysine (gene product 'R') have been shown to act as the key players of λ phage-induced cell lysis in many species. Holines constitute a diverse group of intramembrane proteins that control timing of lysis by perforating the inner membrane. Endolysine proteins are hydrolases that degrade the peptidoglycan layer after

crossing the inner membrane through channels that have been formed by holins [228, 298, 299]. Other components such Rz and Rz1 (part of the spanin complex) that have been shown to be part of the λ lysis cassette in other organisms [300, 301], were not identified in prophage λ So. This might be the result of low sequence homologies and/or a high diversity of these components in different species. In addition, a putative endonuclease belonging to the HNH family (SO_2969) and a bacteriophage terminase (SO_2967) were identified within the same gene region. Further downstream in this locus, starting with gene SO_2965 (encoding a putative λ portal protein), a series of genes are found that encode putative structural components of head and tail structural units (Figure 6). In the excised and circularized form of the λ prophage genome of *E. coli*, the head and tail gene cassettes reside directly downstream of the lysis gene cassette. Furthermore, lysis genes and the head and tail genes are being cotranscribed as one operon under the control of promoter P_R . In *E. coli*, promoter P_R locates directly upstream of gene S that encodes the holin protein [302].

To gain more insights into the transcriptional organization of the putative lysis genes SO_2971 and SO_2973 in *S. oneidensis* MR-1, and in particular to determine which genes are being cotranscribed between gene SO_2963 and gene SO_2975, operon mapping by RT-PCR was performed (Figure 5B). PCR amplification products were obtained for all genes except SO_2974 and SO_2975, strongly indicating that genes SO_2963 to SO_2974 reside on a single transcript. Genes that reside downstream of SO_2963 (encoding the major capsid protein) were not included in this assay. However, analyses of the genetic organization of downstream genes by the VIMSS operon prediction tool suggested that all genes until gene SO_2942 (encoding a hypothetical protein) reside on the same operon [303]. Since RT-PCR failed to detect a cDNA amplification product for the primer pair bracketing genes SO_2974 and SO_2975, it is likely that putative promoter P_R locates upstream of gene SO_2974. Accordingly, a large noncoding region (476 bps) exists between SO_2974 and SO_2975 that might contain operator sequences required for regulation of transcription initiation. In conclusion, the putative lysis cassette of prophage λ So seems to be cotranscribed in a single operon with the head and tail gene cassettes, analogously to *E. coli* phage λ . For further analyses, genes SO_2966 to SO_2974 were designated as the putative 'lysis operon' (genes encoding structural head and tail components start with gene SO_2965), although a reliable bioinformatic prediction of all genes within this region was not possible.

To generate a mutant that is completely incapable of λ So-induced cell lysis, the putative 'lysis operon' was deleted (Δ SO_2966-SO_2974 or Δ lysis-operon). To determine the role of cell lysis during biofilm formation *S. oneidensis* MR-1, the mutant was subjected to phenotypic analyses in comparison to the $\Delta\lambda$ So prophage mutant and the wild type.

As control, the capacity of the Δ lysis-operon mutant to induce λ So-mediated cell lysis was elucidated. To this end, strain Δ lysis-operon, strain $\Delta\lambda$ So, and the wild type were equipped with plasmid pME6031-*P_{motB}-lacZ* for constitutive cytoplasmic expression of β -galactosidase. To induce the prophage's lytic cycle, the cultures were treated with mitomycin C. Cell lysis was assayed as a measure of relative β -galactosidase activity in culture supernatants as described previously [38]. Compared to the wild type, the extracellular β -galactosidase activity in strain $\Delta\lambda$ So and strain Δ lysis-operon was reduced to a similar degree of 27 % and 32 %, respectively (Figure 5C). In conclusion, λ So-induced lysis was completely suppressed by deletion of genes SO_2966 to SO_2974. To further characterize the Δ lysis-operon mutant in comparison to the $\Delta\lambda$ So prophage mutant and the wild type, biofilm formation was assayed under hydrodynamic condition in flow cells. Compared to the wild type, both mutants showed impaired biofilm phenotypes with respect to surface coverage

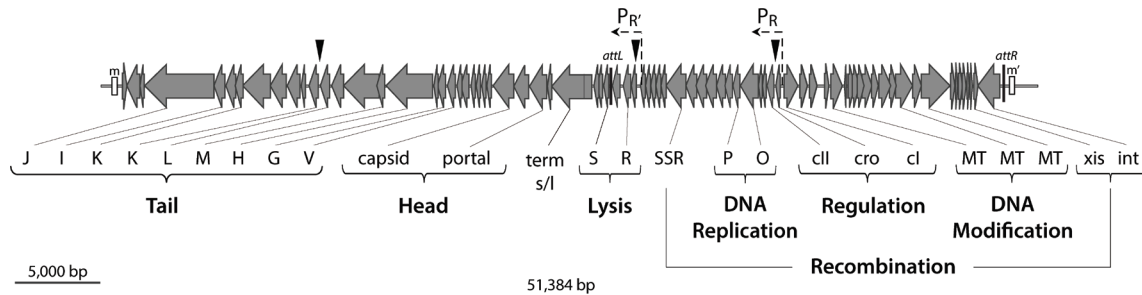
Prophage λ So (*S. oneidensis* MR-1)

Figure 6. Genetic organization of prophage λ So and site-specific transcriptional fusion constructs. Predicted genes are indicated as grey arrows. Gene nomenclature is based on homologies to *E. coli* phage Lambda [302]. Abbreviations for predicted putative genetic elements: m/m', cohesive ends (cos sites); attL/R, attachment sites; terms/term, small and large subunit of phage terminase; SSR, site-specific recombination protein; MT, methyltransferase; P_R, promoter for early transcription; P_R', promoter for late transcription. Black arrows indicate the integration site for venus constructs used for transcriptional fusion to genes cro, promoter P_R', and gene L.

and total biofilm biomass during later phases of biofilm formation (Figure 5D). Twenty-four hours after the initial attachment, Δ lysis-operon and $\Delta\lambda$ So mutant biofilms had formed 32 % and 31 % of biofilm biomass, respectively (Figure 5E). These data indicate that suppression of λ So-induced cell lysis and deletion of prophage λ So result in inhibited biofilm formation to a similar degree. It was concluded that cell lysis is the major biofilm-promoting factor of the λ So prophage.

1.4.2 Biofilm conditions trigger λ So prophage induction

Transcriptome analyses and Western immunoblot analysis performed by J. Gödeke strongly indicated induction and production of phage λ So under biofilm conditions [291]. However, it has still remained obscure which subpopulation of cells is actually subjected to λ So-mediated cell lysis within the biofilm community.

To identify and to characterize such cells *in vivo*, an approach was developed that aimed at monitoring the spatiotemporal induction of prophage λ So during biofilm formation. To this end, strains were generated carrying transcriptional fusions of prophage genes to *venus*. Production and fluorescence of Venus was utilized as an *in vivo* marker of λ So induction at the single-cell level. To this end, the coding sequence for *venus* was inserted into the prophage λ So genome downstream of SO_2989 (encoding the putative transcriptional regulator Cro) by homologous recombination, resulting in strain P λ cro::venus (Figure 6). The *cro* gene has been shown to be one of the first genes of phage λ that is induced after transition from lysogeny to the lytic cycle. *Cro* encodes a repressor protein that binds to the operator region *O_{R3}* to inhibit transcription of the λ repressor *cI*, which maintains the lytic cycle [304, 305]. Further, it has been suggested that *Cro* mediates weak repression of early lytic promoters, a process that might be required to establish expression of the complete prophage [306]. Thus, the predicted regulatory patterns of *cro* expression (remaining silent during lysogeny and being one of the first genes to be induced after transition to the lytic cycle) suggested it to be a suitable transcriptional marker for λ prophage induction. However, if these regulatory patterns observed for *E. coli* also apply in *S. oneidensis* MR-1 had still to be verified. For

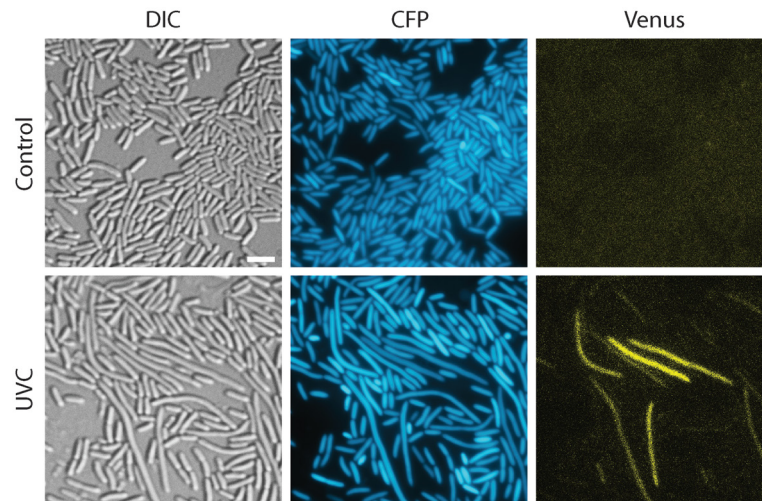


Figure 7. Induction of Venus fluorescence in strain $P\lambda_{cro}::venus$ after UVC exposure. Strain $P\lambda_{cro}::venus$ was grown to mid exponential phase (OD_{600} 0.6), exposed UVC light (1200 J/m^2 at 254 nm), incubated at 30 °C with orbital shaking, and subjected to differential interference contrast microscopy (DIC) and CFP/Venus fluorescence microscopy. As control, strain $P\lambda_{cro}::venus$ was equally cultured without UVC exposure. The scale bar equals 5 μm .

CLSM analyses, the strain was additionally equipped with constitutively expressed *ecfp* at the Tn7 site. Constitutive expression of eCFP allows visualization of all cells during CLSM and subsequent induction-to-biomass (Venus-to-CFP) normalization.

Analogous strains harboring transcriptional fusions to the putative λ So lysis promoter (P_R , upstream of gene SO_2974) and putative tail protein L (downstream of SO_2949) were equally generated. Genes under control of promoter P_R belonging to the lysis and head/tail assembly cassettes are predicted to be induced at the end of the lytic cycle, shortly before cell lysis and release of phage particles [302]. Strain $P\lambda_R::venus$ and $P\lambda_L::venus$ were constructed to cover different transcriptional phases during the lytic cycle, and thus to obtain a broader picture of λ So induction during biofilm formation. More precisely, analyzing different transcriptional units of the prophage aimed to determine whether the complete genetic cascade of the lytic cycle is executed during biofilm formation, or whether induction is restricted to single operons (e.g. the lysis operon). Furthermore, selection of early and late genes of the lytic cycle aimed to distinguish between the different transcriptional phases during biofilm formation. However, induction patterns observed for strain $P\lambda_R::venus$ and $P\lambda_L::venus$ were spatiotemporally congruent with those obtained for strain $P\lambda_{cro}::venus$ (see below). The results indicated that the complete genetic program of λ So's lytic cycle is executed during biofilm formation, but a clear distinction between different transcriptional phases was not possible. For this reason, this study focuses exclusively on strain $P\lambda_{cro}::venus$, if not indicated otherwise.

To demonstrate that prophage induction correlates with Venus fluorescence in strain $P\lambda_{cro}::venus$, cultures were exposed to UVC light or mitomycin C and analyzed by fluorescence microscopy. Approximately 2 hours after exposure, a significant fraction of cells started to display filamentous growth and Venus fluorescence, whereas no filamentous growth or fluorescence was detected in the control cultures (Figure 7). CFP fluorescence was unaltered in cultures exposed to UVC light and the control cultures. Comparable fluorescence phenotypes were observed for cultures of strain $P\lambda_{cro}::venus$ treated with mitomycin C, exhibiting Venus fluorescence approximately 2 hours after

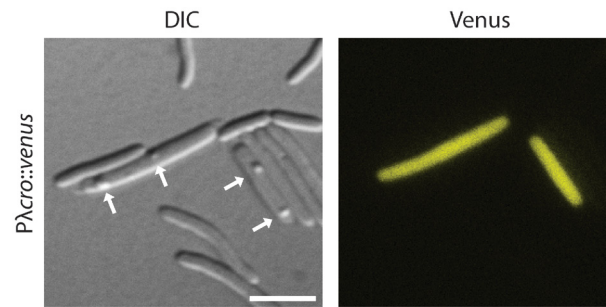


Figure 8. Appearance of blister-like protuberances on cell bodies of strain *Pλcro::venus* after UVC exposure. Strain *Pλcro::venus* was grown to mid exponential phase (OD_{600} 0.6), exposed UVC light (1200 J/m^2 at 254 nm), incubated at 30 °C with orbital shaking, and subjected to differential interference contrast microscopy (DIC) and Venus fluorescence microscopy. White arrows indicate excrescences. The scale bar equals 5 μm .

addition of the chemical. These results strongly indicated that induction of λSo by DNA-damaging agents correlates with Venus fluorescence in planktonic cultures of strain *Pλcro::venus*. Notably, a large fraction of cells showing both filamentous morphologies and Venus fluorescence simultaneously exhibited small blister-like protuberances on the cell envelopes. Potentially, these protuberances might be due to a destabilized cell wall during late phases of λSo 's lytic cycle.

To further determine whether phage induction is ultimately followed by cell lysis, a mitomycin C-treated culture of strain *Pλcro::venus* was immobilized on a propidium iodide-containing agar pad and analyzed by time lapse microscopy (Figure 9A). Propidium iodide is a cell impermeable DNA-stain commonly used to identify dead cells in live/dead imaging assays. Single cells were observed which exhibited a simultaneous loss of turgor pressure and Venus fluorescence in concert with sudden appearance of propidium iodide fluorescence, strongly indicating cell lysis. The time interval between induction and lysis was highly variable and induction did not necessarily result in complete lysis of the *Pλcro::venus* population. However, the number of filamentous cell bodies exhibiting propidium iodide fluorescence increased over time, indicating gradual cell lysis of a significant fraction of the population. Based on these results, strain *Pλcro::venus* was evaluated to be a useful tool to monitor spatiotemporal induction of the prophage's lytic cycle.

Biofilms of strain *Pλcro::venus* were cultivated under hydrodynamic conditions and visualized by CLSM over a time period of 48 hours (0.5, 4, 24, and 48 h). Induction of prophage λSo peaked at around 24 hours after initial attachment (Figure 9B). At this phase, wild type-like biofilms of *S. oneidensis* MR-1 cultured under standard conditions cover the entire glass surface with a thin layer of cells, and (micro)colonies have been formed with a diameter of approximately 10 – 30 μm . Under hydrodynamic conditions, this is the developmental transition phase prior to extensive three-dimensional growth. While only single cells produced Venus during the first hours at a degree comparable to spontaneous induction in planktonic cultures, a large subpopulation of mainly filamentous cells displayed increased fluorescence after 24 hours (Figure 9D). When *S. oneidensis* MR-1 biofilms were treated with cell-impermeable (e)DNA stain 7-hydroxy-9H-(1,3-dichloro-9,9-dimethylacridin-2-one (DDAO), similar string-like structures appeared, a phenotype that has been observed earlier [38]. However, fluorescence signals of both structures did not colocalize, strongly implicating that the DDAO-stained string-like structures represent dead cells after λSo -induced lysis. Staining with 4',6-Diamidino-2-phenylindole (DAPI) of filamentous cells

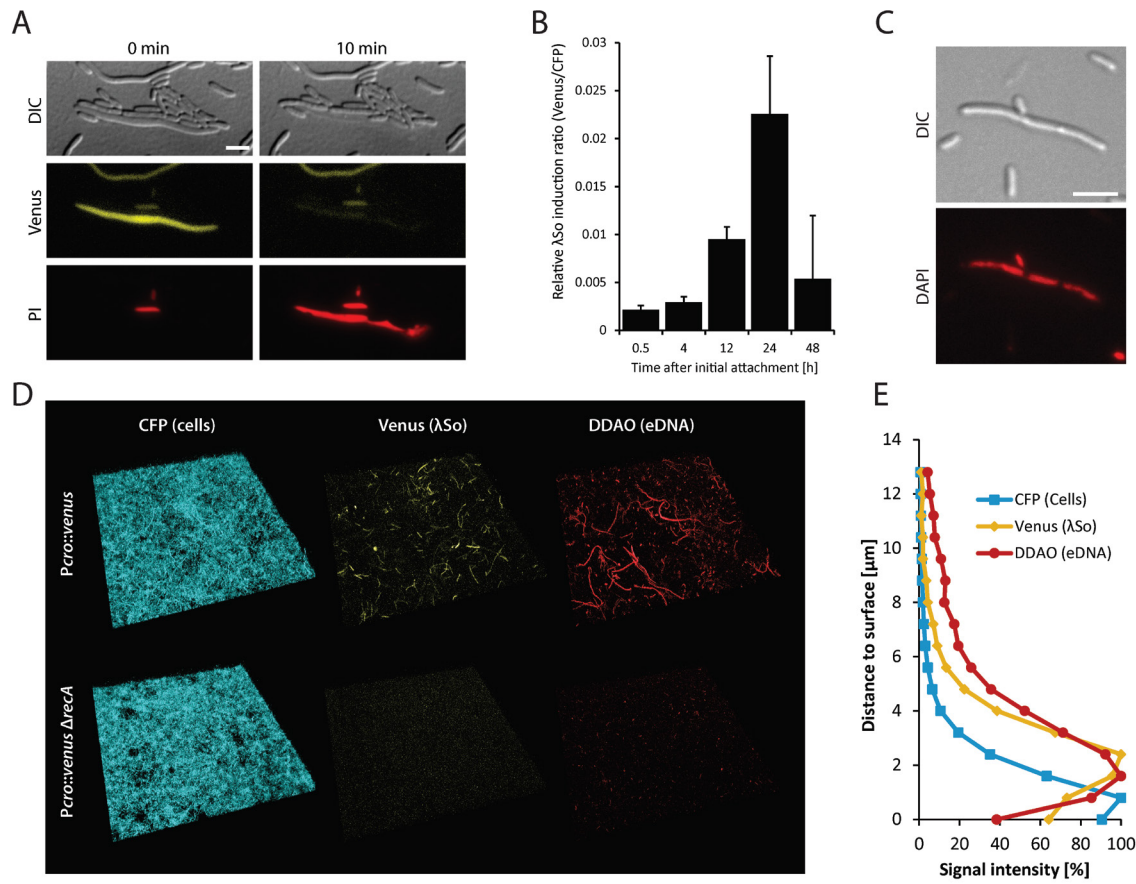


Figure 9. Determination of λ So prophage induction and eDNA release. (A) Visualization of λ So prophage-induced cell lysis by differential interference contrast microscopy (DIC), detection of Venus fluorescence and propidium iodine (PI) fluorescence in cells of strain $P_{\lambda cro::venus}$ after UV exposure. Scale bar equals 5 μ m. (B) Relative λ So induction over time in biofilms formed by strain $P_{\lambda cro::venus}$ under hydrodynamic conditions in flow cells. Total Venus signal intensities from CLSM images were normalized to total CFP signal intensities to obtain an induction-to-biomass ratio. Black bars represent the mean values with standard deviations displayed as error bars, obtained from two independent experiments conducted each in triplicates. (C) DAPI staining of nucleoids (red) in filamentous biofilm cells of *S. oneidensis* MR-1. Scale bar equals 5 μ m. (D) Projections of CLSM images displaying the induction of prophage λ So (Venus fluorescence) and eDNA (stained with DDAO) in biofilms formed by the CFP-tagged strains $P_{\lambda cro::venus}$ and $P_{\lambda cro::venus} \Delta recA$ under hydrodynamic conditions in flow cells 24 hours after the initial attachment. The lateral edge of each micrograph is 250 μ m. (E) Distribution of total CFP, Venus and DDAO signal intensities (as percentage of maximal intensity of each channel) over the z-axis (distance to surface) of CLSM images of biofilms formed by strain $P_{\lambda cro::venus}$ under hydrodynamic conditions in flow cells 24 hours after the initial attachment. Relative signal intensities are derived from the mean pixel values of triplicates in a representative experiment.

isolated from biofilms revealed the presence of multiple chromosomes, indicating that the cell length of filamentous cells positively correlates with the amount of DNA per cell body (Figure 9C). Analysis of the distribution of cells exhibiting Venus fluorescence along the z-axis in 24 hours-old biofilms revealed that signal intensities were strongest in a distance of approximately 1.5 - 2.5 μ m to the glass surface at the top of the yet thin cell layer, whereas the basal CFP signal displayed strongest fluorescence at a distance of 0 - 0.8 μ m, representing the bottom layers of the biofilm. DDAO signals showed a pattern similar to that of Venus, indicating that induction of prophage λ So and cell lysis predominantly occurs within the upper layers of the biofilm during this developmental stage. Along the x- and y-axis signals were evenly distributed, except in densely packed micro- or macrocolonies which mostly lacked *venus*-expressing filamentous cells or string-

like eDNA structures. A time-lapse analysis was performed for 1 hour (with 5-minutes intervals) to follow λ So-induced lysis, as described above for immobilized planktonic cells. Both *venus* expressing filamentous cells and DDAO-stained eDNA structures were highly dynamic within the biofilm and not restricted to distinct positions. Thus, detection of single cell-lysis events was not possible under these conditions.

1.4.3 RecA controls λ So prophage induction and eDNA release

Induction of the lytic cycle in λ -like phages is thought to occur via the RecA-mediated autocleavage of phage repressor cI in response to DNA-damaging agents. Phage λ So shows great similarities to *E. coli* phage λ regarding its genetic organization and protein homologies (Figure 5). Furthermore, DNA-damaging agents such as UV-light and mitomycin C can be used to induce the lytic cycle of λ So, as described in section 1.4.2. Thus, induction of λ So might similarly be RecA-dependent. To test this hypothesis, a $\Delta recA$ in-frame deletion was generated in strain $P\lambda cro::venus$ and the wild type, and characterized by phenotypic analyses. To this end, the response of planktonic cultures to DNA damaging agents was examined by fluorescence microscopy and immunoblot analysis. No Venus fluorescence of strain $P\lambda cro::venus \Delta recA$ was observed at any time point after exposure to UV light or incubation with mitomycin C (data not shown). Immunoblot analyses of the same cultures

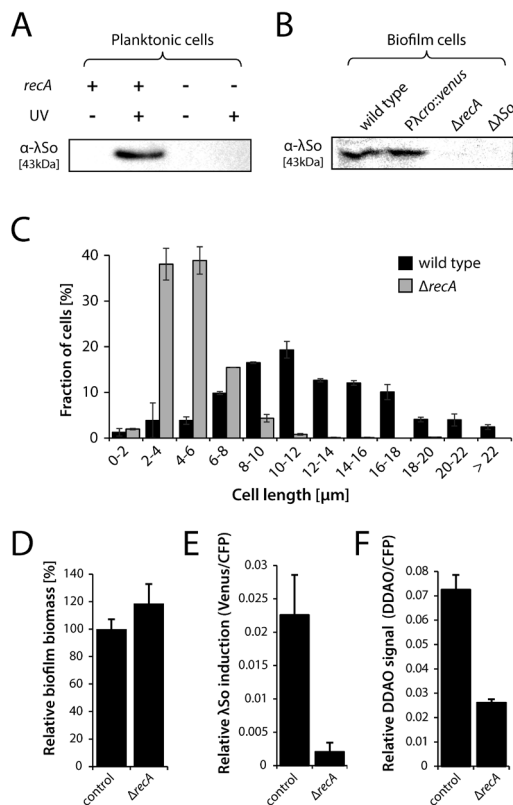


Figure 10. Induction of prophage λ So and filamentous cell growth in $\Delta recA$ deletion mutants. (A) λ So production in planktonic cells of the wild type (*recA* +) and $\Delta recA$ deletion mutants (*recA* -) after UV exposure (UV +) or without UV exposure (UV -). Whole cell lysates were separated by SDS-PAGE followed by Western immunodetection of major capsid protein SO_2963. Sample normalization was achieved by adjusting cell suspensions to the same OD₆₀₀ and analysis of stained SDS-PAGE gels. Representative immunoblot patterns are presented of at least two independent experiments. (B) Production of phage λ So in biofilm cells (static conditions) in the wild type, strain $P\lambda cro::venus$, a $\Delta recA$ deletion mutant and the $\Delta \lambda So$ deletion mutant of prophage λ So. Whole cell lysates were separated by SDS-PAGE followed by Western immunodetection of major capsid protein SO_2963. (C) Cell length distribution of planktonic wild-type and $\Delta recA$ deletion mutant cells in response to mitomycin C. Black and grey bars (*S. oneidensis* MR-1 wild type and $\Delta recA$ mutant, respectively) represent the mean values with standard deviations displayed as error bars of the percentages of each cell length obtained from at least 800 cells per strain. (D-F) CLSM analysis of relative biomass (D, total CFP signal compared to the wild type), relative λ So induction (E, total Venus signal normalized to total CFP signal to obtain an induction-to-biomass ratio), and relative eDNA levels (F, total DDAO signal fluorescence) in 24 hours-old biofilms formed by strain $P\lambda cro::venus$ and $P\lambda cro::venus \Delta recA$ under hydrodynamic conditions in flow cells. Black bars represent the mean values with standard deviations displayed as error bars.

verified that deletion of *recA* not only suppressed λ So induction but also production of phage particles (Figure 10A).

The results described in section 1.4.2 suggest filamentous growth and induction of λ So in response to DNA damage. Inhibition of cell division has been shown to be part of the RecA-mediated SOS response in *E. coli* [307]. Light microscopy analyses were performed to determine whether filamentous growth in planktonic cultures of *S. oneidensis* MR-1 is also under control of RecA in response to DNA damage. The distribution of lengths was determined for the wild type and $\Delta recA$ mutants treated with mitomycin C. The results suggest that filamentous growth was largely suppressed by deletion of the *recA* gene (Figure 10C). Only 5.6 % of the $\Delta recA$ population reached cell lengths above 8 μ m, in contrast to 81.1 % of wild-type cells. However, filamentous growth was not entirely suppressed in all $\Delta recA$ cells, indicating an additional redundant route for the inhibition of DNA-damage induced cell division in *S. oneidensis* MR-1.

To determine whether induction of prophage λ So is also a RecA-dependent process in biofilms, strain $P\lambda cro::venus \Delta recA$ was cultured under hydrodynamic conditions and analyzed by CLSM. No Venus fluorescence above the background level was observed in any of the biofilm developmental stages (Figure 9D, Figure 10E). Accordingly, phage production in biofilm cells was suppressed as confirmed by immunoblot analysis (Figure 10B). Unexpectedly, the total biomass of $P\lambda cro::venus \Delta recA$ biofilms (CFP signal) was slightly increased in comparison to the wild type and did not phenocopy the $\Delta \lambda$ So strain (Figure 10D, Figure 5E), possibly due to pleiotropic effects of the $\Delta recA$ deletion. eDNA staining of 24 hours-old biofilms formed by $P\lambda cro::venus \Delta recA$ demonstrated that the relative signal intensity of DDAO was reduced at least 2.8-fold in comparison to strain $P\lambda cro::venus$, indicating that deletion of *recA* suppressed λ So-mediated eDNA release (Figure 10F). In addition, significantly less string-like structures were observed after DDAO-staining of eDNA (Figure 9D). These data indicate that RecA-controlled induction of prophage λ So mediates cell lysis and eDNA release in a subpopulation of filamentous cells in *S. oneidensis* MR-1 biofilms, mainly at the developmental transition phase prior to extensive three-dimensional growth.

1.4.4 Regulation by OxyR and Fur affects λ So prophage induction

Under biofilm conditions, both induction of Venus fluorescence of strain $P\lambda cro::venus$ and production of phage λ So have been shown to be controlled by RecA (1.4.3). RecA is one of the most conserved proteins in nature and known to control the SOS response in bacteria [308]. RecA recognizes DNA damage such as single-strand gaps or double-strand breaks by forming a filamentous nucleoprotein complex in which the RecA protein switches to its active state. The activated RecA protein exhibits coprotease function, facilitating the autocatalytic cleavage of the LexA repressor, as required for induction of the SOS response in bacteria [309]. Conclusively, induction of prophage λ So under biofilm conditions is likely triggered by DNA damage that is recognized by RecA. However, the cause for such DNA damage in *S. oneidensis* MR-1 that appears to be specific to surface-associated growth is still unknown. In a previous study in our lab, J. Gödeke established an assay to harvest biofilm cells cultured under hydrodynamic conditions to perform whole transcriptome microarray analyses [286]. The results indicate that early surface-associated growth induces the expression of genes belonging to the putative OxyR (oxidative stress defense regulator) and Fur (ferric uptake regulator) regulons in *S. oneidensis* MR-1 (Table 2). Based

Table 2. Differentially regulated genes of the *OxyR* or *Fur* regulons during early surface-associated growth (adapted from Gödeke and coworkers [286])

Locus	Gene	Product	log ₂ ratio
Oxidative Stress (<i>OxyR</i>-regulated genes^a)			
SO_0725	<i>katG-1</i>	Catalase/peroxidase HPI	1.47
SO_1070	<i>katB</i>	Catalase	1.37
SO_0956	<i>ahpF</i>	Alkyl hydroperoxide reductase, F subunit	2.38
SO_0958	<i>ahpC</i>	Alkyl hydroperoxide reductase, C subunit	2.22
Iron homeostasis (<i>Fur</i>-regulated genes^b)			
SO_0139	<i>fln</i>	Ferritin	1.80
SO_0630	<i>nosA</i>	TonB-dependent receptor	1.51
SO_1482	-	TonB-dependent receptor, putative	5.02
SO_1580	-	TonB-dependent heme receptor	2.42
SO_2907	-	TonB-dependent receptor domain-containing protein	1.56
SO_3030	<i>alcA</i>	Siderophore biosynthesis protein (AlcA)	5.33
SO_3031	<i>alcB</i>	Siderophore biosynthesis protein (AlcB)	3.94
SO_3032	<i>alcC</i>	Siderophore biosynthesis protein (AlcC)	5.81
SO_3033	<i>alcD</i>	Ferric alcaligin siderophore receptor (AlcD)	5.61
SO_3667	-	Heme iron utilization protein	3.62
SO_3668	-	HugX family protein	3.64
SO_3669	<i>hugA</i>	Heme transport protein	2.71
SO_3670	<i>tonB1</i>	TonB1 protein	3.51
SO_3671	<i>exbB1</i>	TonB system transport protein ExbB1	5.70
SO_3672	<i>exbD1</i>	TonB system transport protein ExbD1	5.38
SO_3673	<i>hmuT</i>	Hemin ABC transporter, periplasmic hemin-binding protein	4.04
SO_3674	<i>hmuU</i>	Hemin ABC transporter, permease protein	2.33
SO_3675	<i>hmuV</i>	Hemin importer ATP-binding subunit	5.03
SO_3914	-	TonB-dependent receptor, putative	3.15
SO_4077	-	TonB-dependent receptor, putative	4.70
SO_4516	<i>vinA</i>	Ferric vibriobactin receptor	3.60
SO_4523	<i>irgA</i>	Enterobactin receptor protein	1.80
SO_4743	-	TonB-dependent receptor, putative	1.76

^a according to Jiang and coworkers [310]; ^b according to Wan and coworkers [311]

on these observations it was hypothesized that iron-mediated oxidative stress might generate DNA damage under biofilm conditions, which might ultimately result in λ So induction via RecA.

To investigate the role of oxidative stress and intracellular iron levels for the induction of prophage λ So in *S. oneidensis* MR-1 biofilms, we generated in-frame deletion mutants in *oxyR* (SO_1328) and *fur* (SO_1937). A recent study demonstrated that OxyR in *S. oneidensis* MR-1 is analogous to OxyR in *E. coli* and mediates the response to hydrogen peroxide (H₂O₂)-induced stress by acting both as an activator and repressor of defense genes [310]. Hence, *oxyR* mutants were expected to exhibit a partially impaired response to oxidative stress. Deletion of *fur* should result in an increase in intracellular iron levels, since Fur acts as a repressor of iron uptake genes in *S. oneidensis* MR-1 [311].

Immunoblot analysis of λ So in Δ *oxyR* and Δ *fur* biofilm cells (static conditions) indicated increased levels of λ So production in both mutants compared to that of the wild type (Figure 11A). To further investigate the impact on λ So prophage induction during biofilm formation under hydrodynamic conditions, both genes were deleted in strain P λ cro::*venus*. In both mutants, relative

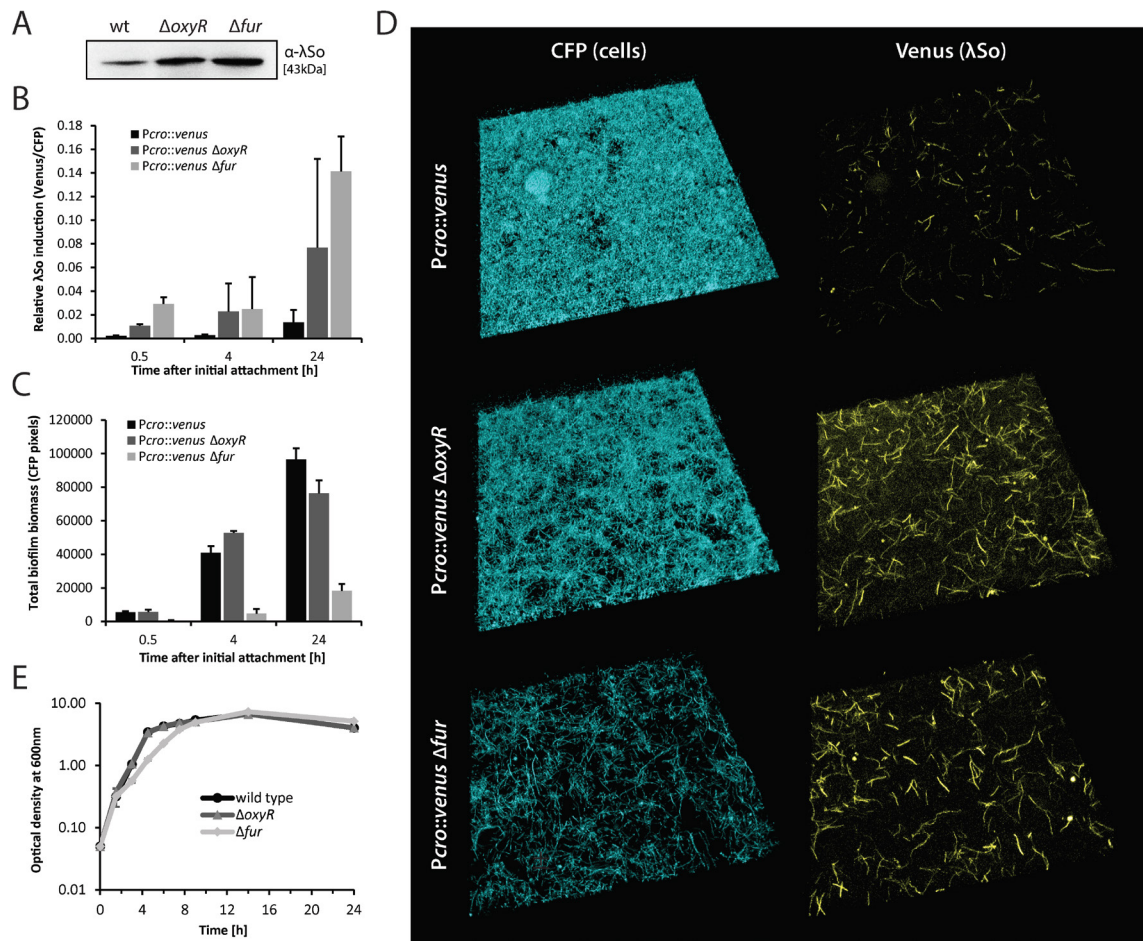


Figure 11. Regulation by OxyR and Fur affects λ So prophage induction and biofilm development. (A) Detection of phage λ So by immunoblot analysis in biofilms formed by the wild type, the $\Delta oxyR$ deletion mutant, and the Δfur deletion mutant under static conditions in petri dishes. Sample normalization was achieved by adjusting cell suspensions to the same OD600 and analysis of stained SDS-PAGE gels. Representative immunoblot patterns are presented of at least two independent experiments. (B) Relative induction of λ So prophage over time in biofilms formed by strain *P λ cro::venus* (black), *P λ cro::venus $\Delta oxyR$* (dark grey), and *P λ cro::venus Δfur* (light grey) under hydrodynamic conditions in flow cells. Bars represent the mean values of Venus/CFP ratios with standard deviations displayed as error bars, obtained from two independent experiments conducted at least in duplicates. (C) Accumulation of biofilm biomass (CFP signal) over time of strain *P λ cro::venus*, *P λ cro::venus $\Delta oxyR$* and *P λ cro::venus Δfur* under hydrodynamic conditions in flow cells. Bars represent the mean values of total CFP pixel values with standard deviations displayed as error bars, obtained from two independent experiments conducted at least in duplicates. (D) CLSM images of 24 hours-old biofilms formed by strain *P λ cro::venus*, *P λ cro::venus $\Delta oxyR$* , and *P λ cro::venus Δfur* under hydrodynamic conditions in flow cells. CFP fluorescence represents all cells and Venus fluorescence indicates λ So prophage induction. (E) Planktonic growth of *S. oneidensis* MR-1 wild type, the $\Delta oxyR$ deletion mutant and the Δfur deletion mutant in LB medium under aerobic conditions. Growth curves are derived from one representative experiment conducted in triplicates. Error bars represent standard deviations.

induction of λ So was severely increased throughout biofilm development during the first 24 hours (approximately 6-fold for $\Delta oxyR$ and 12-fold for Δfur ; Figure 11B). $\Delta oxyR$ mutants produced loosely packed and unstructured biofilms mostly consisting of filamentous cells, however, the total biofilm biomass was only slightly reduced 24 hours after the initial attachment (Figure 11C,D). The Δfur mutant was strongly defective in biofilm formation during all developmental phases tested. The accumulated biomass ranged between 10 – 20 % compared to that of the wild-type biofilms (Figure 11C). Twenty-four hour-old biofilms consisted almost exclusively of randomly oriented and

loosely packed filamentous cells (Figure 11D). Δfur mutants were also unable to produce densely packed macrocolonies under the conditions tested. Notably, under planktonic growth conditions in LB medium the $\Delta oxyR$ mutant exhibited no growth defect and the Δfur mutant had only slightly reduced growth rates in late exponential phase (Figure 11E). All mutant phenotypes could be complemented by reintegration of the wild-type gene copy into the same locus (data not shown). The results indicate that surface-associated growth of *S. oneidensis* MR-1 strongly requires an inducible defense against oxidative stress and tight control of iron uptake. Deregulation of either process triggers λ So prophage induction to abnormal levels resulting in defective biofilm formation.

1.4.5 λ So induction in biofilms cannot be suppressed by an increase in cellular H₂O₂ turnover

Since deregulation of the oxidative stress response in the $\Delta oxyR$ mutant and elevated uptake of iron in the Δfur mutant both increased the level of λ So prophage induction the question arose whether elevated H₂O₂ levels might occur under biofilm conditions, resulting in Fenton-mediated DNA damage and λ So prophage induction. Accordingly, reduction or elimination of intracellular H₂O₂ by an increase in cellular turnover of H₂O₂ would be expected to indirectly reduce, or even suppress, RecA-mediated induction of prophage λ So.

To explore the role of H₂O₂, a mutant screen was performed for the isolation of randomly occurring H₂O₂-resistant clones that possess a constitutively active response to oxidative stress. To select for H₂O₂-resistant clones, potentially possessing mutations in *oxyR*, *S. oneidensis* MR-1 was cultured overnight on LB agar plates containing 2 mM H₂O₂. Yet, exposure to H₂O₂ could likewise trigger mutations in prophage genes instead of *oxyR*. Suppression of phage-induced cell lysis could produce false-positive clones with fitness benefits under these conditions. To overcome this problem, the triple prophage deletion mutant ($\Delta\lambda$ So Δ MuSo2 Δ MuSo1) was used as template strain for this mutant screen. In total, approximately 1.5×10^{10} cells were screened for growth on H₂O₂-containing agar plates to theoretically obtain at least one (up to 60) mutations per base pair, assuming a rate of beneficial mutations (*E. coli*) in the order of 2×10^{-9} per cell and generation [312]. Out of four isolated resistant clones, sequencing of *oxyR* genes revealed a single point mutation causing a T104N amino acid substitution in 3 isolates, and another single point mutation causing a L197P substitution in one isolate. Sequence alignments of *S. oneidensis* MR-1 OxyR with that of other proteobacteria species suggested a high degree of conservation of residue T104. Residue L197P was conserved in many but not all tested proteobacteria species (Figure 12). Reintroduction of both point mutations into the wild-type background revealed that both mutations individually provide *S. oneidensis* MR-1 with a strongly increased resistance (> 20-fold) against H₂O₂ compared to the wild type and the $\Delta oxyR$ mutant (Figure 13A). In plain LB medium the mutants showed slightly reduced growth rates compared to the wild type (Appendix, Figure 36).

Quantitative real-time RT-PCR was performed to better understand the effect of both amino acid substitutions in OxyR on the expression of potential target genes in the absence and the presence of H₂O₂. In both mutants (OxyR^{T104N} and OxyR^{L197P}), the expression of *katB* (SO_1070), *dps* (SO_1158), *ahpC* (SO_0958) and *katG-1* (SO_0725) was strongly induced by factors ranging from 170 (*dps* in OxyR^{T104N}) to 1860 (*katG-1* in OxyR^{L197P}) compared to those wild-type cells, regardless of the presence or absence of H₂O₂ (Figure 13B; Appendix, Figure 36B). Transcript

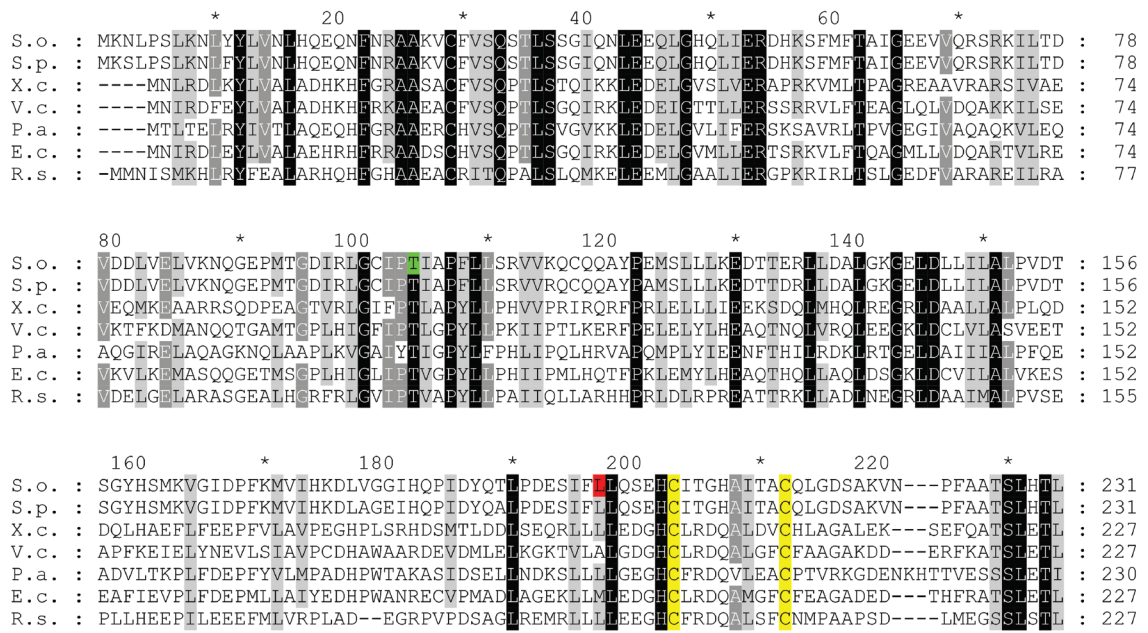


Figure 12. Amino acid substitutions T104N and L197P in *S. oneidensis* MR-1 OxyR. Alignment of OxyR protein sequences of *Shewanella oneidensis* MR-1 (S.o.), *Shewanella putrefaciens* CN-32 (S.p.), *Xanthomonas campestris* (X.c.), *Vibrio cholera* (V.c.), *Pseudomonas aeruginosa* PAO1 (P.a.), *Escherichia coli* (E.c.), and *Rhodobacter sphaeroides* (R.s.). Protein sequences were aligned with ClustalW2 (EMBL-EBI) using standard slow pairwise alignment options. Grey and black background colors highlight highly conserved amino acid residues. Green highlights the position of the T104N amino acid substitution, red the position of the L197P amino acid substitution, and yellow highlights conserved cysteine residues for potential disulfide bond formation under oxidizing conditions.

levels of *tonB* (SO_3670) were also examined to determine whether deletion of *oxyR* or expression of the OxyR variants OxyR^{T104N} and OxyR^{L197P} influences the expression of the Fur regulon. However, no differential expression of *tonB* was observed in the absence of H₂O₂, and only slight down-regulation in the OxyR variants occurred in the presence of H₂O₂ (Appendix, Figure 36B). It was concluded that resistance against H₂O₂ of strains expressing the OxyR variants OxyR^{T104N} and OxyR^{L197P} is conferred by constitutive overexpression of H₂O₂-defense genes and an increase in H₂O₂ turnover.

To determine whether expression of the OxyR variant OxyR^{T104N} or OxyR^{L197P} suppresses λ So induction by H₂O₂, planktonic cultures were treated with 2 mM H₂O₂ and analyzed by immunoblot analysis. The results demonstrate that λ So production was strongly reduced in both mutants compared to that of the wild type (Figure 13C, left lane). Accordingly, cell morphologies of the mutants were unaffected by H₂O₂, while the wild type displayed filamentous cell morphologies (Appendix, Figure 36C).

To finally determine whether induction of prophage λ So is also suppressed under biofilm conditions by expression of the OxyR variant OxyR^{T104N} or OxyR^{L197P}, both *oxyR* mutations were individually introduced into strain P λ cro::venus. Surprisingly, λ So induction levels and biofilm morphologies of the mutants were indistinguishable from those of the wild type as indicated by CLSM analyses (data not shown). Immunoblot analysis of phage λ So in biofilm cells cultivated under hydrodynamic conditions confirmed similar levels of phage λ So production in both mutants

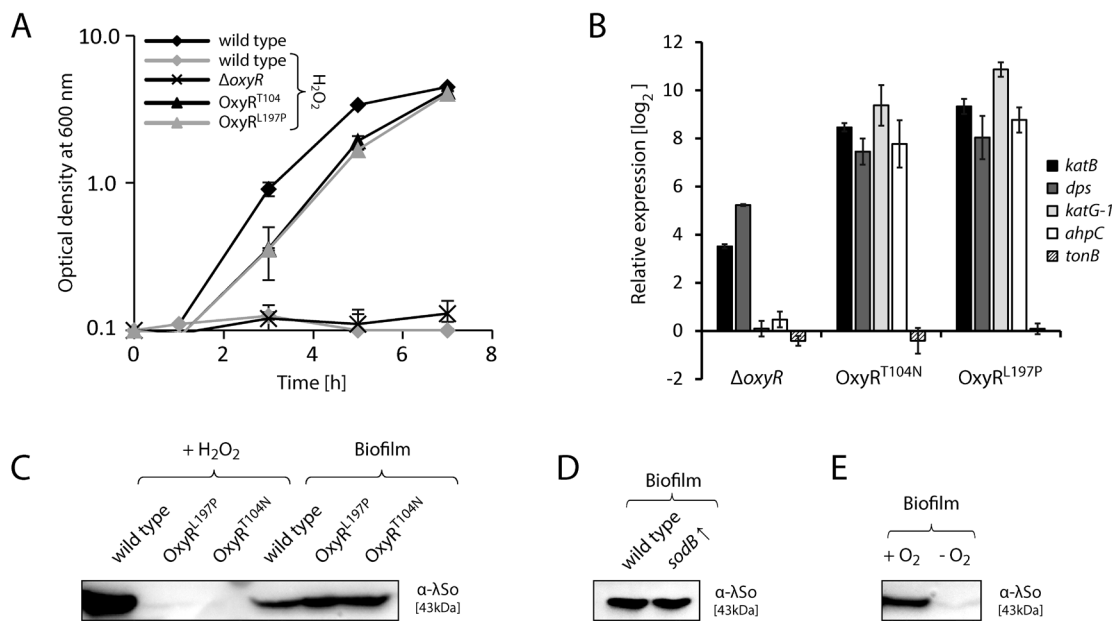


Figure 13. Induction of prophage λ So in biofilms is independent of hydrogen peroxide and superoxide. (A) Planktonic growth under aerobic conditions in LB medium containing 10 mM H_2O_2 of the *S. oneidensis* MR-1 wild type, the ΔoxyR mutant and mutant strains that harbor single amino acid substitutions T104N or L197P in OxyR (OxyR^{T104N} and OxyR^{L197P}). As reference, the growth curve of the wild type in the absence of H_2O_2 is also presented. Growth curves are derived from a representative experiment conducted in triplicates. Error bars represent standard deviations. (B) Relative expression to the wild type of *katB* (SO_1070), *dps* (SO_1158), *ahpC* (SO_0958), *katG-1* (SO_0725) and *tonB* (SO_3670) in the ΔoxyR and the OxyR^{T104N} and OxyR^{L197P} mutant strains, determined by quantitative real-time RT-PCR. Bars represent the mean values of two independent experiments, each normalized to the 16s rRNA and *recA* house-keeping genes. Standard deviations are displayed as error bars. (C) Left three lanes (+ H_2O_2): Immunoblot analysis of phage λ So production in planktonic cells of the wild type and the OxyR^{T104N} and OxyR^{L197P} mutants. Cells were cultivated in LB medium until mid-exponential phase and subjected to 2 mM H_2O_2 for 2 hours. Right three lanes (Biofilm): Immunoblot analysis of phage λ So production in biofilm cells of the wild type and both OxyR mutants. Cells were harvested from 24 hours-old biofilms formed on glass beads under hydrodynamic conditions. Representative immunoblot patterns are presented of at least two independent experiments. (D) Immunoblot analysis of phage λ So production in wild-type biofilm cells harboring plasmid pBBR1-TT-Ptac-MSC5-*sodB* for constitutive overexpression of superoxide dismutase gene *sodB*. Cells were harvested from 24 hours-old biofilms formed on glass beads under hydrodynamic conditions. Representative immunoblot patterns are presented of at least two independent experiments. (E) Immunoblot analysis of phage λ So production in wild-type cells harvested from biofilms formed under oxic conditions (+ O_2) on glass beads (constant medium flow) and cells harvested from biofilms formed under anoxic conditions (- O_2 ; N_2 headspace) on glass beads (static conditions). Representative immunoblot patterns are presented of at least two independent experiments.

and the wild type, indicating that H_2O_2 is not a limiting factor for λ So induction in *S. oneidensis* MR-1 biofilms (Figure 13C).

In addition to H_2O_2 , it was tested whether elevated superoxide levels might influence λ So activation under biofilm conditions. However, addition of paraquat (known to generate superoxide by reaction with molecular oxygen) did not stimulate λ So production in planktonic cells (Appendix, Figure 37) [313]. Furthermore, overexpression of the Fe/Mn superoxide dismutase *sodB* gene (SO_2881) in biofilm cells did not suppress λ So production (Figure 13D). The results indicate that superoxide has a minor if any role in λ So induction in *S. oneidensis* MR-1 biofilms. A range of molecules (glutathione, ascorbic acid, N-acetyl-cysteine, L-proline, L-cysteine) was also tested that might act as antioxidants and have previously been shown to suppress cellular oxidative stress, but none had any significant effect on phage induction during biofilm formation (data not shown).

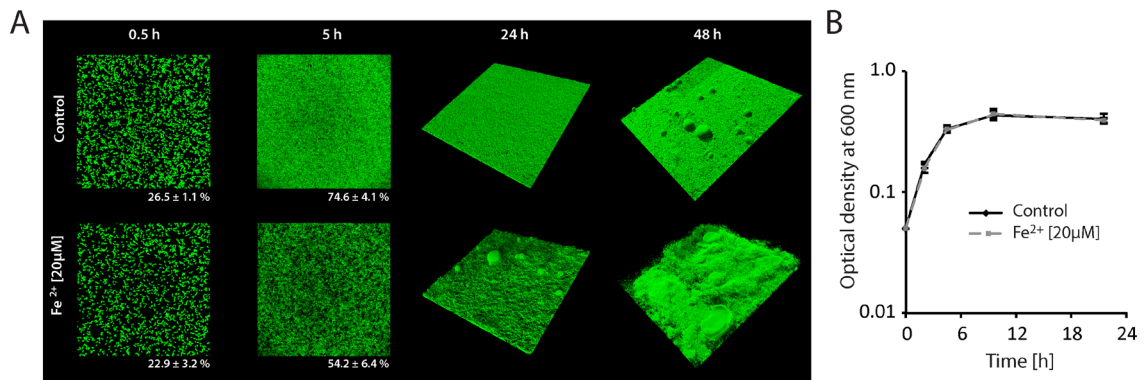


Figure 14. Influence of iron addition to *S. oneidensis* MR-1 biofilms formation and planktonic growth. (A) GFP-tagged (*Tn7::egfp*) *S. oneidensis* MR-1 wild-type cells were incubated in flow chambers under hydrodynamic conditions in plain LM medium (upper panel) and LM medium supplemented with 20 μ M FeCl_2 (lower panel). Biofilm formation was analyzed by CLSM at the indicated time points, displayed are three-dimensional shadow projections. The numbers below the images recorded after 0.5 and 5 hours represent the average surface coverage. At 0.5 and 5 hours, the lateral edge of each image is 250 μ m in length. At 24 and 48 hours the lateral edge of each image is 750 μ m in length. (B) Influence of iron addition (20 μ M FeCl_2) to planktonic growth of *S. oneidensis* MR-1 in LM medium. The values represent the average of 6 independent growth experiments. The error bars represent the standard deviation.

To determine whether induction of λ So under biofilm conditions depends on the presence of molecular oxygen, an assay was developed to harvest biofilm cells grown under anoxic conditions. To this end, *S. oneidensis* MR-1 biofilms were grown on glass beads (covered with LM medium) in glass bottles flushed with nitrogen. Twenty-four hours after the initial attachment, biofilm cells were harvested and subjected to SDS-PAGE and immunoblot analysis (Figure 13E). The results indicate that cultivation of biofilms under anoxic conditions strongly decreased the level of λ So production in comparison to those grown aerobically. Thus, dioxygen seems to play an important role in the induction of λ So under hydrodynamic biofilm conditions. However, it has to be noted that the setup used for the cultivation of anaerobic biofilms differs considerably from that used for aerobic biofilms and therefore represents only a limited control.

From this set of experiments it was concluded that an inducible defense against reactive oxygen species (ROS) is required for normal biofilm formation, however, neither increased H_2O_2 nor increased superoxide levels seem to represent a biofilm-specific stimulus of prophage λ So.

1.4.6 Availability of iron controls timing and level of λ So prophage induction and eDNA release

Transcriptome analysis performed by J. Gödeke demonstrated that genes of the Fur regulon of *S. oneidensis* MR-1 were strongly induced upon surface contact, indicating a high demand of iron during this phase [286, 291]. To gain more insights into the role of iron, biofilms of *S. oneidensis* MR-1 were cultured under hydrodynamic conditions in the presence of additional iron. Addition of physiological concentrations of ferrous iron (20 μ M Fe^{2+}) strongly stimulated structural biofilm development during later phases (24 and 48 hours) (Figure 14A). Addition of the same amount of iron to planktonic cells cultured in LM medium had no detectable effect on growth rates

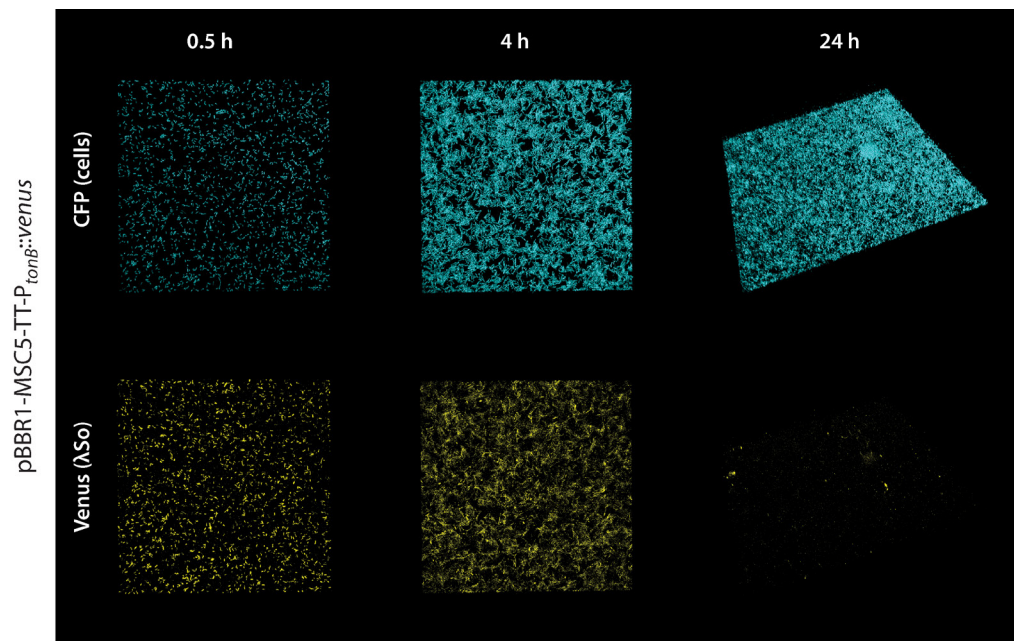


Figure 15. Activity of promoter P_{tonB} during biofilm development. Displayed are CLSM images of 24 hours-old biofilms formed by a CFP-tagged *S. oneidensis* MR-1 wild-type strains harboring plasmid pBBR1-TT-MSC5- $P_{tonB}::venus$ under hydrodynamic conditions in flow cells. Venus fluorescence is expected to positively correlate with promoter activity of the *tonB1* gene (SO_3670). The lateral edge of each micrograph is 250 μ m.

(Figure 14B). While the coverage of the surface was delayed in earlier biofilm stages (22.9 % to 26.5 % after 30 minutes and 54.2 % to 74.6 % after 5 hours), formation of three-dimensional structures occurred earlier and more structures were formed. Furthermore, at 24 and 48 hours a dense network of filamentous cells was observed that pervaded the entire biofilm surface. In the control samples without additional iron, filamentous growth was also observed, but it occurred to a much lower extent. It was concluded that iron plays an important role for the development of biofilms under hydrodynamic conditions, both in terms of biofilm structure and biomass.

Nevertheless, it was unclear whether iron is constantly assimilated during the course of biofilm development or whether iron uptake is restricted to the early phases of biofilm formation, as indicated by the results of J. Gödeke [286, 291]. To investigate TonB-mediated iron uptake during biofilm formation, the putative promoter region of the *tonB1* gene (P_{tonB}) was cloned into vector pBBR1-TT-MSC5-RBS-*venus*. Venus fluorescence was expected to positively correlate with promoter activities of P_{tonB} and accordingly active assimilation of iron via the TonB-mediated iron uptake system. The *tonB1* gene (SO_3670) is predicted to be the first gene in an operon with *exbB1* (SO_3671), *exbD1* (SO_3672), *bmuT* (SO_3673), *bmuU* (SO_3674), and *bmuV* (SO_3675) (VIMSS, [303]). Consistently, all these genes were found to be upregulated during early phases of biofilm formation (Table 2). Upstream of *tonB1* resides a noncoding intergenic region of 245 bps, potentially harboring the putative promoter P_{tonB} of the *tonB1* operon. This region was cloned into vector pBBR1-TT-MSC5-RBS-*venus* upstream of the *venus* gene that is carrying its own ribosomal binding site. Plasmid pBBR1-TT-MSC5- P_{tonB} -*venus* was transformed into wild-type *S. oneidensis* MR-1, and the strain was tagged with eCFP (Tn7::*ecfp*) for subsequent analyses of biofilm formation by CLSM in flow chambers. During the first hours (approximately 0 - 5 hours) after the initial attachment, almost all cells exhibited fluorescence of Venus, indicating transcription

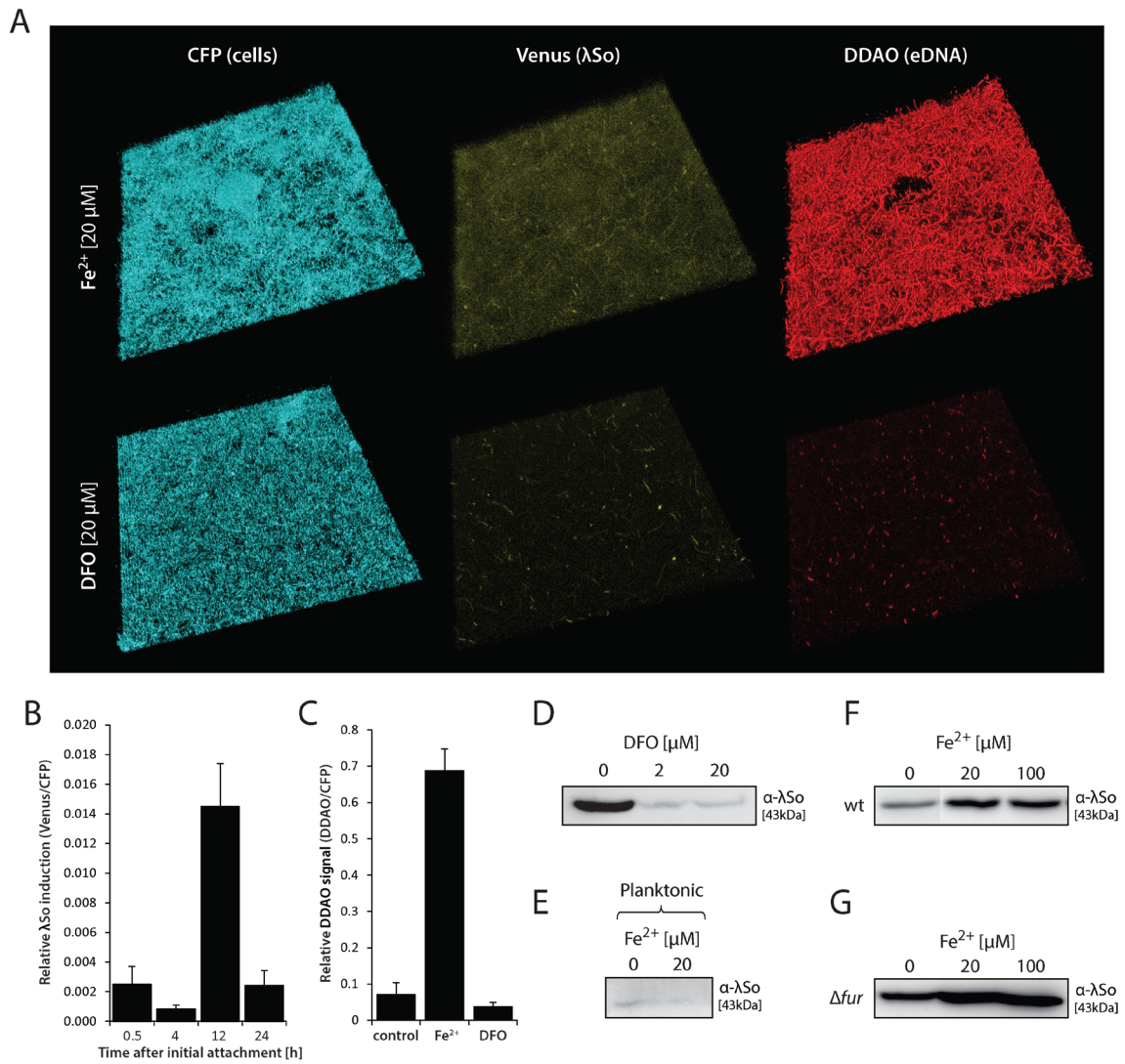


Figure 16. Iron controls level and timing of λ So prophage induction and eDNA release. (A) CLSM image projections of 24 hours-old biofilms formed by strain *P λ cro::venus* under hydrodynamic conditions in flow cells in the presence of 20 μM FeCl_2 (Fe^{2+}) or 20 μM iron chelator desferrioxamine (DFO). CFP fluorescence represents all cells and Venus fluorescence indicates λ So prophage induction. The biofilms were stained with DDAO to visualize eDNA. The lateral edge of each micrograph is 250 μm . **(B)** Relative induction of λ So prophage over time in biofilms formed by strain *P λ cro::venus* under hydrodynamic conditions in flow cells in the presence of 20 μM Fe^{2+} . Total Venus signal intensities from CLSM images were normalized to total CFP signal intensities to obtain an induction-to-biomass ratio. Black bars represent the mean values with standard deviations displayed as error bars. **(C)** eDNA levels as a measure of relative DDAO fluorescence in biofilms formed under hydrodynamic conditions in flow cells in the presence of 20 μM Fe^{2+} or 20 μM iron chelator desferrioxamine (DFO). Total DDAO signal intensities from CLSM files were normalized to total CFP signal intensities to obtain an eDNA-to-biomass ratio. Black bars represent the mean values with standard deviations displayed as error bars. **(D)** Detection of phage λ So by immunoblot analysis in biofilms formed under hydrodynamic conditions on glass beads in the presence or absence of desferrioxamine (DFO). Representative immunoblot patterns are presented of at least two independent experiments. **(E)** Detection of phage λ So by immunoblot analysis in wild type cells cultivated under planktonic growth conditions in the absence or presence of 20 μM Fe^{2+} . The cells were harvested during logarithmic growth phase. Representative immunoblot patterns are presented of at least two independent experiments. **(F)** Detection of phage λ So by immunoblot analysis in biofilms formed by the wild type and **(G)** the Δfur deletion mutant under static conditions in petri dishes in the presence of 20 μM and 100 μM Fe^{2+} . Cell lysates of biofilm cells were subjected by SDS-PAGE followed by immunoblot analysis of major capsid protein SO_2963. Representative immunoblot patterns are presented of at least two independent experiments.

of the *tonB* operon and active uptake of ferric iron (Figure 15). These results confirm the transcriptome data of early surface-attached cells obtained by J. Gödeke [286, 291]. However, a few hours after the initial attachment, Venus signals started to decrease. After 24 hours, Venus fluorescence had vanished in almost all cells, indicating suppression of *P_{tonB}* promoter activity and diminished assimilation of ferric iron via the TonB system. Notably, planktonic cells cultured in LM medium exhibited Venus fluorescence similar to biofilm cells during the first hours after the initial attachment. Conclusively, planktonic cells and early biofilm cells seem to have a high demand for iron, as indicated by expression the TonB operon and additional Fur-regulated genes. However, assimilation of ferric iron appears to be suppressed in later phases of biofilm development.

Increased intracellular levels of free iron in concert with aerobic respiration have often been suggested to result in oxidative stress and DNA damage, a well-known stimulus for the RecA-mediated SOS response [for review: 314, 315, 316]. Thus, it was concluded that iron might act as an indirect stimulus for λ So phage induction and eDNA release in *S. oneidensis* MR-1 biofilms. To follow this hypothesis, biofilms of strain *P_{Acro::venus}* were cultivated in the presence of 20 μ M Fe²⁺. After 12 hours of incubation, Venus fluorescence (as a measure of λ So prophage induction) increased in comparison to that of biofilms without additional iron, but decreased after 24 hours after initial attachment, indicating that addition of iron stimulated an earlier λ So induction (Figure 16B). DDAO staining of 24 hours-old biofilms revealed drastically increased levels of eDNA (9.5-fold) in comparison to biofilms grown without additional iron (Figure 16A,C). The eDNA appeared as densely packed string-like structures, probably representing filamentous multinucleated cell bodies that pervaded the entire biofilm except the area of microcolonies (Figure 16A).

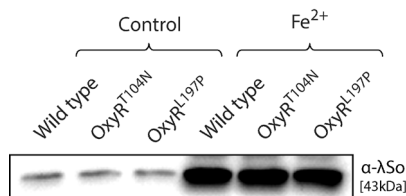


Figure 17. Production of λ So in H₂O₂-resistant mutants in the presence of additional iron. Detection of phage λ So by immunoblot analysis in biofilms formed by the wild type and the OxyRT^{104N} and OxyRL^{197P} mutant strains under static conditions in LM medium in the presence of 20 μ M Fe²⁺. Cell lysates of biofilm cells were subjected to SDS-PAGE followed by immunoblot analysis of major capsid protein SO_2963. Representative immunoblot patterns are presented of at least two independent experiments.

However, to demonstrate that iron is the major stimulus for the induction of λ So under biofilm conditions, it was crucial to investigate whether λ So induction and the release of eDNA can also be suppressed by the removal of the potential stimulus. Addition of desferrioxamine (DFO), a chelating agent for ferric and ferrous iron [317], reduced the relative signal intensities of both Venus and DDAO, indicating that decreasing the levels of available iron indeed inhibits λ So phage induction and eDNA release. Accordingly, the presence of DDAO-stained string-like structures was largely diminished. Suppression of λ So production by desferrioxamine in hydrodynamically-grown biofilms was additionally verified by immunoblot analysis (Figure 16D). Notably, the observed effect of iron on λ So induction appeared to be biofilm-specific since addition of Fe²⁺ to cells grown under planktonic conditions did not have any effect on λ So production (Figure 16E).

The effect of iron was additionally investigated by immunoblot analysis in wild-type and Δfur biofilms grown under static conditions. In both strains, addition of ferrous iron increased the level of λ So production compared to the untreated controls. Moreover, addition of iron to Δfur biofilms

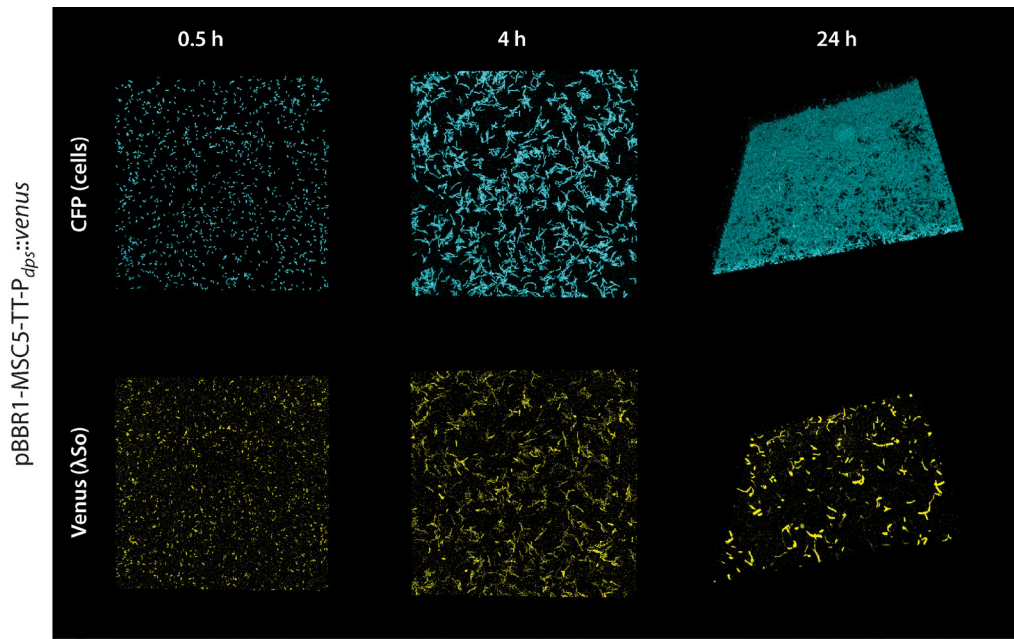


Figure 18. Activity of promoter P_{dps} during biofilm development. Displayed are CLSM images of 24 hours-old biofilms formed by a CFP-tagged *S. oneidensis* MR-1 wild-type strains harboring plasmid pBBR1-MSC5-TT- $P_{dps}::venus$ under hydrodynamic conditions in flow cells. Venus fluorescence is expected to positively correlate with promoter activity of the *dps* gene (SO_1158). The lateral edge of each micrograph is 250 μ m.

had an additive effect, resulting in strongly increased levels of λ So production (Figure 16 F,G). These results suggested that the level of intracellular iron positively correlates (in the range of concentrations tested) with the degree of λ So production in *S. oneidensis* MR-1 biofilms. Notably, addition of Fe^{2+} to biofilms formed by the OxyR^{T104N} and OxyR^{L197P} mutant strains also strongly increased the level of λ So production in comparison to the untreated controls, further indicating that iron and not H_2O_2 is the predominant factor for λ So induction in *S. oneidensis* MR-1 biofilms (Figure 17). From this set of experiments we concluded that addition of Fe^{2+} to biofilms of *S. oneidensis* MR-1 stimulates λ So prophage induction and enhances the level of eDNA release, likely by an increase in fluorescence solely occurred in filamentous cells in the upper layers of the biofilm.

This hypothesis was further supported by monitoring *dps* (SO_1158) promoter activity during biofilm formation (Figure 18). Dps is predicted to be a ferritin-like protein that binds and oxidizes Fe^{2+} to protect DNA against oxidative damage [318, 319]. In *S. oneidensis* MR-1, *dps* transcription has been shown to depend on derepression by OxyR [310]. Operon prediction by VIMSS suggests *dps* to be transcribed monocistronically. Upstream of *dps* resides a noncoding intergenic region of 219 bps that is probably harboring putative promoter P_{dps} and other regulatory elements. This region was cloned into vector pBBR1-TT-MSC5-RBS-*venus* and transformed into eCFP-tagged *S. oneidensis* MR-1 for subsequent analyses of biofilm formation by CLSM in flow chambers. *Dps* appeared to be actively expressed in almost all cells during early phases of biofilm formation, indicative of iron-mediated stress. In contrast, *dps* expression in planktonic cells (LM medium) was mostly below the detection limit of the reporter system. Remarkably, during later phases of biofilm formation (24 hours after the initial attachment) Venus fluorescence solely occurred in filamentous cells in the upper layers of the biofilm. Reporter activity was mostly absent in the bottom layers or

in micro- or macrocolonies. Thus, induction patterns observed for the *dps* gene in later phases of biofilm formation, appear similar to the induction patterns observed for prophage λ So. Conclusively, the results indicate that iron-mediated oxidative damage is exceedingly pronounced in filamentous cells, a phenotypic variant specific to later phases of *S. oneidensis* MR-1 biofilm development.

1.5 Functional specificity of extracellular nuclease EndA

S. oneidensis MR-1 harbors three extracellular nucleases, ExeM, ExeS and EndA. The phenotypes of *exeM* and *exeS* deletion mutants were attributed predominantly to biofilm formation [241]. In contrast, deletion mutants of *endA* were shown to form cellular aggregates under planktonic conditions [320]. To better understand the role of EndA with regard to both lifestyles, this chapter focuses on the enzymatic characteristics of the EndA protein and the role of EndA *in vivo* under both conditions. Furthermore, the role of the extracellular phosphatase PhoA that is encoded with *endA* in an operon was examined with regard to its role in growth on DNA as sole phosphorus source.

The results suggest that EndA is an Mg^{2+}/Mn^{2+} -dependent extracellular nuclease that is secreted into the medium supernatant during exponential phase to exploit DNA as nutrient source and to prevent from accumulation of high-molecular-weight eDNA to abnormal levels under planktonic growth conditions. In contrast to EndA, PhoA is not required to exploit DNA as sole source of phosphorus. Surprisingly, addition of purified MBP-EndA protein to established biofilms did not result in the release of biofilm biomass and endogenous overexpression of *endA* had no effect, indicating a minor role of EndA under biofilm conditions.

Most of the work presented in this chapter was accomplished in close collaboration with Max Kreienbaum as part of his Master thesis that was supervised by me [321].

1.5.1 Purification and *in vitro* analyses of EndA

To investigate EndA's nucleolytic activity *in vitro*, the protein was overproduced in *E. coli* BL21Star (DE3) and enriched by affinity chromatography. For this purpose, the pMAL-P2X vector system (NEB, USA) was utilized to produce a translational fusion of EndA (lacking its native signal peptide) to the maltose binding protein (MBP). Plasmid pMAL-P2X encodes the MBP protein with an N-terminal SecYEG-dependent signal peptide to mediate periplasmic secretion of the fusion protein. EndA contains 8 conserved cysteine residues that are probably required for disulfide bond formation and proper folding in the extracellular space [292]. SDS-PAGE analysis of the elution fractions revealed that high amounts of fusion protein were obtained by MBP-amylose affinity chromatography (Figure 19A). As control, the single MBP protein was overproduced and purified in parallel without any fusion. For the MBP-EndA sample, a second band appeared corresponding to the molecular mass of the pure MBP protein. It was speculated that this band represents MBP protein which was unspecifically cleaved off from the fusion construct.

To characterize the activity of the fusion protein, DNA degradation was determined upon addition of purified MBP-EndA. An assay was developed allowing real-time monitoring of DNA-degradation *in vitro*. To this end, the decrease in fluorescence due to the release of DNA-bound Gel-Red™ nucleic acid stain was measured as a function of DNA degradation using the plasmid pBluescript as substrate (Figure 19B). The results were confirmed by visualization of the residual DNA by separation on agarose gels after incubation with MBP-EndA (data not shown). The same concentration of pure MBP protein being produced and purified in parallel was used as negative control. These assays demonstrated that pBluescript was readily degraded by MBP-EndA, while no DNA degradation occurred when the same amount of MBP was added. Furthermore, the results demonstrated that EndA exhibits endonucleolytic activity on circular plasmid DNA.

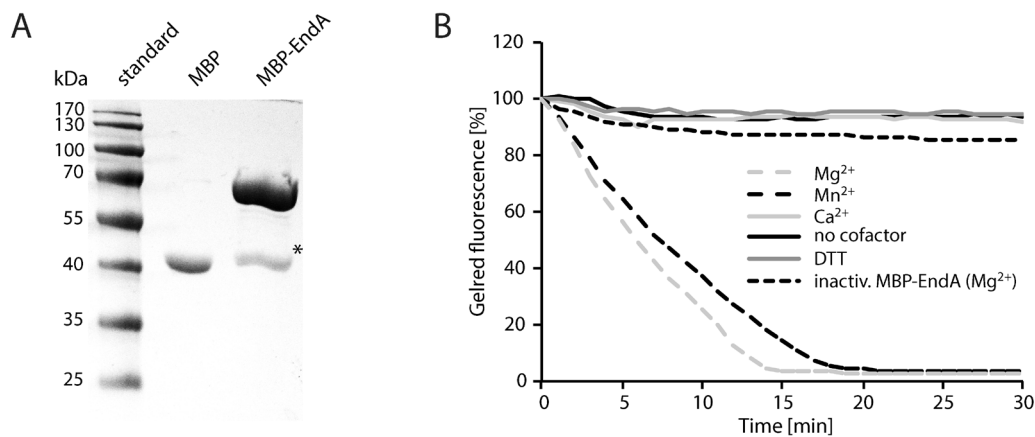


Figure 19. Purification and *in vitro* activity of MPB-EndA. (A) SDS-PAGE on proteins after enrichment using amylose resin. MBP without fusion was produced and enriched in parallel (middle lane). MBP-EndA migrated at a position corresponding to a molecular mass of about 70 kDa in close agreement with the estimated mass of 73.1 kDa. A single major contaminating band (marked by an asterisk), likely representing MBP (42 kDa), was visible after enrichment. (B) Activity of MBP-EndA (0.12 μ g) on purified vector pBluescript (250 ng). The activity was determined by the loss of fluorescence of DNA-bound GelRedTM nucleic acid stain due to DNA degradation. Several cofactors (Mg²⁺, Mn²⁺, Ca²⁺) were tested at a concentration of 2.5 mM, and control assays were carried out without cofactor, after addition of DTT, after heat inactivation of MBP-EndA, and by addition of MBP that was analogously produced and purified. The identity of the different assays is indicated. Only the addition of Mg²⁺ or Mn²⁺ as cofactor to EndA resulted in rapid degradation of DNA.

EndA is predicted to belong to the endonuclease I family of proteins (NCBI BLASTP), showing significant homologies to other nucleases of this family that have been characterized earlier, such as *Vibrio vulnificus* Vvn, *E. coli* EndA, *V. cholerae* Dns, and *A. hydrophila* Dns [292]. Members of this family have been shown to require divalent ions for enzyme activity [322]. Accordingly, no DNA degradation was observed when only Tris buffer was used in the sample or EDTA was added to the reaction. DNA degradation occurred upon addition of Mg²⁺ and significant enzyme activity was also observed with Mn²⁺. In contrast, supplementation of the reaction mixture with Ca²⁺, Fe²⁺, Zn²⁺, Ni²⁺, or Cu²⁺ did not or only weakly support DNA degradation. *Shewanella* EndA is not thermostable and was inactivated after heating to 70 °C for 10 minutes. To test for nucleolytic activity under reducing conditions, DTT was added to the reaction. As expected, no degradation of DNA was observed, indicating that EndA requires oxidizing conditions for nucleolytic activity, probably relying on proper disulfide bond formation. Defining one unit of enzyme activity as the amount of MBP-EndA required to completely degrade one μ g of pBluescript vector within 10 minutes at 30 °C in reaction buffer supplemented with 2.5 mM Mg²⁺, the specific activity of purified MBP-EndA was up to 9,100 U/mg. Similar to plasmids, linear DNA fragments as well as chromosomal DNA from *B. subtilis*, *S. oneidensis*, and *C. crescentus*, eukaryotic DNA of high molecular weight and RNA were readily degraded (Appendix, Figure 38).

1.5.2 PhoA is not essential for growth on DNA as sole source of phosphorus

Deletion mutants in *endA* have been shown to be incapable of growing on DNA as the sole source of phosphorus and to lack nucleolytic activity in culture supernatants [292]. These data strongly

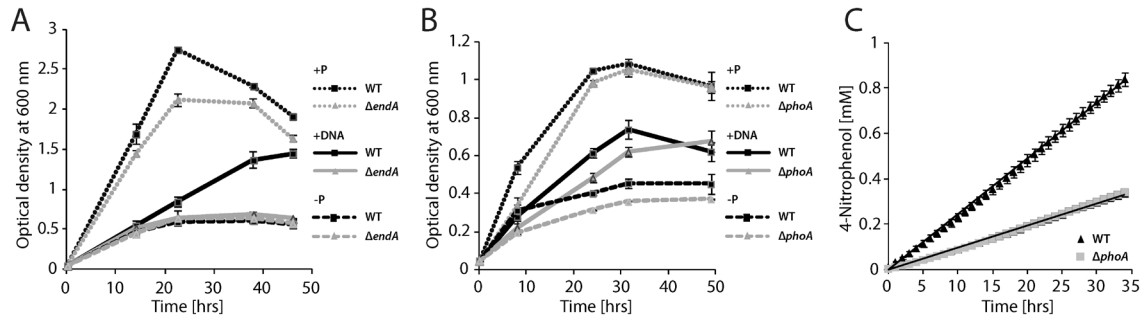


Figure 20. Contribution of PhoA to growth on eDNA as sole source of phosphorous. Growth of the wild type (black squares) and the $\Delta endA$ (A) and $\Delta phoA$ (B) mutant (grey triangles) in M1 mineral medium supplemented with either 0.86 mM NaH_2PO_4 (dotted lines), salmon sperm DNA (0.5 g l⁻¹; solid lines), or no source of phosphorus (dashed lines). (C) Activity of PhoA in medium supernatants. The phosphatase activity in M1 medium supernatants was determined for wild-type (black triangles) and $\Delta phoA$ mutant (grey squares) cultures. The graph displays the formation of 4-nitrophenol from *p*-nitrophenylphosphate over time. The error bars display the standard deviation.

indicated that EndA is required for utilizing eDNA as a nutrient. Interestingly, *endA* resides in an operon with gene SO_0830, encoding the putative alkaline phosphatase PhoA. PhoA is a protein of 454 amino acids with an estimated molecular mass of 48.5 kDa. Like EndA, PhoA is predicted to have a signal peptide likely to be cleaved between positions 23 and 24 [323]. The question arose whether PhoA is required for growth on DNA under phosphorus-limiting conditions, similar to EndA. Thus, the ability of a $\Delta phoA$ strain to grow on DNA of high molecular weight was determined in the absence of other sources of phosphorus (Figure 20). For comparison, the growth of $\Delta endA$ mutants was also assayed in parallel. As shown before by M. Heun, $\Delta endA$ displayed no growth on salmon sperm DNA whereas in the presence of NaH_2PO_4 the mutants grew indistinguishable to the wild type [292]. In contrast to $\Delta endA$, a mutant in *phoA* did not display a significantly decreased growth rate on the DNA, indicating that PhoA is not strictly required to exploit eDNA as phosphorus source. To determine whether PhoA is an active extracellular phosphatase, the corresponding activity in cell-free supernatants of exponentially growing cultures of the wild type and a *phoA* mutant were determined (Figure 20C). The phosphatase activity in supernatants of a *phoA* mutant was decreased by up to 40 % compared to that of wild-type supernatants. In conclusion, PhoA is an active extracellular phosphatase, significantly contributing to the phosphatase activity in medium supernatants. However, the phosphatase activity in culture supernatants was not completely suppressed by deletion of *phoA*, indicating the presence of further redundant enzymes exhibiting extracellular phosphatase activity. Thus, the residual phosphatase activity appears to be sufficient to release enough phosphate to enable growth on DNA under the conditions tested.

1.5.3 EndA is a planktonic growth-specific nuclease

Probably the most distinct phenotypes of a *S. oneidensis* MR-1 $\Delta endA$ deletion mutant are the formation of cell aggregates and the lack of nucleolytic activity in $\Delta endA$ planktonic cultures [292]. These phenotypes suggest an extracellular localization of EndA, either secreted into the culture supernatant or associated to the cell surface. In contrast, nucleolytic activity of *E. coli* EndA was detected only in the fluids released from the periplasm [295], suggesting variable localizations of EndA homologs among different species.

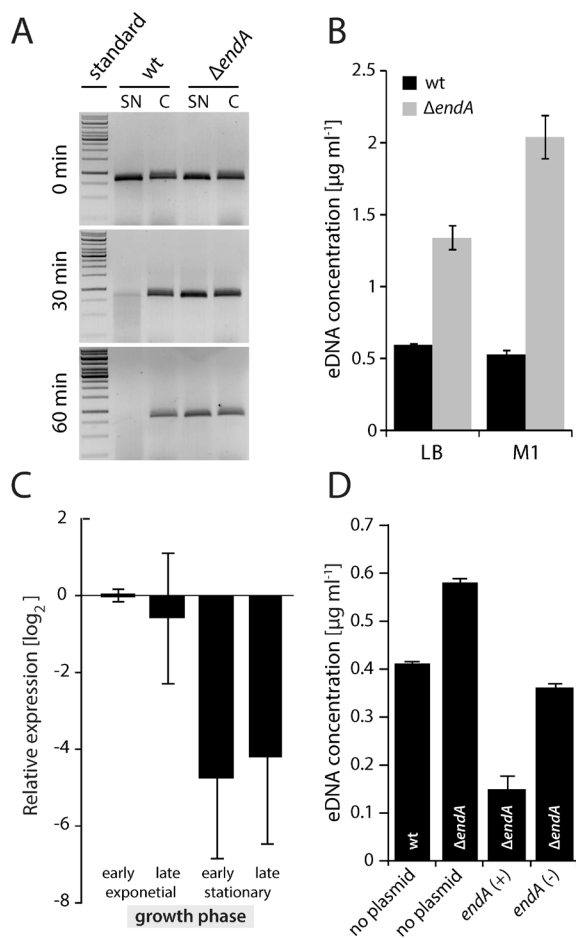


Figure 21. *In vivo* activity of EndA in planktonic cultures (A) Nuclease activity in medium supernatants of the wild type and the $\Delta endA$ mutant. The cultures were grown in LB medium to exponential phase and production of novel protein was blocked by addition of chloramphenicol. Subsequently, an 833 bp DNA fragment was directly added to the supernatant of the cultures (SN) and to supernatant of cultures in which the cell sediment has been washed prior to addition of the PCR fragment (B) Amount of eDNA in medium supernatants of wild-type (black) and $\Delta endA$ mutant cultures grown in LB (left) or M1 medium (right). The error bars display the standard deviation. (C) Growth-dependent regulation of *endA* in planktonic cultures. qRT-PCR was performed to determine transcript levels of *endA* in cells in the late exponential growth phase (OD₆₀₀ 2.0) and early and late stationary growth phase (OD₆₀₀ 4.0 and 6.0) compared to the early exponential growth phase in LB medium (OD₆₀₀ 0.6). Error bars represent the standard deviations of two independent experiments performed each in duplicates (D) eDNA concentrations in supernatants of the wild type, the $\Delta endA$ mutant and the $\Delta endA$ mutant overexpressing *endA* (pLacTac-*endA*) in the presence (+) or absence (-) of IPTG. The strains were cultured in 4M medium for 24 hours. To induce overexpression of *endA* from pLacTac-*endA*, IPTG was added prior to inoculation. Error bars represent the standard deviations of two independent experiments performed each in triplicates.

To determine whether *S. oneidensis* MR-1 EndA is secreted into the culture supernatant or associated to the cell surface, cell-free supernatants of exponentially growing wild-type and $\Delta endA$ cultures were tested for nucleolytic activity. In the absence of *endA*, no degradation of a defined linear DNA fragment was observed whereas in the wild-type sample the DNA was rapidly degraded within the first hour. Assays with washed cells in which protein synthesis was arrested by addition of chloramphenicol revealed that DNA degradation exclusively occurred in the medium supernatant but not within the cell fraction (Figure 21A). These observations strongly indicate that active EndA is released into the supernatant and not localized in the periplasm or associated with the cell surface.

In addition to the formation of cell aggregates in planktonic cultures, it was observed that late stationary phase cultures of $\Delta endA$ mutants generate a highly mucoid culture supernatant, indicative of high concentrations of eDNA. Accordingly, culture supernatants were found to contain more than two-fold and four-fold higher concentrations of eDNA after 72 hours in complex media and mineral medium, respectively (Figure 21B).

Quantitative real-time RT-PCR (qPCR) analyses of transcript levels performed by M. Heun indicated that *endA* is not significantly regulated under phosphorus-limiting conditions, in the presence of high DNA concentration, or under biofilm conditions [292]. To determine whether *endA* is differently regulated during different phases of planktonic growth, qPCR analyses were

performed on early- and late-exponential, and early- and late-stationary phase cells (Figure 21C). Unexpectedly, the results strongly suggest that highest expression of *endA* occurs during exponential phase and that expression levels strongly decrease in stationary phase. By contrast, eDNA accumulation and cell aggregation was mainly observed during later stages of cultivation. The relative transcript abundance of *pbaA* showed similar patterns as observed for *endA*, further indicating that both genes reside in the same operon (data not shown).

Based on these results, the question arose whether EndA's nucleolytic activity in supernatants directly correlates with its expression levels. Therefore, the *endA* gene was cloned into plasmid pLacTac for IPTG-inducible overexpression of *endA* in *S. oneidensis* MR-1. Overexpression of *endA* resulted in decreased eDNA concentrations in medium supernatants (Figure 21D). The uninduced controls showed eDNA levels similar to those of the wild type. Correspondingly, degradation assays of a linear PCR product showed that overexpression of *endA* results in increased nuclease activity in culture supernatants (Appendix, Figure 39). Taken together, the results demonstrated that EndA is produced and transported into the medium supernatant during exponential growth

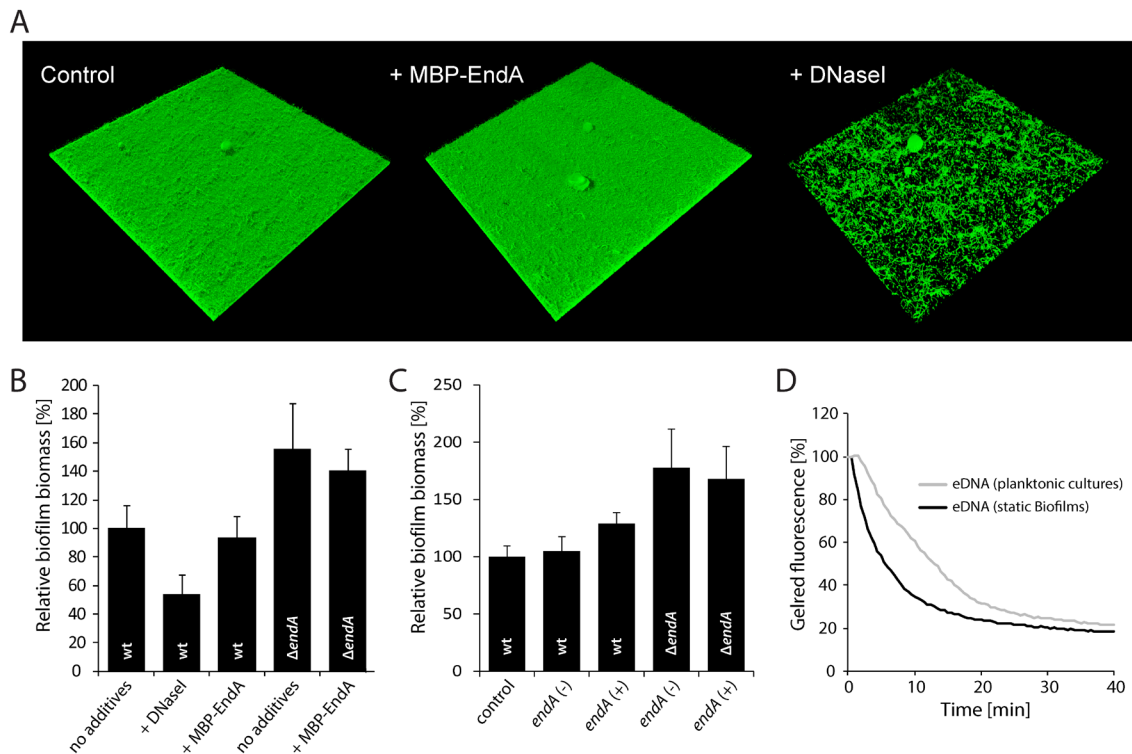


Figure 22. The role of EndA in biofilm formation and degradation of biofilm-eDNA. (A) A wild-type biofilm formed after 24 h in flow chambers was treated with MBP-EndA (center) or DNase I (right) for 45 min. The lateral edge of each micrograph measures 250 μ m. (B) Biofilm formation (static conditions) of the wild type and the $\Delta endA$. The strains were grown for 24 h in microtiter plates, and DNase I (approximately 4 U according to NEB, USA) or MBP-EndA (approximately 0.2 U) was added as indicated. The values are means of three replicates. Error bars represent standard deviations. (C) Biofilm formation of the wild type, the $\Delta endA$ mutant, and both strains overexpressing *endA* (pLacTac-*endA*) in the presence (+) or absence (-) of IPTG. The strains were grown for 24 hours in microtiter plates. To induce overexpression of *endA* from pLacTac-*endA*, IPTG was added prior to inoculation. Error bars represent the standard deviations of two independent experiments performed each at least in triplicates. (D) Activity of MBP-EndA on eDNA in the supernatant of planktonic cultures (light grey) and on eDNA prepared from the matrix of statically grown biofilms. The activity was determined by the loss of fluorescence of DNA-bound GelRed™ nucleic acid stain due to DNA degradation.

phase. Gödeke and coworkers have previously demonstrated that eDNA is involved in mediating cell-cell and cell-surface interactions in *S. oneidensis* MR-1 which are both affected by nucleolytic activity [38]. Surprisingly, flow chamber assays performed by M. Heun demonstrated that $\Delta endA$ deletion mutants are not impaired in biofilm formation under hydrodynamic conditions in terms of surface coverage and colony morphology. Staining of eDNA by DDAO also revealed no differences between biofilms formed by the wild type and the $\Delta endA$ mutant [292]. Conclusively, the results indicate a minor role of EndA under the conditions tested.

It was hypothesized that this may be due to low *endA* expression levels under hydrodynamic biofilm conditions or that the secreted protein is rapidly diluted by the constant medium flow. It was therefore explored whether externally added MBP-EndA would lead to biofilm dispersal, as has been observed with DNaseI treatments [38]. Rather unexpectedly, addition of MBP-EndA did not affect the integrity of flow chamber-grown biofilms, while addition of DNaseI resulted in rapid release of large amounts of biomass (Figure 22A). Accordingly, addition of MBP-EndA only had a minor effect on the integrity of biofilms grown under static conditions (Figure 22B). Also the addition of excess Mg^{2+} did not improve the function of MBP-EndA (data not shown). In contrast to EndA, addition of DNaseI to the same biofilm resulted in a significant loss of surface-associated cells, indicating that MBP-EndA is either not active under biofilm conditions or that biofilm eDNA is not accessible to MBP-EndA. To determine whether biofilm dispersal can be induced by endogenous induction of *endA* expression, biofilm formation was assayed of the wild type and the $\Delta endA$ mutant carrying plasmid pLacTac-*endA*. However, addition of IPTG had no significant effect on biofilm dispersal of *S. oneidensis* MR-1 (Figure 22C). To determine whether eDNA in biofilms is protected from cleavage by EndA, degradation assays were performed with eDNA isolated from planktonic cultures and from static biofilms of the *S. oneidensis* MR-1 wild type (Figure 22D). Notably, a rapid decrease in Gel-RedTM fluorescence in both samples indicated that eDNA, both from planktonic and biofilm cultures can be readily degraded by addition of MBP-EndA. Complete degradation of both eDNA forms was confirmed by agarose gel electrophoresis (data not shown). Conclusively, rather biofilm conditions than specific modifications of biofilm eDNA seem to inactivate EndA or protect eDNA from degradation by EndA.

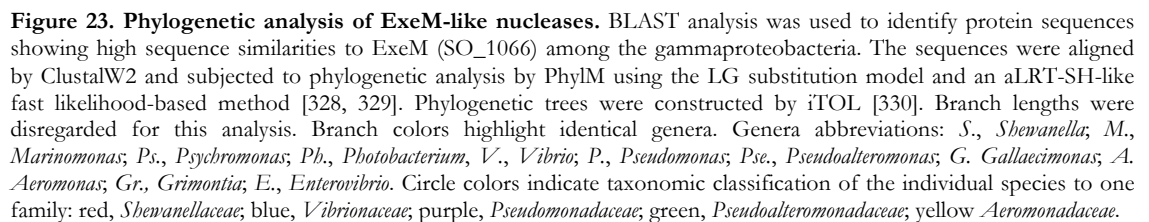
1.6 Molecular characterization of ExeM nuclease activity and transport

S. oneidensis MR-1 harbors three distinct extracellular nucleases that seem to be important under different conditions, including planktonic growth and surface-associated growth. However, specific structural, biochemical, and regulatory characteristics that might attribute specialized functions to extracellular nucleases such as ExeM, remain to be elucidated.

The first section in this chapter focuses on a bioinformatic characterization of ExeM to gain a better understanding of its structure and function (1.6.1). ExeM exhibits a unique domain organization that might confer specific features for its nucleolytic activity, transport and localization, including a putative C-terminal transmembrane domain and a predicted Gly-Gly-C-Term rhombosortase cleavage site. Purification and *in vitro* analyses of a MBP-ExeM fusion indicated that ExeM is a sugar-unspecific endonuclease that requires Ca^{2+} and either Mg^{2+} or Mn^{2+} as cofactors for function (1.6.2. and 1.6.3). Under the conditions tested, immunoblot analyses of truncated variants of ExeM in different cellular (membrane) fractions indicated that ExeM locates primarily in the inner membrane. Furthermore, substitution of the putative rhombosortase cleavage site results in extensive accumulation of ExeM protein in the inner membrane, indicating that this motif has an important role in processing and transport of ExeM (1.6.4). In contrast to MBP-EndA, addition of MBP-ExeM to the medium prior to inoculation strongly inhibited biofilm formation of *S. oneidensis* MR-1, further indicating functional specificity of ExeM to biofilm conditions.

1.6.1 *In silico* analyses of ExeM

ExeM-like proteins with high sequence homologies to SO_1066 can be found in many gammaproteobacteria, especially among *Shewanellaceae*, *Vibrionaceae*, *Aeromonadaceae*, and *Pseudoalteromonadaceae*. Phylogenetic analysis suggests that *Shewanella*-ExeM is most closely related to the corresponding nucleases in *Vibrio* species, whereas ExeM-like nucleases found in other genera of the *Vibrionaceae* family, like *Photobacterium* and *Enterovibrio*, are more distantly related to *Shewanella* ExeM (Figure 23). ExeM-like nucleases in *P. aeruginosa*-strains represent the most distantly related proteins of this analysis. Comparative sequence analysis of ExeM by BLASTP reveals a unique domain organization with partially conserved structural motifs (Figure 24). SignalP 4.0 software identified a putative N-terminal highly hydrophobic signal peptide predicted to be cleaved between position 24 and 25 [323]. Consequently, ExeM seems to be secreted into the periplasm through Sec-mediated cotranslational transport. The N-terminal signal sequence is followed by a domain showing structural homologies to lamin tail domains (LTD) found in eukaryotic nuclear lamins and several uncharacterized proteins from phylogenetically diverse bacteria, and the archaea *Methanosarcina* and *Halobacterium*. In bacteria it occurs mainly with membrane-associated hydrolases of the metallo- β -lactamase, synaptojanin, calcineurin-like phosphoesterase superfamilies, or in secreted or periplasmic proteins associated with oligosaccharide-binding domains or as multiple tandem repeats in a single protein [324, 325]. Mans and coworkers suggest a potential role of prokaryotic LTDs in directing proteins to the membrane or membrane-associated structures [325]. LTDs share a characteristic immuno globulin fold (Ig) formed by a β -sandwich composed of two β -sheets consisting of nine β -strands connected by short loops (Figure 24) [326, 327]. Immuno globulin folds are known to mediate diverse protein-protein and protein-ligand interactions [324].



The LTD domain is followed by a region exhibiting sequence homologies to the oligonucleotide binding structural motif (OB-fold) that is similar to that of a domain of the sugar-nonspecific extracellular nuclease YhcR from *B. subtilis*. YhcR cleaves DNA and RNA endonucleolytically in the presence of Ca^{2+} and Mn^{2+} , but seems to be the major Ca^{2+} -dependent nuclease in *B. subtilis* [331, 332]. Between the putative LTD and YhcR domain and in within the putative YhcR domain of ExeM, two conserved cysteine residues can be found at position 187 and 272, respectively, which might be involved in disulfide bond formation (Figure 24). Furthermore, a number of residues that exclusively reside within the YhcR domain are predicted to compose two generic binding domains: generic binding surface I (residue: 225-227, 235-238, 240, 245-247, 249, 269, 276-278, 285-287) and generic binding surface II (residue: 220, 270, 272, 274). A large domain belonging to the Exonuclease-Endonuclease-Phosphatase (EEP) domain superfamily can be identified adjacent to the C-terminal hydrophobic domains. EEP domains can be found in a diverse set of proteins (including deoxyribonuclease 1) that cleave phosphodiester bonds in nucleic acids, phospholipids and proteins. The EEP domain in ExeM contains two conserved cysteine residues (C650, C670) that might be involved in disulfide bond formation, two predicted metal binding sites (E521, D822) and three residues (H642, N699, H823) that are probably involved in phosphate binding (Figure 24). The putative EEP domain of ExeM is followed by a semi-hydrophobic prolin-rich sequence (position 833-845, PAPVVPPKPQPTP) which is conserved in *Shewanellaceae* (Appendix, Figure 40)

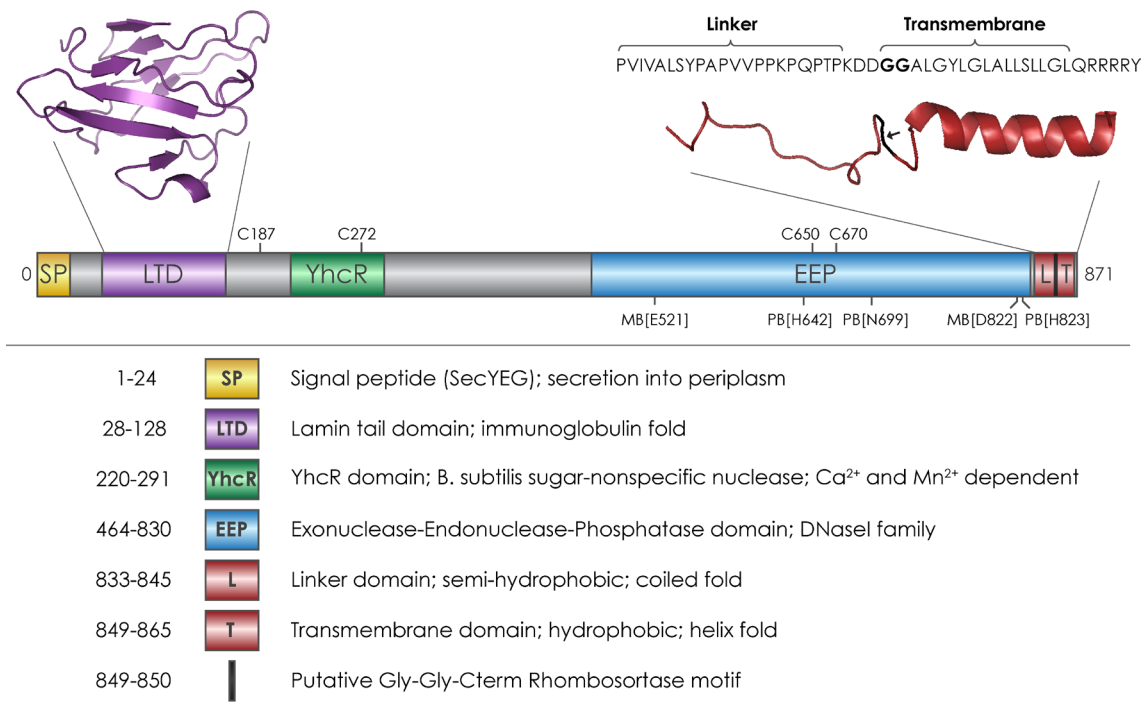


Figure 24. Domain architecture of ExeM. Schematic illustration of conserved domains identified by sequence comparison (BLASTP). Cysteine residues that are potentially involved in disulfide bond formation are indicated on the upper side. Putative metal binding sites (MB) and putative phosphate binding sites (PB) are indicated on the lower side. Three-dimensional protein structure predictions of the putative LTD domain (predicted by Phyre2, Protein Homology/analogy Recognition Engine V 2.0) and the putative linker and transmembrane region (predicted by (PS)2-v2, Protein Structure Prediction Server) are illustrated in violet and red color, respectively. The putative Gly-Gly-Cterm motif is highlighted with a black arrow in the predicted protein structure and with bold letters in the one letter code of the linker and transmembrane region.

but absent in other ExeM-like nucleases such as *V. cholera*-Xds [242]. Peptide structure analysis by (PS)2-v2 predicts a coiled but stretched conformation that might act as a linker between the bulky ExeM protein and the terminal transmembrane domain. It is possible that this region may contain unknown cleavage sites for periplasmic or membrane-associated proteases. The terminal hydrophobic domain (position 849-865, GGALGYLGLALLSLLGL) may direct ExeM to the inner membrane once secreted into the periplasm. Peptide structure analysis by (PS)2-v2 predicts a helical conformation, typical for membrane anchors. The membrane anchor is flanked by a periplasmic DD motif and a cytoplasmic RRRR motif (Figure 24), which might embed it into the membrane in the correct orientation during secretion, according to the positive-inside rule [333-335]. Finally, a Gly-Gly-Cterm motif has been identified in ExeM proteins belonging to *Shewanellaceae*, *Vibrionaceae*, *Aeromonadaceae* and others. Recently, Gly-Gly-Cterm motifs, consisting of a GG motif, a hydrophobic transmembrane helix, and a cluster of basic residues (RRRR), have been predicted by a bioinformatic many-to-one approach and are believed to constitute a processing signal for novel intramembrane serine proteases, named rhombosortases [336]. Thus, putative rhombosortase SO_2504 in *S. oneidensis* MR-1 might be involved in processing, secretion and regulation of ExeM. Notably, the putative C-terminal “linker” region is absent in closely related ExeM-like nucleases found in *Vibrio* species, posing intriguing questions about the role of this region in *Shewanella* (Appendix, Figure 40). ExeM-like nucleases in *P. aeruginosa*-strains lack both the “linker” and the transmembrane region. Consequently, these nucleases do not harbor any Gly-Gly-CTERM motif.

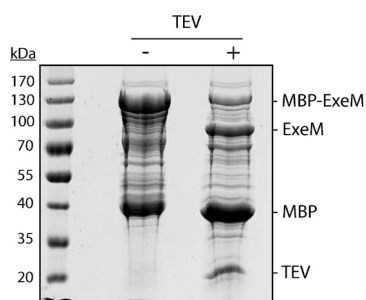


Figure 25. Purification and cleavage of MBP-ExeM. SDS-PAGE of enriched MBP-ExeM after amylose affinity chromatography. TEV protease cleavage was performed to separate ExeM from the MBP protein (+). The molecular weight (kDa) of each band of the ladder is indicated on the left side. Bands representing the different proteins (or fragments) are indicated on the right side.

Apart from the C-terminal regions, ExeM-like nucleases in *Vibrio* species and *P. aeruginosa* share the same domain organization with ExeM in *Shewanella*.

1.6.2 Purification of ExeM

ExeM was purified to investigate its nucleolytic activity *in vitro* including enzymatic characteristics such as metal ion cofactor requirements, sugar-specificity (DNA or RNA), and molecular mechanisms controlling ExeM activity. ExeM is predicted to be localized either in the periplasmic or extracellular space [293, 294]. Thus, ExeM may require oxidizing conditions for disulfide bond formation and proper folding. Additionally, excessive overproduction of an active nuclease in the cytoplasm might result in cleavage of host DNA, making overproduction difficult. Direction of ExeM to the periplasmic space of the host cell (*E. coli*) may therefore be required. Accordingly, cytoplasmic overexpression of His- or Strep-tagged ExeM was not successful, resulting either in arrested growth or very low protein amounts (data not shown). In contrast, fusion of ExeM to maltose binding protein (MBP) MalE, containing a N-terminal Sec signal sequence, yielded high amounts of protein when expressed via the pMAL-P2X vector system (NEB, USA) in strain *E. coli* BL21Star at moderate temperatures (18 – 25 °C). However, overproduction was only successful with truncated versions of ExeM (27-846) missing the N-terminal signal peptide and the C-terminal hydrophobic region. Further, SDS-PAGE analysis of the elution fractions revealed the presence of degradation fragments, including one major fragment with an estimated size similar to the MBP fusion protein. Plasmid pMAL-P2X encodes a linker region (10xN) followed by a Factor Xa cleavage site (IEGR) between the MBP protein and the fusion protein (ExeM). Factor Xa protease digests were performed under various conditions to separate the MBP protein from ExeM. However, cleavage was incomplete and partially unspecific (data not shown). To potentially achieve better cleavage, the Factor Xa site was exchanged with a TEV (tobacco etch virus) protease cleavage site (ENLZFQG) that has been shown to enable efficient and highly specific cleavage with MBP fusions [337]. Overproduction and purification with the newly constructed plasmid pMAL-TEV-ExeM yielded high amounts of MBP-ExeM fusion protein. However, similar to the observations made with plasmid pMAL-P2X, degradation and unspecific cleavage of the MBP protein occurred (Figure 25). Cleaved-off ExeM protein (SDS-PAGE gel fragment) was utilized for antibody generation (α -ExeM). Anion exchange chromatography and gel filtration was performed to further purify both the MBP-ExeM fusion protein and cleaved-off ExeM protein after TEV digestion. Relatively pure protein was obtained, however, ExeM tended to precipitate during the procedure and only small amounts of active nuclease protein were obtained. Thus, MBP-ExeM fusion protein was utilized for most *in vitro* assays (1.6.3).

1.6.3 *In vitro* analyses of ExeM

To investigate the nucleolytic characteristics of ExeM *in vitro*, a similar approach to that described for EndA (1.5.1) was utilized. To this end, the decrease in fluorescence due to the release of DNA-bound Gel-RedTM nucleic acid stain was measured as a function of DNA degradation using the plasmid pBluescript as substrate for most assays. *In silico* characterization (1.6.1) suggested that ExeM contains a large domain belonging to the Exonuclease-Endonuclease-Phosphatase (EEP) superfamily. The most prominent member of this family is DNase I [338]. At physiological pH, the activity of DNase I is highest in the presence of Mg²⁺ and Ca²⁺ metal ions [339]. Accordingly, equimolar amounts of Mg²⁺ and Ca²⁺ (5 mM) were added to the reaction mixture to test for nucleolytic activity of ExeM. DNA degradation in the presence of MBP-ExeM was observed for both circular and linearized plasmid DNA, suggesting that ExeM exhibits endonucleolytic activity

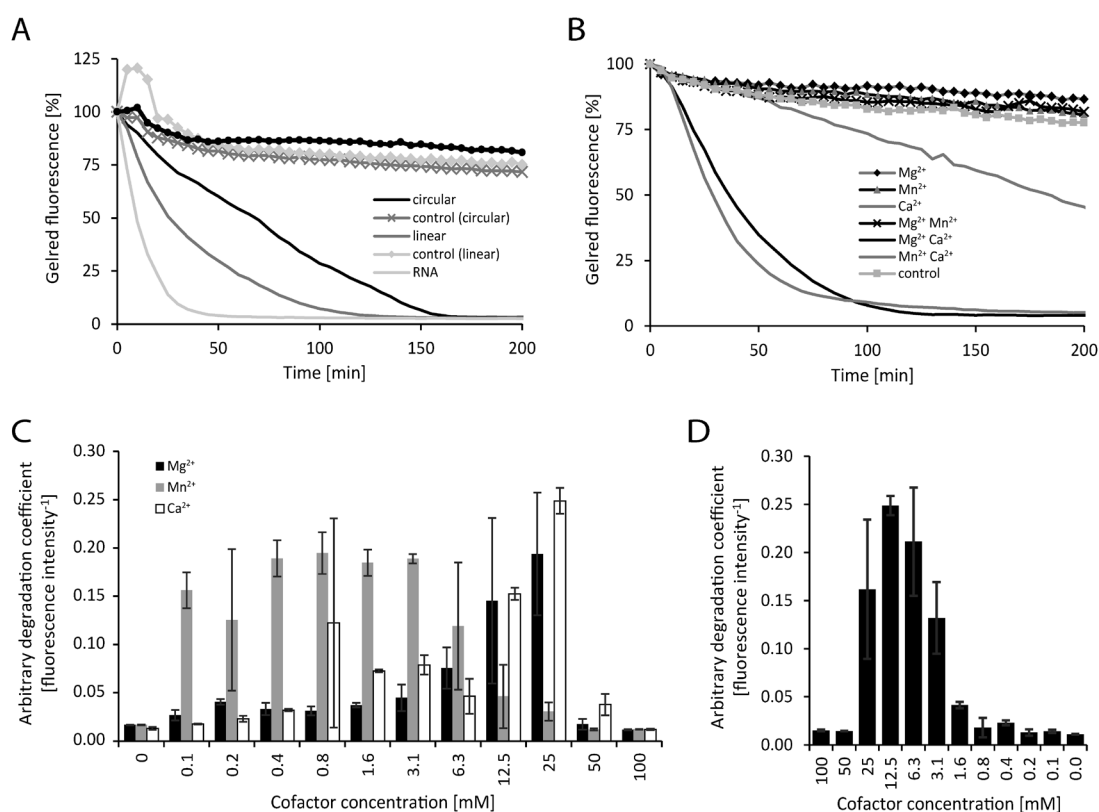


Figure 26. *In vitro* characterization of MBP-ExeM nucleolytic activity. (A) Degradation of pBluescript plasmid DNA (circular and linear; 250 ng) and RNA (1.8 μ g) by MBP-ExeM (8 μ g) as indicated by a loss in fluorescence of nucleic acid stain GelRedTM. The buffer contained 5 mM Mg²⁺ and Ca²⁺ to support ExeM's nucleolytic activity. Control samples contained no MBP-ExeM. The assay was performed in triplicates in two independent experiments. The curves are based on the mean values of one representative experiment. (B) Degradation of pBluescript plasmid DNA (250 ng) by MBP-ExeM (8 μ g) as indicated by a loss in fluorescence of nucleic acid stain GelRedTM. The buffer contained 5 mM Mg²⁺, Mn²⁺, or Ca²⁺ (or combinations) to support ExeM's nucleolytic activity. The control samples contained no additional metal ions. The assay was performed in triplicates in two independent experiments. The curves are based on the mean values of one representative experiment. (C) Comparison of pBluescript plasmid DNA (250 ng) degradation by MBP-ExeM (8 μ g) in the presence of a range of concentrations of one cofactor, at which the second cofactor remains at a constant concentration of 5 mM or at equimolar concentrations of Mg²⁺ and Ca²⁺ (D). The arbitrary degradation coefficient in C and D represents the reciprocal mean value of the fluorescence intensity (in % of the initial value) of nucleic acid stain GelRedTM after 150 minutes (time point at which the fluorescence of at least one sample approached 0). Error bars represent standard deviations of two independent experiments performed each at least in triplicates.

(Figure 26A). RNA was also readily degraded by MBP-ExeM, suggesting sugar-unspecific cleavage by ExeM. To further explore the role of other potential cofactors for ExeM's nucleolytic activity, Mg^{2+} , Ca^{2+} , Mn^{2+} , Zn^{2+} , Ni^{2+} , and Cu^{2+} were tested in all possible dual combinations to support degradation of circular plasmid DNA by MBP-ExeM (Appendix, Table 13). The results indicated that in the presence of Ca^{2+} , both Mg^{2+} and Mn^{2+} support DNA degradation to a similar degree (Figure 26B). In the absence of other metal ions, Ca^{2+} weakly supports degradation by MBP-ExeM. Under the conditions tested, none of the other metal ions supported DNA degradation by MBP-ExeM. Taken together, Ca^{2+} seems to be indispensable for ExeM's nucleolytic activity, whereas either Mg^{2+} or Mn^{2+} can function as second cofactor. To further determine optimal cofactor concentrations required for ExeM's nucleolytic activity, each cofactor was tested in a range of concentrations from 0.1 mM to 100 mM at which the second cofactor (Ca^{2+} was tested in combination with Mg^{2+}) was kept constant at 5 mM (Figure 26C). Due to high variances between the replicates only a rough estimation can be given, however, the results indicated that DNA degradation by MBP-ExeM is highest at a concentration of approximately 6 – 25 mM for Mg^{2+} , 0.1 – 6 mM for Mn^{2+} , and 12 – 25 mM for Ca^{2+} . Thus, Mg^{2+} and Ca^{2+} supported DNA degradation by ExeM in a very similar range of concentrations, whereas Mn^{2+} supported ExeM's function at much lower concentrations. An additional dilution row with equimolar concentrations of Mg^{2+} and Ca^{2+} was generated to determine the optimal concentration of the combination of both cofactors for further assays. The results suggest that DNA degradation is highest at an equimolar concentration of approximately 12.5 mM (Figure 26D).

Defining one unit of enzyme activity as the amount of MBP-ExeM required to completely degrade one μ g of pBluescript vector within 10 minutes at 30 °C in reaction buffer supplemented with 12.5 mM Mg^{2+} and 12.5 mM Ca^{2+} , the specific activity of purified MBP-ExeM was approximately 3 U/mg.

1.6.4 Processing and transport of ExeM

ExeM contains a N-terminal signal sequence for Sec secretion, a putative linker region, a predicted C-terminal transmembrane anchor, and a putative Gly-Gly-C-Term rhombosortase cleavage site (1.6.1). Earlier analyses of the membrane and subcellular proteomes detected ExeM both in the inner and the outer membrane, whereas DNA degradation assays indicated weak nucleolytic activity of ExeM in culture supernatant (see section 1.2.1). Thus, transport across the cell envelope as well as the final destination of ExeM remains controversial.

To gain a better understanding of the role of the C-terminal hydrophobic regions and the putative cleavage site, truncated variants of ExeM were constructed for episomal expression in *S. oneidensis* MR-1 (Figure 27). The pBBMT-kan vector system was utilized for arabinose-inducible overproduction of native ExeM (ExeM[full]), ExeM lacking the putative linker region (ExeM[Δ linker]), ExeM lacking both the putative linker and transmembrane region (ExeM[Δ linker-TM]), and ExeM harboring a GG-to-AA (G849A; G850A) amino acid substitution (ExeM[GG-AA]) (Figure 27). To rule out possible interferences with natively expressed nucleases, the nuclease deletion mutant (Δ endA Δ exeS Δ exeM) was utilized for all following assays, if not stated otherwise.

DNA degradation assays with supernatants of planktonic cultures were performed to determine which strains exhibit extracellular nucleolytic activity. Detection of nucleolytic activity would indicate efficient transport of native or truncated ExeM, whereas a lack of DNA degradation would

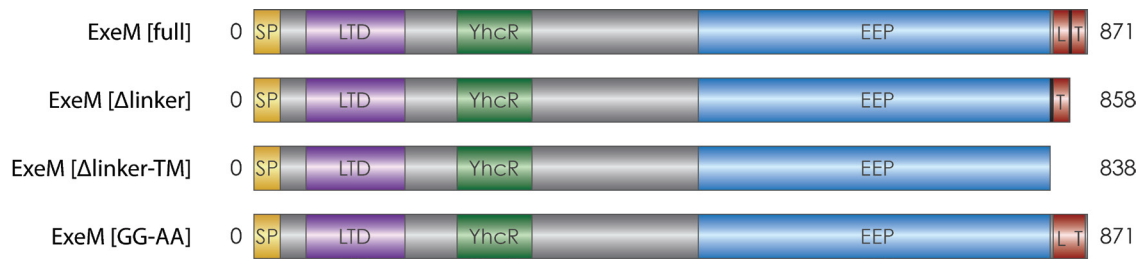


Figure 27. ExeM constructs for episomal expression in *S. oneidensis* MR-1. Truncated variants of ExeM were constructed lacking the putative linker region (ExeM[Δlinker]; Δ833-845), lacking both the putative linker and transmembrane region (ExeM[Δlinker-TM]; Δ833-865), and ExeM harboring a GG-to-AA amino acid substitution in the putative linker region (ExeM[GG-AA]; G849A and G850A). ExeM[full] represents the native full-length protein of ExeM. Numbers indicate the proteins lengths (amino acids) of each construct.

indicate suppression of ExeM transport across the cell envelope. However, neither strains overexpressing native ExeM nor strains overexpressing truncated variants of ExeM generated extracellular nucleolytic activity (data not shown). In fact, DNA molecules (both linear and circular DNA) were shown to remain completely stable in culture supernatants without any indications of cleavage or degradation, even after adjustment of optimal metal ion cofactor concentrations. Immunoblot analysis of ExeM and truncated variants demonstrated that all constructs were stably produced. The results indicate that expression levels of *exeM* do not positively correlate with extracellular nucleolytic activity in planktonic culture supernatants of *S. oneidensis* MR-1.

To further investigate ExeM processing and transport across the cell envelope, immunoblot analysis was performed on different cellular fractions. To this end, ExeM and truncated variants were overproduced in planktonic cultures in exponential growth phase. Membrane fractions were isolated and purified by a sarkosyl-based fractionation protocol according to Brown and coworkers and the periplasm was prepared using osmotic shock according to Ross and coworkers [294, 340]. The periplasmic fraction and the supernatant was approximately concentrated 10-fold by filter centrifugation. Detection of PomB and MtrB-Strep in the inner and outer membrane, respectively, demonstrated efficient separation of both fractions (Figure 28). Notably, the protein contents of all samples within each fraction were adjusted to the same level but for technical reasons it was not possible to adjust equal protein levels within different fractions. Thus, signal intensities can only be compared between samples of one fraction.

The results indicate that ExeM localizes at least transiently to the inner membrane (Figure 28A). Surprisingly, constructs lacking the C-terminal hydrophobic regions (ExeM[Δlinker] and ExeM[Δlinker-TM]) were similarly detected in the inner membrane. However, signal intensities were mostly weaker than those of full-length ExeM, indicating that the hydrophobic regions contribute to the localization in the inner membrane. No bands were visible for any of the constructs in the periplasmic fraction, in the outer membrane fraction, or the supernatant, indicating that ExeM primarily localizes to the inner membrane. Signal intensities of ExeM[GG-AA] were strongly increased compared to full-length ExeM, suggesting that substitution of the putative rhombosortase cleavage site suppresses processing and causes accumulation of ExeM in the inner membrane.

To examine the effect of putative rhombosortase gene SO_2504 on the localization and accumulation of ExeM in the different fractions, full-length ExeM was overproduced in a

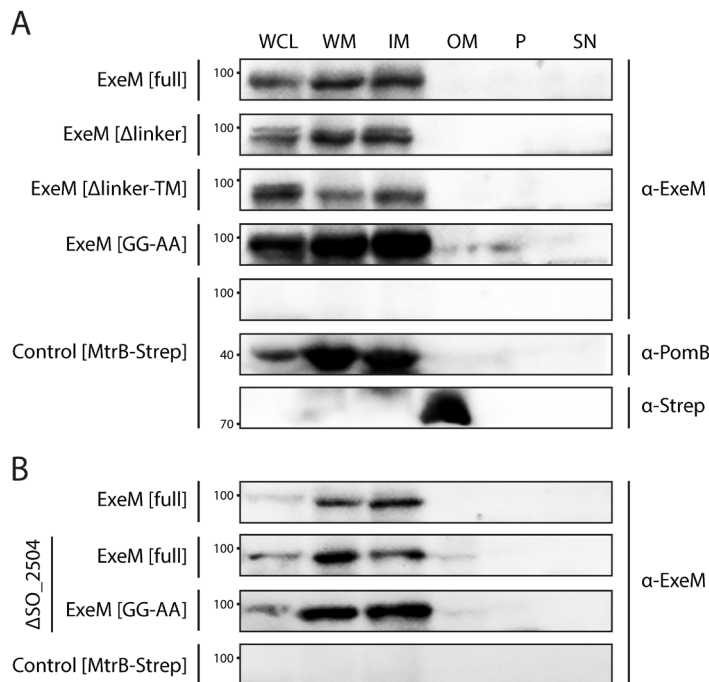


Figure 28. Localization of full-length ExeM and truncated ExeM constructs in various cellular fractions of *S. oneidensis* MR-1. Immunodetection of ExeM (α -ExeM antibody), PomB (α -PomB antibody), and MtrB-Strep (α -Strep antibody) in the whole cell lysate (WCL), the whole membrane fraction (WM), the inner membrane fraction (IM), the outer membrane fraction (OM), the periplasmic fraction (P), and the cell-free culture supernatant (SN). Full-length ExeM and truncated variants were overproduced in the $\Delta endA \Delta exeS \Delta exeM$ nuclease mutant (A) or the ΔSO_{2504} mutant (B). The $\Delta endA \Delta exeS \Delta exeM$ nuclease mutant overproducing MtrB-Strep was utilized as control. Membrane fractions were isolated by a sarkosyl-based fractionation method as described previously [294].

ΔSO_{2504} mutant. However, deletion of gene *SO_2504* did not result in a drastic increase of ExeM levels in the inner membrane as observed for the wild-type strain overproducing ExeM[GG-AA]. If any, only a minor increase of ExeM levels was observed. Additionally, ExeM[GG-AA] was overproduced in the ΔSO_{2504} mutant to test for cumulative effects of both mutations, but immunoblot analysis indicated similar or even lower levels of ExeM[GG-AA] in the ΔSO_{2504} mutant compared to the wild type strain (high variances between replicates). Thus, the results may indicate that putative rhombosortase *SO_2504* has only minor if any effect on localization and accumulation of ExeM in different fractions. However, additional experiments are required to further elucidate the role of *SO_2504* in processing and transport of ExeM (see section 1.9).

1.6.5 Effect of ExeM on biofilm formation

Deletion of *exeM* in *S. oneidensis* MR-1 has been shown to result in reduced biofilm formation under static conditions, and indicated that it may be required for the structural integrity and modulation of the biofilm matrix under these conditions [241]. To further investigate the effect of ExeM on biofilm formation, purified MBP-ExeM was added to biofilms formed under static conditions in microtiter plates. Addition of MBP-ExeM to the medium prior to inoculation of the culture, resulted in inhibition of biofilm formation, as indicated by a reduction of approximately 60 % of the total biomass compared to the untreated control after 24 hours of incubation (Figure 29A). To rule out that the observed effect was due to the glycerol that was present in the MBP-ExeM buffer, the same volume of buffer containing 20 % of glycerol was added to control cultures. Notably, no effect of glycerol on biofilm formation was observed under the conditions tested. To further determine whether biofilm dispersal can be induced by addition of MBP-ExeM to pre-existing biofilms, the same amount of purified MBP-ExeM (0.025 U) was added to 24 hour-old biofilms.

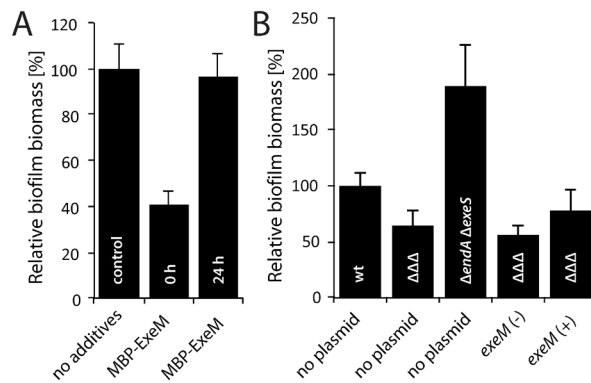


Figure 29. Effect of exogenously added MBP-ExeM and endogenously induced *exeM* on biofilm formation. (A) Biofilm formation (static conditions) of the *S. oneidensis* MR-1 wild type after addition of MBP-ExeM (0.025 U) compared to an untreated control culture. MBP-ExeM was added prior to inoculation (0 h) or after 24 hours of incubation (24 h; and incubated for further 2 hours after addition). The values are means of three replicates. Error bars represent standard deviations. (B) Biofilm formation of the wild type, the $\Delta endA \Delta exeS \Delta exeM$ mutant ($\Delta\Delta\Delta$), the $\Delta endA \Delta exeS$ mutant, and the $\Delta\Delta\Delta$ mutant overexpressing *exeM* (pBBMT-kan-*exeM*) in the absence (-) or presence (+) of L-arabinose. The strains were grown for 24 hours in microtiter plates. To induce overexpression of *exeM* from pBBMT-kan-*exeM*, L-arabinose was added prior to inoculation. Error bars represent the standard deviations of two independent experiments performed each at least in triplicates.

After two hours of incubation, the total biofilm biomass was determined. However, no significant release of biomass could be detected, indicating that exogenously added ExeM protein does not induce biofilm dispersal, in contrast to the observations made for DNaseI (1.5.3) (Figure 29A). Notably, analogous observations were made for a strain lacking all extracellular nucleases ($\Delta endA \Delta exeS \Delta exeM$), indicating that exogenously added ExeM protein cannot complement the mutant phenotype (data not shown). However, additional experiments (e.g. under hydrodynamic conditions) are required to further elucidate the effect of exogenously added ExeM on biofilm formation.

To determine the effect of endogenous induction of *exeM* expression on biofilm formation, the nuclease triple mutant was equipped with plasmid pBBMT-kan-*exeM* for episomal overexpression of *exeM* in that strain. The *S. oneidensis* MR-1 wild type, the triple nuclease mutant, and strain $\Delta endA \Delta exeS$ that harbors only *exeM*, were assayed in parallel as reference strains. Biofilm formation of strain $\Delta endA \Delta exeS$ was strongly increased under the conditions tested, indicating that in the absence of EndA and ExeS, ExeM stimulates biofilm formation under static conditions (Figure 29B). Induction of *exeM* expression in the triple nuclease mutant resulted only in a minor increase in biofilm formation after 24 hours, indicating that simple overexpression of *exeM* is not sufficient for complementation of the $\Delta endA \Delta exeS$ phenotype. Notably, overexpression of *exeM* in the wild type had no effect on biofilm formation under static conditions (data not shown). Thus, ExeM functioning in biofilms might require coordinated coexpression of other unknown factors, possibly involved in processing and transport of ExeM.

Based on these results it can be concluded that biofilm formation is inhibited in the presence of purified MBP-ExeM (when present prior to inoculation), whereas overexpression of *exeM* weakly supports biofilm formation. Further experiments are required to better understand the role of ExeM in biofilm formation and to identify unknown factors that are required for ExeM functioning.

DISCUSSION

1.7 Analyses of λ So prophage induction in biofilms

The ubiquitous presence of prophages in bacterial genomes has numerous implications with respect to host physiology and ecology, which we are just beginning to understand. Since biofilms are the predominant form of bacterial existence, the question arises to what extent prophages impact biofilm formation. For different species, including *S. oneidensis* MR-1, it has been suggested that prophage-induced lysis promotes biofilm formation, *e.g.* by the release of matrix components such as eDNA [38, 218, 237]. To my knowledge, this is the first study in which high-resolution CLSM was utilized to elaborate the spatiotemporal induction of a prophage during biofilm formation at the single cell level and to visualize the heterogeneity of this process within the biofilm community. The results strongly suggest that λ So induction in *S. oneidensis* MR-1 mainly occurs in upper biofilm layers in a subpopulation of filamentous cells. I could show that induction and, ultimately, cell-lysis and eDNA accumulation are strictly controlled by RecA and likely correlate with intracellular iron levels. Additionally, the results indicate that surface-associated growth of *S. oneidensis* MR-1 strongly requires a defense system against oxidative stress and tight control of iron uptake; however, levels of free intracellular iron and not hydrogen peroxide seem to limit induction and production of λ So on *S. oneidensis* MR-1 biofilms.

1.7.1 RecA-mediated induction of prophage λ So in biofilms

The results of this study suggest that λ So prophage-mediated lysis of a subpopulation of cells in *S. oneidensis* MR-1 biofilms is controlled by RecA, indicating that DNA damage represents an indirect trigger for matrix production and biofilm maturation. Correspondingly, stress-inducing factors such as antibiotics have been demonstrated to enhance biofilm formation of different species. For example, subinhibitory concentrations of aminoglycoside antibiotics have been shown to induce biofilm formation of *P. aeruginosa* and *E. coli* by altering c-di-GMP levels [341]. A variety of other antibiotics have been shown to increase biofilm formation and virulence of *P. aeruginosa* [342]. Linares and coworkers suggest that stress-inducing antibiotics can be beneficial for the behavior of susceptible bacteria in natural environments and may act as signaling molecules that regulate the homeostasis of microbial communities [342]. In addition, DNA replication inhibitors such as hydroxyurea or nalidixic acid have also been shown to induce biofilm formation of *P. aeruginosa* [343, 344]. Recent reports have also demonstrated the involvement of the SOS response in stress-inducible biofilm formation and the regulation of motility of *P. aeruginosa* [345, 346]. Interestingly, addition of the DNA-damaging antibiotic ciprofloxacin increased both biofilm formation and motility [346].

Involvement of the SOS response in biofilm formation has also been described for *Listeria monocytogenes*, which depends on cell division inhibitor YneA that is under control of RecA [347]. Conclusively, these results indicate that bacteria use environmental stresses as stimuli to induce biofilm formation. Moreover, DNA damage seems to represent a common trigger during biofilm formation that induces the SOS response, which in turn seems to regulate a variety of processes

being important for biofilm formation. Accordingly, in this study it has been demonstrated that λ So prophage induction and eDNA release is under control of the RecA-mediated SOS response in *S. oneidensis* MR-1. To date, this study describes the first example of RecA-controlled prophage induction that is beneficial for the biofilm community. However, similar RecA-dependent mechanisms may exist in many other species as well. Remarkably, about two third of all bacteria contain at least one prophage and prophage DNA may constitute up to 20 % of bacterial genomes [232, 233]. For example, *E. coli* contains nine cryptic prophages that have been shown to provide multiple benefits to the host for surviving adverse environmental conditions [233]. Moreover, most prophages in environmental isolates are inducible by DNA-damaging agents such as mitomycin C or UV light [232, 348-351]. Stopar and coworkers investigated the abundance of lysogens in microbial communities in Adriatic sea and demonstrated that 71 % of the bacterial isolates contained mitomycin C-inducible prophages. In earlier studies, Jiang and Paul determined frequencies of approximately 40 % of inducible prophages in microbial communities in the Atlantic Ocean (USA) [349, 352]. The fact that such a high percentage of prophages respond to DNA-damaging agents indicates the existence of common physiological and molecular principles for the control of prophage induction, which might also apply during biofilm growth of the corresponding host bacteria. The RecA-mediated SOS response may be involved in many of the induction mechanisms that remain to be elucidated. RecA has probably evolved very early and is one of the highest conserved proteins in bacteria [308, 353]. Thus, mechanisms that mediate prophage induction of lambdoid and related phages may predominantly involve RecA-mediated phage repressor cleavage. However, alternative pathways for the induction of lambdoid phages have also been identified that exclude the RecA-mediated SOS response [354, 355]. Nevertheless, the results of this study clearly demonstrate that induction of prophage λ So is strictly RecA-dependent in *S. oneidensis* MR-1 under the conditions tested, both in planktonic cultures and in biofilms. Induction of the lysis operon was completely suppressed in $\Delta recA$ mutants under all conditions tested, indicating that *S. oneidensis* MR-1 lacks bypass-mechanisms that may directly control the induction of lysis genes instead of the classical induction pathway via the lambda repressor cI. Unexpectedly, $\Delta recA$ deletion mutants did not phenocopy $\Delta \lambda$ So deletion mutants with regard to biofilm biomass and biofilm architecture. Hypothetically, this effect may be due to secondary effects of the $\Delta recA$ mutation or due to the inability of $\Delta recA$ mutants to repair double strand breaks. As previously suggested, cell death might occur more often in $\Delta recA$ mutants during biofilm growth [356]. In *S. oneidensis* biofilms, increased cell lysis in $\Delta recA$ deletion mutants might trigger the release of biofilm promoting factors such as eDNA, which might partially complement the loss of λ So prophage-induced lysis [356].

1.7.2 Filamentous cells in biofilms

CLSM analysis of *P λ cro::venus* biofilms demonstrated that λ So induction is mainly restricted to filamentous cells, a commonly occurring but so far uncharacterized phenotypic variant in *S. oneidensis* MR-1 biofilms. The occurrence of filamentous growth indicates that these cells suffer from increased levels of DNA damage, the trigger for RecA. Elongated cell morphologies in response to DNA damage have been observed by Gates already in the early nineteen thirties [357]. Later, they were shown to be a consequence of cell division inhibition while cellular growth proceeds, a process that is predominantly regulated by the RecA-mediated SOS response. In addition to simply gaining time for DNA repair prior to cell division, filamentation can also

represent a fitness advantage in stressful environments or increase virulence [for review: 307]. In microbial biofilms, the occurrence of filamentous cells appears to be a common but so far not well-understood phenomenon. In *L. pneumophila* biofilms, filamentous growth appears to be temperature-dependent but independent of the RecA-mediated SOS response. At 37°C, *L. pneumophila* was shown to form mat-like biofilms that consisted of filamentous bacteria, whereas biofilms that were grown at 25°C, were composed of rod-shaped cells [358]. Thus, filamentation of *L. pneumophila* may represent a response to body temperature and an adaption for intracellular survival. Accordingly, invasion of Vero cells by multiple species of *Legionella* has been shown to be accompanied filamentous growth [359]. Similar observations have been made for other pathogens such as *Mycobacterium tuberculosis* and *S. enterica* serovar Typhimurium that seem to use filamentous growth as a strategy to survive phagocytosis by macrophages. Filamentation is likely controlled by the SOS response in both organisms; however, direct evidence for this hypothesis is still missing [360-362]. In *P. aeruginosa* biofilms, cell elongation correlates with nutrient deprivation under aerobic conditions and is triggered by nitric oxide production during anaerobic respiration [363, 364], two processes that might increase DNA damage and induce the SOS response. Analogously, formation of knitted chains in *L. monocytogenes* biofilms is controlled by SOS response factor YneA in response to oxidative stress [347, 365]. Filamentous cells were also observed in environmental biofilm communities attached to microbial fuel cells, indicating that these morphologies might play a role in naturally occurring mixed electrogenic communities [366]. Correspondingly, artificially induced elongation of *S. oneidensis* MR-1 cells was shown to enhance microbe-electrode interactions in microbial fuel cells [367].

To date, the exact role of filamentous growth in *S. oneidensis* MR-1 biofilm formation remains to be elucidated. It is still unclear whether filamentous growth itself is required for normal biofilm formation, or whether it occurs as a side effect of the SOS response, prior to λ So-induced lysis and eDNA release. Furthermore, it would be interesting to determine the role of filamentous cells in natural environments of *S. oneidensis* MR-1 and accordingly under diverse environmental conditions. For this purpose, analysis of biofilm formation of mutants that specifically suppress filamentation would be a straightforward approach to gain more insights in the role of this phenotypic variant. Qui and coworkers proposed that gene SO_4604 encodes a SulA-like protein possibly involved in RecA-regulated cessation of cell division [368]. To determine whether SO_4604 is required for filamentous growth, I constructed an in-frame deletion mutant in gene SO_4604 and analyzed the response to mitomycin C. Unexpectedly, the cell length distribution after mitomycin C treatment of strain Δ SO_4604 did not differ significantly in comparison to the wild type, suggesting that SO_4604 has another yet unknown function and is not under control of the RecA-mediated SOS response (data not shown). In contrast, filamentous growth in response to mitomycin C treatment was significantly suppressed in Δ recA mutants. However, complete suppression of filamentation was not attained, indicating the existence of other factors that contribute to this phenotype. Similarly, filamentous growth in *S. oneidensis* MR-1 biofilms was strongly reduced but not completely absent in biofilms of the Δ recA mutant. To identify additional factors that mediate filamentation, transcriptomic and proteomic analyses of filamentous cells isolated from biofilms may be conducted in future experiments.

1.7.3 The role of iron

The results of this study suggest a correlation between λ So prophage-mediated cell lysis and environmental iron levels in *S. oneidensis* MR-1 biofilms. Iron is present in almost all living organisms where it is required for many essential cellular functions, mostly as an integral biological cofactor. Unique chemical characteristics, including the versatility oxidation states, reduction potential, coordination number, spin state, ligand characteristics, and structure, may explain the significance of this transition metal in biological systems [369]. Moreover, iron is one of the most abundant elements in earth's crust and therefore easily accessible for living organisms. However, the role of iron in biological systems is a paradox. Although it is required for many cellular functions, it can also catalyze deleterious oxidations of biomolecules, including proteins, DNA, and lipids [370].

Iron has been shown to affect biofilm formation of multiple bacterial species [97, 371-378]. However, exact regulatory pathways and physiological roles of iron during biofilm formation remain mostly unknown and likely vary among the species. Iron limitation has been demonstrated to induce biofilm formation in *L. pneumophila*, *S. aureus* and *S. mutans* [371-373], but inhibits this process in *E. coli* and *V. cholera* [374, 375]. However, depending on the concentration, the effect of iron on biofilm formation can be completely oppositional for each species. In *P. aeruginosa*, biofilm assays with varying concentrations of ferric iron indicated that low concentrations (5 μ M) stimulate biofilm formation whereas higher concentrations (100 μ M) inhibit biofilm formation [376]. Furthermore, it was shown in another study that high concentrations of iron suppress eDNA release and structural biofilm development [377]. Complete removal of iron by chelation or addition of excess iron to non-physiological concentrations was even shown to disrupt *P. aeruginosa* biofilms or to induce dispersal [97, 378]. Thus, iron seems to impact *P. aeruginosa* biofilm formation in a strictly concentration-dependent fashion. Presumably, this applies similarly for other species, making it unsuitable to generalize or trivialize the effect of iron on biofilm formation.

The ability of *S. oneidensis* MR-1 to perform dissimilatory reduction of ferric iron indicates that it occurs in habitats rich of insoluble iron oxides and has made it a model organism in this field of research. Although surface-associated growth can be assumed to be the predominant mode of existence in these habitats, little is known about the impact of iron on biofilm formation of *S. oneidensis* MR-1. In fact, this is the first study demonstrating that physiological concentrations of iron strongly impact *S. oneidensis* MR-1 biofilm development and eDNA release. Addition of 20 μ M or 100 μ M of ferrous iron amplified structural biofilm development into complex three-dimensional cell clusters and increased λ So prophage-induction and eDNA accumulation. Given that bacteria respond differentially to environmental iron levels, this may be a consequence of individual metabolic requirements of iron for each organism, including the repertoire of iron metallo-enzymes involved in specific metabolic pathways [374]. As mentioned above, *S. oneidensis* MR-1 is capable of utilizing multiple organic and inorganic alternative terminal electron acceptors. For this respiratory versatility *S. oneidensis* MR-1 requires a large array of iron-containing cytochromes [269]. Thus, the ability to grow on diverse redox-active surfaces might simultaneously account for a high demand for iron. Accordingly, a transcriptome analyses performed in our lab indicated induction of genes involved in iron uptake in response to early surface-associated growth, suggesting elevated iron uptake under biofilm conditions [286]. As a consequence, increased intracellular levels of free iron may trigger oxidative stress, resulting in elevated levels of DNA damage that ultimately induce λ So prophage induction in a subpopulation of cells (Figure 30). This effect of iron might be augmented by the lack of an inducible manganese import system (MntH) in

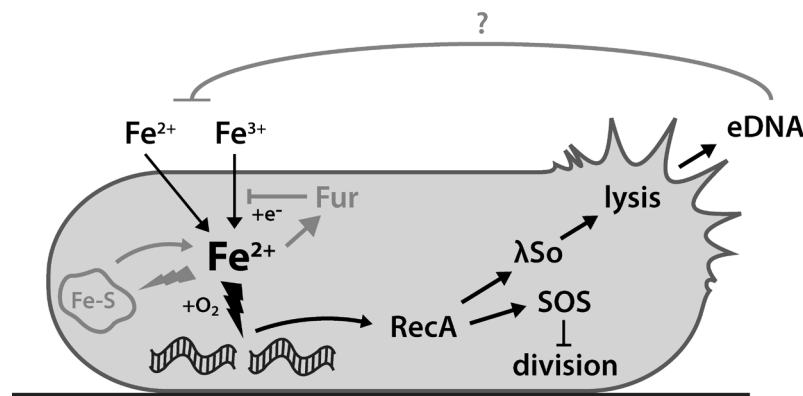


Figure 30. Schematic model of RecA-controlled λ So prophage induction, eDNA release and filamentous growth in response to ferrous iron-induced DNA damage. Ferrous iron is either directly acquired from the environment, or taken up as ferric iron and subsequently reduced to ferrous iron within the cell. Intracellular iron levels negatively regulate ferric iron uptake via Fur. In the presence of molecular oxygen and elevated levels of free iron, DNA is damaged, possibly by a Fenton-independent reaction. Iron-sulfur clusters subjected to oxidative damage might release additional iron. DNA damage is recognized by RecA, which induces the SOS response and the lytic cycle of phage λ So. Induction of prophage λ So ultimately leads to the host cell's lysis resulting in eDNA release, whereas filamentous growth of the host cell occurs as a consequence of inhibition of cell division by the SOS response. Chelation of divalent cations by eDNA might reduce free iron levels and protect against oxidative stress.

S. oneidensis MR-1 [310]. Accumulation of reduced manganese (Mn^{2+}) has been shown to provide bacteria with increased resistance against radiation and oxidative stress [379]. Bacteria such as *Deinococcus radiodurans* resist high levels of gamma-radiation by limiting intracellular iron concentrations and accumulating manganese, whereas bacteria such as *S. oneidensis* MR-1 and *P. putida* accumulate high levels of iron and low levels of manganese, and thus show a higher sensitivity to radiation and oxidative stress [310, 379].

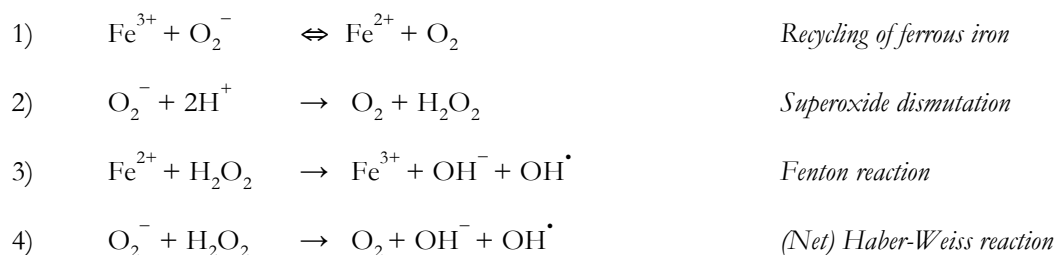
Expression profiles of *S. enterica* serovar Typhimurium suggest that the lag phase involves transient accumulation of iron and oxidative stress [380]. Cells in lag phase might therefore adapt their physiological status to new environmental conditions similarly to the response of cells during early surface contact. In *S. oneidensis* MR-1, significant expression of *tonB* (SO_3670) was observed during early phases of biofilm formation, as indicated by fluorescence of Venus expressed from an episomal promoter fusion of the putative *tonB* promoter region and *venus*. In contrast, no fluorescence was detected in 24 hour-old biofilms. The results confirm the transcriptome data of Gödeke and coworkers and indicate that ferric iron uptake is repressed at later stages, possibly to control iron-induced oxidative damage [286]. In agreement with this hypothesis, levels of λ So prophage induction have been observed to decrease in late phases of biofilm development.

Extracellular DNA has been shown to chelate divalent cations in *P. aeruginosa* biofilms [198]. Although chelation by eDNA has only been demonstrated indirectly for Mg^{2+} , Ca^{2+} , Mn^{2+} , and Zn^{2+} , binding of ferrous iron to eDNA might similarly occur under natural conditions. Thus, another possible explanation for the decrease in prophage induction during later phases of biofilm formation could be that extensive accumulation of eDNA may limit oxidative stress, DNA damage, and λ So prophage induction by chelation of free iron. Consequently, production of a biofilm matrix that consists of significant amounts of eDNA may help to reach a balance between prophage-induced lysis and protection of the biofilm community from detrimental effects of free iron. Accordingly, biofilm formation has been shown to protect bacteria from oxidative stress in

comparison to the planktonic lifestyle [12]. Taken together, a negative feedback-loop may balance iron-stimulated eDNA release and iron-mediated oxidative stress by chelation of free iron by eDNA (Figure 30). However, this hypothesis needs to be evaluated in future experiments. In addition to eDNA, other matrix components, such as exopolysaccharides, may also be involved in binding of divalent cations, as has been shown for the exopolysaccharide alginate from *P. aeruginosa* biofilms [381]. Generally, chelation of metal cations is thought to occur by attraction to the negative charges carried by many exopolysaccharides and the phosphate backbone of eDNA molecules, resulting in neutralization of the net charge of the biofilm matrix [382].

In natural habitats of *S. oneidensis* MR-1, reduction and solubilization of solid iron oxides likely results in locally increased ferrous iron concentrations in proximity to the substratum [383]. This would be expected to enhance λ So prophage induction and eDNA accumulation, as has been observed in the presence of additional ferrous iron in flow chamber biofilms in this study. Accordingly, Xu and coworkers observed induction of λ So genes during growth of *S. oneidensis* MR-1 on Fe-nanoparticle-decorated anodes in microbial electrolysis cells, indicative of λ So prophage-mediated cell lysis [384]. In contrast, in flow chamber-grown biofilms, oxygen and iron levels are presumably highest in the media and decrease within the depth of the biofilm. Teal and coworkers demonstrated that *S. oneidensis* MR-1 biofilm structures stratified with respect to oxygen and nutrients as a function of size. Local microenvironments were shown to be quite distinct within biofilm structures and oxygen and nutrient concentration decreased rapidly within the depth of large biofilm structures [279]. Accordingly, λ So prophage induction and eDNA accumulation was mainly observed to occur in upper biofilm layers. Analogously, filamentous growth was observed to occur mainly in the upper layers of the biofilm. In filamentous cells, the nutrient collection surface is enlarged while the surface to volume ratio remains similar [363]. Hence, filamentous growth itself might indirectly contribute to an increase in intracellular iron levels (forming a positive feedback loop) and thereby triggering DNA damage and further filamentous growth. Moreover, iron-induced DNA damage might be enhanced by the release of additional iron from iron-sulfur clusters that were damaged by oxidative stress (Figure 30) [385]. These processes might, at least in part, elicit the observed heterogeneity in *S. oneidensis* MR-1 biofilms.

In addition to biofilm formation at solid surfaces, pellicle formation at liquid-air interfaces represents another important community lifestyle. Recently, iron levels have been shown to strongly impact pellicle formation of *S. oneidensis* MR-1 [382]. Initially, transcriptome analyses indicated increased expression of iron uptake proteins in comparison to planktonic cells, as has been observed for early surface-attached cells in our lab [286, 386]. Based on this observation, Yuan and coworkers further investigated the role of iron in pellicle formation and found that small amounts of ferrous iron are essential for pellicle formation, but presence of over-abundant ferrous or ferric iron led to pellicle disassociation [382]. Strikingly, under such conditions *S. oneidensis* MR-1 switched to the biofilm lifestyle to perform dissimilatory anaerobic respiration on insoluble iron oxide substrates. Yuan and coworkers conclude that biofilm formation and anaerobic respiration is metabolically less costly to maintain, although pellicle lifestyle allows for better oxygen rates [382]. Thus, iron seems to represent an important signal for biofilm formation of *S. oneidensis* MR-1. In good agreement with this conclusion, this study demonstrates increased structural biofilm formation and eDNA accumulation in response to elevated iron levels at physiological concentrations. Notably, we primarily utilized ferrous iron throughout this study, however, spontaneous oxidation will have produced significant amounts of ferric iron over time, and thus a clear distinction between the effects of both forms was not possible. However, addition of ferric



iron had similar effects on structural development of flow chamber-grown biofilms, indicating that both forms of iron have analogous effects with regard to λ So prophage induction and eDNA release.

1.7.4 Iron-mediated oxidative stress

A combination of genetic, physiological, and fluorescence microscopy approaches indicated that λ So prophage-induced cell lysis and eDNA release in *S. oneidensis* MR-1 biofilms is triggered by iron and is under control of RecA. The fact that the activating signal of RecA is DNA damage, in conjunction with the observation of Gödeke and coworkers that early surface-associated cells induce both the OxyR and the Fur regulon, indicated involvement of Fenton chemistry in the induction process [286].

The term Fenton chemistry comes from H.J.H Fenton who more than 120 years ago discovered the oxidation of organic molecules (tartaric acid) in the presence of H_2O_2 and ferrous iron ions [387]. Forty years later, Haber and Weiss postulated that reaction of ferrous iron with H_2O_2 in aqueous solution leads to generation of a hydroxyl radical as reactive intermediate [388]. With limiting ferrous iron concentration under oxic conditions, the first step of the cycle was postulated to involve the reduction of ferric to ferrous iron by reaction with superoxide (1). In cellular environments, superoxide can be generated accidentally by incomplete reduction of O_2 during aerobic respiration and through flavin-mediated reductive processes [389]. It has later been suggested that superoxide might also be generated spontaneously by autooxidation of ferrous iron, the reverse reaction of (1) [390]. Superoxide can either undergo spontaneous dismutation to H_2O_2 , or accelerated by the catalytic action of cellular superoxide dismutases that protect cells from increased levels of superoxide to prevent oxidative stress (2) [391]. The actual reaction (3) of ferrous iron with H_2O_2 was called Fenton reaction, even though H.J.H Fenton never wrote it. The net reaction of (1) and (3) is known as Haber-Weiss reaction (4) which is catalysed in the presence of ferric and ferrous iron [392]. It is now well established that ROS, such as the hydroxyl radical can cause oxidative damage in various biomolecules, including DNA, protein, lipids, and small molecules [370]. In addition to superoxide dismutases, anaerobically living organisms utilize a variety of catalases and peroxidases to protect the cells from oxidative damage by elimination of intracellular H_2O_2 . Simultaneously, control of intracellular iron levels has evolved as an important strategy to minimize iron-mediated oxidative damage. In most bacteria, the defense against ROS and regulation of ferrous iron uptake is under synchronous control of transcriptional regulators such as OxyR and Fur, respectively [315, 316].

Phenotypic analyses of deletion mutants ΔoxyR and Δfur was performed to elucidate the role of

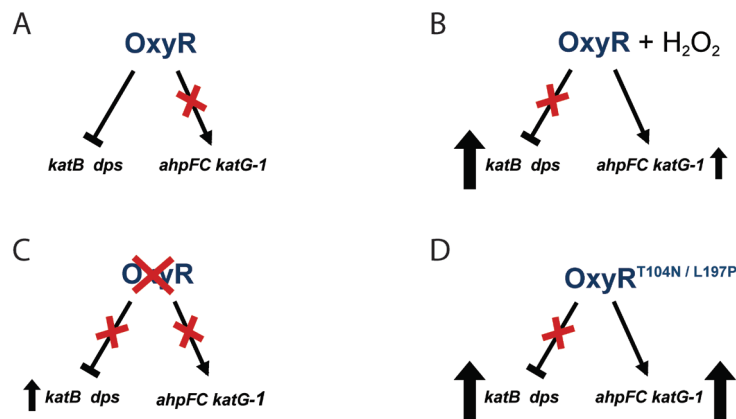


Figure 31. Regulatory patterns of OxyR in *S. oneidensis* MR-1. (A) In the absence of H_2O_2 , wild-type OxyR represses *katB* and *dps* and does not induce *ahpFC* and *katG-1* (B) In the presence of H_2O_2 , derepression of *katB* and *dps* and induction of *ahpFC* and *katG-1* results in strong induction and moderate induction, respectively. (C) Deletion of *oxyR* results in moderate derepression of *katB* and *dps* and no induction *ahpFC* and *katG-1*. (D) Mutated OxyR^{T104N} and OxyR^{L197P} variants act both as strong derepressor of *katB* and *dps* and strong activator of *ahpFC* and *katG-1*, regardless of the presence or absence of H_2O_2 .

both regulators in *S. oneidensis* MR-1 biofilm formation and to investigate whether classical Fenton chemistry might be involved in RecA-mediated induction of prophage λ So. Similar to Δfur , deletion of *oxyR* resulted in an increase in λ So prophage induction during biofilm formation, indicating that the OxyR-mediated response is involved, to some extent, in protecting biofilm cells against oxidative stress. It should be noted that the *fur* gene itself often belongs to the OxyR regulon [315]. However, quantitative real-time RT-PCR analyses indicated that this is not the case in *S. oneidensis* MR-1. To further explore the role of Fenton chemistry in the induction of λ So under biofilm conditions, a mutant screen was performed to isolate mutations that render OxyR constitutively active to suppress H_2O_2 -mediated induction of λ So. This approach helped to successfully isolate two mutants (OxyR^{T104N} and OxyR^{L197P}) that exhibit highly increased resistance towards H_2O_2 . Moreover, H_2O_2 -mediated induction of λ So in planktonic cultures was strongly suppressed. Very recently, OxyR in *S. oneidensis* MR-1 has been shown to act both as an activator and repressor of transcription [310]. Strikingly, substitution of only a single residue (either T104N or L197P) resulted both in strong derepression and strong induction of central genes of the OxyR regulon in *S. oneidensis* MR-1 (Figure 31). Protein structure prediction of the catalytic domain indicated that both residues locate in spacial proximity to the cysteine residues involved in disulfide bond formation in the oxidized state of OxyR (Appendix, Figure 42) [393]. I propose that both substitutions render a conformational change in OxyR that mimics disulfide bond formation and alters DNA binding. Hypothetically, depending on the specific regulatory locus (operator site), DNA binding might result in suppression or activation of transcription of downstream genes. Notably, the OxyR threonine residue at position 104 is highly conserved among proteobacteria and can be easily utilized as functional “on-switch” of the OxyR regulon by substitution to asparagine (Figure 12). Thus, I propose that substitution T104N may be broadly applied as molecular tool for OxyR research in further studies.

Although iron has been proven to be a central catalyst of oxidative damage in aerobic organisms for a long time, the mechanisms of the Fenton reaction are still under intense and controversial

- 5) $\text{Fe}^{2+} + \text{H}_2\text{O}_2 \rightarrow \text{Fe}^{2+}\text{-O} + \text{H}_2\text{O}$ *Ferryl ion generation with H_2O_2*
- 6) $\text{Fe}^{2+} + \text{O}_2 \rightleftharpoons [\text{Fe}^{2+}\text{-O}_2 \rightleftharpoons \text{Fe}^{3+}\text{-O}_2^-] \rightleftharpoons \text{Fe}^{3+} + \text{O}_2^-$ *Perferryl ion generation*
- 7) $\text{Fe}^{2+} + \text{Fe}^{2+}\text{-O}_2 \rightarrow 2\text{Fe}^{2+}\text{-O}$ *Ferryl ion generation from perferryl*

discussion. Especially reactive oxidizing products or intermediates of Fenton chemistry, including radicals such as the hydroxyl radical or iron-oxygen complexes such as ferryl ($\text{Fe}^{2+}\text{-O}$) or perferryl ions ($\text{Fe}^{2+}\text{-O}_2$), have been the subject of controversy [392, 394]. Generally, this may be due to the fact that the efficiency of the Fenton reaction depends drastically on H_2O_2 concentration, iron/ H_2O_2 ratio, pH, and reaction time.

In contrast to the general assumption that DNA lesions in the presence of ferrous iron are the result of Fenton-generated (hydroxyl) radicals, the data of this study indicate that iron and not H_2O_2 levels appear to be limiting for prophage λ So induction in biofilms, since the level of λ So induction was unaffected in biofilms formed by the H_2O_2 -resistant OxyR mutants (OxyR^{T104N}; OxyR^{L197P}). It has been suggested earlier that oxidation of biomolecules by ferrous iron and dioxygen without participation of H_2O_2 is more relevant under physiological conditions than oxidation by hydroxyl radicals generated by Fenton chemistry. A study comparing Fenton-mediated radical oxidations of biomolecules to those induced by iron-oxygen complexes strongly indicated that at ratios of $[\text{O}_2]/[\text{H}_2\text{O}_2] \geq 100$ detrimental effects of iron-oxygen complexes become predominant over Fenton-derived radicals [394]. Notably, physiological ratios of $[\text{O}_2]/[\text{H}_2\text{O}_2]$ range from 10^3 to 10^5 , suggesting a negligible role of Fenton-derived radicals under such conditions. Accordingly, the presence of free iron and dioxygen was assumed to be sufficient for damaging biomolecules such as DNA in various studies [394-396]. For example, Flemmig and Arnhold observed Fe^{2+} -induced DNA strand breaks in plasmid pBBR322 that were not mediated by H_2O_2 [396].

Although the exact nature of reactive iron-oxygen complexes is still under discussion, alternative routes for the oxidation of biomolecules have been suggested in addition to the classical Fenton reaction. On the one hand, hydroxyl radical production by the Fenton chemistry has been questioned by several studies, proposing that the reaction between ferrous iron and H_2O_2 might produce reactive intermediates such as the ferryl ion, which might also induce detrimental oxidation reactions of biomolecules (5) [316, 392, 397, 398]. On the other hand, iron and oxygen have been also been suggested to form the reactive perferryl (6) and ferryl ion (7) without participation of H_2O_2 . Such a mechanisms might explain that iron and not H_2O_2 appeared to be the limiting factor of λ So prophage induction in *S. oneidensis* MR-1 biofilms. Based on these observations I hypothesize that elevated iron uptake under oxic conditions might result in DNA damage without significant participation of the classical Fenton reaction including H_2O_2 , and ultimately in RecA-mediated λ So prophage induction and cell lysis in *S. oneidensis* MR-1 biofilms. However, direct evidence is missing and further studies focusing on effects of iron on the integrity of chromosomal DNA in biofilm cells are required to explore the exact radical chemistry that might indirectly trigger λ So induction.

Biofilm conditions have been reported to promote DNA damage in both Gram-negative and Gram-positive species, generating genetic diversity that may help the community to adapt to

varying environmental conditions or to generate antibiotic resistance [347, 356, 365, 399, 400]. Thus, the occurrence of oxidative damage of DNA seems to represent a common phenomenon under biofilm conditions. Mostly, oxidative stress has been suggested to be responsible for the emergence of DNA lesions by a yet unknown mechanism. Based on the results of this study, I propose that intracellular iron levels might play a central role in these processes. Possibly, iron-induced H₂O₂-independent oxidative damage of DNA could be a ubiquitous phenomenon with so far underestimated and/or overlooked impacts on microbial physiology and ecology.

1.8 Functional specificity of extracellular nuclease EndA

Extracellular nucleases have been shown to exhibit important functions in biofilm formation, biofilm dispersal, structural modulation of the biofilm matrix, utilization of DNA as nutrient source, control of horizontal gene transfer, protection from detrimental concentrations of DNA, and escape from NETs [118, 173, 184, 198, 242, 247, 248, 255]. The fact that many bacteria produce multiple structurally distinct extracellular nucleases suggests specialized functions for distinct purposes [241-243, 245]. However, we are still far from understanding the exact molecular, regulatory, and physiological principles that mediate specialized functions of extracellular nucleases. Thus, detailed investigation of these principles is required to better understand the physiological roles of extracellular nucleases under different conditions. In this study, we investigated the role of extracellular nuclease EndA in *S. oneidensis* MR-1 during biofilm formation and planktonic growth, using a combination of *in vitro* and *in vivo* assays.

1.8.1 *In vitro* analyses of EndA

Purification of an MBP-EndA fusion and characterization of its nucleolytic activity *in vitro* demonstrated that EndA in *S. oneidensis* MR-1 is a sugar-unspecific endonuclease. Accordingly, homologous extracellular nucleases such as Vvn in *V. vulnificus*, Dns in *V. cholera*, or EndA in *S. pneumonia* (low sequence homology to *Shewanella* EndA) have also been shown to cleave DNA endonucleolytically, and in the case of Vvn, to degrade both DNA and RNA [242, 250, 255]. Extracellular DNA isolated from biofilms has often been shown to consist of large strands of genomic DNA or entire chromosomes [194]. Thus, the ability to cleave eDNA endonucleolytically might be more efficient than exonucleolytic degradation in natural environments. Likewise, utilization of both DNA and RNA as nutrient source might represent an important fitness benefit under starvation conditions. I propose that sugar-unspecific endonucleolytic degradation might be a common feature of extracellular nucleases. However, little is known about nucleolytic characteristics of other extracellular nucleases and further studies are required to gain a better understanding.

EndA belongs to the $\beta\beta\alpha$ -Me superfamily of endonucleases that are predicted to require a single metal ion for function. Especially Mg^{2+} , Ca^{2+} , and Zn^{2+} have been described as preferred cofactors of nucleases of that class [322]. However, the results of this study demonstrate that either Mg^{2+} or Mn^{2+} support nucleolytic activity of *Shewanella* EndA. *S. oneidensis* MR-1 is a dissimilatory metal ion-reducing bacteria that can utilize oxidized forms of manganese as terminal electron acceptor. Thus, Mn^{2+} may be an abundant ion produced by anaerobic respiration of manganese oxides and thus may be available in the organism's natural environments. Accordingly, levels of reduced manganese in Lake Oneida (New York), the origin of strain *S. oneidensis* MR-1, were found to be relatively high [263]. Adaptation of *S. oneidensis* MR-1 and possibly other species to elevated levels of reduced manganese might have resulted in structural modifications of EndA to exploit Mn^{2+} as alternative cofactor.

S. oneidensis MR-1 EndA contains all highly conserved amino acid residues that were previously identified as critical for the production of a functional enzyme, including eight cysteine residues that

are likely required for disulfide bond formation. Proper folding and activation of EndA might therefore be restricted to oxidizing milieus such as the extracellular space to protect the cells from deleterious effects of nuclease activity in the cytoplasm [250, 401]. Accordingly, the nucleolytic activity of purified EndA was completely inhibited upon addition of DTT to generate a reducing environment. Interestingly, *endA* (SO_0833) resides in an operon with gene SO_0831, encoding a putative ATP-dependent glutathione synthetase (GshB). Cotranscription of *gshB* with *endA* and GshB-mediated synthesis of glutathione might provide reducing conditions in the cytoplasm that prevent folding of EndA prior to cotranslational transport into the periplasm. Strikingly, *gshB* genes seem to be closely associated with *endA* genes in other species as well, including *dns* in *V. cholerae* and *endA* in *E. coli*, further indicating linked functions of both proteins (data not shown).

1.8.2 Regulation of EndA-mediated extracellular nucleolytic activity

Quantitative real-time RT-PCR analysis performed by M. Heun indicated that *endA* is not differentially regulated in response to phosphorus starvation. This was a rather surprising finding since EndA had also been shown to enable *S. oneidensis* MR-1 to exploit DNA as sole source of phosphorus under starvation conditions [292]. However, the results of this study demonstrated that deletion of *endA* results in extensive accumulation of eDNA in stationary phase cultures, both in minimal and rich medium. This clearly shows that even under non-starvation conditions, $\Delta endA$ deletion mutants exhibit abnormal phenotypes that might impact *S. oneidensis* MR-1 physiology and long-term survival. On the one hand, eDNA might be an important alternative energy and nutrient source in addition to other common sources such as N-acetylglucosamine, small organic acids, or amino acids. On the other hand, extensive accumulation of eDNA resulted in a highly viscous environment that might inhibit motility or reach toxic concentrations in late stationary phase [198]. Accordingly, the results of this study demonstrate that *endA* transcription is regulated by growth phase and not in response to phosphorus starvation. In planktonic cultures of wild-type *S. oneidensis* MR-1, native *endA* transcription was induced during exponential phase and decreased in stationary phase, indicating that EndA is required already in early phases of planktonic growth or that EndA might be stable in the supernatant over longer periods. Notably, episomal overexpression of *endA* in planktonic cultures resulted in strongly decreased eDNA levels and elevated nucleolytic activity in culture supernatants, indicating that transcription is the limiting factor under the conditions tested. However, factors involved in transcriptional regulation of *endA* remain to be identified. The fact that *endA* is induced even under optimal growth conditions during exponential phase, indicates that it is of general importance. Extracellular DNA has been shown to occur in high amounts in marine sediments and to play important roles in microbial ecosystems in the deep-sea [172]. Natural habitats of *S. oneidensis* and other members of the *Shewanellaceae* family comprise marine sediments. Thus, EndA may be a crucial factor for growth and long-term survival of *Shewanella* species in their natural environment. Finally, the control of DNA uptake and horizontal gene transfer might be another role of EndA that could be of particular importance in eDNA-rich environments such as marine sediments. However, conclusive evidence for the occurrence of natural transformation in *Shewanella* species is still missing.

EndA resides in an operon with *phoA*, encoding extracellular alkaline phosphatase PhoA. PhoA contributes significantly to extracellular phosphatase activity in culture supernatants but is not essential for growth on eDNA. In the absence of PhoA, residual phosphatase activity was observed, indicating the presence of additional enzymes that exhibit redundant functions in

S. oneidensis MR-1. Indeed, several other extracellular phosphatases can be identified in *S. oneidensis* MR-1, and the resulting activity is likely sufficient for growth on eDNA in the absence of other phosphorus sources [173].

EndA is homologous to other bacterial nucleases, such as *V. vulnificus* Vvn, *E. coli* EndA, *V. cholerae* Dns, and *A. hydrophila* Dns. All of these enzymes contain signal peptides for Sec-dependent secretion and remain either in the periplasm, like Vvn and *E. coli* EndA, or are exported into the extracellular space, like Dns in *V. cholerae* and *A. hydrophila* [250, 295, 402]. *In vivo* DNA degradation assays in planktonic cultures demonstrated nucleolytic activity in cell-free supernatants but not in suspensions with washed cells, suggesting that *Shewanella* EndA is an extracellular enzyme similar to Dns and does not remain in the periplasm like Vvn or *E. coli* EndA. However, release through vesiculation or cell lysis cannot be ruled out, but this is rather unlikely to occur under the conditions tested (short incubation time, logarithmic phase cultures) [38, 403].

1.8.3 EndA is a planktonic growth-specific nuclease

Deletion of *endA* was shown to result in cellular aggregation during planktonic growth of *S. oneidensis* MR-1 [292]. Although this might suggest a possible role in community behavior of *S. oneidensis* MR-1, deletion of *endA* did not result in abnormal biofilm formation under hydrodynamic conditions and did not exhibit uncontrolled eDNA accumulation, as observed in Δ *exeM* mutants [241]. Overexpression of *endA* in static biofilms did not result in biofilm dispersal, although expression levels of *endA* were shown to correlate with nucleolytic activity in supernatants of planktonic cultures. Moreover, external addition of MBP-EndA did not release biomass from biofilms while addition of DNaseI readily induced biofilm dispersal, both under hydrodynamic and static conditions.

These data pose intriguing questions about structural and functional differences of extracellular nucleases that might determine whether a nuclease is functional under biofilm conditions or under planktonic growth conditions. Since purified MBP-EndA was shown to exhibit significant nucleolytic activity *in vitro*, it is rather unlikely that it lacks access to eDNA in biofilms due to the MBP fusion. Possibly, biofilm conditions render EndA inactive, e.g. as a result of reducing conditions in anaerobic biofilm areas, loss of the metal cofactor, or presence of other inhibitory cofactors. Indeed, slight inhibition of MBP-EndA nucleolytic activity was observed *in vitro* in the presence of Ca^{2+} (data not shown). However, it is unclear whether locally increased Ca^{2+} levels occur in biofilm environments, and if so, whether this would suffice to inactivate the nucleolytic activity of EndA. Furthermore, at least a residual loss of biomass from the upper layers of the biofilms would be expected in any of the mentioned cases. Recently, it has been demonstrated that eDNA physically interacts with other matrix components in biofilms formed by *M. xanthus* and *P. aeruginosa* [131, 146]. In starvation biofilms and fruiting bodies of *M. xanthus*, eDNA was bound to an unknown exopolysaccharide, resulting in greater physical strength and stress resistance compared to DNase I treated matrices [131]. Similarly, exopolysaccharide Psl in *P. aeruginosa* biofilms was shown to interact with eDNA to form a web of Psl-eDNA fibers in the center of pellicles to give structural support [146]. Possibly, binding of exopolysaccharides or other matrix components might mask eDNA and protect it from unspecific cleavage by extracellular nucleases under biofilm conditions. It would be interesting to determine whether similar interactions occur in *S. oneidensis* MR-1 biofilms and whether removal of such matrix components would make eDNA

susceptible to cleavage by EndA. Another possibility is that biofilm-specific eDNA is modified as protection from degradation by EndA, as has been suggested for methylated eDNA in *N. gonorrhoeae* biofilms that was resistant to degradation by extracellular nuclease Nuc [184]. However, this study reveals that a significant fraction of eDNA that is required for structural biofilm formation, is released by prophage-induced cell lysis and therefore represents genomic DNA that is most likely identical to eDNA in planktonic stationary phase cultures. Moreover, *in vitro* degradation assays with biofilm eDNA indicated that most of the eDNA was readily degraded by the MBP-EndA fusion protein. However, only a small fraction of the eDNA might exhibit structural functions in biofilms. Under static conditions, deletion of *endA* resulted in increased accumulation of biofilm biomass, indicating that native EndA plays at least a minor role in biofilm formation. However, it is possible that improved cell aggregation in $\Delta endA$ mutants supports initial attachment or early biofilm formation but does not affect the structural integrity of the eDNA matrix in later phases. The phenotype of the $\Delta endA$ deletion mutant would therefore be rather indirect. Notably, extracellular nuclease Dns in *V. cholerae* has been shown to affect biofilm formation [242]. To better understand why homologous enzymes such as EndA and Dns exhibit different functions, it would be interesting to determine whether addition of purified Dns to biofilms formed either by *V. cholerae* or by *S. oneidensis* MR-1, would result in biofilm dispersal.

In conclusion, the role of EndA in biofilm formation requires further elucidation, mainly regarding biofilm-specific conditions or eDNA modifications that protect biofilms from dissolution by EndA. The results of this study strongly suggest functional specificity of extracellular nucleases in *S. oneidensis* MR-1. The fact that many bacteria possess various structurally distinct extracellular nucleases indicates that functional specificity and ‘division of labor’ by extracellular nucleases might represent a common phenomenon and likely an adaptation to variable lifestyle and environments, including planktonic growth and biofilm formation.

1.9 Molecular characterization of ExeM

ExeM is a large extracellular nuclease that is conserved in *Shewanellaceae*, *Vibrionaceae*, *Aeromonadaceae*, and *Pseudoalteromonadaceae*. Bioinformatic analyses identified several domains and motifs that form the basis for this and prospective studies on correlations between the molecular structure and function of this class of extracellular nucleases. Its size, unique domain architecture (including transmembrane domain and processing motif), and regulatory pattern indicate structural and functional complexity that we are only beginning to understand. The predominant role of ExeM has been attributed to biofilm formation; however, molecular features that determine this functional specificity remained to be elucidated. Furthermore, characteristics inherent by ExeM that are required for modulation, processing, and degradation of biofilm-specific eDNA were unknown. Although not all of the questions have been answered in this study, the results represent a first basis for the decryption of ExeM's structure-function relationships and its role in biofilm formation of *S. oneidensis* MR-1.

1.9.1 *In silico* analyses of ExeM

Protein sequence alignments identified an N-terminal signal sequence that has been predicted to mediate Sec secretion into the periplasm. Signal peptides of Sec-secreted membrane protein are generally more hydrophobic and therefore recognized by the signal recognition particle (SRP) for cotranslational transport into the periplasm [404]. Indeed, analysis of ExeM's signal sequence demonstrated that it is highly hydrophobic and that both other extracellular nucleases, ExeS and EndA, contain much less hydrophobic signal peptides. Thus, I propose that upon initiation of translation, ExeM is directed to the SecYEG secretion machinery by SRP (and FtsY) and secreted into the periplasmic space by cotranslational transport (Figure 32). Experimental clarification might only be achieved by following ExeM transport in a $\Delta secB$ mutant that suppresses posttranslational transport. However, it has to be noted that suppression of Sec-dependent protein export might produce a conditionally lethal phenotype as in many other species, including *E. coli* [405]. Protein sequence comparison further identified three major domains that were termed LTD domain, YhcR domain, and EEP domain. Notably, putative metal and phosphate binding sites reside exclusively within the large C-terminal EEP domain which is present in a diverse superfamily of enzymes that mostly cleave phosphodiester bonds, indicating that the catalytic core resides within this region of ExeM [406]. Correspondingly, the question arises how the residual domains may contribute to ExeM function, or whether these exhibit rather important structural than catalytic roles. Direct comparison with EndA points out that a small enzyme of an estimated molecular weight of only 29.1 kDa (compared to 93.7 kDa for ExeM) is sufficient to exhibit significant extracellular endonucleolytic activity. It is therefore unclear why bacteria such as *S. oneidensis* MR-1 bear higher metabolic cost for a larger enzyme, if a smaller one such as EndA may conduct the same catalytic function. Possible reasons may be that specific environmental conditions require a more complex enzyme structure (*e.g.* integration of different regulatory signals or interaction with other structures such as EPS) or that ExeM may exhibit more complex functions in comparison to EndA (*e.g.*

specific modulation of eDNA). Accordingly, the results of this study demonstrate functional specificity of both nucleases with regard to different conditions. To determine the specific roles of single domains of ExeM, purification and *in vitro* characterization (nucleolytic activity) of truncated ExeM variants that lack single domains or that consist only of one domain (e.g. EEP) may be necessary in future studies.

1.9.2 *In vitro* analyses of ExeM

In vitro degradation assays with purified MBP-ExeM fusion protein indicated that ExeM is a sugar-unspecific endonuclease. As already discussed for EndA (1.8), the capacity to endonucleolytically degrade both DNA and RNA may be a common feature of extracellular nucleases to achieve efficient and unspecific cleavage of high molecular weight eDNA and to possibly to exploit RNA as additional nutrient source. Notably, region 220-291 has been predicted to exhibit sequence homologies to the oligonucleotide-binding domain of YhcR in *B. subtilis*, which is also an extracellular sugar-unspecific endonuclease. However, the exact role of this domain remains to be elucidated. In contrast to our results, only exonucleolytic activity has been observed for highly homologous Xds in *V. cholera* [242]. However, the results are based on DNA degradation assays with culture supernatants and thus experiments with the purified protein may be required.

Protein sequence alignment suggested that ExeM belongs to the diverse superfamily of two-metal-ion-dependent nucleases that also include DNaseI [322]. Indeed, sequential analyses of potential metal ion cofactors (Mg^{2+} , Mn^{2+} , Ca^{2+} , Zn^{2+} , Ni^{2+} , Cu^{2+}) demonstrated that Ca^{2+} and additionally either Mg^{2+} or Mn^{2+} are required for function. Since all putative metal ion-binding sites have been predicted to reside within the EEP domain, it is likely that this region determines ExeM's specific cofactor requirements. Though it is interesting that YhcR in *B. subtilis* similarly requires Ca^{2+} and Mn^{2+} as cofactors while no metal binding sites have been predicted within the YhcR domain in ExeM. Thus, further *in vitro* assays may be required to determine the exact role of the putative YhcR domain and whether this region in ExeM is only involved in oligonucleotide binding or whether it exhibits additional catalytic functions [331].

Magnesium and calcium ions are common cofactors of many nucleases and other enzymes, likely due to their high abundance in natural environments, solubility, and redox stability [322]. In seawater, Mg^{2+} and Ca^{2+} belong to the most abundant ions and play important roles in a variety of biological processes [407]. Although *S. oneidensis* MR-1 has been isolated from the sediments of the freshwater Lake Oneida (New York) [263], it is possible that it originates from marine environments, similar to its closest relatives *Shewanella* sp. MR-4 and *Shewanella* sp. MR-7 that were isolated from the Sargasso Sea [408, 409]. In contrast to Mg^{2+} and Ca^{2+} , Mn^{2+} is normally present at very low concentrations in natural environments [407, 410]. However, in Lake Oneida, concentrations of reduced manganese were shown to reach remarkably high levels during the summer months and it was speculated that this process was due to biological activity in the sediments. In 1988, *S. oneidensis* MR-1 was isolated from the sediments of Lake Oneida and shown to contribute to Mn^{2+} accumulation in the lake water [263]. Thus, utilization of Mn^{2+} as alternative cofactor by extracellular enzymes of *S. oneidensis* MR-1 might represent a recent adaptation to increased Mn^{2+} levels in Lake Oneida that result from its own respiratory metabolism. Determining cofactor requirements of EndA and ExeM in closely related species, such as *S. sp.* MR-4 and *S. sp.* MR-7, could help to answer these questions. However, sequence comparison of SO_1066 with its

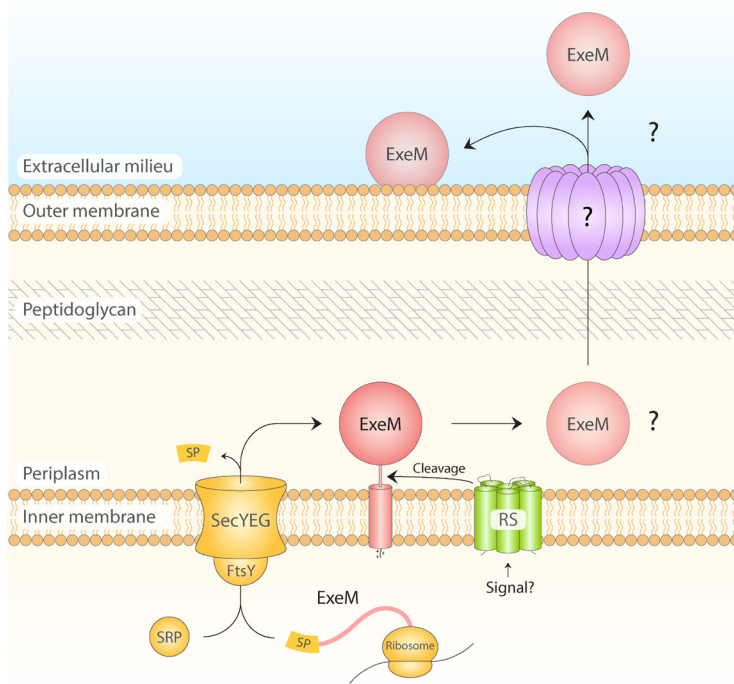


Figure 32. Schematic illustration of putative ExeM transport across the cell wall. Upon translation of ExeM, signal recognition particle (SRP) recognizes the hydrophobic signal peptide (SP) of ExeM and is recruited to its receptor FtsY at the SecYEG translocon. Cotranslational transport secretes ExeM directly into the periplasm (signal peptide is cleaved off) and embeds its C-terminal membrane anchor into the inner membrane. Putative rhombosortase (RS) cleaves ExeM at the Gly-Gly-Cterm motif, possibly in response to an unknown signal. ExeM remains either transiently in the periplasm or is directly secreted into the extracellular milieu, likely by a Type II secretion mechanism. Potential interaction of ExeM with the outer cell envelope remains to be elucidated.

orthologs in both species demonstrates a high degree of conservation of up to 100 %, making major catalytic differences between the nucleases rather unlikely (Figure 23). In fact, local concentrations of Mn^{2+} in marine sediments may similarly reach levels in the presence of bacteria that perform dissimilatory reduction of manganese oxides, resulting in habitat-specific adaptations that may include metal ion cofactors. Finally, it cannot be excluded that the observed *in vitro* nucleolytic activity in the presence of Mn^{2+} may also represent a false-positive result, since both ions exhibit similar chemical properties, including inner and outer shell complexation that might trigger coincidental binding without actual physiological relevance [411].

To gain a better understanding of ExeM's catalytic requirements and being a prerequisite for further approaches, optimal cofactor concentrations of ExeM were determined by *in vitro* DNA degradation assays in the presence a various concentration of Mg^{2+} , Mn^{2+} , and Ca^{2+} . For Mg^{2+} and Ca^{2+} , nucleolytic activity peaked at approximately 25 mM and was only observed in a relatively narrow range of concentrations, indicating that not only a shortage but also excess of cofactors inhibits ExeM function. Notably, studies on the composition of seawater demonstrated Mg^{2+} and Ca^{2+} concentrations of approximately 50 mM and 10 mM, whereas freshwater concentrations ranged only between 0.06 – 0.25 mM and 0.1 – 1 mM, respectively [407, 410]. Thus, optimal nucleolytic activity of ExeM occurred within the range of concentrations typical for marine environments rather than freshwater habitats, further supporting the hypothesis that ancestors of *S. oneidensis* MR-1 originate from in the ocean. Interestingly, optimal concentrations of Mn^{2+} ranged much lower at approximately 0.1 – 6 mM, possibly reflecting the overall lower abundance of reduced manganese in natural environments, compared to other metal ions such as Mg^{2+} and Ca^{2+} . Furthermore, determining the maximal nucleolytic activity under optimal conditions, the results of this study indicate approximately 3000-fold lower activity of purified MBP-ExeM compared to

MBP-EndA. Thus, the question arises again why *S. oneidensis* MR-1 invests high ‘metabolic costs’ to produce a large protein that exhibits much lower catalytic activity compared to an analogous nuclease that achieves much higher rates at a much smaller size. Conclusively, high catalytic rates may not be limiting for ExeM’s specific functions. In contrast to ExeM, EndA is essential for growth on DNA as sole source of phosphorus under planktonic conditions. To exploit DNA as a nutrient, high nucleolytic rates may be crucial to provide sufficient substrates for downstream catabolic processes. On the other hand, the role of ExeM has been attributed to structural biofilm formation and the control of eDNA levels in the biofilm matrix. These processes might require a higher degree of regulation to enable catalytic fine-tuning, and thus a more complex enzyme. It has to be noted that purified MBP-ExeM was less stable than MBP-EndA *in vitro*. Thus, it is unclear whether ExeM exhibits higher nucleolytic rates under physiological conditions *in vivo*. Seper and coworkers investigated the role of Dns and Xds in *V. cholera*, the orthologs of *Shewanella* EndA and ExeM, respectively [242]. Interestingly, DNA degradation assays with culture supernatants indicated higher nucleolytic activities of Dns compared to Xds, supporting the *in vitro* data of this study.

1.9.3 Processing and transport of ExeM

To investigate ExeM processing and transport, truncated variants of ExeM were constructed to gain a better understanding of the C-terminal hydrophobic regions including the putative Gly-Gly-CTerm motif. DNA-degradation assays with supernatants of planktonic cultures failed to identify nucleolytic activity for any of the strains. Thus, in sharp contrast to the results obtained for EndA, extracellular nucleolytic activity of ExeM does not directly correlate with its expression levels. It remains unclear whether this was due to a missing signal for ExeM secretion under the conditions tested, or whether the nucleolytic activity of ExeM was simply below the detection limit of this approach. In contrast, the nucleolytic activity of orthologous Xds in supernatants of *V. cholerae* cultures was readily detectable and the authors concluded that Xds is not surface-associated but rather secreted [242]. Possibly, Xds might have a different function in *V. cholerae* compared to ExeM in *S. oneidensis* MR-1. Accordingly, Xds was shown to be essential for growth on DNA as nutrient source whereas ExeM was shown to play only a minor role [241, 242].

Transport and localization of ExeM was further investigated by immunoblot detection of the truncated variants of ExeM in different cellular fractions. The results indicate that ExeM localizes, at least transiently, to the inner membrane (Figure 32). Surprisingly, significant amounts of construct ExeM[Δlinker-TM] were also detected in the inner membrane fraction, although the constructs lack the C-terminal membrane anchor. Assuming that cotranslational transport is the bottleneck of ExeM transport across the cell envelope, overproduction to non-physiological levels might have resulted in an overload of the SecYEG machinery. Thus, immunoblot signals obtained for ExeM in the inner membrane might represent, in part, unfolded ExeM peptide that is still associated with the SecYEG translocon. Since expression levels of native ExeM were too low for detection by immunoblot analysis, adequate expression levels may be achieved by incubation of the *S. oneidensis* MR-1 overexpression strain with lower concentrations of the inducer (L-arabinose). Alternatively, cells harboring the overexpression plasmids may be incubated initially in the presence of the inducer followed by an incubation period without the inducer to allow completion of cotranslational transport into the periplasm.

Table 3. Predicted targets of putative rhombosortase SO_2504

Gene	Protein	Predicted function
SO_0130	PrtV	Extracellular metalloprotease
SO_1066	ExeM	Extracellular nuclease
SO_1854	-	HP, putative outer membrane protein required for motility and nitrate resistance
SO_1915	-	Serine protease, subtilase family
SO_2529	-	HP, rhombotail lipoprotein
SO_3302	-	Serine protease, extracellular peptidase family S8A
SO_3718	-	DsbA family, required for disulfide bond formation of some periplasmic proteins
SO_3800	-	Serine protease, surface-associated serine protease
SO_4539	-	Serine protease, extracellular peptidase family S8
SO_4645	-	Putative bifunctional autotransporter, serine protease domain

HP, Hypothetical protein; Adapted from Haft and Varghese, 2011 [336]

Immunoblot detection of ExeM[GG-AA] indicated strongly elevated levels in the inner membrane compared to native ExeM, indicating that the putative Gly-Gly-CTerm motif is indeed involved in ExeM processing, as suggested by Haft and coworkers [336]. However, it remains unclear whether putative rhombosortase SO_2504 is involved in specific cleavage of ExeM at the Gly-Gly site, since deletion of SO_2504 did not result in extensive accumulation of native ExeM. It has to be noted that Δ SO_2504 mutants show reduced growth rates in mid-exponential phase that might alter protein production and transport (Appendix, Figure 41). Furthermore, deletion of putative rhombosortase SO_2504 might have pleiotropic effects that could indirectly impact ExeM stability. Bioinformatic analyses by Haft and coworkers predicted 10 putative targets that harbor a conserved Gly-Gly-CTerm motif (Table 3). More than half of the proteins are predicted to exhibit proteolytic functions. Thus, suppression of Gly-Gly-CTerm cleavage in Δ SO_2504 mutants might result in excessive accumulation of inner membrane-attached proteases and possibly in unspecific degradation of other membrane-bound or periplasmic proteins, including ExeM. Interestingly, among the predicted targets of rhombosortase SO_2504 resides a DsbA-like protein (SO_3718). Proteins of the Dsb family have been shown to be required for disulfide bond formation of several extracellular proteins, including PhoA [412, 413]. It would be interesting to determine whether SO_3718 in *S. oneidensis* MR-1 exhibits similar functions, possibly facilitating disulfide bond formation of ExeM and other extracellular proteins.

Generally, a more detailed investigation of the role of rhombosortase SO_2504 in biofilm formation and in particular in processing of ExeM is required, including indirect effects of its target proteins. Preliminary results strongly indicate an important role in structural biofilm formation and prevention of cellular aggregation in planktonic cultures (data not shown). However, further experimental elucidation is required to gain a better understanding of this protein. For example, nothing is known about the regulatory control of rhombosortase activity. Thus, analysis of promoter activities or transcript levels under various environmental conditions (*e.g.* sessile vs. motile lifestyle) by promoter fusion studies (*e.g.* fusion to *gfp*) or qPCR, respectively, might give important insights. Further, overexpression of SO_2504 and analysis of ExeM levels in different cellular fractions and the supernatant might demonstrate whether levels of rhombosortase SO_2504 can be correlated with processing and transport of ExeM across the cell envelope.

Surprisingly, neither full-length ExeM nor the truncated variants of ExeM could be detected in the periplasmic fraction or in the supernatant. As it is rather unlikely that ExeM remains in the inner membrane to fulfill its function, the negative results may be due to technical limitations of this approach or due to the conditions tested. The antibody that was utilized for these assays was specific but not very sensitive and the protein-to-volume ratios of the periplasmic fraction and the supernatant are both very low. Thus, levels of processed ExeM protein in both fractions may have been too low to obtain significant signals, although the fractions were at least 10-fold concentrated prior to immunoblot analysis. In contrast, protein concentrations of the outer membrane fraction were adequate and a good degree of separation was achieved, as revealed by the MtrB-Strep control. In contradiction to earlier results from Tang and coworkers who detected ExeM in the outer membrane fraction, these results indicate that ExeM is not attached to the outer membrane [293]. However, it cannot be excluded that ExeM may interact with the cell envelope by weak binding forces under physiological conditions that may be interrupted during sarkosyl-based separation of both membranes. On the other hand, it is also possible that the conditions used for this assay do not stimulate processing and activation of ExeM, and thus the protein may rest in the inner membrane without being transported to the extracellular space. Biofilm growth, phosphorus limitation, and anaerobic conditions have been shown to induce ExeM expression [241]. Accordingly, factors involved in processing and transport of ExeM may be analogously induced under the same conditions. Hence, it would be interesting to elucidate whether the observed patterns may vary under different conditions. However, deletion of SO_2504 results in reduced growth rates in mid-exponential phase in planktonic cultures, indicating that putative rhombosortase is expressed and active under these conditions (Appendix, Figure 41). In addition to the putative rhombosortase, other, so far unknown, factors may be involved in processing and transport of ExeM that remain to be identified. For prospective experiments, it has to be noted that sarkosyl-based fractionation and immunoblot analysis of ExeM in different cellular fractions is a relatively laborious and complex procedure, including numerous intermediate steps that may influence ExeM stability and thus the significance and reliability of the results. Although detection of ExeM in different cellular fractions has already helped to gain a better understanding of ExeM processing and transport, alternative approaches may be required to obtain a more complete picture. Kiedrowski and coworkers investigated localization of membrane bound extracellular nuclease Nuc2 in *S. aureus* by utilizing fluorescence microscopy and alkaline phosphatase localization approaches using Nuc2-GFP and Nuc2-PhoA fusions [245]. Similar approaches may be used for the investigation of ExeM. Moreover, to better understand the role of the C-terminal hydrophobic domains including the Gly-Gly-CTerm motif, this region may be translationally fused to other extracellular enzymes such as EndA or PhoA. Both enzymes exhibit high catalytic activities that may facilitate detection in supernatants. Alternatively, the C-terminal region may be fused to sfGFP that has been used successfully for localization studies in the periplasm and the extracellular space [414]. However, rapid folding of sfGFP may result in suppression of SecYEG-mediated transport and accumulation of the fusion protein in the cytoplasm. To overcome this problem, sfGFP should be fused to a highly hydrophobic signal peptide (e.g. ExeM's native signal peptide) to ensure efficient cotranslational (and not posttranslational) transport via SecYEG [414]. Otherwise, mCherry can also be used for periplasmic localization studies. Fluorescence microscopy analysis of such a construct may help to gain important insights in the role of the C-terminal transmembrane anchor and the Gly-Gly-CTerm motif. Furthermore, highly specific and sensitive antibodies against sfGFP are commercially available and may help to detect sfGFP in culture supernatants. *S. oneidensis* MR-1 is predicted to encode most protein components required for Type I and Type II-mediated secretion (KEGG, Kyoto Encyclopedia of Genes and Genomes). Thus, analysis of ExeM secretion

into the extracellular space may be determined in specific deletion mutants such as $\Delta aggA$ and $\Delta gspD$ to suppress Type I and Type II secretion, respectively [290, 415].

As summarized in Figure 32, ExeM is likely secreted into the periplasm by cotranslational transport and directly embedded into the inner membrane with its C-terminal membrane anchor. Upon an unknown stimulus, putative rhombosortase may recognize the Gly-Gly-CTerm motif and cleave off the C-terminal transmembrane domain, resulting in release of ExeM into the periplasm. It is unclear, whether ExeM is directly secreted into the extracellular milieu or whether it may endure transiently in the periplasm. Furthermore, it remains to be elucidated in more detail whether secreted ExeM might interact with the cell envelope or whether it is freely released into the supernatant (Figure 32).

1.9.4 Effect of ExeM on biofilm formation

An important function that has been attributed to extracellular nucleases is the induction of biofilm dispersal by degradation of eDNA as structural matrix component [92]. Accordingly, deletion mutants that lack extracellular nucleolytic activity were shown to produce thicker biofilms, containing high levels of eDNA [184, 242, 247]. However, the role of ExeM in biofilm formation of *S. oneidensis* MR-1 appears to be more complex. Under static conditions, deletion of *exeM* had been shown to result in decreased biofilm formation, indicating that it supports biofilm formation rather than inducing dispersal. Under hydrodynamic conditions, excessive accumulation of eDNA and abnormal structural biofilm formation was observed for the $\Delta exeM$ deletion mutant [241]. The results of this study indicate that biofilm formation is inhibited in the presence of purified MBP-ExeM; however, addition of the enzyme to pre-existing biofilms had no effect. In contrast, expression of *exeM* in the absence of other nucleases or episomal overexpression of *exeM* in a triple nuclease mutant, stimulated biofilm formation compared to the controls. Thus, based on these data it is not possible to attribute a strictly inhibitory or strictly supportive role of ExeM on biofilm formation. Furthermore, it is unlikely that ExeM is specifically required for induction of biofilm dispersal, otherwise significant biofilm dissolution would have occurred upon addition of MBP-ExeM to pre-existing biofilms or upon endogenous induction. However, it cannot be excluded that biofilm dispersal requires additional factors such as proteases or polysaccharide-degrading enzymes and that coproduction of enzymes under specific conditions might result in efficient biofilm dispersal [107, 117]. Nevertheless, taking the structural and regulatory complexity of ExeM into consideration, it is more likely that it is required for fine-tuning of biofilm-specific processes such as modulation of the eDNA matrix for successful structural biofilm formation, rather than dispersal. Modulation of the eDNA matrix might require balanced levels of nucleolytic activity within biofilm structures to avoid premature dissolution that would likely decrease community fitness. Thus, low levels of nucleolytic activity, as observed for ExeM, might be desired to enable controlled biofilm development. It is also possible that specific stimuli might induce local expression of *exeM* within biofilm structures. Localization of *exeM* expression during biofilm development (e.g. by CLSM analysis of strains carrying a fluorescence promoter fusion to *exeM*) might help to better understand the role of ExeM in biofilm formation.

Conclusively, biofilm formation is a complex process that is only successful when a delicate equilibrium of a multitude of parameters is maintained. ExeM presents one of these parameters and its functionality is likely dependent on several other factors that remain to be identified and/or

characterized to fully understand the role of ExeM in biofilm formation. The results of this and prospective studies might also help to gain a better understanding of molecular processes that are required for structural biofilm formation in general.

MATERIAL AND METHODS

1.10 Materials

1.10.1 Reagents and Enzymes

Common reagents used in this studies were purchased from Bioline (Germany), Carl-Roth (Germany), GE Healthcare (Germany), Invitrogen (Germany), Merck (Germany), Millipore (Germany), Perkin Elmer (USA), Peqlab (USA), Sigma-Aldrich (Germany), Thermo Scientific (USA), Zymo Research Europe GmbH (Germany) or VWR International GmbH (Germany). Specific chemicals used in this thesis are described in the respective parts.

Enzymes required for the molecular manipulation and cloning of DNA were acquired from New England Biolabs (NEB, USA), Fermentas (Canada), or Thermo Scientific (USA).

Size standards for DNA and proteins were obtained from NEB (USA) and Thermo Scientific (USA), respectively.

1.10.2 Buffers and solutions

Standard buffers and solutions were prepared according to Green and Sambrook [416]. When required, buffers and solutions were autoclaved (20 min at 121 °C) or filter sterilized (Sarstedt, Germany; pore size 0.22 µm). Specific buffers and solutions are described along with the respective method.

1.10.3 Media

Complex media used for growth of *E. coli* and *S. oneidensis* are listed in Table 4. Media were autoclaved for 21 min at 121°C and 2 bar, unless otherwise stated. Media additives are listed in Table 5 and Table 6. To solidify media, 1.5 % (w/v) agar was added prior to autoclaving. Heat instable components were sterilized by filtration using 0.22 µm pore diameter filter units (Sarstedt, Germany).

Table 4. Media.

Media	Component		Reference
LB (lysogeny broth, Miller)	Tryptone	10 g/l	[417]
	Yeast Extract	5 g/l	
	NaCl	10 g/l	
	pH	7.0	
SOB (super optimal broth)	Tryptone	20 g/l	[418]
	Yeast Extract	5 g/l	
	MgCl ₂	0.95 g/l	
	NaCl	0.5 g/l	
	KCl	0.186 g/l	
	pH	7.0	
SOC (SOB with catabolite repression)	SOB		[418]
	Glucose	20 mM	
LM (lactate medium)	Yeast Extract	0.2 g/l	[419]
	Peptone	0.1 g/l	
	HEPES	2.38 g/l	
	NaCl	5.8 g/l	
	Lactate [85 % (v/v)]	15 mM	
	pH	7.5	
LM_{FC} (lactate medium, flow chamber)	Yeast Extract	0.2 g/l	[24]
	Peptone	0.1 g/l	
	HEPES	2.38 g/l	
	NaCl	5.8 g/l	
	Lactate, [85 % (v/v)]	44.8 µl	
	pH	7.5	

* stock concentration is displayed in brackets []

Antibiotics were prepared as stock solutions and added to the media in the following concentration. If not otherwise stated the same final concentration was used for both, *E. coli* and *S. oneidensis* (Table 5).

Table 5: Antibiotics.

Antibiotic	Stock concentration	Final concentration	Solvent
Ampicillin-sodium salt	100 mg/ml	100 µg/ml	ddH ₂ O
Chloramphenicol	30 mg/ml	<i>E. coli</i> 30 µg/ml <i>S. oneidensis</i> 10 µg/ml	96 % (v/v) EtOH
Kanamycinsulfate	50 mg/ml	50 µg/ml	ddH ₂ O
Tetracyclinhydrochlorid	10 mg/ml	2.5 µg/ml	96 % (v/v) EtOH
Gentamycinsulfat	10 mg/ml	10 µg/ml	ddH ₂ O

Filter sterilized (Sarstedt, Germany; pore size 0.22 µm) additives are listed in Table 6.

Table 6: Additives.

Other additives	Stock concentration	Final concentration	Solvent
IPTG (isopropyl- β -D-thiogalactopyranoside)	1 M	1 mM	ddH ₂ O
L-Arabinose	20 % (w/v)	0.2 % (w/v)	ddH ₂ O
DAP (Meso-diaminopimelic acid)	60 mM	300 μ M	ddH ₂ O
Sucrose	80 % (w/v)	10 % (w/v)	ddH ₂ O

1.10.4 Kits

The ‘kits’ used for this work are listed in Table 7.

Table 7: ‘Kits’.

Label and company	Application
DNA Clean & Concentrator (Zymo Research, Germany)	DNA purification
Zymo Clean™ Gel DNA Recovery Kit (Zymo Research, Germany)	Isolation and purification of DNA from agarose gels
Zyppy™ Plasmid Miniprep Kit (Zymo Research, Germany)	Isolation and purification of plasmid DNA
E.Z.N.A.® DNA Probe Purification, Omega Bio-tek (VWR International GmbH, Germany)	DNA purification
E.Z.N.A.® Gel Extraction Kits, Omega Bio-tek (VWR International GmbH, Germany)	Isolation and purification of DNA from agarose gels
E.Z.N.A.® Plasmid Mini Kit I, Omega Bio-tek (VWR International GmbH, Germany)	Isolation and purification of plasmid DNA
E.Z.N.A.® Genomic DNA Isolation Kit, Omega Bio-Tek (VWR International GmbH, Germany)	Isolation and purification of genomic DNA
HiSpeed Plasmid Maxi Kit (QIAGEN GmbH, The Netherlands)	Isolation and purification of plasmid DNA
Pierce™ BCA Protein Assay Kit (Thermo Scientific, USA)	Quantification of protein concentrations
Western Lightning™ Chemiluminescence Reagent Plus (Perkin Elmer, Germany)	Chemiluminescent reagent for HRP-dependent immunodetection
CDP-Star® Reagent (New England Biolabs, Germany)	Chemiluminescent reagent for HRP-dependent immunodetection

1.10.5 Laboratory equipment and software

Standard equipment and software used during this work is listed in Table 8. Specific equipment and software is listed with the respective method.

Table 8: Equipment and software.

Equipment or software	Label and manufacturer
Agarose gel photochamber	2UV-Transilluminator (UVP, USA)
Fluorescence microscope	Axio Imager.M1 (Zeiss, Germany) DMI6000B (Leica, Germany)
Bioanalyzer	Tecan infinite M200 (Tecan, Switzerland)
PCR cyclers	Mastercycler personal (Eppendorf, Germany) Mastercycler epgradient
pH meter	CyberScan 510 (USA)
Spectral photometer	Ultrospec 2100 pro (Amersham Biosciences, Germany) NanoDrop® ND-1000 (Pqclab, Germany)
Thermo mixer	Thermomix compact (Eppendorf, Germany)
Centrifuges	Sorvall RC 5B Plus (Kendro laboratory products, Germany) Multifuge 1 S-R (Heraeus, Germany) Biofuge fresco (Heraeus, Germany) Biofuge pico (Heraeus, Germany)
Electro power supply for electroporation	Consort Power Supply E835/E865 (Pqclab, Germany)
Chemoluminescence imager	FUSION-SL4 (Pqclab, Germany)
Electroblotter for western transfer	TE 77 ECL Semi Dry (Amersham Biosciences, Germany) MetaMorph® 7.1.2 (Molecular Device; USA)
Imaging software	ImageJ 1.47v software (National Institute of Health, USA) Adobe® Illustrator® CS6 (Adobe Systems Software, Ireland) Adobe® Photoshop® CS6 (Adobe Systems Software, Ireland)
<i>In silico</i> cloning	Vector NTI Advance™ 11 (Invitrogen, Germany)

1.10.6 Oligonucleotides

Oligonucleotides were designed using OligoCalc [420] and generated by Sigma-Aldrich (Germany) or SEQLAB GmbH (Germany). Vector NTI Advance™ 11 (Invitrogen, Germany) or Clone Manager Professional 9 software (Scientific & Educational Software, USA) was used for *in silico* plasmid construction. A complete list for the synthesised oligonucleotides can be found in Table 9.

Table 9: Oligonucleotides.

Name	Sequence (5'-3')	Enzyme
<i>Knock-out/knock-in constructs</i>		
EcoRI-KO_lys-us-Fw	TCT ATG AAT TCC AAC CCA TCT AAC GAG AAT GCA GG	EcoRI
Sall-KO_lys-ds-Rev	CTA GTC GAC GGC AGA TTT ATC GGC TGG AGC	Sall
Ol-KO_lys-SO_2966-up-Rev	TAT GAA TAA GAC AGC GTG AAA CAA AAA AAC TCA CTT G	-
Ol-KO_lys-SO_2974-ds-Fw	TTC ACG CTG TCT TAT TCA TAG ATG CCC CAA AAC AAA AAG	-
chk-KO_lys-Fw	ATT GGC ACC GTA AGA GAT GGT GG	-
chk-KO_lys-Rev	ATA AGC TTC TTG CGA GAC TAA ACC G	-
BamHI-drecA-us-fw	ATA GGA TCC GGC GTG TTG AAA TTG ATA AGG GA	BamHI
drecA-OL-us-rev	ATG AAG GTC GAT GGC GAA GTG TTC TGA GTC AGT C	-
drecA-OL-ds-fw	GAA CAC TTC GCC ATC GAC CTT CAT TCC TGT TCC C	-
Sall-drecA-ds-rev	CTA GTC GAC CCA CGG GCA GTG AGA GAA ATA CC	Sall
drecA-chk-fw	GTG GCG TAA AAG TGG TGG AAA CG	-
drecA-chk-rev	AGG GAA TGC CCG CCA TAG GG	-
NheI_KO_oxR-Fw	ACT GCT AGC CAA TTG GTG CCG GTA CTC TAC T	NheI
US_KO_oxR-Rev	ATT GTG CCG TTA AAT TTT TCA TTT TAT CGA TTG CCA C	-
DS_KO_oxR-Fw	GAA AAA TTT AAC GGC ACA ATA ACT GAG TAT TTT GCC TG	-
Sall_KO_oxR-Rev	ACT GTC GAC GCG ATT ATC GTT TTA GCC GCT TG	Sall
chk_oxR-Fw	CCT AGA TCT CAA TAC ATT AGA ACA G	-
chk_oxR-Rev	GTT GCC TCG ACT ACC CAC GC	-
PspOMI_KO_fur-Fw	ACT GGG CCC CAG TAA CCC TGC GAT GTT GA	PspOMI
US_KO_fur-Rev	GAC AGA TGG AAA CGA CGA ATA AGC TTG CTC GGC	-
DS_KO_fur-Fw	ATT CGT CGT TTC CAT CTG TCA TTG CTA ATC TCT TG	-
NheI_KO_fur-Rev	ACT GCT AGC CAA CCA ATA ACT GCC CAG AAA ACT C	NheI
chk_fur-Fw	CGA GCA GGA TGT TGA TGC CCT C	-
chk_fur-Rev	CCA GCA CGC TCA TGT AAA TCA TC	-
EcoRI_KO_oxR-Rev	ACT GAA TTC GCG ATT ATC GTT TTA GCC GCT TG	EcoRI
Seq-oxR-Fw	TCC ATA ACC TTA GTG GCA ATC G	-
Seq-oxR-Rev	CCT TTA TAA GAC TCA CAA CAG GC	-
PspOMI_KO_LTD-Fw	ACT GGG CCC TTT ATT TGG GAA CGT GAT TAT TTG G	PspOMI
US_KO_LTD-Rev	TTG GCA CGT CCA TTA CAT TAG CGT TTG CCA TC	-
DS_KO_LTD-Fw	TAA TGT AAT GGA CGT GCC AAC CCC TGT GG	-
NheI_KO_LTD-Rev	ACT GCT AGC ACT TCA CCC TTA GTG CCA GC	NheI
chk_LTD-Fw	TAT CAG TAA ACC TAG TCA TAT TAA GGG	-
chk_LTD-Rev	CTT CTG CAA CAT AGA AAG GCG C	-
PspOMI_KO_YhcR-Fw	ACT GGG CCC CAA TAC AGC AAT AGA TCT TAC CGG	PspOMI
US_KO_YhcR-Rev	CAA ATT TCT TTA CTT CGC TTT CAG ACT CGA ATG C	-
DS_KO_YhcR-Fw	AAG CGA AGT AAA GAA ATT TGA AGC TGG CAC TAA GG	-
NheI_KO_YhcR-Rev	ACT GCT AGC CCT TTG GTG GCC ACG CTG G	NheI
chk_YhcR-Fw	GAA GGT AGC TCA AAT AAC AAA GCG	-
chk_YhcR-Rev	CAC GTT GAA ACT GGC CAC ACG	-
PspOMI_KO_EEP-Fw	ACT GGG CCC GAA ATT TGA AGC TGG CAC TAA GGG	PspOMI
US_KO_EEP-Rev	CTG GAT AGC TAT CGC CTT TGG TGG CCA CGC	-
DS_KO_EEP-Fw	CAA AGG CGA TAG CTA TCC AGC ACC TGT GGT G	-
NheI_KO_EEP-Rev	ACT GCT AGC GAA TTA ACA AAC AAC CTA CAA CCC C	NheI
chk_EEP-Fw	GTA AGG TGA AGG AAT ACT TCG GC	-
chk_EEP-Rev	CTA TTA CCG CGA CGA ACG AAG C	-
PspOMI_KI_L-TM-Fw	ACT GGG CCC TAA AAA TAC CGC CCT AGG GCG G	PspOMI
US_KI_L-TM-Rev	AAA CAG TTC AAT AGC TTA ACG CCA CAA TCA CAG G	-
DS_KI_noL_noTM-Fw	GTT AAG CTA TTG AAC TGT TTG CAC TCT CAC GAC	-
NheI_KI_noL_noTM-Rev	ACT GCT AGC GAT CAC CAC ACT TGG CAT CAC C	NheI

Material & Methods

US_KI_noL_Rev	CGC CAT CAT CAT AGC TTA ACG CCA CAA TCA CAG G	-
DS_KI_noL_Fw	GTT AAG CTA TGA TGA TGG CGG TGC GCT AGG	-
NheI_KI_noL_Rev	ACT <u>GCT AGC</u> CCA TTT GCA CTA TTA CCG CGA CG	NheI
chk_noL_noTM-Fw	GTA CTG GCA CTT ACT CAT ACA GC	-
chk_noL_noTM-Rev	CGA TGC CAA TAA GAC GCT ACA CC	-
OL-GG-AA-Rev	ACC TAG CGC <u>TGC CGC</u> ATC ATC CTT TGG CGT CGG CTG C	-
OL-GG-AA-Fw	AAG GAT GAT <u>GCG GCA</u> GCG CTA GGT TAC TTG GGC TTA GC	-
PspOMI-US-dSO_2504-Fw	ACT <u>GGG CCC</u> CTC AAC GAA TTA GCC ATT TCT GCC	PspOMI
OL-US-dSO_2504-Rev	TTT ACG CTT TCA GTT TCA CGC CTG TGG CTT ACC	-
OL-DS-dSO_2504-Fw	CGT GAA ACT GAA AGC GTA AAT ACT TGA TTC TTC TTT GAT G	-
EcoRI-US-dSO_2504-Rev	TCT <u>ATG AAT TCG</u> CGT AAC TTG GAG TTT GAA CAG G	EcoRI
chk-dSO_2504-Fw	CGA AAT CCC TCG CCC AAC GC	-
chk-dSO_2504-Rev	GCG CAG CTT AGC CAT GAT ATC G	-

Venus insertions

lambdaSo- <i>cro</i> -6xHis-OL-Rev	AAG CAT CAT CAT CAT CAT CAT TAA TTA ACT TAC GAA CAG GAT AAC	-
<i>venus</i> -6xHis-OL-Rev	TTA ATG ATG ATG ATG ATG ATG CTT GTA CAG CTC GTC CAT GCC GAG	-
lambdaSo- <i>cro</i> -RBS-OL-Fw	CTT GCT CAC CAT GTC AGT CCT CCT CTA GGC AAC TTG GTT TGA TTC	-
<i>venus</i> -RBS-OL-Fw	AGG AGG ACT GAC ATG GTG AGC AAG GGC GAG GAG	-
BamHI-lambdaSo- <i>cro</i> -US-Fw	ATA <u>GGA TCC</u> GCT GGA ATG GTA TGA ACG	BamHI
EcoRI-lambdaSo- <i>cro</i> -DS-Rev	TCT <u>ATG AAT TCG</u> AGT CTC AGC ATC AAT AG	EcoRI
lambdaSo-KLtail-6xHis-OL-Rev	AAG CAT CAT CAT CAT CAT CAT TAA AAG CAT TTT CCC GCC GTC AGC	-
lambdaSo-KLtail-RBS-OL-Fw	CTT GCT CAC CAT GTC AGT CCT CCT TTA ACG TAT TAG CCG CAC GCT	-
BamHI-lambdaSo-KLtail-US-Fw	ATA <u>GGA TCC</u> CTT GCT CGC CTT CCC ACC	BamHI
EcoRI-lambdaSo-KLtail-DS-Rev	TCT <u>ATG AAT TCG</u> GCC AGC GCA GTT AGA AG	EcoRI
chk-lambdaSo- <i>cro-venus</i> -Fw	GCG CTT CAT GCT CGA TTG CGG C	-
chk-lambdaSo- <i>cro-venus</i> -Rev	CAT AGA GGA TCT CAG CAG GTG TTA CG	-
chk-lambdaSo-KLtail- <i>venus</i> -Fw	CAG CGC TAC AAA TCC AGC CTT GGC	-
chk-lambdaSo-KLtail- <i>venus</i> -Rev	CCC GCG CGG ATT ATC CAT TGG C	-
<i>venus</i> -Strep-OL-Rev	GAT TTA TTT TTC GAA CTG CGG GTG GCT CCA GCC CTT GTA CAG CTC GTC CAT GCC GAG	-
lambdaSo-2974-RBS-OL-Fw	CTT GCT CAC CAT GTC AGT CCT CCT AGA TGC CCC AAA ACA AAA AGC	-
lambdaSo-2974-Strep-OL-Rev	TGG AGC CAC CCG CAG TTC GAA AAA TAA ATC ATG AAT AAG ATT TTG ATG AGT	-
EcoRI-lambdaSo-2974-US-Fw	TCT <u>ATG AAT TCC</u> CGT ATT GAT ACG TCC AAT CG	EcoRI
SalI-lambdaSo-2974-DS-Rev	CTA <u>GTC GAC</u> GAC TAA ACC GTA CTA GCG GCG GC	SalI
chk-PR ¹ -SO_2974- <i>venus</i> -Rev	CCA CGC ATC GGA GAG GCT AAC C	-
chk-PR ¹ -SO_2974- <i>venus</i> -Fw	GTG TAC TGG CGT GCA GCA AAT AAG C	-

Operon mapping (lysis operon)

OM-2974-2975-Fw	GAT TAG TAA CAC TCA TCA AAA TCT TAT TC	-
OM-2974-2975-Rev	GGA ATT AAG GAT GAG TTT GGC CG	-
OM-2973-2974-Fw	ACC TTG GAT AAG ATG GCC ACG	-
OM-2973-2974-Rev	GTT GCA CAT GAT AAA AGT GAA TTA GC	-
OM-2972-2973-Fw	GCC AGC AAA TCA AGA CTG CCG	-
OM-2972-2973-Rev	CAT TGC TGT TGC CAG AGT ATC G	-
OM-2971-2972-Fw	GAA GAG TGC GAT TGT TGA TGC G	-
OM-2971-2972-Rev	CAG GTA TTC GAA AGG TCC AGC	-
OM-2970-2971-Fw	CTA TTT ACC AAG TGG CTG ATG GC	-
OM-2970-2971-Rev	GCG ATG ATT ATG GAT AAA GCA ACG	-

OM-2969-2970-Fw	CGT GGC AAT GCT TGC ACA GC	-
OM-2969-2970-Rev	CCA CTG GTA CCT GCT GAT TGG	-
OM-2968-2969-Fw	GAG TAC GCC CAT GTC TTT AAG C	-
OM-2968-2969-Rev	AGC GTG GTT ACG GTG GAC G	-
OM-2967-2968-Fw	ATC CTT CCA GCC GAA CAG CG	-
OM-2967-2968-Rev	AAC TTA CCA AAG CAT CAA AAT CAT CG	-
OM-2966-2967-Fw	GAC CAA CCA AGT CCA AAC AGG	-
OM-2966-2967-Rev	CAC TGT TTG AGA TAA AAA GCA TCG G	-
OM-2965-2966-Fw	AAG TCG ATA TCC ATG CGG TGC	-
OM-2965-2966-Rev	TGG TCG CTG TTA TCT GGT TCG	-
OM-2964-2965-Fw	GCC TGG GGA ATT GAT ATA AAC GG	-
OM-2964-2965-Rev	ACA ACG GCA AAC CCA ATA CGC	-
OM-2963-2964-Fw	CTC ACC GAT TGA CTG CTC GC	-
OM-2963-2964-Rev	AGC CGA TGA AAT TGG TGA GAC C	-
OM2-2968-2969-Fw	CAT GCG GCT TTG GCT CTT GGG	-
OM2-2968-2969-Rev	CTT CTT AAA GCG CAA TCC TCT CTG C	-
OM2-2970-2971-Fw	CGT TGG TTT GGG CAG TAA TGG C	-
OM2-2970-2971-Rev	GCT ATG TCG CTT CAA TCT CTA CGG	-

Promoter fusion studies (pBBR1-TT-MSC5-RBS-venus)

PspOMI_pXVENC-2_RBS_venus_Fw	ACT <u>GGG CCC</u> AGG AGG GCA AAT ATG GTG AGC AAG GGC GAG GAG	PspOMI
KpnI_pVENC-2_venus_Rev	ACT <u>GGT ACC</u> TTA CTT GTA CAG CTC GTC CAT GCC	KpnI
EcoRI_PtonB_Fw	ACT <u>GAA TTC</u> ACC CGT AAC AGT CAT TCG CCC	EcoRI
PspOMI_PtonB_Rev	ACT <u>GGG CCC</u> GGC AAA CCT TCC AAT TCC AAA AGC	PspOMI
BamHI_Pdps_Fw	ACT <u>GGA TCC</u> AGG GTT AAT AGG ATT TTC ACT GG	BamHI
EcoRI_Pdps_Rev	ACT <u>GAA TTC</u> TCC TCC TAT TGT CCT ACT CGA TG	EcoRI

pBBR1-TT-Ptac inserts

XhoI-RBS-sodB-Fw	TAT <u>CTC GAG</u> AGG AGG GCA AAT ATG GCT TTC GAA TTA CCC GCA TTA CC	XhoI
KpnI-sodB-Rev	CTG <u>GGT ACC</u> TTA ACC TGC GAA GTT TTG GTT CAC G	KpnI

Quantitative real-time RT-PCR

<i>katB</i> -qPCR-Fw	CAC TTC AAA TCG CAG CAA GGC G	-
<i>katB</i> -qPCR-Rev	GGC ATG ATC TGC ACA TTC ACC G	-
<i>dps</i> -qPCR-Fw	TGG CAT AGG CTG AAT AGG AGC C	-
<i>dps</i> -qPCR-Rev	CGT CAC TGG TCC TAT GTT CAC C	-
<i>katG1</i> -qPCR-Fw	ATC TAC CGC GAA ATC ACC ACG C	-
<i>katG1</i> -qPCR-Rev	CTT GCC AAA TCA GTG CTT CGG C	-
<i>ahpC</i> -qPCR-Fw	TCA CGA AAG TAC CAC GCA GTG C	-
<i>ahpC</i> -qPCR-Rev	CAT GGC ACG ATA CTT CTG ACA CC	-
<i>tonB</i> -qPCR-Fw	TCG CAG GAG CAT CAC TAC ACC	-
<i>tonB</i> -qPCR-Rev	AAC CAC GGT TTG ATG AGG CGC	-
16s-rRNA-qPCR-Fw	AGG TTC ATC CAA TCG CGA GAG G	-
16s-rRNA-qPCR-Rev	GTT TAC TCA TGA GGT GGC GAG C	-
<i>recA</i> -qPCR-Fw	TCA CAT CAA CCG CAC CAG AAC G	-
<i>recA</i> -qPCR-Rev	CGC TCT TGA TCC TAT CTA CGC G	-

pMal-TEV (plasmid construction and inserts)

TEV-pMAL-Fw	GAA AAC CTG TAT TTT CAG GGC ATT TCA GAA TTC GGA TCC TCT AGA G	
OL-Tev-Rev	GCC CTG AAA ATA CAG GTT TTC CCC GAG GTT GTT GTT ATT GTT ATT G	-
OL-His9x-TEV-Fw	CAT CAT CAC CAC CAT CAC CAT CAT CAC GAA AAC CTG TAT TTT CAG GGC ATT TCA GAA TTC GGA TCC TCT AGA GTC G	-
OL-His9x-Rev	GCC CTG AAA ATA CAG GTT TTC GTG ATG ATG GTG ATG GTG GTG ATG ATG CCC GAG GTT GTT GTT ATT GTT ATT GTT G	-
pMAL_MBP_intern_Rev	GCG ATA ACG CTT CAA CAG CG	-
pMAL_Seq_promoter_Fw	CAT CGG AAG CTG TGG TAT GG	-
Seq-exeM1-Fw	GAC AAA GCA TCG CAC CTA AAG C	-
Seq-exeM2-Fw	CAC TTT CTG CCG AGG CGA CG	-
Seq-exeM3-Fw	GTA GCG ATG CCA TTA CTG TTG G	-

pBBMT-kan (overproduction of ExeM and derivatives in S. oneidensis MR-1)

NheI-RBS-exeM-pBBMT-Fw	ACT <u>GCT AGC</u> AGG AGG GCA AAT ATG GAA AAT GTT AAT AAG TTA ACA GCT GTT TC	NheI
PspOMI-exeM-pBBMT-Rev	ACT <u>GGG CCC</u> TCA ATA ACG GCG ACG ACG TTG TAA ACC	PspOMI
PspOMI-exeM-GGAA-pBBMT-	ACT <u>GGG CCC</u> TCA ATA ATA GCT TAA CGC CAC AAT CAC	PspOMI

1.10.7 Strains and plasmids

S. oneidensis MR-1 was used as the wild-type strain during this work [421]. The host strains for molecular cloning were *E. coli* DH5 α λ pir [422] and *E. coli* WM3064 (W. Metcalf, University of Illinois, USA). More detailed information on the construction and properties of plasmids can be found in section 1.12.7. Table 10 summarizes all strains and plasmids used and constructed during this work.

Table 10: Bacterial strains and plasmids

Strain or plasmid	Relevant genotype / insert	Source or reference
<i>Escherichia coli</i>		
DH5 α λ pir	ϕ 80d λ lacZ Δ M15 Δ (lacZYA-argF)U169 <i>recA1</i> <i>hsdR17</i> <i>deoR</i> <i>thi-1</i> <i>supE44</i> <i>gyrA96</i> <i>relA1</i> / λ pir	[422]
WM3064	<i>thrB1004</i> <i>pro</i> <i>thi</i> <i>rpsL</i> <i>hsdS</i> <i>lacZ</i> Δ M15 RP4-1360 Δ (<i>araBAD</i>) 567 Δ <i>dapA</i> 1341::[<i>erm</i> <i>pir</i> (wt)]	W. Metcalf, University of Illinois, Urbana-Champaign
BL21 Star (DE3)	F ⁻ <i>ompT</i> <i>hsdSB</i> (<i>rB</i> ⁻ , <i>mB</i> ⁻), <i>gal</i> <i>dem</i> <i>rne131</i> (DE3)	M. Thanbichler, MPI, Marburg
<i>Shewanella oneidensis</i> MR-1		
S79	wild type	[421]
S176	<i>Tn7::egfp</i> , tagged with <i>egfp</i> in a mini-Tn7 construct	[38]
S198	<i>Tn7::egfp</i> , tagged with <i>egfp</i> in a mini-Tn7 construct	[241]
S1387	Δ LambdaSo (Δ λ So), deletion of SO_2939 - SO_3013	[38]
S1419	Δ LambdaSo (Δ λ So) Δ MuSo2 Δ MuSo1, deletion of genes SO_2939 - SO_3013, SO_2651 - SO_2704 and SO_0641 - SO_0685	[38]

S1393	S198 Δ LambdaSo ($\Delta\lambda$ So), deletion of genes SO_2939 - SO_3013 in strain S198	[38]
S2933	$\Delta\lambda$ lysis- <i>operon</i> , deletion of genes SO_2966 - SO_2974	This work
S2933	S198 $\Delta\lambda$ lysis- <i>operon</i> , deletion of genes SO_2966 - SO_2974 in strain S198	This work
S2391	<i>Tn7::egfp</i> P λ cro:: <i>venus</i> , insertion of RBS and <i>venus-his6x</i> sequence downstream of putative <i>λcro</i> (SO_2989) in strain S176	This work
S2502	Δ <i>recA</i> , deletion of gene SO_3430	This work
S3173	<i>recA</i> complementation strain, insertion of <i>recA</i> (SO_3430) wild type copy in S2502	This work
S2425	S2391 Δ <i>recA</i> , deletion of gene SO_3430	This work
S2623	<i>Tn7::egfp</i> P λ R:: <i>venus</i> , insertion of RBS and <i>venus-his6x</i> sequence upstream of SO_2974 in strain S176	This work
S2395	<i>Tn7::egfp</i> P λ L:: <i>venus</i> , insertion of RBS and <i>venus-his6x</i> sequence downstream of SO_2949 in strain S176	This work
S2991	Δ <i>oxyR</i> , deletion of gene SO_1328	This work
S2989	Δ <i>fur</i> , deletion of gene SO_1937	This work
S2993	S2391 Δ <i>oxyR</i> , deletion of gene SO_1328 in strain S2391	This work
S3065	S2391 Δ <i>fur</i> , deletion of gene SO_1937 in strain S2391	This work
S3104	<i>oxyR</i> complementation strain, insertion of <i>oxyR</i> (SO_1328) wild type copy in S2993	This work
S3112	<i>fur</i> complementation strain, insertion of <i>fur</i> (SO_1937) wild type copy in S3065	This work
S3169	Hydrogen peroxide-resistant strain, OxyR T104N substitution	This work
S3170	Hydrogen peroxide-resistant strain, OxyR L197P substitution	This work
S3171	OxyR T104N encoded substitution in strain S2391	This work
S3172	OxyR L197P encoded substitution in strain S2391	This work
S2095	Δ <i>endA</i> , deletion of gene SO_0833	[320]
S2303	<i>endA</i> complementation strain, insertion of <i>endA</i> (SO_0833) wild type copy in S2095	[320]
S2212	<i>Tn7::egfp</i> , S2303 tagged with <i>egfp</i> in a mini-Tn7 construct	[320]
S2373	Δ <i>pboA</i> , deletion of gene SO_0830	[320]
S988	Δ <i>exxM</i> , deletion of gene SO_1066	[241]
S2160	Δ <i>exxS</i> (SO_1844), Δ <i>exxM</i> (SO_1066), Δ <i>endA</i> (SO_0833)	M. Heun, MPI Marburg
S3187	Deletion mutant of putative rhombosortase SO_2504	This work
S3709	SO_2504 complementation strain, insertion of SO_2504 wild type copy in S3187	This work
S3314	<i>Tn7::egfp</i> Δ SO_2504, strain S3187 tagged with <i>egfp</i> in a mini-Tn7 construct	This work
S3191	Δ LTD-ExeM, deletion of putative LTD domain in <i>exxM</i> (encoding aa 28-128)	This work
S3195	Δ YhcR-ExeM, deletion of putative YhcR domain in <i>exxM</i> (encoding aa 220-291)	This work
S3199	Δ EEP-ExeM, deletion of putative EEP domain in <i>exxM</i> (encoding aa 464-830)	This work
S3207	Δ linker-ExeM, deletion of putative linker (L) region in <i>exxM</i> (encoding aa 833-845)	This work
S3203	Δ L-TM-ExeM, deletion of putative linker (L) and transmembrane (TM) region in <i>exxM</i> (encoding aa 833-865)	This work
S3211	GG-AA-ExeM, G849A and G850A aa substitutions in putative linker region of ExeM	This work

Plasmids

pNPTS138-R6KT	mobRP4 ⁺ ori-R6K <i>sacB</i> ; β -galactosidase fragment alpha; suicide plasmid for in-frame deletions or integrations; Km ^r	[423]
pNPTS138-R6KT- Δ <i>recA</i>	Fragment for in-frame deletion of <i>recA</i> (SO_3430) in pNPTS138-R6KT; Km ^r	This work
pNPTS138-R6KT-KI <i>recA</i>	<i>recA</i> wild type gene copy for complementation by insertion into locus	This work
pNPTS138-R6KT- Δ lysis- <i>operon</i>	Fragment for in-frame deletion of gene region SO_2939-SO_3013 (putative lysis operon) in pNPTS138-R6KT; Km ^r	This work
pNPTS138-R6KT- Δ <i>oxyR</i>	Fragment for in-frame deletion of <i>oxyR</i> (SO_1328) in pNPTS138-	This work

	R6KT; Km ^r	
pNPTS138-R6KT-KoxyR	<i>oxyR</i> wild type gene copy for complementation by insertion into locus	This work
pNPTS138-R6KT- Δfur	Fragment for in-frame deletion of <i>fur</i> (SO_1937) in pNPTS138-R6KT; Km ^r	This work
pNPTS138-R6KT-KI fur	<i>fur</i> wild type gene copy for complementation by insertion into locus	This work
pNPTS138-R6KT-P λcro ::RBS- <i>venus</i> -His6x	Fragment for insertion of RBS and venus-his6x sequence downstream of putative <i>λcro</i> gene (SO_2989) in pNPTS138-R6KT; Km ^r	This work
pNPTS138-R6KT-P $\lambda R'$::RBS- <i>venus</i> -His6x	Fragment for insertion of RBS and venus-his6x sequence upstream of SO_2974 in pNPTS138-R6KT; Km ^r	This work
pNPTS138-R6KT-P λL ::RBS- <i>venus</i> -His6x	Fragment for insertion of RBS and venus-his6x sequence downstream of SO_2949 in pNPTS138-R6KT; Km ^r	This work
pNPTS138-R6KT-KI-OxyR-T104N	Fragment for in-frame insertion of OxyR T104N construct (H ₂ O ₂ resistance); Km ^r	This work
pNPTS138-R6KT-KI-OxyR-L187P	Fragment for in-frame insertion of OxyR L187P construct (H ₂ O ₂ resistance); Km ^R	This work
pXVENC-2	Template vector for cloning of <i>venus</i> sequence; Km ^r	M. Thanbichler, MPI, Marburg
pME6031-P $motB$ - <i>lacZ</i>	Constitutive expression of <i>lacZ</i> , <i>motAB</i> promoter fused to <i>lacZ</i> , Tc ^R	[38]
pBBR1-MCS5-TT	Terminators <i>lambda T0</i> and <i>rrnB1 T1</i> cloned into pBBR1-MCS5, Gm ^R	Dr. S. Bubendorfer, Medizinische Hochschule Hannover
pBBR1-TT-MSC5-RBS- <i>venus</i>	Vector for promoter fusions, optimal RBS sequence upstream of venus gene, Gm ^R	This work
pBBR1-TT-MSC5-P dps -RBS- <i>venus</i>	Putative promoter region of <i>dps</i> (SO_1158) in pBBR1-TT-MSC5-RBS- <i>venus</i> , Gm ^R	This work
pBBR1-TT-MSC5-P $tonB$ -RBS- <i>venus</i>	Putative promoter region of <i>tonB</i> (SO_3670) in pBBR1-TT-MSC5-RBS- <i>venus</i> , Gm ^R	This work
pBBR1-TT-Ptac-MCS5	Tac promoter region in pBBR1-MCS5-TT for constitutive expression, Gm ^R	This work
pBBR1-TT-Ptac-MCS5- <i>sodB</i>	<i>sodB</i> (SO_2881) in pBBR1-TT-Ptac-MCS5, Gm ^R	This work
pNPTS138-R6KT- $\Delta endA$	Fragment for in-frame deletion of <i>endA</i> (SO_0833) in pNPTS138-R6KT; Km ^r	[320]
pNPTS138-R6KT-KI- <i>endA</i>	Wild type gene copy of <i>endA</i> (SO_0833) in pNPTS138-R6KT for complementation by insertion; Km ^r	[320]
pNPTS138-R6KT- $\Delta phoA$	Fragment for in-frame deletion of <i>phoA</i> (SO_0830) in pNPTS138-R6KT; Km ^r	[320]
pLacTac	<i>repA oriV_{pVS1} oriVp15A oriT lacI^{q1}</i> -P _{tac} , Tet ^R	[320]
pLacTac-endA	<i>endA</i> (SO_0833) gene copy in pLacTac	[320]
pMal-P2X	pMB1 <i>ori lacI^q malE</i> , vector for overproduction of proteins fused N-terminally to the maltose-binding protein to be targeted to the periplasm; Amp ^R	New England Biolabs
pMal-P2-0833-N	<i>endA</i> (SO_0833) lacking the N-terminal signal sequence (aa 31-258) in pMal-P2X, Amp ^R	[320]
pMAL_P2_TEV	Overexpression vector, N-terminal MBP fusion, TEV protease cleavage site, periplasmic secretion	This work
pMAL_P2_9xHis_TEV	Overexpression vector, N-terminal MBP fusion, TEV protease cleavage site, periplasmic secretion, 9xHis-tag at C-terminus of MBP	This work
pMAL_P2_TEV_exeM	Encoding ExeM without N-terminal signal peptide and C-terminal transmembrane region (aa 27-849) in pMAL_P2_TEV	This work
pMAL_P2_TEV_exeM-Strep	Encoding C-terminally Strep-tagged ExeM without N-terminal signal peptide and C-terminal transmembrane region (aa 27-849) in pMAL_P2_TEV	This work
pNPTS138-R6KT- ΔSO_{2504}	Fragment for in-frame deletion of putative rhombosortase SO_2504 in pNPTS138-R6KT; Km ^r	This work
pNPTS138-R6KT-KI-SO_2504	Wild type gene copy of putative rhombosortase SO_2504 in pNPTS138-R6KT for complementation by insertion; Km ^r	This work
pBBMT-kan-exeM	Wild type gene copy of <i>exeM</i> and RBS in pBBMT-kan for overproduction in <i>Shewanella oneidensis</i> MR-1	This work
pBBMT-kan-exeM- ΔLTD	Deletion of putative LTD domain in <i>exeM</i> (encoding aa 28-128) + RBS	This work

	in pBBMT-kan for overproduction in <i>Shewanella oneidensis</i> MR-1	
pBBMT-kan-exeM-ΔYhcR	Deletion of putative YhcR domain in <i>exeM</i> (encoding aa 220-291) + RBS in pBBMT-kan for overproduction in <i>Shewanella oneidensis</i> MR-1	This work
pBBMT-kan-exeM-ΔEEP	Deletion of putative EEP domain in <i>exeM</i> (encoding aa 464-830) + RBS in pBBMT-kan for overproduction in <i>Shewanella oneidensis</i> MR-1	This work
pBBMT-kan-exeM-Δlinker	Deletion of putative linker region in <i>exeM</i> (encoding aa 833-845) + RBS in pBBMT-kan for overproduction in <i>Shewanella oneidensis</i> MR-1	This work
pBBMT-kan-exeM-ΔL-TM	Deletion of putative linker region in <i>exeM</i> (encoding aa 833-865) + RBS in pBBMT-kan for overproduction in <i>Shewanella oneidensis</i> MR-1	This work
pBBMT-kan-exeM-GG-AA	<i>exeM</i> construct encoding G849A and G850A aa substitutions in putative linker region + RBS in pBBMT-kan for overproduction in <i>Shewanella oneidensis</i> MR-1	This work
pBAD-mtrB-Strep	Construct for overproduction of Strep-tagged MtrB (SO_1776) in <i>Shewanella oneidensis</i> MR-1	J. Gescher, Universität Freiburg

Abbreviations: Amp^R, Ampicillin Resistance; Kan^R, Kanamycin Resistance; Cm^R, Chloramphenicol Resistance; Gm^R, Gentamycin Resistance; Tet^R, Tetracycline Resistance; aa, amino acid residue; RBS, Ribosomal Binding Site

1.11 Microbiological methods

If not indicated otherwise, microbiological assays were performed in triplicates in at least two independent experiments.

1.11.1 Cultivation of *E. coli*

E. coli strains were grown aerobically in LB medium at 37 °C overnight. Liquid cultures were incubated in a shaker at 220 rpm. When necessary, liquid media were solidified using 1.5 % (w/v) agar and supplemented with the respective antibiotics/additives (Table 5 and Table 6).

1.11.2 Cultivation of *S. oneidensis* MR-1

S. oneidensis strains were cultivated aerobically at 30 °C in LB or LM in a shaking culture (220 rpm). For growth on solid media 1.5 % (w/v) agar was added. Media were supplemented with the listed additives and antibiotics when necessary (Table 5 and Table 6). Before inoculation in liquid media from a frozen stock, *S. oneidensis* strains were streaked on LB 1.5 % (w/v) agar plates, with the respective antibiotics.

Optical density of bacterial cultures was measured in a spectral photometer at 600 nm (OD₆₀₀).

1.11.3 Storage of bacteria

For long-term storage in the strain collection, strains were grown to mid log phase and supplemented with DMSO to a final concentration of 10 % (v/v) and stored at -80 °C.

1.11.4 Cultivation of biofilms under static conditions

Quantification of biofilm biomass

To determine the biomass of biofilms grown under static conditions, the cells were cultivated in 96-well microtiter plates as described previously [24]. Each microtiter plate well was filled with 175 μ l of LM medium (15 mM lactate) and inoculated with 5 μ l of an overnight culture. After incubation for 24 h at 30 °C, the OD₆₀₀ was determined for each well using the Tecan Infinite M200 microplate reader (Tecan, Switzerland). Subsequently, the biofilms were stained by addition of 10 μ l of a 0.5 % (w/v) crystal violet solution, followed by incubation for 10 min at room temperature. The supernatant was removed and the cells were washed once with water. Subsequently, 200 μ l of 96 % (v/v) ethanol was added to dissolve the crystal violet stain. Finally, the absorbance at 580 nm was quantified spectrophotometrically as a measure of total biofilm biomass, using the Tecan Infinite M200 microplate reader. The values were normalized with the OD₆₀₀ of the supernatant to obtain a biofilm-to-growth ratio.

Harvesting biofilm biomass

For harvesting of biofilm biomass, the cells were cultivated in petri dishes in LM medium as described earlier [38] and collected by scraping and centrifugation in fresh medium. Cultivation and harvesting of anaerobically grown biofilms was performed in glass bottles containing glass beads (5 mm diameter, soda-lime glass, Carl-Roth, Karlsruhe, Germany). The glass beads were completely covered with LM medium containing 15 mM lactate. To remove oxygen from the media, the bottles were stoppered, sealed, and flushed with nitrogen for several minutes with periodic shaking. Cells were adjusted to an OD₆₀₀ of 0.05 and incubated at room temperature for 24 hours. After removal of the supernatant the cells were harvested by shaking in fresh medium.

1.11.5 Cultivation of biofilms in flow cells

For image acquisition, biofilms were cultivated under hydrodynamic conditions in three-channel flow cells essentially as previously described [24, 38, 424]. The setup was assembled as follows:

Preparation of flow cells and media reservoirs

Flow cells (1x4x40 mm) were prepared by gluing 24x60 mm glass slides (Carl-Roth, Germany) onto the flow cells as illustrated in Figure 33. Either white or black ‘aquarium silicone’ was used for glueing, to facilitate visual control of glueing procedure and to prevent the release of potentially toxic substances, respectively.

LM medium (0.5 mM lactate) was prepared and autoclaved in a large Erlenmeyer flask that was supplied with silicone tubing (2x4 mm) for the medium reservoir, appropriate connectors (VWR International GmbH, Germany) and 1.65x3.35 mm Tygon® 3350 tubes for the peristaltic pump (VWR International GmbH, Germany). The tubes were closed with clamps to prevent loss of media by capillary forces or vapor pressure during autoclaving. If required, sterile-filtered FeCl₂ or desferrioxamine mesylate salt was added to the medium reservoir after autoclaving.

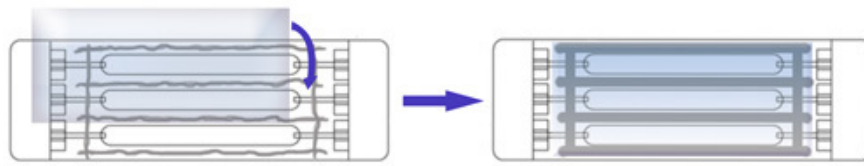


Figure 33. Gluing technique to attach glass slides on flow cells with silicone glue. A syringe and a pipette tip were used to apply an appropriate amount of silicone glue onto the flow cell without any gaps. The glass slide (24 x 60 mm) was pressed evenly on the flow cell using a flat object. Figure derived from Weiss Nielsen and coworkers [424].

Assembly, sterilization, pre-culture

Bubble traps equipped with 5 ml Injekt® Syringes (Brown Melsungen AG, Germany), silicone tubes (1x3 mm), connectors (VWR International GmbH), and flow cells (equipped with silicone glue and glass slides a day in advance) were assembled as illustrated in Figure 34 and placed in a vessel for subsequent sterilization. To prevent the bubble traps and flow cells from damage by heat, the setup is 'sterilized' at 100 °C for 30 min (agar melting program).

As pre-culture, strains of interest were inoculated in 10 ml LB medium containing appropriate antibiotics, and incubated overnight with orbital shaking (220 rpm).

Initiation and inoculation

The entire system was assembled as depicted in Figure 34 and the medium flow was set to maximal velocity (90 rpm). Once filled with approximately 4 ml medium, the bubble traps were closed with short silicon tubes and clamps. Remaining gas bubbles in the flow cells were removed by gentle 'knocking' against a solid surface. The medium flow was set to 0.5 rpm for 2 hours. Meanwhile, the overnight cultures were diluted 1:10 in fresh LM medium (15 mM lactate) and incubated for 2 hours with orbital shaking (220 rpm). Subsequently, the OD₆₀₀ of all cultures was adjusted to 0.05 in LM medium (0.5 mM lactate). Five hundred microliters of each cell suspension were injected with a 2 ml-syringe (equipped with a thin 0.45x23 mm needle) into the silicone tube directly 'upstream' of the flow cell. The silicone tube was closed with a clamp 'upstream' of the injection site to

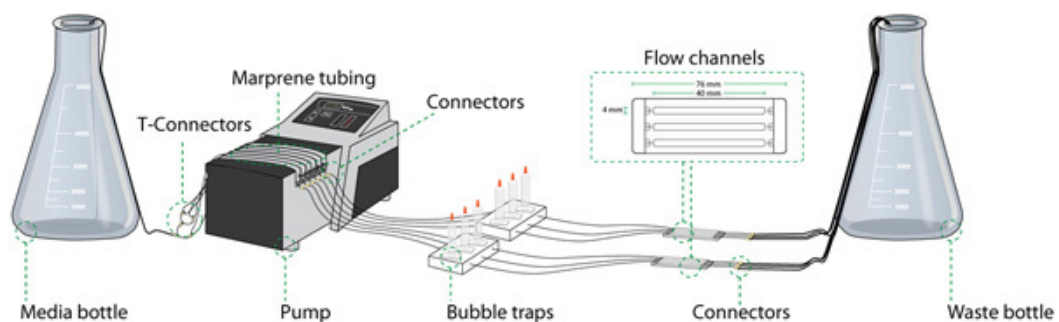


Figure 34. Setup of the flow cell system. Schematic illustration of the essential components of the flow cell system: Medium bottle, silicone tubing, connectors, peristaltic pump, bubble trap, flow cells with three flow channels, and waste bottle. Figure derived from Weiss Nielsen and coworkers [424].

minimize growth in the influx system. The bacteria were allowed to attach for 20 min before the flow was raised to 0.75 rpm (66 $\mu\text{l}/\text{min}$ per channel).

Analysis and image acquisition by confocal laser scanning microscopy

Confocal laser scanning microscopy and image acquisition was performed as described in section 1.14.2. If not indicated otherwise, microscopic visualization was performed at defined locations close to the inflow at 0.5, 4, 24, and 48 hours.

For eDNA staining, DDAO (7-hydroxy-9H-(1,3 dichloro-9,9-dimethylacridin-2-one); Invitrogen, Darmstadt, Germany) was added to a final concentration of 4 μM directly in the bubble trap 45 min prior to microscopy.

Wash, sterilization, storage

The system was flushed with 70 % ethanol (v/v) overnight, then sterilized with 0.5 % (v/v) sodium hypochloride (Sigma-Aldrich, Germany) for 1 hour, and finally washed with ddH₂O for 3-4 hours. Bubble traps, syringes and flow cells were stored in 96 % ethanol (v/v). Silicone tubes and connectors were stored at room temperature in the dark.

1.11.6 Cultivation of biofilms in the cell harvesting system

To harvest biofilm cells grown under hydrodynamic conditions for subsequent Western immuno detection analyses, we utilized the ‘cell harvesting system’. A similar setup and protocol was established earlier in our lab for transcriptome analyses of biofilm cells [286].



Figure 35. Setup of the biofilm cell harvesting system. The system consist of medium reservoirs (right), a peristaltic pump, syringes with glass beads, waste bottles (left), and silicon tubing connecting the different components.

Assembly of the ‘cell harvesting system’

The system consists of 50-ml syringes (Brown Melsungen AG, Germany) filled approximately with 200 glass beads (5 mm diameter, soda-lime glass, Carl-Roth, Germany) that serve as a surface for

biofilm formation. Approximately 3 cm of LM medium (0.5 mM lactate) was added to the syringes to ensure that all glass beads are barely covered with medium to avoid oxygen gradients. The syringes were locked with rubber plugs and connected to a peristaltic pump and a medium and waste reservoir reservoir by 2x4 mm silicone tubes, connectors (Sigma-Aldrich, Germany) and 1.2x40 mm Sterican® Needles (Brown Melsungen AG, Germany) as illustrated in Figure 33. A constant medium flow of 3 ml min⁻¹ (25 rpm) was applied to provide a highly oxic hydrodynamic environment that resembles that of flow cell biofilms.

Preculture, calibration, inoculation

For calibration, the system was run at least two hours without cells. For inoculation, an overnight culture grown in LB medium was diluted 1:10 in LM medium, incubated with orbital shaking (220 rpm) for 2 hours and adjusted to an OD₆₀₀ of 0.1. The flow was stopped and the medium supernatant in the syringes was exchanged with cell suspension (outflow was interrupted by clamps). The cells were allowed to attach to the glass beads for 20 min before the flow was started again. Notably, for the removal or insertion of the rubber plugs, the silicon tubes need to be disconnected to avoid generation of pressure variances.

Cell harvest

After 24 hours, the medium supernatant in the syringes was gently removed and the glass beads were collected in 50-ml reaction tubes. After the addition of 10 ml fresh LM medium, the reaction tubes were ‘vortexed’ for 1 min and the supernatant was collected in a 15-ml reaction tube. The OD₆₀₀ of the cell suspension was determined for sample-normalization. Finally, the biofilm cells were collected by centrifugation and stored at -20 °C for further analyses.

Wash, sterilization, storage

Fresh syringes and glass beads were used for each run. Silicone tubes were flushed with 70 % ethanol (v/v) overnight, then sterilized with 0.5 % (v/v) sodium hypochloride (Sigma-Aldrich, Germany) for 1 hour and finally washed with ddH₂O for 3-4 hours. The tubes were stored at room temperature in the dark.

1.11.7 β-galactosidase activity in culture supernatants

Extracellular β-galactosidase activity of culture supernatants was determined as previously described [38]. Exponentially growing planktonic cultures of *S. oneidensis* MR-1 were incubated with mitomycin C for 3 hours. All strains harbored plasmid pME6031-*PmotB-lacZ* for constitutive cytoplasmic expression of β-galactosidase. To obtain cell-free supernatant, the samples were centrifuged at 2,500 x g for 5 min and subsequently filtered (0.2 μm filter). β-galactosidase assays on supernatants were carried out in reaction tubes at 30 °C according to standard protocols [425]. The β-galactosidase activity was normalized to the OD₆₀₀ of the culture prior to incubation with mitomycin C.

1.11.8 Time-lapse analysis of phage-induced lysis

Exponentially growing cultures of strain S2391 were exposed to UVC light and incubated at 30 °C with orbital shaking at 220 rpm for 3 hours. Four microliters of propidium iodide (Sigma-Aldrich, Steinheim, Germany) stock solution (1 mg ml⁻¹) was added on top of agar pads and incubated for several minutes to be completely absorbed into the agar. Subsequently, 4 µl of the cell suspension (OD₆₀₀ 0.5) were placed on the same agar pad (1 % agarose in PBS Buffer, 137 mM NaCl, 2.7 mM KCl, 6.6 mM Na₂HPO₄, 1.8 mM KH₂PO₄) and analyzed by fluorescence microscopy in 10-min intervals using an Axio Imager.M1 microscope (Zeiss, Wetzlar, Germany) equipped with a Zeiss Plan Achromate 100x/1.4 DIC objective.

1.11.9 Determination of cell length

Exponentially growing planktonic cultures of *S. oneidensis* MR-1 were incubated with mitomycin C at a final concentration of 10 µg ml⁻¹ for 4 hours. All cell suspensions were adjusted to an OD₆₀₀ of 0.5 and 4 µl of each suspension was placed on an agar pad. Image acquisition was carried out by differential interference contrast microscopy (DIC) using a Leica DMI6000B microscope equipped with a Leica HCX PlanApo 100x/1.4-0.7 Oil objective. Cell lengths were determined of at least 800 cells per strain using ImageJ 1.47v software (National Institute of Health, USA) from duplicates in two independent experiments.

1.11.10 Isolation of H₂O₂-resistant mutants

For the isolation and identification of an *oxyR* mutation that provides increased resistance against H₂O₂ in *S. oneidensis* MR-1, we used a similar approach as described earlier for *Xanthomonas campestris* [426, 427]. To avoid selection of mutations in prophage genomes that would reduce induction and/or lysis, we used the prophage-deficient strain S1419 as template. In total, approximately 1.5 x 10¹⁰ cells in mid-exponential phase were transferred to LB agar plates (1.5 x 10⁸ cells/plate) containing 2 mM H₂O₂ (Carl-Roth, Germany). To verify that mutants retain resistance after non-selective growth, single colonies were cultivated overnight in plain LB and reinoculated in LB medium containing 10 mM H₂O₂. Mutated *oxyR* regions were sequenced, then cloned into pNPTS-128-R6K and reintroduced in strain S2991 and strain S2391 by markerless in-frame insertion. Resistance was confirmed by cultivation in LB containing 10 mM H₂O₂.

1.12 Molecular biological methods

Molecular biological methods carried out according to standard protocols [416, 428] or by following manufacturer's instructions. The used kits are listed in 1.10.4. If not indicated otherwise, experimental assays were performed in triplicates in at least two independent experiments.

1.12.1 Isolation of DNA

Plasmid DNA

Plasmid DNA from *E. coli* was isolated using the Zyppy™ Plasmid Miniprep Kit (Zymo Research, Germany) or E.Z.N.A. Plasmid Mini Kit (VWR International GmbH, Germany).

Chromosomal DNA

S. oneidensis MR-1 chromosomal DNA was isolated following the protocol by Pospiech and coworkers [428]. Cells were grown overnight in 10 ml LB medium, harvested by centrifugation (10 min, 3,000 x g), and resuspended in 2 ml SET-buffer. Lysozyme was added to a concentration of 1 mg ml⁻¹ and the suspension was supplemented with 10 µl RNase (stock concentration: 20 µg ml⁻¹) and incubated at 37 °C for 1 hour. Subsequently, 200 µl of 10 % (w/v) SDS (1/10 of the volume) and 0.5 mg ml⁻¹ proteinase K were added to the mixture and incubated at 55 °C for 2 hours. Afterwards, 1/3 volumes 5 M NaCl and 1 volume chloroform were added and incubated at room temperature for 0.5 hours with frequent inversions. After centrifugation (15 min, 5000 x g) the upper (aqueous) phase was transferred to a new reaction cup using a clipped pipette tip. The DNA was then precipitated by adding 1 volume of isopropanol, gentle inversion and transferred to a 2-ml reaction cup with a Pasteur pipette, rinsed with 70 % (v/v) ethanol, dried at room temperature and dissolved in 500 µl TE buffer. The concentration of the extracted DNA was determined using a NanoDrop ND-100 (Peqlab, Germany) and/or by agarose gel-electrophoresis.

SET buffer (Salt-EDTA-Tris), pH 7.5	NaCl	75 mM
	EDTA	25 mM
	Tris/HCl	20 mM
TE buffer (Tris-EDTA), pH 7.5	Tris/HCl	10 mM
	EDTA	1 mM

1.12.2 Polymerase chain reaction (PCR)

PCR amplification of specific gene regions of chromosomal or plasmid DNA was carried out using the Phusion™ Polymerase (Biozym Scientific GmbH, Germany) along with the supplied Phusion HF reaction buffer (5x) following the manufacturer's instructions. Successful amplification of PCR fragments was verified by agarose gel electrophoresis (1.12.5). Gene fragments were purified with the DNA Clean & Concentrator Kit (Zymo Research, Germany) or E.Z.N.A. Probe Purification Kit (VWR International GmbH, Germany).

Plasmid uptake or correct integration into the genome of *E. coli* or *S. oneidensis* was verified by 'colony'-PCR. *E. coli* colony material was directly added to the reaction mix, whereas *S. oneidensis* colonies were resuspended in 50 µl ddH₂O and denatured at 95 °C for 7 minutes. Two microlitres

Taq-Polymerase PCR

0.15 µl	Forward primer (50µM)
0.15 µl	Reverse primer (50 µM)
2.5 µl	10x Taq buffer
2.1 µl	MgSO ₄ (60 mM)
0.5 µl	dNTP's (10 mM)
1 µl	Taq- Polymerase
1 µl	chromosomal DNA
17.6 µl	ddH ₂ O

Phusion^R-Polymerase PCR

0.6 µl	Forward primer (50µM)
0.6 µl	Reverse primer (50 µM)
10 µl	5x HF buffer
1 µl	dNTP's (10 mM)
0.25 µl	Phusion ^R -Polymerase
1 µl	chromosomal DNA
36.55 µl	ddH ₂ O

were added to the reaction mix and a standard PCR (35 cycles) was performed using Taq-Polymerase.

To construct either N- or C-terminal protein fusions or markerless *in-frame* deletions of specific genes in *S. oneidensis* MR-1, an 'overlap-PCR' with PhusionTM polymerase was performed. For this purpose, fragments 500-600 bps upstream and downstream of the target gene were PCR-amplified and fused in a second PCR by overlap extension (10 bps) using the outer primer pairs with respective restriction sites. 5'-overhanging regions of the primers were designed in a manner that each fragment was supplemented with an outer restriction site and an inner 10 bp overlapping region.

1.12.3 Restriction enzyme digests

DNA fragments or plasmids (2-5 µg) were digested with the respective restriction endonucleases (New England Biolabs, Germany; Fermentas, Germany) with the recommended buffer for 3 to 12 h at 37 °C following the manufacturer's instructions. Restricted DNA fragments or plasmid separated by gel electrophoresis were excised and purified with the Zymo CleanTM Gel DNA Recovery Kit (Zymo Research, Germany) or E.Z.N.A.[®] Gel Extraction Kit (VWR International GmbH, Germany).

1.12.4 Ligation of DNA

Ligation of PCR fragments and plasmid DNA was performed using T4 Ligase and appropriate buffer systems (New England Biolabs, Germany) according to the manufacturer's instructions. Ligation mixtures were incubated on melting ice overnight or at room temperature for 2 hours. In general, a 5-fold molar excess of DNA insert was incubated with 50 ng of the recipient vector.

$$\text{Mass of insert DNA (ng)} = \frac{50 \text{ ng} \times \text{size of insert (bp)}}{\text{size of plasmid (bp)}}$$

1.12.5 Agarose gel electrophoresis

DNA probes were supplemented with 5x loading dye (50 % (v/v) glycerine, 0.25 % (w/v) bromphenol blue added to 1 x TAE) and separated by size in 1 % agarose gels prepared in 0.5 x TAE (0.175 % acetic acid, 20 mM Tris base, 0.5 mM EDTA) and 0.005 % EtBr. DNA fragments were visualised using a 2UV-Transilluminator (UVP, USA).

1.12.6 DNA sequencing

DNA fragments or plasmids were sequenced using a method that is based on chain-termination sequencing by Sanger [429]. DNA sequencing was outsourced to MWG Operon (Germany) or SEQLAB GmbH (Germany). Digital raw data were analyzed by VectorNTI™ software (Invitrogen, Germany) or Clone Manager Professional 9 software (Scientific & Educational Software, USA).

1.12.7 Plasmid construction

In silico generation of plasmids was done using Vector NTI Advance™ 11 (Invitrogen, Germany) or Clone Manager Professional 9 software (Scientific & Educational Software, USA). A list of the constructed plasmids can be found in Table 10. Specific oligonucleotides used for plasmid construction carried restriction enzyme recognition sites at their 5'-end, as annotated in Table 9.

High-copy plasmids for arabinose-inducible gene expression

To achieve high levels of proteins or fusion proteins in *S. oneidensis* MR-1, genes of interest or modified gene constructs were inserted into pBBMT-kan, a self-replicating plasmid. To this end, the corresponding target gene was PCR amplified with oligonucleotides carrying the specific restriction enzyme recognition sites at their 5'-end. Additionally, an optimal ribosomal binding site (AGGAGGNNNNN) was inserted by PCR amplification directly upstream of the start codon. The resulting fragment as well as pBBMT-kan were restricted and ligated, following the protocol in section 1.12.3 and 1.12.4. Truncated gene variants were constructed using either 'overlap-PCR' or were directly amplified from chromosomal DNA isolated from the corresponding *S. oneidensis* MR-1 mutants, and then cloned into pBBMT-kan as described above. The resulting vectors were transferred into *S. oneidensis* by conjugation (section 1.12.9).

High-copy plasmids for constitutive gene expression

For constitutive overexpression of genes of interest in *S. oneidensis* MR-1, the high-copy plasmid pBBR1-MCS5-TT (Table 10) was supplied with the *tac*-promoter sequence (*P_{tac}*). The *tac* promoter is a functional hybrid of the *trp* and *lac* promoter and repressed by the *lac* repressor in *E. coli* [430]. *S. oneidensis* MR-1 does not harbor a *lacI* gene homolog, resulting in constitutive expression of the gene of interest. To end transcription, the plasmid pBBR1-MCS5-TT contains two terminator sequences downstream of the multiple cloning site. The insertion construct was supplied with a

ribosomal binding site (AGGAGGNNNNNN) by PCR amplification. The resulting plasmid was introduced into *S. oneidensis* MR-1 by conjugation (section 1.12.9).

High-copy plasmids for fluorescence-based promoter fusion studies

For plasmid-based promoter fusion studies vector pBBR1-MCS5-TT-RBS-venus was constructed using pBBR1-MCS5-TT as vector backbone and pXVENC-2 as template for the *Venus* coding sequence. A ribosomal binding site (AGGAGGNNNNNN) was added to the *Venus* insertion construct by PCR amplification. Putative promoter regions were identified by bioinformatic analyses and cloned into the multiple cloning sites. The resulting plasmid was introduced into *S. oneidensis* MR-1 by conjugation (section 1.12.9).

pMal-P2-0833-N for overproduction and purification of MBP-EndA

To construct a plasmid for the overproduction of EndA, gene SO_0833 was amplified without the sequence encoding the native signal peptide and was cloned into pMal-P2X using BamHI and SalI to result in an *in-frame* fusion to *malE*, encoding the maltose-binding protein (MBP). The primers used are listed in Table 9.

pMAL-TEV plasmids for overproduction and purification of MBP-ExeM

The pMAL-P2X vector system (NEB, USA) was used as template to construct the pMAL-TEV vectors that encode instead of a Factor Xa protease cleavage site a TEV protease cleavage site (pMAL-TEV) and optionally an additional His9x-tag at the C-terminus of the MBP protein for Immunodetection and affinity chromatography. For this study, plasmid pMAL-TEV-exeM was used for overproduction and purification of ExeM, lacking the N-terminal signal sequence and C-terminal hydrophobic regions (see section 1.13.7).

Plasmids for markerless in-frame gene deletion and insertion

In-frame deletion and insertion fragments were constructed using the ‘overlap-PCR’ described in 1.12.2. Overlap-fragments and the suicide vector pNPTS-138-R6K were restricted with the corresponding enzymes, purified by agarose gel electrophoresis and subsequently ligated (see section 1.12.3, 1.12.5, 1.12.4).

Plasmids for genome-integrated transcriptional fusions to *Venus*

Genome-integrated transcriptional fusions to *Venus* were constructed using plasmid pXVENC-2 (1.10.7) as template for the *Venus* coding sequence and pNPTS-138-R6K for markerless insertion downstream of each gene of interest. The *Venus* coding sequence was supplied with overlapping regions at both ends, and a ribosomal binding site (AGGAGGNNNNNN) was inserted upstream of the *Venus* start codon, using PCR amplification with appropriate primer pairs (see section 1.12.2 and Table 9). The up- and downstream flanking regions (500-600 bps) of the target insertion sites were also PCR amplified and supplied with overlapping regions to the insertion construct and terminal restriction enzyme sites for ligation into pNPTS-138-R6K. A final ‘overlap-PCR’ (as

described in section 1.12.2) using all three DNA fragments in a 1:1:1 ratio was performed using the outer primer pairs of the upstream and downstream fragment. The resulting gene fusion was restricted and ligated into the suicide vector pNPTS138-R6KT (see section 1.12.3, 1.12.4).

All vectors were propagated in *E. coli* DH5 α and, for the purpose of conjugation, transferred in *E. coli* WM3064. The vectors were then transferred to *S. oneidensis* MR-1 by conjugation as described in section 1.12.9.

1.12.8 Preparation and transformation of chemically competent *E. coli* cells

Preparation of chemically competent *E. coli* cells was done using an optimized protocol of Inoue and coworkers [431]. *E. coli* was grown to an OD₆₀₀ of 0.6 in 250 ml SOB media at 18 °C and placed onto ice for 10 min. Subsequently, cells were centrifuged (10 min, 4,600 x g, 4 °C) and the cell pellet was resuspended in 80 ml ice-cold TB buffer and incubated on ice for 10 min. After an additional centrifugation step the cell pellet was resuspended in 20 ml TB buffer supplemented with 7 % (v/v) DMSO. The cells were placed again on ice for 10 min before aliquoted (400 μ l) and snap-frozen in liquid nitrogen.

E. coli WM3064 cells were grown in SOB media containing 300 μ M DAP.

TB (Transformation Buffer) , pH 6.7	Pipes	10 mM
	MnCl ₂	55 mM
	CaCl ₂	15 mM
	KCl	250 mM

Transformation of chemically competent *E. coli* cells was done according to the protocol of Inoue and coworkers [431]. To introduce plasmids, 100 μ l of chemically competent *E. coli* cells were thawed on ice, mixed with 20 μ l of the ligation mixture or 20 ng plasmid DNA and incubated for 30 min on ice. After performing a heat-shock at 42 °C for 30 seconds, cells were placed on ice and supplemented with 1 ml SOB (SOB with 300 μ M DAP for WM3064). The cultures were allowed to recover for 1 to 2 h at 37 °C under shaking conditions and spread on LB agar plates supplemented with the appropriate additives. After 12 h single colonies of recombinant *E. coli* cells were restreaked on fresh LB plates and verified by colony PCR.

1.12.9 Conjugation of *S. oneidensis* MR-1 cells

Conjugation of *S. oneidensis* was performed using an optimized protocol of Thormann and coworkers [99]. Plasmids were introduced in *S. oneidensis* by mating, using *E. coli* WM3064 as a donor strain. After overnight cultivation of recipient and donor strain, 1 ml of the culture was centrifuged (1 min, 13,000 rpm) and washed three times in LB medium. Both pellets were unified in 250 μ l LB medium and spotted as one drop on a LB-agar plate containing 300 μ M DAP. After incubation for 12 h at 30 °C, colonies were suspended in 2 ml LB, washed three times in LB and

plated on LB-agar plates supplemented with the respective antibiotics for selection. Single crossover integration mutants were restreaked on LB-agar plates, containing the appropriate antibiotics and finally verified by colony PCR.

The standard protocol as described above was expanded for the purpose of markerless *in-frame* deletions or insertions by using pNPTS138-R6KT. Kanamycin resistant colonies were cultured overnight in LB without antibiotics and plated on LB agar plates containing 10 % (w/v) sucrose to select for double crossover events. Subsequently, cells were restreaked in parallel on LB and LB-kanamycin plates to screen for kanamycin-sensitive colonies. In-frame deletions or insertions were confirmed by colony PCR. Complementation of in-frame deletions was achieved by reinsertion of the wild-type copy into the native locus (Appendix, Figure 43).

1.12.10 Total-RNA extraction and reverse transcriptase PCR (RT-PCR)

For operon mapping of the putative lysis operon of prophage λ So, total RNA was extracted from *S. oneidensis* MR-1 cells by using a hot-phenol method [432] as described previously [38]. To induce transcription of the putative lysis operon, exponentially growing planktonic cultures were incubated with mitomycin C for two hours, harvested by centrifugation (1 min at 13,000 x *g* and 4°C), frozen in liquid nitrogen and stored at -80 °C. Residual contaminating DNA was removed by using the Turbo DNA-free kit (Applied Biosystems, Darmstadt, Germany) according to the manufacturer's instructions. The quality of the RNA was determined by agarose gel electrophoresis. The extracted total RNA was then applied as the template for random-primed first-strand cDNA synthesis using BioScript reverse transcriptase (Bioline, Luckenwalde, Germany) according to the manufacturer's instructions. Operon mapping was carried out by PCR, using the resulting cDNA as template and appropriate primer pairs, bracketing the gaps between the genes to be analyzed. A corresponding total-RNA sample that was taken prior to the reverse transcriptase reaction served as a negative control, and chromosomal DNA served as a positive control. The PCR products were analyzed by 2 % agarose gel electrophoresis.

1.12.11 Quantitative real-time RT-PCR (qPCR)

To perform a transcriptomic analysis by qPCR of the OxyR regulon in response to H₂O₂, *S. oneidensis* MR-1 cultures were grown in LB medium at 30 °C to an OD₆₀₀ of 1 and exposed to 2 mM H₂O₂ for 15 minutes. Directly before and after the H₂O₂-treatment cells were harvested by centrifugation (1 min at 13,000 *g* and 4°C) and stored immediately in liquid nitrogen.

Total RNA extraction and cDNA synthesis was carried out essentially as described for RT-PCR. The cDNA was used as template for quantitative real-time RT-PCR (C1000™ Thermal Cycler with CFX96™ Real-Time System, Bio-Rad Laboratories GmbH, München, Germany), by using the Sybr green detection system, MicroAmp™ Optical 96-well Reaction Plates and Optica Adhesive Covers (Applied Biosystems Deutschland GmbH, Darmstadt, Germany). Primers that were used to determine the expression of the corresponding genes are summarized in Table 9. The cycle threshold (C_T) was determined automatically by use of Real-Time CFX Manager 2.1 software (Bio-Rad Laboratories GmbH) after 40 cycles. All C_T values were normalized separately to C_T values obtained for the 16s rRNA and *recA* (SO_3430) genes of each sample. Primer efficiencies and

relative expression values were determined according to Pfaffl [433]. Each strain was assayed in biological duplicates in two independent experiments.

1.12.12 Chromosome staining

Biofilm cells were harvested in LM medium and washed with PBS buffer. Subsequently, the cells were resuspended in PBS containing 0.1 % Triton X and incubated for 10 minutes on ice. The cells were then sedimented and resuspended in 4 % PBS-buffered paraformaldehyde solution containing 10 $\mu\text{g ml}^{-1}$ 4',6-Diamidino-2-phenylindole (DAPI, Sigma-Aldrich, Steinheim, Germany). After 15 minutes of incubation, fluorescence microscopy and image acquisition was carried out using an Axio Imager.M1 microscope equipped with a Zeiss Plan Apochromate 100x/1.4 DIC objective.

1.13 Biochemical methods

1.13.1 SDS-PAGE

Protein samples were separated by **S**odium-**D**odecyl **S**ulfate **P**olyacrylamide **G**el-**E**lectrophoresis (SDS-PAGE) according to Laemmli [434]. Protein lysates were obtained from logarithmically growing cultures. Cells corresponding to an OD_{600} of 0.25 were sedimented by centrifugation and resuspended in 25 μl 2 x SDS sample buffer (0.125 M Tris base, 20 % (w/v) Glycerine, 4 % SDS, 10 % (v/v) beta-mercaptoethanol, 0.02 % bromphenol blue, pH 6.8). Subsequently, cells were boiled for 5 min and stored at -20°C . Frozen samples were boiled for 5 min prior to loading on a SDS-gel, consisting of a 5 % stacking and an 11 % resolving gel. Five μl of a prestained molecular weight marker were loaded as a standard (PageRuler™ Prestained Protein Ladder). Electrophoresis was performed in a Tris/Glycine based buffer system at 50 mAh^{-1} (100 to 150 V) in a custom-made electrophoresis system. The resulting SDS-PAGES were either stained in Roti®-Blue Coomassie stain (Carl-Roth, Germany) overnight, and destained for 3-4 hours in dH_2O for visualization of proteins, or used for immunodetection of specific proteins (see section 1.13.2.).

Table 11: Buffers for SDS-PAGE.

11 % SDS-PAGE	11 % resolving gel	5 % stacking gel
4 x resolving buffer	2.5 ml	1.25 ml
4 x stacking buffer	80 μl	840 μl
10 % (w/v) APS (Ammonium persulfate)	6 μl	50 μl
TEMED (N,N,N,N-Tetramethylethylenediamine)		
30 % Rotiphorese® NR-Acrylamide/Bis-(29:1)	3.7 ml	3.8 μl

4 x Resolving buffer, pH 8.8

SDS	0.4% (w/v)
Tris base	1.5 M

4 x Stacking buffer, pH 6.8

SDS	0.4 % (w/v)
Tris base	0.5 M

1.13.2 Immunoblot assays

Resolved proteins on a SDS-PAGE were transferred onto a polyvinylidene fluoride (PVDF)-membrane (Millipore Immobilon™ P Transfer Membrane, (Millipore, USA)) by semidry western blot transfer (Electroblotter TE 77 ECL Semi Dry (Amersham Biosciences, Germany). Prior assembly, PVDF membranes were first incubated for 20 s in 100 % Methanol, washed in ddH₂O for 2 min and equilibrated for 5 min in Western transfer buffer (25 mM Tris base, 192 mM glycine, 10 % (v/v) Methanol). The activated PVDF membrane and the SDS-gel were sandwiched between blotting papers soaked in Western transfer buffer (6 x) according to manufacturer's instructions. Proteins were blotted onto the PVDF membrane by applying an electric current of 2 mA/cm² for 1 hour. Afterwards, the membrane was blocked overnight at 4 °C in 5 % (w/v) milk powder dissolved in PBST (6.6 mM Na₂HPO₄ x 7 H₂O, 1.8 mM KH₂PO₄, 137 mM NaCl, 2.7 mM KCl, 1 % (v/v) Tween-20, pH 7.5).

Table 12: Antibodies.

Antibody	Dilution	Company/Comment
Primary antibodies		
anti-λSo	1:20,000	SO_2973; polyclonal antibody raised against the major capsid protein of phage λSo; Eurogentec, Germany
anti-ExeM	1:3,000	SO_1066; polyclonal antibody raised against ExeM; Eurogentec, Germany
anti-PomB	1:20,000	SO_PomB2; polyclonal antibody raised against PomB2 lacking the transmembrane region; Eurogentec, Germany
Secondary antibodies		
anti-rabbit-HRP	1:20,000	Goat-anti-rabbit, IgG horseradish peroxidase conjugate; Perkin Elmer, USA
anti-rabbit-AP	1:20,000	Goat-anti-rabbit, IgG alkaline phosphatase conjugate; Sigma-Aldrich, Germany

In order to detect specific proteins, the membrane was briefly washed in 'TBST' and incubated for at least 1 h with the primary antibody at the desired dilution. Afterwards, membranes were washed trice with 'TBST' and incubated for 1 h with the secondary anti-rabbit IgG, coupled to horseradish peroxidase (HRP). Antibodies were diluted in 'TBST' supplemented with 2.5 % (w/v) milk powder as listed in Table 12. Subsequently, membranes were washed three times in 'TBST' and incubated with chemiluminescence substrate (Western Lightning™ Chemiluminescence Reagent Plus (Perkin

Elmer, USA) according to manufacturer's instructions. Signals were visualized by exposure to chemoluminescence imager FUSION-SL4 (Peglab, Germany).

1.13.3 Heterologous production and purification of MBP-EndA

For heterologous overproduction of the fusion protein MBP-EndA, plasmid pMal-P2-0833-N was transformed into *E. coli* BL21 Star (DE3). The fusion protein was overproduced and purified essentially as specified for the pMAL Protein Fusion and Purification System (NEB, Germany) using method II for periplasmic secretion of the fusion protein.

IPTG was added to a final concentration of 0.3 mM to exponentially growing cells (OD_{600} of 0.5) in 500 ml SOB medium containing 0.2 % (w/v) sterile-filtered glucose. After 2 h of incubation at 37 °C, cells were harvested by centrifugation and resuspended in 400 ml of 30 mM Tris-HCl 20 % sucrose (pH 8.0). After the addition of 1 mM EDTA, the suspension was incubated for 10 min at room temperature. Subsequently, the cells were sedimented by centrifugation and were resuspended in 5 mM ice-cold $MgSO_4$. After 10 min of shaking in an ice bath, the supernatant (osmotic shock fluid) was collected by centrifugation, and the pH was adjusted by the addition of 8 ml 1 M Tris-HCl (pH 7.4). The fusion protein was purified by binding to 5 ml amylose resin and was eluted in column buffer (20 mM Tris-HCl, 200 mM NaCl, 1 mM EDTA) containing 10 mM maltose (1.5-ml elution fractions). Elution fractions were analyzed by SDS-PAGE, and protein concentrations were quantified using the Roti-Quant assay (Roth, Karlsruhe, Germany) or the Pierce bicinchoninic acid (BCA) protein assay kit (Thermo Fisher Scientific, USA). Fractions 2 to 9 were pooled, supplied with 30 % glycerol, and stored at -20 °C for further analyses.

1.13.4 EndA nuclease assays

Nuclease activity in culture supernatants

Qualitative nuclease assays in medium supernatants were carried out essentially as described previously [241]. Cells from an overnight LB preculture were incubated in fresh medium at an OD_{600} of 0.05 and were grown to an OD_{600} of 1.5. Aliquots (230 μ l) of cell-free filter-sterilized supernatant were mixed with an appropriate nucleic acid sample at a final concentration of 5 μ g ml⁻¹. The samples were incubated at 30°C, aliquots were removed at regular intervals and the integrity of the DNA was analyzed by agarose gel electrophoresis. The assay was repeated in at least two independent experiments.

Nuclease activity of washed cells

For a comparison of nuclease activity in culture supernatants and washed cells, cultures were grown to an OD_{600} of 1.5. In order to inhibit further protein synthesis, chloramphenicol was added to a final concentration of 30 μ g ml⁻¹ and cultures were incubated for 20 min at 30 °C. To determine the nuclease activity of washed cells, 230- μ l aliquots were washed three times in LB medium containing chloramphenicol (30 μ g ml⁻¹). For a comparable determination of nuclease activity in the respective culture supernatants, 230- μ l aliquots of the same culture were used without washing in LB.

Subsequently, cell suspensions were mixed with a 20- μ l nucleic acid sample (833-bp PCR product) at a final concentration of 5 μ g ml⁻¹. The samples were incubated at 30 °C, and 20- μ l aliquots of each supernatant were removed, centrifuged and analyzed by agarose gel electrophoresis at regular intervals.

Nuclease activity of purified protein (plasmid DNA)

The nuclease activity of purified MBP-EndA was determined by monitoring the decrease in fluorescence of DNA probes incubated with GelRed nucleic acid stain (Biotrend, Germany) after the addition of the proteins. Each sample contained 0.02 μ g of purified protein, 260 ng purified DNA [pBluescript II KS(+)], and 30 μ l of 3x GelRed nucleic acid stain in a final volume of 100 μ l in 10 mM Tris-HCl (pH 7.6) supplemented with the respective metal ion cofactors (2.5 mM) or dithiothreitol (DTT; 10 mM). Emission was monitored at 1-min intervals at 600 nm (excitation at 290 nm) and 30 °C using a Infinite M200 microplate reader (Tecan, Switzerland). For this assay, we defined 1 U of enzyme activity as the amount of enzyme that completely degraded 1 μ g of pBluescript DNA in 10 min at 30 °C in a buffer supplemented with 2.5 mM Mg²⁺.

Nuclease activity of purified protein (eDNA)

To determine the degradation of eDNA that was isolated from medium supernatants, 0.18 U MBP-EndA in 10 μ l buffer (10 mM Tris-HCl [pH 7.6], 2.5 mM Mg²⁺) and 30 μ l GelRed nucleic acid stain (Biotrend, Germany) were added directly to 40 μ l of medium supernatant after centrifugation and filtration. To harvest eDNA from biofilms, static biofilms were cultivated in petri dishes, the supernatant was discarded, and the cells were carefully scraped from the surface after the addition of fresh medium. Subsequent to centrifugation and filter sterilization, the eDNA in the supernatant was used for degradation assays as described for medium supernatants. Control assays ensured that the degradation of eDNA as measured by fluorescence corresponded to the disappearance of DNA as visualized by agarose gel electrophoresis (data not shown). Qualitative control assays were carried out by the addition of 0.09 U MBP-EndA to 2.5 μ g of the nucleic acid sample dissolved in 100 μ l of 10 mM Tris-HCl (pH 7.6) supplemented with 2.5 mM Mg²⁺. Samples were taken at the desired time points and were separated by agarose gel electrophoresis.

1.13.5 Determination of eDNA concentration in planktonic cultures

The concentration of eDNA in planktonic *S. oneidensis* MR-1 cultures was assayed by mixing 70 μ l of culture supernatant with 30 μ l of 3x GelRed nucleic acid stain (Biotrend, Germany). Emission at 600 nm (excitation at 290 nm) was quantified using the Tecan (Tecan, Switzerland) Infinite M200 microplate reader. DNA concentrations in the supernatants were calculated based on a calibration curve prepared with appropriate amounts of *S. oneidensis* MR-1 chromosomal DNA in the corresponding medium.

1.13.6 Quantification of eDNA in static biofilms

Static biofilms were cultivated in microtiter dishes for 24 hours as described in section 1.11.4. The supernatant was removed by vacuum pumping and exchanged with 1x PBS buffer containing 30 % (v/v) GelRed nucleic acid stain (Biotrend, Germany). The suspensions were incubated for 15 min with occasional gentle shaking. The fluorescence of each suspension was determined using the Tecan infinite M200 (Tecan, Switzerland) microplate reader with an excitation wavelength of 290 nm and an emission wavelength of 600 nm. Total fluorescence values were normalized with the biofilm biomass that was determined in parallel as described in section 1.11.4.

1.13.7 Heterologous production and purification of MBP-ExeM

For heterologous production of ExeM, plasmid pMAL-TEV-exeM (Table 10) was constructed as described in section 1.12.7 and transformed in *E. coli* BL21 Star (DE3). An overnight culture in LB medium (containing 50 µg ml⁻¹ ampicillin) was used to inoculate 400 ml SOB medium containing 0.2 % (w/v) of sterile filtered glucose. The culture was incubated at 37 °C with orbital shaking (220 rpm). At an OD₆₀₀ of 0.5, the culture was rapidly cooled down on ice for 10 minutes. IPTG was added to a final concentration of 0.3 mM and the cultures were incubated with orbital shaking (220 rpm) at 25 °C for 4 hours. The cells were harvested by centrifugation, frozen in liquid nitrogen and stored at -20 °C. For cell lysis, the cell pellets were resuspended in 30 ml ice-cold 1x PBS buffer containing 0.5 mM AEBSF-hydrochloride (Carl-Roth, Germany). For lysis, the cells were passed three times through a prechilled 'French press'. Unbroken cells were removed by centrifugation at 8,000 x g for 10 min and 4 °C. To remove insoluble cell debris and/or inclusion bodies, the cells were ultracentrifuged at 30,000 x g at 4 °C for 1 hour. The fusion protein was purified by binding to 5 ml amylose resin and eluted in column buffer (20 mM Tris-HCl, 200 mM NaCl, without EDTA!) containing 10 mM maltose (1.5-ml elution fractions). Affinity purification was performed at 4 °C. Elution fractions were analyzed by SDS-PAGE, and protein concentrations were quantified using the Pierce bicinchoninic acid (BCA) protein assay kit (Thermo Fisher Scientific, USA). Elution fractions containing high concentrations of pure MBP-ExeM protein were pooled, supplied with 30 % (v/v) glycerol, frozen in liquid nitrogen, and stored at -20 °C. The amylose resin was regenerated for further uses with 3 column volumes of water, 3 column volumes of 0.1 % SDS, 1 column volume of water, 3 column volumes of column buffer, and stored at 4 °C.

Optionally, the MBP-ExeM protein was concentrated using anion exchange chromatography in combination with an ÄKTA purification system (Amersham Biosciences, GE Healthcare, UK). To this end, the protein sample (MBP-ExeM) was diluted 1:5 in buffer A (20 mM Tris-HCl, pH 7.4, 10 % glycerol) to reduce the NaCl concentration of the column buffer, and loaded on a 5-ml HiTrap Q HP sepharose anion exchange column (GE Healthcare, UK). Two milliliter elution fractions were collected from a sharp 50 mM to 1 M NaCl gradient (buffer B: 1 M Tris-HCl, pH 7.4, 10 % glycerol) with a total volume of 12 milliliters. Elution fractions were analysed by SDS-PAGE. Fractions containing concentrated MBP-ExeM protein were pooled, either directly used for further analyses, or frozen in liquid nitrogen and stored at -20 °C.

1.13.7.1 TEV protease cleavage and purification of ExeM

As described in section 1.10.7, a TEV protease recognition site (ENLYFQG) was inserted into the fusion protein MBP-ExeM for optional separation of ExeM from the maltose binding protein MBP. TEV protease was kindly provided by Chris van der Does (MPI Marburg). The reaction was performed at room temperature in 'TEV glutathione reaction buffer' overnight, if not indicated otherwise. The completeness of the digest was analysed by SDS-PAGE. Gel filtration chromatography was applied in combination with an ÄKTA purification system (Amersham Biosciences, GE Healthcare, UK) to separate pure ExeM protein from cleaved MBP, TEV protease, and uncleaved MBP-ExeM protein. To this end, the protein sample was loaded on a HiLoad 16/600 Superdex 200 PG gel filtration column and separated in gel filtration buffer (20 mM Tris-HCl, pH 7.4, 150 mM NaCl, 20 % glycerol). If required, the protein sample was concentrated by anion exchange chromatography prior to gel filtration chromatography (as described in section 1.13.7). Elution fractions were analysed by SDS-PAGE. Fractions containing 'pure' ExeM protein were either directly subjected to further analyses, or frozen in liquid nitrogen and stored at -20 °C.

TEV glutathione reaction buffer, pH 8.0

Tris/HCl	50 mM
EDTA	0.5 mM
Glutathione (reduced)	3 mM
Glutathione (oxidized)	0.3 mM

1.13.8 ExeM nuclease assays

Nuclease activity of purified ExeM protein (or MBP-ExeM fusion protein) was assayed essentially as described for MBP-EndA (section 1.13.4) by following the decrease of fluorescence of GelRed nucleic acid stain (Biotrend, Germany) using the Tecan Infinite M200 microplate reader (Tecan, Switzerland). Each sample contained 8 µg of purified protein, 250 ng purified DNA [pBluescript II KS(+)], and 67 µl of 3x GelRed nucleic acid stain in a final volume of 200 µl in 10 mM Tris-HCl (pH 7.6) supplemented with the respective metal ion cofactors. For this assay, I defined 1 U of enzyme activity as the amount of enzyme that completely degraded 1 µg of pBluescript DNA in 10 min at 30 °C in a buffer supplemented with 12.5 mM Mg²⁺ and Ca²⁺.

1.13.9 Fractionation of inner and outer membrane of *S. oneidensis* MR-1

Inner and outer membrane fractions were separated and purified according to a Sarkosyl-based protocol presented by Brown and coworkers [294]. *S. oneidensis* MR-1 was cultured overnight in 10 ml LB medium and reinoculated in 250 ml LB medium at an OD₆₀₀ of 0.05. Strains harboring plasmid pBBMT-kan-*exeM* or derivatives (for the overproduction of ExeM or truncated ExeM variants) were cultured in the presence of 50 µg ml⁻¹ kanamycin and induced with 0.2 % (w/v) L-arabinose at an OD₆₀₀ of 0.6. At an OD₆₀₀ of 2, the cells were harvested by centrifugation at 10,000 x g for 10 minutes. An 80 ml fraction of the culture was kept for isolation of the periplasmic fraction (see below). Unless otherwise noted, all centrifugations were performed at 4 °C. The supernatant (SN) was ultracentrifuged twice at 35,000 x g for 1 h and stored at -20 °C for further

analyses. The cell pellet was suspended in 30 ml ice-cold 20 mM sodium phosphate buffer (pH 7.5) and passed one time through a prechilled 'French press'. The clear lysate was centrifuged at $8,000 \times g$ for 10 min to remove unbroken cells, and an aliquot of the supernatant was stored as 'whole cell lysate sample'. Ten milliliter of the remaining supernatant were ultracentrifuged at $45,000 \times g$ for 1 hour. The supernatant was removed and centrifuged again to remove residual membrane fractions and insoluble protein, and stored at -20°C as soluble fraction. The tube containing the whole membrane fraction was inverted to drain, and a sample was frozen in liquid nitrogen and stored at -20°C for further analyses. The remaining whole membrane fraction was suspended in 0.5 % Sarkosyl (20 mM sodium phosphate) by frequent 'pipetting' and orbital shaking at 220 rpm for 30 min at room temperature. The crude membrane suspension was ultracentrifuged at $45,000 \times g$ for 1 hour to sediment the outer membrane. The supernatant containing the inner membrane was removed and the outer membrane sample was washed in ice-cold sodium phosphate buffer, spun down again by ultracentrifugation at $45,000 \times g$ for 1 hour, suspended in 500 μl sodium phosphate, frozen in liquid nitrogen, and stored at -20°C . The supernatant containing the inner membrane was washed and concentrated to 500 μl using Vivaspin®6 centrifugation filter tubes (Sartorius Stedim Biotech GmbH, Germany) with a 5 kDa molecular weight cutoff. The inner membrane sample was frozen in liquid nitrogen and stored at -20°C for further analyses.

The periplasm was isolated by osmotic shock according to Ross and coworkers [340]. Eighty milliliters of the initial culture were centrifuged at $8,000 \times g$ for 10 min and suspended in 10 ml of 50 mM Tris-HCl, pH 8.0, 250 mM sucrose. The suspension was incubated for 5 min at room temperature and centrifuged at $8,000 \times g$ for 15 min. The pellet was suspended in ice-cold 5 mM MgSO_4 and kept on ice with occasional inversion. The soluble periplasmic fraction was obtained from the supernatant after centrifugation at $8,000 \times g$ for 15 min. The periplasmic fraction was concentrated to a final volume of 500 μl using Vivaspin®6 centrifugation filter tubes (Sartorius Stedim Biotech GmbH, Germany) with a 5 kDa molecular weight cutoff.

1.14 Microscopic methods

1.14.1 Fluorescence microscopy and image acquisition

Fluorescence microscopy and image acquisition was carried out either on an Axio Imager.M1 microscope (Zeiss, Germany) equipped with a Zeiss Plan Apochromate 100x/1.40 Oil DIC objective and a Cascade 1K CCD camera (Photometrics, USA), or on a Leica DMI6000B inverse microscope (Leica, Germany) equipped with a Leica HCX PlanApo 100x/1.4-0.7 Oil objective and a sCMOS camera (Visitron Systems, Germany). Images were processed with the MetaMorph® 7.1.2 software (Molecular Device, USA), ImageJ 1.47v software (National Institute of Health, USA), or Adobe® Photoshop® CS2 9.0.2 (Adobe Systems Software, Ireland).

1.14.2 Confocal laser scanning microscopy (CLSM) and image acquisition

Microscopic visualization of biofilms and image acquisition was performed using an inverted Leica TCS SP5 confocal laser scanning microscope (Microsystems, Germany) equipped with x10/0.3.

Plan-Neofluar and x63/1.2 W C-Apochromate objectives. Images were acquired in 0.8 μm or 1 μm z-stacks. CLSM images were processed using the IMARIS software package (Bitplane AG, Switzerland) and Adobe Photoshop. Image analysis (*e.g.* quantification of prophage induction) was conducted using ImageJ 1.47v software (National Institute of Health, USA) including the LOCI Bio-Formats plugin. CLSM stacks were split into individual channels (CFP/Venus/DDAO) and thresholds were adjusted adequately to remove noise. Total signal intensities (limited to the threshold range) were quantified by applying the area-multi-measurement tool on each stack. CFP signals (constitutively expressed in all cells) were used as reference to obtain a normalized signal-to-biomass ratio. Biofilm cultivation and measurements were conducted in triplicate in at least two independent experiments.

1.15 Bioinformatic methods

Source and analysis of bacterial nucleotide- and protein sequences:

National Center for Biotechnology Information (NCBI)

<http://www.ncbi.nlm.nih.gov>

Sequence alignments based on NCBI database:

Basic Local Sequence Alignment Search Tool (BLAST) for proteins (BLASTP) and nucleotide (BLASTN) alignments

<http://blast.ncbi.nlm.nih.gov/Blast.cgi>

Multiple alignments of nucleic acid and protein sequences:

ClustalW2

<http://www.ebi.ac.uk/Tools/clustalw2/index.html>

Prediction of transmembrane helices in proteins:

TMHMM Server v. 2.0

<http://www.cbs.dtu.dk/services/TMHMM/>

Operon prediction:

Prediction by VIMSS [303] and visualization on MicrobesOnline

<http://www.microbesonline.org>

Analysis of oligonucleotide properties:

Oligonucleotide Properties Calculator (Oligo Calc) [420]

<http://www.basic.northwestern.edu/biotools/oligocalc.html>

Signal peptide prediction:

SignalP 4.0 [323]

<http://www.cbs.dtu.dk/services/SignalP/>

Phage prediction:

Phage Search Tool (PHAST) [297]

<http://phast.wishartlab.com>

Phylogenetic trees:

Interactive Tree of Life (iTOL) [330]

<http://itol.embl.de>

Protein structure prediction:

Protein Homology/analogY Recognition Engine V 2.0 (Phyre²) [393]

<http://www.sbg.bio.ic.ac.uk/phyre2/>

APPENDIX

1.16 Figures

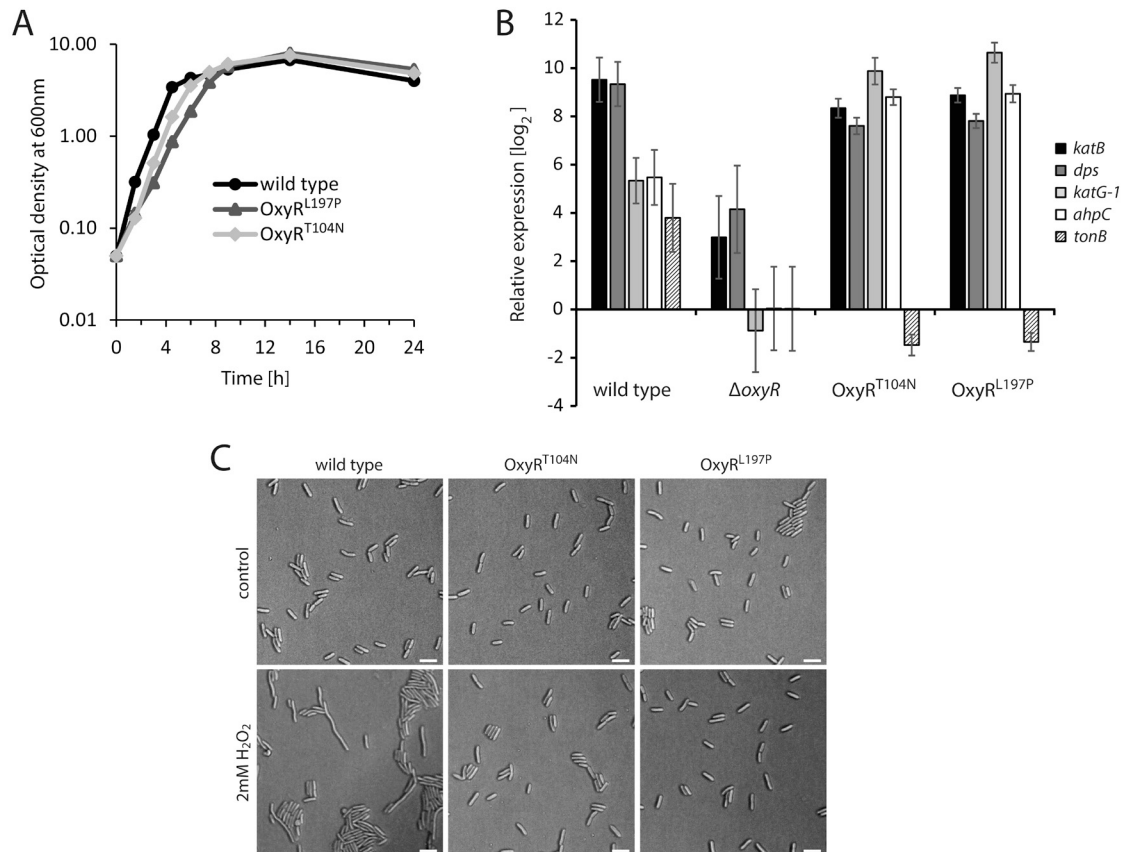


Figure 36. Characterization of H₂O₂ resistant mutants OxyR^{T104N} and OxyR^{L197P}. (A) Planktonic growth under aerobic conditions in LB medium of the *S. oneidensis* MR-1 wild type and the OxyR^{T104N} and OxyR^{L197P} mutant strains. Growth curves are derived from a representative experiment conducted in triplicates. Error bars represent standard deviations (B) Relative expression of *katB* (SO_1070), *dps* (SO_1158), *ahpC* (SO_0958), *katG-1* (SO_0725) and *tonB* (SO_3670) in response to 2 mM H₂O₂ (15 min), in strain $\Delta oxyR$ and the OxyR^{T104N} and OxyR^{L197P} mutant strains compared to the wild type, determined by quantitative real-time PCR. Bars represent the mean values of two independent experiments, each normalized to the 16s rRNA and *recA* housekeeping genes. Standard deviations are displayed as error bars (C) Cell morphologies of the *S. oneidensis* MR-1 wild type and the H₂O₂ hyper-resistant mutants after exposure to 2mM H₂O₂ for 2 hours. The scale bar is 5 μ m.

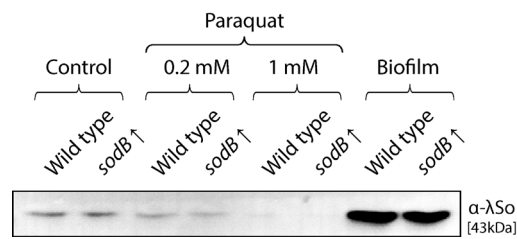


Figure 37. Effect of *sodB* overexpression on production of phage λSo. Western immunodetection of λSo in the *S. oneidensis* MR-1 wild type and a strain carrying plasmid pBBR1-TT-Ptac-MCS5-*sodB* for constitutive overexpression of the *sodB* gene (SO_2881) in the absence or presence of paraquat. The strains were grown until mid-logarithmic phase in plain LM medium (+15 mM lactate), incubated with or without 0.2 mM / 1 mM paraquat for 3h hours at 30°C and finally harvested by centrifugation and subjected to SDS-PAGE and immunodetection. Samples of biofilm cells of both strains grown under hydrodynamic conditions were additionally included for direct comparison.

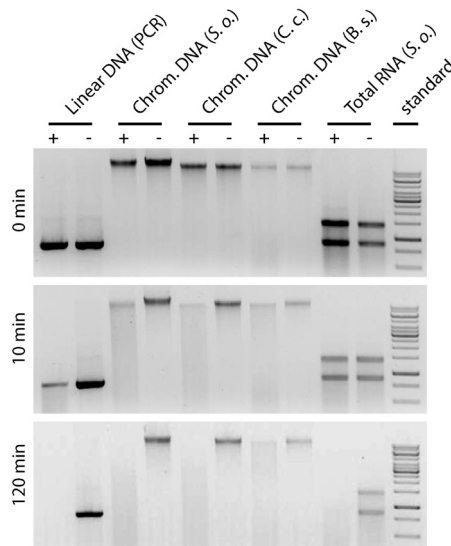


Figure 38. Degradation of different nucleic acids by MBP-EndA. 0.09 U of MBP-EndA (+) or the equimolar amount of MBP (-) were added to the indicated type of nucleic acid and incubated at 30 °C for the indicated amount of time prior to separation on a 1 % agarose gel. The chromosomal DNA was prepared from *S. oneidensis* MR-1 (*S. o.*), *C. crescentus* (*C. c.*), and *B. subtilis* (*B. s.*), the total RNA was prepared from *S. oneidensis* MR-1.

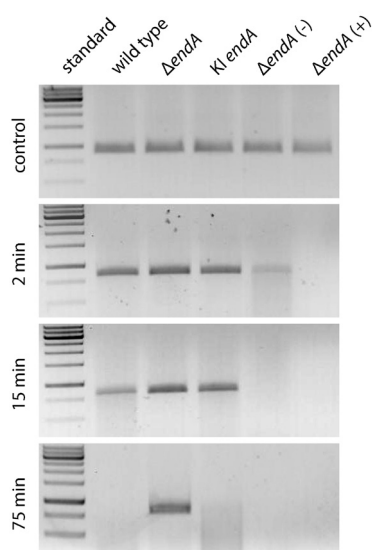


Figure 39. Nuclease activity in supernatants of the *endA* complementation strain and the wild type overexpressing *endA*. Visualization of the degradation of a 1.2 kbp PCR fragment by supernatants of the wild type, the $\Delta endA$ deletion mutants, the *endA* knock-in complementation strain (KI *endA*), and a wild-type strain overexpressing *endA* (pLacTac-*endA*) in the presence (+) or absence (-) of IPTG. The strains were cultured in 4M medium for 24 hours. To induce overexpression of *endA* from pLacTac-*endA*, IPTG was added prior to inoculation. Samples were taken at the indicated time points. Representative band patterns are presented of at least two independent experiments.

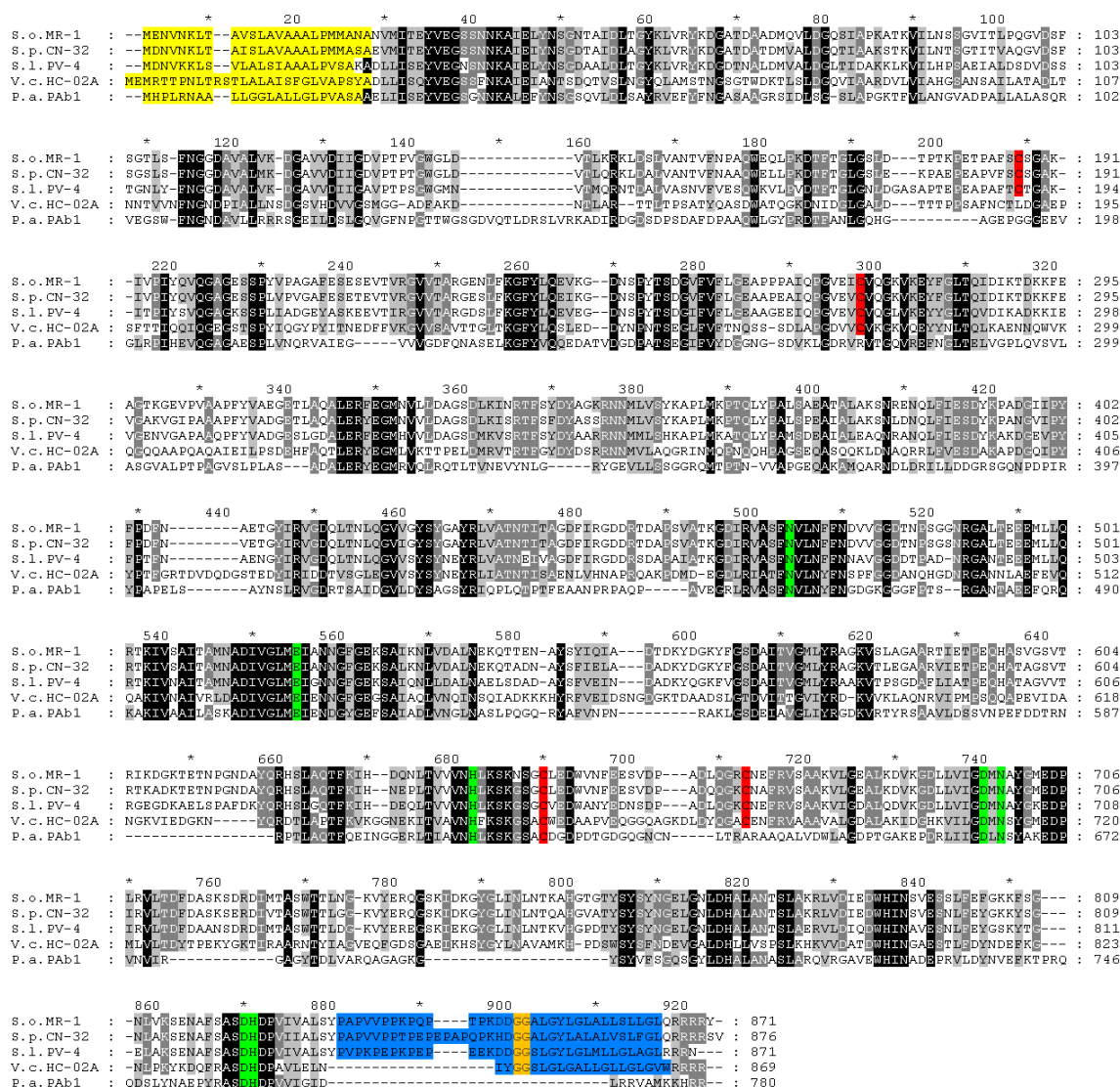


Figure 40. Amino acid sequence alignment of ExeM. GeneDoc software was utilized to generate sequence alignments of putative ExeM proteins of *S. oneidensis* MR-1 (S. o. MR-1), *S. putrefaciens* CN-32 (S. p. CN-32), *S. loihica* PV-4 (S. l. PV-4), *Vibrio cholera* HC-02A (V. c. HC02A) and *Pseudomonas aeruginosa* Pab1 (P. a. Pab1). Colorless shadings from white to black indicate the degree of conservation, yellow shading indicates putative signal peptides, red shadings indicate conserved cysteine residues and green shadings indicate metal- or phosphate-binding sites. Orange shading indicates the putative Gly-Gly C-Term rhombosortase cleavage site.

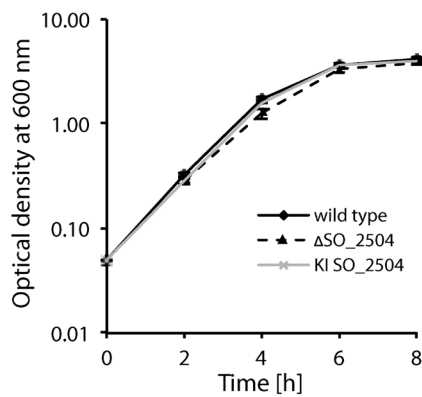


Figure 41. Growth defect of the Δ SO_2504 deletion mutant in late exponential phase. Planktonic growth of the *S. oneidensis* MR-1 wild type, an in-frame deletion mutant in gene SO_2504 (Δ SO_2504), and the knock-in complementation strain in SO_2504 (KI SO_2504) was assayed under aerobic conditions in LB medium at 30 °C with orbital shaking (200 rpm). Growth curves are derived from a representative experiment conducted in triplicates. Error bars represent standard deviations.

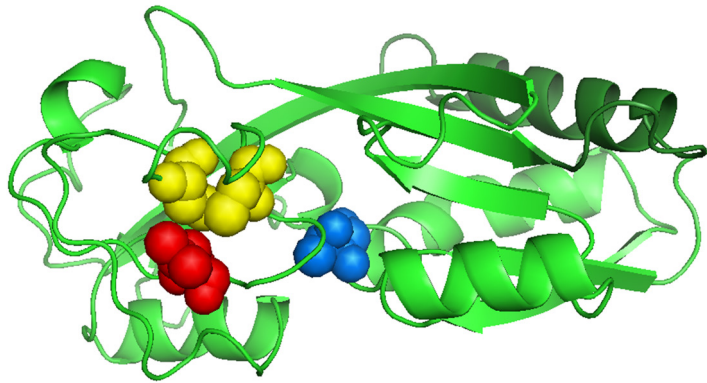


Figure 42. Prediction of the regulatory domain of OxyR (SO_1328) in *S. oneidensis* MR-1. Protein structure prediction was performed with the Protein fold recognition server (Phyre²) [393]. The structure of the regulatory domain (residue 91 to 301) of SO_1328 was predicted in the oxidized state based on OxyR in *E. coli* and *Porphyromonas gingivalis*. The protein structure is illustrated as ribbon diagram. Conserved cysteine residues that are involved in disulfide bond formation are highlighted as yellow spheres. Residue 104 is highlighted as blue spheres and residue 197 as red spheres.

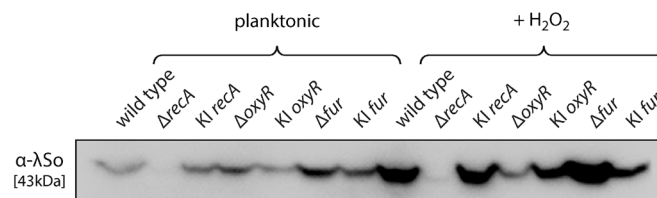


Figure 43. Production of phage λ So in *S. oneidensis* MR-1 in-frame deletion strains and complementation strains (KI, in-frame reinsertion/knock-in) in the absence and presence of H₂O₂. The strains were grown until mid-logarithmic phase in plain LM medium (+15 mM lactate) and then incubated or without 2 mM H₂O₂ for 3 hours at 30 °C and then subjected to SDS-PAGE and immunoblot analysis.

1.17 Tables

Table 13. Metal ion cofactors required for nucleolytic activity of MBP-ExeM.

	Mg ²⁺	Mn ²⁺	Ca ²⁺	Zn ²⁺	Ni ²⁺	Cu ²⁺
Mg ²⁺	✗	✗	✓	✗	✗	✗
Mn ²⁺		✗	✓	✗	✗	✗
Ca ²⁺			✗	✗	✗	✗
Zn ²⁺				✗	✗	✗
Ni ²⁺					✗	✗
Cu ²⁺						✗
-	✗	✗	(✓)	✗	✗	✗

✓ Degradation of circular plasmid DNA in the presence of the specified metal ions (5 mM each)
 (✓) Slow or incomplete degradation
 ✗ No degradation occurred in the presence of the specified metal ions

ABBREVIATIONS

aa	A mino a cid
bp	B ase p airs
c-di-GMP	bis-(3'-5')- c yclic d imeric g uanosine m onophosphate
cDNA	C omplementary DNA
CFP	C yan f luorescent p rotein
CLSM	C onfocal laser s canning m icroscopy
DAPI	4',6- D iamidino-2- p henylindole
DDAO	7-hydroxy-9H-(1,3 d ichloro-9,9- d imethylacridin-2- o ne
Δ	Delta (gene deletion)
DMSO	D imethyl sulfoxide
eDNA	Extracellular DNA
EDTA	E thylenediaminetetraacetic a cid
EPS	E xtracellular p olymeric s ubstances
GFP	G reen f luorescent p rotein
h	H our(s)
IPTG	I sopropyl- β -D- t hiogalactopyranoside
λ	Lambda
LB	L uria- B ertani (medium)
LM	L actate m edium
MBP	M altose b inding p rotein
min	M inute(s)
OD	O ptical d ensity
PCR	P olymerase c hain r eaction
qPCR	Q uantitative real-time p olymerase c hain r eaction
rpm	R ounds p er m inute
RT-PCR	R everse t ranscriptase p olymerase c hain r eaction
SDS-PAGE	S odium- d odecyl sulfate p olyacrylamide g el- e lectrophoresis
sfGFP	S uper-folding G reen f luorescent p rotein
UV	U ltraviolet

ACKNOWLEDGEMENT

- removed for protection of data privacy -

CURRICULUM VITAE

- removed for protection of data privacy -

REFERENCES

1. Costerton JW, Lewandowski Z, Caldwell DE, Korber DR, Lappin-Scott HM. 1995. Microbial biofilms. *Annu Rev Microbiol* **49**:711-745.
2. Flemming HC. 2000. Biofilme - das Leben am Rande der Wasserphase. *Nachrichten aus der Chemie* **48**:442-447.
3. Costerton JW, Stewart PS, Greenberg EP. 1999. Bacterial biofilms: a common cause of persistent infections. *Science* **284**:1318-1322.
4. Drenkard E. 2003. Antimicrobial resistance of *Pseudomonas aeruginosa* biofilms. *Microbes Infect* **5**:1213-1219.
5. Mah TF, O'Toole GA. 2001. Mechanisms of biofilm resistance to antimicrobial agents. *Trends Microbiol* **9**:34-39.
6. Stewart PS, Costerton JW. 2001. Antibiotic resistance of bacteria in biofilms. *Lancet* **358**:135-138.
7. Hoyle BD, Costerton JW. 1991. Bacterial resistance to antibiotics: the role of biofilms. *Prog Drug Res* **37**:91-105.
8. Elasi MO, Miller RV. 1999. Study of the response of a biofilm bacterial community to UV radiation. *Appl Environ Microbiol* **65**:2025-2031.
9. Davey ME, O'Toole G A. 2000. Microbial biofilms: from ecology to molecular genetics. *Microbiol Mol Biol Rev* **64**:847-867.
10. Jefferson KK. 2004. What drives bacteria to produce a biofilm? *FEMS Microbiol Lett* **236**:163-173.
11. Chang WS, van de Mortel M, Nielsen L, Nino de Guzman G, Li X, Halverson LJ. 2007. Alginate production by *Pseudomonas putida* creates a hydrated microenvironment and contributes to biofilm architecture and stress tolerance under water-limiting conditions. *J Bacteriol* **189**:8290-8299.
12. Van Acker H, Van Dijck P, Coenye T. 2014. Molecular mechanisms of antimicrobial tolerance and resistance in bacterial and fungal biofilms. *Trends Microbiol* **22**:326-333.
13. Moller S, Pedersen AR, Poulsen LK, Arvin E, Molin S. 1996. Activity and three-dimensional distribution of toluene-degrading *Pseudomonas putida* in a multispecies biofilm assessed by quantitative *in situ* hybridization and scanning confocal laser microscopy. *Appl Environ Microbiol* **62**:4632-4640.
14. Moller S, Sternberg C, Andersen JB, Christensen BB, Ramos JL, Givskov M, Molin S. 1998. *In situ* gene expression in mixed-culture biofilms: evidence of metabolic interactions between community members. *Appl Environ Microbiol* **64**:721-732.
15. Okabe S, Satoh H, Watanabe Y. 1999. *In situ* analysis of nitrifying biofilms as determined by *in situ* hybridization and the use of microelectrodes. *Appl Environ Microbiol* **65**:3182-3191.
16. Hall-Stoodley L, Costerton JW, Stoodley P. 2004. Bacterial biofilms: from the natural environment to infectious diseases. *Nat Rev Microbiol* **2**:95-108.
17. Lawrence JR, Korber DR, Hoyle BD, Costerton JW, Caldwell DE. 1991. Optical sectioning of microbial biofilms. *J Bacteriol* **173**:6558-6567.
18. Nyvad B, Kilian M. 1990. Comparison of the initial streptococcal microflora on dental enamel in caries-active and in caries-inactive individuals. *Caries Res* **24**:267-272.
19. O'Toole GA, Kolter R. 1998. Initiation of biofilm formation in *Pseudomonas fluorescens* WCS365 proceeds via multiple, convergent signalling pathways: a genetic analysis. *Mol Microbiol* **28**:449-461.
20. Pratt LA, Kolter R. 1998. Genetic analysis of *Escherichia coli* biofilm formation: roles of flagella, motility, chemotaxis and type I pili. *Mol Microbiol* **30**:285-293.
21. Genevaux P, Muller S, Bauda P. 1996. A rapid screening procedure to identify mini-Tn10 insertion mutants of *Escherichia coli* K-12 with altered adhesion properties. *FEMS Microbiol Lett* **142**:27-30.
22. O'Toole GA, Kolter R. 1998. Flagellar and twitching motility are necessary for *Pseudomonas aeruginosa* biofilm development. *Mol Microbiol* **30**:295-304.
23. Watnick PI, Kolter R. 1999. Steps in the development of a *Vibrio cholerae* El Tor biofilm. *Mol Microbiol* **34**:586-595.
24. Thormann KM, Saville RM, Shukla S, Pelletier DA, Spormann AM. 2004. Initial Phases of biofilm formation in *Shewanella oneidensis* MR-1. *J Bacteriol* **186**:8096-8104.
25. Palmer J, Flint S, Brooks J. 2007. Bacterial cell attachment, the beginning of a biofilm. *J Ind Microbiol Biotechnol* **34**:577-588.
26. Kumar CG, Anand SK. 1998. Significance of microbial biofilms in food industry: a review. *Int J Food Microbiol* **42**:9-27.
27. Marshall KC, Stout R, Mitchell R. 1971. Mechanism of the initial events in the sorption of marine bacteria to surfaces. *Microbiology* **68**:337-348.

28. **Gilbert P, Evans DJ, Evans E, Duguid IG, Brown MR.** 1991. Surface characteristics and adhesion of *Escherichia coli* and *Staphylococcus epidermidis*. *J Appl Bacteriol* **71**:72-77.
29. **Vanloosdrecht MCM, Lyklema J, Norde W, Schraa G, Zehnder AJB.** 1987. Electrophoretic mobility and hydrophobicity as a measure to predict the initial steps of bacterial adhesion. *Appl Environ Microbiol* **53**:1898-1901.
30. **Carpentier B, Cerf O.** 1993. Biofilms and their consequences, with particular reference to hygiene in the food-industry. *J Appl Bacteriol* **75**:499-511.
31. **Froeliger EH, Fives-Taylor P.** 2001. *Streptococcus parvus* fimbria-associated adhesin fap1 is required for biofilm formation. *Infect Immun* **69**:2512-2519.
32. **Hinsa SM, Espinosa-Urgel M, Ramos JL, O'Toole GA.** 2003. Transition from reversible to irreversible attachment during biofilm formation by *Pseudomonas fluorescens* WCS365 requires an ABC transporter and a large secreted protein. *Mol Microbiol* **49**:905-918.
33. **Bodenmiller D, Toh E, Brun YV.** 2004. Development of surface adhesion in *Caulobacter crescentus*. *J Bacteriol* **186**:1438-1447.
34. **Ivanov IE, Boyd CD, Newell PD, Schwartz ME, Turnbull L, Johnson MS, Whitchurch CB, O'Toole GA, Camesano TA.** 2012. Atomic force and super-resolution microscopy support a role for LapA as a cell-surface biofilm adhesin of *Pseudomonas fluorescens*. *Res Microbiol* **163**:685-691.
35. **Barnhart MM, Chapman MR.** 2006. Curli biogenesis and function. *Annu Rev Microbiol* **60**:131-147.
36. **Vandevivere P, Kirchman DL.** 1993. Attachment stimulates exopolysaccharide synthesis by a bacterium. *Appl Environ Microbiol* **59**:3280-3286.
37. **Cheung HY, Sun SQ, Sreedhar B, Ching WM, Tanner PA.** 2000. Alterations in extracellular substances during the biofilm development of *Pseudomonas aeruginosa* on aluminum plates. *J Appl Microbiol* **89**:100-106.
38. **Gödeke J, Paul K, Lassak J, Thormann KM.** 2011. Phage-induced lysis enhances biofilm formation in *Shewanella oneidensis* MR-1. *ISME J* **5**:613-626.
39. **Dunne WM, Jr.** 2002. Bacterial adhesion: seen any good biofilms lately? *Clin Microbiol Rev* **15**:155-166.
40. **Schwab U, Hu Y, Wiedmann M, Boor KJ.** 2005. Alternative sigma factor sigma σ B is not essential for *Listeria monocytogenes* surface attachment. *J Food Protect* **68**:311-317.
41. **Butler JL, Stewart JC, Vanderzant C, Carpenter ZL, Smith GC.** 1979. Attachment of microorganisms to pork skin and surfaces of beef and lamb carcasses. *J Food Protect* **42**:401-406.
42. **Dickson JS, Koohmaraie M.** 1989. Cell surface charge characteristics and their relationship to bacterial attachment to meat surfaces. *Appl Environ Microbiol* **55**:832-836.
43. **Lorite GS, Rodrigues CM, de Souza AA, Kranz C, Mizaikoff B, Cotta MA.** 2011. The role of conditioning film formation and surface chemical changes on *Xylella fastidiosa* adhesion and biofilm evolution. *J Colloid Interface Sci* **359**:289-295.
44. **Fletcher M.** 1976. The effects of proteins on bacterial attachment to polystyrene. *J Gen Microbiol* **94**:400-404.
45. **Parkar SG, Flint SH, Palmer JS, Brooks JD.** 2001. Factors influencing attachment of thermophilic bacilli to stainless steel. *J Appl Microbiol* **90**:901-908.
46. **Whittaker CJ, Klier CM, Kolenbrander PE.** 1996. Mechanisms of adhesion by oral bacteria. *Annu Rev Microbiol* **50**:513-552.
47. **Hengge R.** 2009. Principles of c-di-GMP signalling in bacteria. *Nat Rev Microbiol* **7**:263-273.
48. **Römling U, Galperin MY, Gomelsky M.** 2013. Cyclic di-GMP: the first 25 years of a universal bacterial second messenger. *Microbiol Mol Biol Rev* **77**:1-52.
49. **Fang X, Gomelsky M.** 2010. A post-translational, c-di-GMP-dependent mechanism regulating flagellar motility. *Mol Microbiol* **76**:1295-1305.
50. **Paul K, Nieto V, Carlquist WC, Blair DF, Harshey RM.** 2010. The c-di-GMP binding protein YcgR controls flagellar motor direction and speed to affect chemotaxis by a "backstop brake" mechanism. *Mol Cell* **38**:128-139.
51. **Boehm A, Kaiser M, Li H, Spangler C, Kasper CA, Ackermann M, Kaever V, Sourjik V, Roth V, Jenal U.** 2010. Second messenger-mediated adjustment of bacterial swimming velocity. *Cell* **141**:107-116.
52. **Huitema E, Pritchard S, Matteson D, Radhakrishnan SK, Viollier PH.** 2006. Bacterial birth scar proteins mark future flagellum assembly site. *Cell* **124**:1025-1037.
53. **Wolfe AJ, Visick KL.** 2008. Get the message out: cyclic di-GMP regulates multiple levels of flagellum-based motility. *J Bacteriol* **190**:463-475.
54. **Baraquet C, Harwood CS.** 2013. Cyclic diguanosine monophosphate represses bacterial flagella synthesis by interacting with the Walker A motif of the enhancer-binding protein FleQ. *Proc Natl Acad Sci U S A* **110**:18478-18483.
55. **Wilksch JJ, Yang J, Clements A, Gabbe JL, Short KR, Cao H, Cavaliere R, James CE, Whitchurch CB, Schembri MA, Chuah ML, Liang ZX, Wijburg OL, Jenney AW, Lithgow T, Strugnell RA.** 2011. MrkH, a novel c-di-GMP-

- dependent transcriptional activator, controls *Klebsiella pneumoniae* biofilm formation by regulating type 3 fimbriae expression. *PLoS Pathog* **7**:e1002204.
56. **Srivastava D, Hsieh ML, Khataokar A, Neiditch MB, Waters CM.** 2013. Cyclic di-GMP inhibits *Vibrio cholerae* motility by repressing induction of transcription and inducing extracellular polysaccharide production. *Mol Microbiol* **90**:1262-1276.
 57. **Monds RD, Newell PD, Gross RH, O'Toole GA.** 2007. Phosphate-dependent modulation of c-di-GMP levels regulates *Pseudomonas fluorescens* Pf0-1 biofilm formation by controlling secretion of the adhesin LapA. *Mol Microbiol* **63**:656-679.
 58. **Mikkelsen H, Sivaneson M, Filloux A.** 2011. Key two-component regulatory systems that control biofilm formation in *Pseudomonas aeruginosa*. *Environ Microbiol* **13**:1666-1681.
 59. **Lapouge K, Schubert M, Allain FHT, Haas D.** 2008. Gac/Rsm signal transduction pathway of gamma-proteobacteria: from RNA recognition to regulation of social behaviour. *Mol Microbiol* **67**:241-253.
 60. **Wei BL, Brun-Zinkernagel AM, Simecka JW, Pruss BM, Babitzke P, Romeo T.** 2001. Positive regulation of motility and flhDC expression by the RNA-binding protein CsrA of *Escherichia coli*. *Mol Microbiol* **40**:245-256.
 61. **Martinez-Gil M, Ramos-Gonzalez MI, Espinosa-Urgel M.** 2014. Roles of cyclic di-GMP and the Gac system in transcriptional control of the genes coding for the *Pseudomonas putida* adhesins LapA and LapF. *J Bacteriol* **196**:1484-1495.
 62. **Wang X, Dubey AK, Suzuki K, Baker CS, Babitzke P, Romeo T.** 2005. CsrA post-transcriptionally represses *pgaABCD*, responsible for synthesis of a biofilm polysaccharide adhesin of *Escherichia coli*. *Mol Microbiol* **56**:1648-1663.
 63. **Klausen M, Heydorn A, Ragas P, Lambertsen L, Aaes-Jorgensen A, Molin S, Tolker-Nielsen T.** 2003. Biofilm formation by *Pseudomonas aeruginosa* wild type, flagella and type IV pili mutants. *Mol Microbiol* **48**:1511-1524.
 64. **Kulasekara HD, Ventre I, Kulasekara BR, Lazdunski A, Filloux A, Lory S.** 2005. A novel two-component system controls the expression of *Pseudomonas aeruginosa* fimbrial cup genes. *Mol Microbiol* **55**:368-380.
 65. **Ruer S, Stender S, Filloux A, de Bentzmann S.** 2007. Assembly of fimbrial structures in *Pseudomonas aeruginosa*: functionality and specificity of chaperone-usher machineries. *J Bacteriol* **189**:3547-3555.
 66. **Lin X, Wu J, Xie H.** 2006. *Porphyromonas gingivalis* minor fimbriae are required for cell-cell interactions. *Infect Immun* **74**:6011-6015.
 67. **Petrova OE, Schurr JR, Schurr MJ, Sauer K.** 2012. Microcolony formation by the opportunistic pathogen *Pseudomonas aeruginosa* requires pyruvate and pyruvate fermentation. *Mol Microbiol* **86**:819-835.
 68. **Stoodley P, Dodds I, Boyle JD, Lappin-Scott HM.** 1998. Influence of hydrodynamics and nutrients on biofilm structure. *J Appl Microbiol* **85 Suppl** 1:19S-28S.
 69. **Kaiser D.** 2003. Coupling cell movement to multicellular development in myxobacteria. *Nat Rev Microbiol* **1**:45-54.
 70. **Reisner A, Haagensen JA, Schembri MA, Zechner EL, Molin S.** 2003. Development and maturation of *Escherichia coli* K-12 biofilms. *Mol Microbiol* **48**:933-946.
 71. **Fux CA, Stoodley P, Hall-Stoodley L, Costerton JW.** 2003. Bacterial biofilms: a diagnostic and therapeutic challenge. *Expert Rev Anti Infect Ther* **1**:667-683.
 72. **Hall-Stoodley L, Keevil CW, Lappin-Scott HM.** 1999. *Mycobacterium fortuitum* and *Mycobacterium chelonae* biofilm formation under high and low nutrient conditions. *J Appl Microbiol* **85**:60S-69S.
 73. **Spormann AM.** 2008. Physiology of microbes in biofilms. *Curr Top Microbiol Immunol* **322**:17-36.
 74. **Prosser BL, Taylor D, Dix BA, Cleeland R.** 1987. Method of evaluating effects of antibiotics on bacterial biofilm. *Antimicrob Agents Chemother* **31**:1502-1506.
 75. **Stewart PS, Franklin MJ.** 2008. Physiological heterogeneity in biofilms. *Nat Rev Microbiol* **6**:199-210.
 76. **Lewis K.** 2007. Persister cells, dormancy and infectious disease. *Nat Rev Microbiol* **5**:48-56.
 77. **Lewis K.** 2008. Multidrug tolerance of biofilms and persister cells. *Curr Top Microbiol Immunol* **322**:107-131.
 78. **Dawson CC, Intapa C, Jabra-Rizk MA.** 2011. "Persisters": survival at the cellular level. *Plos Pathog* **7**.
 79. **Johnson LR.** 2008. Microcolony and biofilm formation as a survival strategy for bacteria. *J Theor Biol* **251**:24-34.
 80. **Schembri MA, Kjaergaard K, Klemm P.** 2003. Global gene expression in *Escherichia coli* biofilms. *Mol Microbiol* **48**:253-267.
 81. **Whiteley M, Bangera MG, Bumgarner RE, Parsek MR, Teitzel GM, Lory S, Greenberg EP.** 2001. Gene expression in *Pseudomonas aeruginosa* biofilms. *Nature* **413**:860-864.
 82. **Beenken KE, Dunman PM, McAleese F, Macapagal D, Murphy E, Projan SJ, Blevins JS, Smeltzer MS.** 2004. Global gene expression in *Staphylococcus aureus* biofilms. *J Bacteriol* **186**:4665-4684.
 83. **Davies DG, Parsek MR, Pearson JP, Iglewski BH, Costerton JW, Greenberg EP.** 1998. The involvement of cell-to-cell signals in the development of a bacterial biofilm. *Science* **280**:295-298.
 84. **Heydorn A, Ersboll B, Kato J, Hentzer M, Parsek MR, Tolker-Nielsen T, Givskov M, Molin S.** 2002. Statistical analysis of *Pseudomonas aeruginosa* biofilm development: impact of mutations in genes involved in twitching motility, cell-to-cell signaling, and stationary-phase sigma factor expression. *Appl Environ Microbiol* **68**:2008-2017.

85. **Parsek MR, Greenberg EP.** 2005. Sociomicrobiology: the connections between quorum sensing and biofilms. *Trends Microbiol* **13**:27-33.
86. **Solano C, Echeverez M, Lasa I.** 2014. Biofilm dispersion and quorum sensing. *Curr Opin Microbiol* **18**:96-104.
87. **Molin S, Tolker-Nielsen T.** 2003. Gene transfer occurs with enhanced efficiency in biofilms and induces enhanced stabilisation of the biofilm structure. *Curr Opin Biotechnol* **14**:255-261.
88. **Sauer K, Camper AK, Ehrlich GD, Costerton JW, Davies DG.** 2002. *Pseudomonas aeruginosa* displays multiple phenotypes during development as a biofilm. *J Bacteriol* **184**:1140-1154.
89. **Jackson DW, Suzuki K, Oakford L, Simecka JW, Hart ME, Romeo T.** 2002. Biofilm formation and dispersal under the influence of the global regulator CsrA of *Escherichia coli*. *J Bacteriol* **184**:290-301.
90. **Thormann KM, Duttler S, Saville RM, Hyodo M, Shukla S, Hayakawa Y, Spormann AM.** 2006. Control of formation and cellular detachment from *Shewanella oneidensis* MR-1 biofilms by cyclic di-GMP. *J Bacteriol* **188**:2681-2691.
91. **Stoodley P, Cargo R, Rupp CJ, Wilson S, Klapper I.** 2002. Biofilm material properties as related to shear-induced deformation and detachment phenomena. *J Ind Microbiol Biotechnol* **29**:361-367.
92. **McDougald D, Rice SA, Barraud N, Steinberg PD, Kjelleberg S.** 2012. Should we stay or should we go: mechanisms and ecological consequences for biofilm dispersal. *Nat Rev Microbiol* **10**:39-50.
93. **Gjermansen M, Ragas P, Sternberg C, Molin S, Tolker-Nielsen T.** 2005. Characterization of starvation-induced dispersion in *Pseudomonas putida* biofilms. *Environ Microbiol* **7**:894-906.
94. **James GA, Korber DR, Caldwell DE, Costerton JW.** 1995. Digital image analysis of growth and starvation responses of a surface-colonizing *Acinetobacter* sp. *J Bacteriol* **177**:907-915.
95. **Sauer K, Cullen MC, Rickard AH, Zeef LA, Davies DG, Gilbert P.** 2004. Characterization of nutrient-induced dispersion in *Pseudomonas aeruginosa* PAO1 biofilm. *J Bacteriol* **186**:7312-7326.
96. **Rowe MC, Withers HL, Swift S.** 2010. Uropathogenic *Escherichia coli* forms biofilm aggregates under iron restriction that disperse upon the supply of iron. *FEMS Microbiol Lett* **307**:102-109.
97. **Musk DJ, Banko DA, Hergenrother PJ.** 2005. Iron salts perturb biofilm formation and disrupt existing biofilms of *Pseudomonas aeruginosa*. *Chem Biol* **12**:789-796.
98. **Glick R, Gilmour C, Tremblay J, Satanower S, Avidan O, Deziel E, Greenberg EP, Poole K, Banin E.** 2010. Increase in rhamnolipid synthesis under iron-limiting conditions influences surface motility and biofilm formation in *Pseudomonas aeruginosa*. *J Bacteriol* **192**:2973-2980.
99. **Thormann KM, Saville RM, Shukla S, Spormann AM.** 2005. Induction of rapid detachment in *Shewanella oneidensis* MR-1 biofilms. *J Bacteriol* **187**:1014-1021.
100. **An S, Wu J, Zhang LH.** 2010. Modulation of *Pseudomonas aeruginosa* biofilm dispersal by a cyclic-di-GMP phosphodiesterase with a putative hypoxia-sensing domain. *Appl Environ Microbiol* **76**:8160-8173.
101. **Barraud N, Schleheck D, Klebensberger J, Webb JS, Hassett DJ, Rice SA, Kjelleberg S.** 2009. Nitric oxide signaling in *Pseudomonas aeruginosa* biofilms mediates phosphodiesterase activity, decreased cyclic di-GMP levels, and enhanced dispersal. *J Bacteriol* **191**:7333-7342.
102. **Plate L, Marletta MA.** 2012. Nitric oxide modulates bacterial biofilm formation through a multicomponent cyclic-di-GMP signaling network. *Mol Cell* **46**:449-460.
103. **Barraud N, Storey MV, Moore ZP, Webb JS, Rice SA, Kjelleberg S.** 2009. Nitric oxide-mediated dispersal in single- and multi-species biofilms of clinically and industrially relevant microorganisms. *Microb Biotechnol* **2**:370-378.
104. **Carlson HK, Vance RE, Marletta MA.** 2010. H-NOX regulation of c-di-GMP metabolism and biofilm formation in *Legionella pneumophila*. *Mol Microbiol* **77**:930-942.
105. **Schmidt I, Steenbakkers PJ, op den Camp HJ, Schmidt K, Jetten MS.** 2004. Physiologic and proteomic evidence for a role of nitric oxide in biofilm formation by *Nitrosomonas europaea* and other ammonia oxidizers. *J Bacteriol* **186**:2781-2788.
106. **Potter AJ, Kidd SP, Edwards JL, Falsetta ML, Apicella MA, Jennings MP, McEwan AG.** 2009. Thioredoxin reductase is essential for protection of *Neisseria gonorrhoeae* against killing by nitric oxide and for bacterial growth during interaction with cervical epithelial cells. *J Infect Dis* **199**:227-235.
107. **Boles BR, Horswill AR.** 2008. Agr-mediated dispersal of *Staphylococcus aureus* biofilms. *PLoS Pathog* **4**:e1000052.
108. **Kolodkin-Gal I, Romero D, Cao S, Clardy J, Kolter R, Losick R.** 2010. D-amino acids trigger biofilm disassembly. *Science* **328**:627-629.
109. **Leiman SA, May JM, Lebar MD, Kahne D, Kolter R, Losick R.** 2013. D-amino acids indirectly inhibit biofilm formation in *Bacillus subtilis* by interfering with protein synthesis. *J Bacteriol* **195**:5391-5395.
110. **Kaplan JB, Ragunath C, Ramasubbu N, Fine DH.** 2003. Detachment of *Actinobacillus actinomycetemcomitans* biofilm cells by an endogenous beta-hexosaminidase activity. *J Bacteriol* **185**:4693-4698.
111. **Lee SF, Li YH, Bowden GH.** 1996. Detachment of *Streptococcus mutans* biofilm cells by an endogenous enzymatic activity. *Infect Immun* **64**:1035-1038.

112. **Boyd A, Chakrabarty AM.** 1994. Role of alginate lyase in cell detachment of *Pseudomonas aeruginosa*. Appl Environ Microbiol **60**:2355-2359.
113. **Otto M.** 2013. Staphylococcal infections: mechanisms of biofilm maturation and detachment as critical determinants of pathogenicity. Annu Rev Med **64**:175-188.
114. **Karatan E, Watnick P.** 2009. Signals, regulatory networks, and materials that build and break bacterial biofilms. Microbiol Mol Biol Rev **73**:310-347.
115. **Allison DG, Ruiz B, SanJose C, Jaspe A, Gilbert P.** 1998. Extracellular products as mediators of the formation and detachment of *Pseudomonas fluorescens* biofilms. FEMS Microbiol Lett **167**:179-184.
116. **Baty AM, 3rd, Eastburn CC, Techkarnjanaruk S, Goodman AE, Geesey GG.** 2000. Spatial and temporal variations in chitinolytic gene expression and bacterial biomass production during chitin degradation. Appl Environ Microbiol **66**:3574-3585.
117. **Gjermansen M, Nilsson M, Yang L, Tolker-Nielsen T.** 2010. Characterization of starvation-induced dispersion in *Pseudomonas putida* biofilms: genetic elements and molecular mechanisms. Mol Microbiol **75**:815-826.
118. **Mann EE, Rice KC, Boles BR, Endres JL, Ranjit D, Chandramohan L, Tsang LH, Smeltzer MS, Horswill AR, Bayles KW.** 2009. Modulation of eDNA release and degradation affects *Staphylococcus aureus* biofilm maturation. PLoS One **4**:e5822.
119. **Tolker-Nielsen T, Brinch UC, Ragas PC, Andersen JB, Jacobsen CS, Molin S.** 2000. Development and dynamics of *Pseudomonas* sp. biofilms. J Bacteriol **182**:6482-6489.
120. **Webb JS, Thompson LS, James S, Charlton T, Tolker-Nielsen T, Koch B, Givskov M, Kjelleberg S.** 2003. Cell death in *Pseudomonas aeruginosa* biofilm development. J Bacteriol **185**:4585-4592.
121. **Sutherland IW.** 2001. The biofilm matrix - an immobilized but dynamic microbial environment. Trends Microbiol **9**:222-227.
122. **Branda SS, Vik S, Friedman L, Kolter R.** 2005. Biofilms: the matrix revisited. Trends Microbiol **13**:20-26.
123. **Flemming HC, Neu TR, Wozniak DJ.** 2007. The EPS matrix: the "house of biofilm cells". J Bacteriol **189**:7945-7947.
124. **Flemming HC, Wingender J.** 2010. The biofilm matrix. Nat Rev Microbiol **8**:623-633.
125. **Wingender J, Neu TR, Flemming HC.** 1999. Microbial extracellular polymeric substances, 1 ed. Springer, Berlin-Heidelberg, Germany.
126. **Schooling SR, Beveridge TJ.** 2006. Membrane vesicles: an overlooked component of the matrices of biofilms. J Bacteriol **188**:5945-5957.
127. **Schooling SR, Hubley A, Beveridge TJ.** 2009. Interactions of DNA with biofilm-derived membrane vesicles. J Bacteriol **191**:4097-4102.
128. **Kadurugamuwa JL, Beveridge TJ.** 1996. Bacteriolytic effect of membrane vesicles from *Pseudomonas aeruginosa* on other bacteria including pathogens: conceptually new antibiotics. J Bacteriol **178**:2767-2774.
129. **Roberts IS.** 1996. The biochemistry and genetics of capsular polysaccharide production in bacteria. Annu Rev Microbiol **50**:285-315.
130. **Pringle JH, Fletcher M.** 1986. Adsorption of bacterial surface polymers to attachment substrata. J Gen Microbiol **132**:743-749.
131. **Hu W, Li L, Sharma S, Wang J, McHardy I, Lux R, Yang Z, He X, Gimzewski JK, Li Y, Shi W.** 2012. DNA builds and strengthens the extracellular matrix in *Myxococcus xanthus* biofilms by interacting with exopolysaccharides. PLoS One **7**:e51905.
132. **Loesche WJ.** 1986. Role of *Streptococcus mutans* in human dental decay. Microbiol Rev **50**:353-380.
133. **Laus MC, van Brussel AA, Kijne JW.** 2005. Role of cellulose fibrils and exopolysaccharides of *Rhizobium leguminosarum* in attachment to and infection of *Vicia sativa* root hairs. Mol Plant Microbe Interact **18**:533-538.
134. **Matthysse AG, Thomas DL, White AR.** 1995. Mechanism of cellulose synthesis in *Agrobacterium tumefaciens*. J Bacteriol **177**:1076-1081.
135. **Zogaj X, Nimtz M, Rohde M, Bokranz W, Romling U.** 2001. The multicellular morphotypes of *Salmonella typhimurium* and *Escherichia coli* produce cellulose as the second component of the extracellular matrix. Mol Microbiol **39**:1452-1463.
136. **Wingender J, Strathmann M, Rode A, Leis A, Flemming HC.** 2001. Isolation and biochemical characterization of extracellular polymeric substances from *Pseudomonas aeruginosa*. Methods Enzymol **336**:302-314.
137. **Nielsen L, Li X, Halverson LJ.** 2011. Cell-cell and cell-surface interactions mediated by cellulose and a novel exopolysaccharide contribute to *Pseudomonas putida* biofilm formation and fitness under water-limiting conditions. Environ Microbiol **13**:1342-1356.
138. **Hay ID, Rehman ZU, Ghafoor A, Rehm BHA.** 2010. Bacterial biosynthesis of alginates. J Chem Technol Biot **85**:752-759.
139. **Leela JK, Sharma G.** 2000. Studies on xanthan production from *Xanthomonas campestris*. Bioprocess Eng **23**:687-689.

140. **Sutherland IW.** 1969. Structural studies on colanic acid, common exopolysaccharide found in Enterobacteriaceae, by partial acid hydrolysis - oligosaccharides from colanic acid. *Biochemical Journal* **115**:935-945.
141. **Stapper AP, Narasimhan G, Ohman DE, Barakat J, Hentzer M, Molin S, Kharazmi A, Hoiby N, Mathee K.** 2004. Alginate production affects *Pseudomonas aeruginosa* biofilm development and architecture, but is not essential for biofilm formation. *J Med Microbiol* **53**:679-690.
142. **Wozniak DJ, Wyckoff TJO, Starkey M, Keyser R, Azadi P, O'Toole GA, Parsek MR.** 2003. Alginate is not a significant component of the extracellular polysaccharide matrix of PA14 and PAO1 *Pseudomonas aeruginosa* biofilms. *Proc Natl Acad Sci U S A* **100**:7907-7912.
143. **Colvin KM, Irie Y, Tart CS, Urbano R, Whitney JC, Ryder C, Howell PL, Wozniak DJ, Parsek MR.** 2012. The Pel and Psl polysaccharides provide *Pseudomonas aeruginosa* structural redundancy within the biofilm matrix. *Environ Microbiol* **14**:1913-1928.
144. **Ma L, Wang S, Wang D, Parsek MR, Wozniak DJ.** 2012. The roles of biofilm matrix polysaccharide Psl in mucoid *Pseudomonas aeruginosa* biofilms. *FEMS Immunol Med Microbiol* **65**:377-380.
145. **Byrd MS, Sadovskaya I, Vinogradov E, Lu HP, Sprinkle AB, Richardson SH, Ma LY, Ralston B, Parsek MR, Anderson EM, Lam JS, Wozniak DJ.** 2009. Genetic and biochemical analyses of the *Pseudomonas aeruginosa* Psl exopolysaccharide reveal overlapping roles for polysaccharide synthesis enzymes in Psl and LPS production. *Mol Microbiol* **73**:622-638.
146. **Wang S, Liu X, Liu H, Zhang L, Guo Y, Yu S, Wozniak DJ, Ma LZ.** 2014. The exopolysaccharide Psl-eDNA interaction enables the formation of a biofilm skeleton in *Pseudomonas aeruginosa*. *Environ Microbiol Rep.*
147. **Friedman L, Kolter R.** 2004. Genes involved in matrix formation in *Pseudomonas aeruginosa* PA14 biofilms. *Mol Microbiol* **51**:675-690.
148. **Vasseur P, Vallet-Gely I, Soscia C, Genin S, Filloux A.** 2005. The pel genes of the *Pseudomonas aeruginosa* PAK strain are involved at early and late stages of biofilm formation. *Microbiology* **151**:985-997.
149. **Gualdi L, Tagliabue L, Bertagnoli S, Ierano T, De Castro C, Landini P.** 2008. Cellulose modulates biofilm formation by counteracting curli-mediated colonization of solid surfaces in *Escherichia coli*. *Microbiology* **154**:2017-2024.
150. **Danese PN, Pratt LA, Kolter R.** 2000. Exopolysaccharide production is required for development of *Escherichia coli* K-12 biofilm architecture. *J Bacteriol* **182**:3593-3596.
151. **Wang X, Preston JF, Romeo T.** 2004. The *pgaABCD* locus of *Escherichia coli* promotes the synthesis of a polysaccharide adhesin required for biofilm formation. *J Bacteriol* **186**:2724-2734.
152. **Yildiz FH, Schoolnik GK.** 1999. *Vibrio cholerae* O1 El Tor: identification of a gene cluster required for the rugose colony type, exopolysaccharide production, chlorine resistance, and biofilm formation. *Proc Natl Acad Sci U S A* **96**:4028-4033.
153. **Yildiz F, Fong J, Sadovskaya I, Grard T, Vinogradov E.** 2014. Structural characterization of the extracellular polysaccharide from *Vibrio cholerae* O1 El-Tor. *PLoS One* **9**:e86751.
154. **Fong JC, Syed KA, Klose KE, Yildiz FH.** 2010. Role of *Vibrio* polysaccharide (vps) genes in VPS production, biofilm formation and *Vibrio cholerae* pathogenesis. *Microbiology* **156**:2757-2769.
155. **Ma L, Conover M, Lu H, Parsek MR, Bayles K, Wozniak DJ.** 2009. Assembly and development of the *Pseudomonas aeruginosa* biofilm matrix. *PLoS Pathog* **5**:e1000354.
156. **Frolund B, Palmgren R, Keiding K, Nielsen PH.** 1996. Extraction of extracellular polymers from activated sludge using a cation exchange resin. *Water Res* **30**:1749-1758.
157. **Jahn A, Nielsen PH.** 1998. Cell biomass and exopolymer composition in sewer biofilms. *Water Sci Technol* **37**:17-24.
158. **Mayer C, Moritz R, Kirschner C, Borchard W, Maibaum R, Wingender J, Flemming HC.** 1999. The role of intermolecular interactions: studies on model systems for bacterial biofilms. *Int J Biol Macromol* **26**:3-16.
159. **Lasa I, Penades JR.** 2006. Bap: A family of surface proteins involved in biofilm formation. *Res Microbiol* **157**:99-107.
160. **Cucarella C, Solano C, Valle J, Amorena B, Lasa I, Penades JR.** 2001. Bap, a *Staphylococcus aureus* surface protein involved in biofilm formation. *J Bacteriol* **183**:2888-2896.
161. **Lynch DJ, Fountain TL, Mazurkiewicz JE, Banas JA.** 2007. Glucan-binding proteins are essential for shaping *Streptococcus mutans* biofilm architecture. *FEMS Microbiol Lett* **268**:158-165.
162. **Tielker D, Hacker S, Loris R, Strathmann M, Wingender J, Wilhelm S, Rosenau F, Jaeger KE.** 2005. *Pseudomonas aeruginosa* lectin LecB is located in the outer membrane and is involved in biofilm formation. *Microbiology* **151**:1313-1323.
163. **Diggle SP, Stacey RE, Dodd C, Camara M, Williams P, Winzer K.** 2006. The galactophilic lectin, LecA, contributes to biofilm development in *Pseudomonas aeruginosa*. *Environ Microbiol* **8**:1095-1104.
164. **Borlee BR, Goldman AD, Murakami K, Samudrala R, Wozniak DJ, Parsek MR.** 2010. *Pseudomonas aeruginosa* uses a cyclic-di-GMP-regulated adhesin to reinforce the biofilm extracellular matrix. *Mol Microbiol* **75**:827-842.
165. **van Schaik EJ, Giltner CL, Audette GF, Keizer DW, Bautista DL, Slupsky CM, Sykes BD, Irvin RT.** 2005. DNA binding: a novel function of *Pseudomonas aeruginosa* type IV pili. *J Bacteriol* **187**:1455-1464.

166. Chapman MR, Robinson LS, Pinkner JS, Roth R, Heuser J, Hammar M, Normark S, Hultgren SJ. 2002. Role of *Escherichia coli* curli operons in directing amyloid fiber formation. *Science* **295**:851-855.
167. Romero D, Aguilar C, Losick R, Kolter R. 2010. Amyloid fibers provide structural integrity to *Bacillus subtilis* biofilms. *Proc Natl Acad Sci U S A* **107**:2230-2234.
168. Irvine GB, El-Agnaf OM, Shankar GM, Walsh DM. 2008. Protein aggregation in the brain: the molecular basis for Alzheimer's and Parkinson's diseases. *Mol Med* **14**:451-464.
169. Vlassov VV, Laktionov PP, Rykova EY. 2007. Extracellular nucleic acids. *Bioessays* **29**:654-667.
170. Niemeyer J, Gessler F. 2002. Determination of free DNA in soils. *J Plant Nutr Soil Sc* **165**:121-124.
171. Palmgren R, Nielsen PH. 1996. Accumulation of DNA in the exopolymeric matrix of activated sludge and bacterial cultures. *Water Sci Technol* **34**:233-240.
172. Dell'Anno A, Danovaro R. 2005. Extracellular DNA plays a key role in deep-sea ecosystem functioning. *Science* **309**:2179.
173. Pinchuk GE, Ammons C, Culley DE, Li SM, McLean JS, Romine MF, Nealson KH, Fredrickson JK, Beliaev AS. 2008. Utilization of DNA as a sole source of phosphorus, carbon, and energy by *Shewanella* spp.: ecological and physiological implications for dissimilatory metal reduction. *Appl Environ Microbiol* **74**:1198-1208.
174. Mulcahy H, Charron-Mazenod L, Lewenza S. 2010. *Pseudomonas aeruginosa* produces an extracellular deoxyribonuclease that is required for utilization of DNA as a nutrient source. *Environ Microbiol* **12**:1621-1629.
175. Hebsgaard MB, Phillips MJ, Willerslev E. 2005. Geologically ancient DNA: fact or artefact? *Trends Microbiol* **13**:212-220.
176. Nicholls H. 2005. Ancient DNA comes of age. *PLoS Biol* **3**:e56.
177. Catlin BW. 1956. Extracellular deoxyribonucleic acid of bacteria and a deoxyribonuclease inhibitor. *Science* **124**:441-442.
178. Catlin BW, Cunningham LS. 1958. Studies of extracellular and intracellular bacterial deoxyribonucleic acids. *J Gen Microbiol* **19**:522-539.
179. Arko RJ, Wong KH, Peacock WL. 1979. Nuclease enhancement of specific cell agglutination in a serodiagnostic test for *Neisseria gonorrhoeae*. *J Clin Microbiol* **9**:517-519.
180. Whitchurch CB, Tolker-Nielsen T, Ragas PC, Mattick JS. 2002. Extracellular DNA required for bacterial biofilm formation. *Science* **295**:1487.
181. Das T, Sharma PK, Busscher HJ, van der Mei HC, Krom BP. 2010. Role of extracellular DNA in initial bacterial adhesion and surface aggregation. *Appl Environ Microbiol* **76**:3405-3408.
182. Allesen-Holm M, Barken KB, Yang L, Klausen M, Webb JS, Kjelleberg S, Molin S, Givskov M, Tolker-Nielsen T. 2006. A characterization of DNA release in *Pseudomonas aeruginosa* cultures and biofilms. *Mol Microbiol* **59**:1114-1128.
183. Rice KC, Mann EE, Endres JL, Weiss EC, Cassat JE, Smeltzer MS, Bayles KW. 2007. The *cidA* murein hydrolase regulator contributes to DNA release and biofilm development in *Staphylococcus aureus*. *Proc Natl Acad Sci U S A* **104**:8113-8118.
184. Steichen CT, Cho C, Shao JQ, Apicella MA. 2011. The *Neisseria gonorrhoeae* biofilm matrix contains DNA, and an endogenous nuclease controls its incorporation. *Infect Immun* **79**:1504-1511.
185. Bockelmann U, Janke A, Kuhn R, Neu TR, Wecke J, Lawrence JR, Szewzyk U. 2006. Bacterial extracellular DNA forming a defined network-like structure. *FEMS Microbiol Lett* **262**:31-38.
186. Jurcisek JA, Bakaletz LO. 2007. Biofilms formed by nontypeable *Haemophilus influenzae* *in vivo* contain both double-stranded DNA and type IV pilin protein. *J Bacteriol* **189**:3868-3875.
187. Thomas VC, Thurlow LR, Boyle D, Hancock LE. 2008. Regulation of autolysis-dependent extracellular DNA release by *Enterococcus faecalis* extracellular proteases influences biofilm development. *J Bacteriol* **190**:5690-5698.
188. Vilain S, Pretorius JM, Theron J, Brozel VS. 2009. DNA as an adhesin: *Bacillus cereus* requires extracellular DNA to form biofilms. *Appl Environ Microbiol* **75**:2861-2868.
189. Nijland R, Hall MJ, Burgess JG. 2010. Dispersal of biofilms by secreted, matrix degrading, bacterial DNase. *PLoS One* **5**:e15668.
190. Kreth J, Vu H, Zhang Y, Herzberg MC. 2009. Characterization of hydrogen peroxide-induced DNA release by *Streptococcus sanguinis* and *Streptococcus gordonii*. *J Bacteriol* **191**:6281-6291.
191. Heijstra BD, Pichler FB, Liang Q, Blaza RG, Turner SJ. 2009. Extracellular DNA and type IV pili mediate surface attachment by *Acidovorax temperans*. *Antonie Van Leeuwenhoek* **95**:343-349.
192. Wu J, Xi C. 2009. Evaluation of different methods for extracting extracellular DNA from the biofilm matrix. *Appl Environ Microbiol* **75**:5390-5395.
193. Sanchez-Torres V, Maeda T, Wood TK. 2010. Global regulator H-NS and lipoprotein NlpI influence production of extracellular DNA in *Escherichia coli*. *Biochem Biophys Res Commun* **401**:197-202.
194. Jakubovics NS, Shields RC, Rajarajan N, Burgess JG. 2013. Life after death: the critical role of extracellular DNA in microbial biofilms. *Lett Appl Microbiol* **57**:467-475.

195. **Zweig MA, Schork S, Koerdt A, Siewering K, Sternberg C, Thormann K, Albers SV, Molin S, van der Does C.** 2013. Secreted single-stranded DNA is involved in the initial phase of biofilm formation by *Neisseria gonorrhoeae*. *Environ Microbiol*:DOI: 10.1111/1462-2920.12291.
196. **Berne C, Kysela DT, Brun YV.** 2010. A bacterial extracellular DNA inhibits settling of motile progeny cells within a biofilm. *Mol Microbiol* **77**:815-829.
197. **Kirkpatrick CL, Viollier PH.** 2010. Cell dispersal in biofilms: an extracellular DNA masks nature's strongest glue. *Mol Microbiol* **77**:801-804.
198. **Mulcahy H, Charron-Mazenod L, Lewenza S.** 2008. Extracellular DNA chelates cations and induces antibiotic resistance in *Pseudomonas aeruginosa* biofilms. *PLoS Pathog* **4**:e1000213.
199. **Lewenza S.** 2013. Extracellular DNA-induced antimicrobial peptide resistance mechanisms in *Pseudomonas aeruginosa*. *Front Microbiol* **4**:21.
200. **Sahu PK, Iyer PS, Oak AM, Pardesi KR, Chopade BA.** 2012. Characterization of eDNA from the clinical strain *Acinetobacter baumannii* AIIMS 7 and its role in biofilm formation. *ScientificWorldJournal* **2012**:973436.
201. **Liao S, Klein MI, Heim KP, Fan Y, Bitoun JP, Ahn SJ, Burne RA, Koo H, Brady LJ, Wen ZT.** 2014. *Streptococcus mutans* extracellular DNA is upregulated during growth in biofilms, actively released via membrane vesicles, and influenced by components of the protein secretion machinery. *J Bacteriol* **196**:2355-2366.
202. **Hamilton HL, Dominguez NM, Schwartz KJ, Hackett KT, Dillard JP.** 2005. *Neisseria gonorrhoeae* secretes chromosomal DNA via a novel type IV secretion system. *Mol Microbiol* **55**:1704-1721.
203. **Barnes AM, Ballering KS, Leibman RS, Wells CL, Dunne GM.** 2012. *Enterococcus faecalis* produces abundant extracellular structures containing DNA in the absence of cell lysis during early biofilm formation. *MBio* **3**:e00193-00112.
204. **Lappann M, Claus H, van Alen T, Harmsen M, Elias J, Molin S, Vogel U.** 2010. A dual role of extracellular DNA during biofilm formation of *Neisseria meningitidis*. *Mol Microbiol* **75**:1355-1371.
205. **Zhao J, Wang Q, Li M, Heijstra BD, Wang S, Liang Q, Qi Q.** 2013. *Escherichia coli* toxin gene *hipA* affects biofilm formation and DNA release. *Microbiology* **159**:633-640.
206. **Beveridge TJ, Makin SA, Kadurugamuwa JL, Li ZS.** 1997. Interactions between biofilms and the environment. *FEMS Microbiol Rev* **20**:291-303.
207. **Halhoul N, Colvin JR.** 1975. The ultrastructure of bacterial plaque attached to the gingiva of man. *Arch Oral Biol* **20**:115-118.
208. **Kahn M, Concino M, Gromkova R, Goodgal S.** 1979. DNA binding activity of vesicles produced by competence deficient mutants of *Haemophilus*. *Biochem Biophys Res Commun* **87**:764-772.
209. **Kolling GL, Matthews KR.** 1999. Export of virulence genes and Shiga toxin by membrane vesicles of *Escherichia coli* O157:H7. *Appl Environ Microbiol* **65**:1843-1848.
210. **Mashburn-Warren LM, Whiteley M.** 2006. Special delivery: vesicle trafficking in prokaryotes. *Mol Microbiol* **61**:839-846.
211. **Lee EY, Choi DY, Kim DK, Kim JW, Park JO, Kim S, Kim SH, Desiderio DM, Kim YK, Kim KP, Gho YS.** 2009. Gram-positive bacteria produce membrane vesicles: proteomics-based characterization of *Staphylococcus aureus*-derived membrane vesicles. *Proteomics* **9**:5425-5436.
212. **Heilmann C, Hussain M, Peters G, Gotz F.** 1997. Evidence for autolysin-mediated primary attachment of *Staphylococcus epidermidis* to a polystyrene surface. *Mol Microbiol* **24**:1013-1024.
213. **Gonzalez-Pastor JE, Hobbs EC, Losick R.** 2003. Cannibalism by sporulating bacteria. *Science* **301**:510-513.
214. **Thomas VC, Hiromasa Y, Harms N, Thurlow L, Tomich J, Hancock LE.** 2009. A fratricidal mechanism is responsible for eDNA release and contributes to biofilm development of *Enterococcus faecalis*. *Mol Microbiol* **72**:1022-1036.
215. **Eldholm V, Johnsborg O, Haugen K, Ohnstad HS, Havarstein LS.** 2009. Fratricide in *Streptococcus pneumoniae*: contributions and role of the cell wall hydrolases CbpD, LytA and LytC. *Microbiology* **155**:2223-2234.
216. **Resch A, Fehrenbacher B, Eisele K, Schaller M, Gotz F.** 2005. Phage release from biofilm and planktonic *Staphylococcus aureus* cells. *FEMS Microbiol Lett* **252**:89-96.
217. **Rice SA, Tan CH, Mikkelsen PJ, Kung V, Woo J, Tay M, Hauser A, McDougald D, Webb JS, Kjelleberg S.** 2009. The biofilm life cycle and virulence of *Pseudomonas aeruginosa* are dependent on a filamentous prophage. *ISME J* **3**:271-282.
218. **Carrolo M, Frias MJ, Pinto FR, Melo-Cristino J, Ramirez M.** 2010. Prophage spontaneous activation promotes DNA release enhancing biofilm formation in *Streptococcus pneumoniae*. *PLoS One* **5**:e15678.
219. **Zafra O, Lamprecht-Grandio M, de Figueras CG, Gonzalez-Pastor JE.** 2012. Extracellular DNA release by undomesticated *Bacillus subtilis* is regulated by early competence. *Plos One* **7**.
220. **Qin Z, Ou Y, Yang L, Zhu Y, Tolker-Nielsen T, Molin S, Qu D.** 2007. Role of autolysin-mediated DNA release in biofilm formation of *Staphylococcus epidermidis*. *Microbiology* **153**:2083-2092.
221. **Guiron PS, Hung CS, Kline KA, Roth R, Kau AL, Hayes E, Heuser J, Dodson KW, Caparon MG, Hultgren SJ.** 2009. Contribution of autolysin and sortase a during *Enterococcus faecalis* DNA-dependent biofilm development. *Infect Immun* **77**:3626-3638.

222. Thomas VC, Hancock LE. 2009. Suicide and fratricide in bacterial biofilms. *Int J Artif Organs* **32**:537-544.
223. Vuong C, Gerke C, Somerville GA, Fischer ER, Otto M. 2003. Quorum-sensing control of biofilm factors in *Staphylococcus epidermidis*. *J Infect Dis* **188**:706-718.
224. Lou Q, Zhu T, Hu J, Ben H, Yang J, Yu F, Liu J, Wu Y, Fischer A, Francois P, Schrenzel J, Qu D. 2011. Role of the SaeRS two-component regulatory system in *Staphylococcus epidermidis* autolysis and biofilm formation. *BMC Microbiol* **11**:146.
225. Bayles KW. 2003. Are the molecular strategies that control apoptosis conserved in bacteria? *Trends Microbiol* **11**:306-311.
226. Rice KC, Bayles KW. 2008. Molecular control of bacterial death and lysis. *Microbiol Mol Biol Rev* **72**:85-109.
227. Bayles KW. 2007. The biological role of death and lysis in biofilm development. *Nat Rev Microbiol* **5**:721-726.
228. Wang IN, Smith DL, Young R. 2000. Holins: the protein clocks of bacteriophage infections. *Annu Rev Microbiol* **54**:799-825.
229. Engelberg-Kulka H, Amitai S, Kolodkin-Gal I, Hazan R. 2006. Bacterial programmed cell death and multicellular behavior in bacteria. *PLoS Genet* **2**:e135.
230. Magnuson RD. 2007. Hypothetical functions of toxin-antitoxin systems. *J Bacteriol* **189**:6089-6092.
231. Montanaro L, Poggi A, Visai L, Ravaioli S, Campoccia D, Speziale P, Arciola CR. 2011. Extracellular DNA in biofilms. *Int J Artif Organs* **34**:824-831.
232. Paul JH. 2008. Prophages in marine bacteria: dangerous molecular time bombs or the key to survival in the seas? *ISME J* **2**:579-589.
233. Wang X, Kim Y, Ma Q, Hong SH, Pokusaeva K, Sturino JM, Wood TK. 2010. Cryptic prophages help bacteria cope with adverse environments. *Nat Commun* **1**:147.
234. Fortier LC, Sekulovic O. 2013. Importance of prophages to evolution and virulence of bacterial pathogens. *Virulence* **4**:354-365.
235. Hong SH, Wang X, Wood TK. 2010. Controlling biofilm formation, prophage excision and cell death by rewiring global regulator H-NS of *Escherichia coli*. *Microb Biotechnol* **3**:344-356.
236. Wang X, Kim Y, Wood TK. 2009. Control and benefits of CP4-57 prophage excision in *Escherichia coli* biofilms. *ISME J* **3**:1164-1179.
237. Petrova OE, Schurr JR, Schurr MJ, Sauer K. 2011. The novel *Pseudomonas aeruginosa* two-component regulator BfmR controls bacteriophage-mediated lysis and DNA release during biofilm development through PhdA. *Mol Microbiol* **81**:767-783.
238. Webb JS, Lau M, Kjelleberg S. 2004. Bacteriophage and phenotypic variation in *Pseudomonas aeruginosa* biofilm development. *J Bacteriol* **186**:8066-8073.
239. Domka J, Lee J, Bansal T, Wood TK. 2007. Temporal gene-expression in *Escherichia coli* K-12 biofilms. *Environ Microbiol* **9**:332-346.
240. Garcia-Contreras R, Zhang XS, Kim Y, Wood TK. 2008. Protein translation and cell death: the role of rare tRNAs in biofilm formation and in activating dormant phage killer genes. *PLoS One* **3**:e2394.
241. Gödeke J, Heun M, Bubendorfer S, Paul K, Thormann KM. 2011. Roles of two *Shewanella oneidensis* MR-1 extracellular endonucleases. *Appl Environ Microbiol* **77**:5342-5351.
242. Seper A, Fengler VH, Roier S, Wolinski H, Kohlwein SD, Bishop AL, Camilli A, Reidl J, Schild S. 2011. Extracellular nucleases and extracellular DNA play important roles in *Vibrio cholerae* biofilm formation. *Mol Microbiol* **82**:1015-1037.
243. Kiedrowski MR, Kavanaugh JS, Malone CL, Mootz JM, Voyich JM, Smeltzer MS, Bayles KW, Horswill AR. 2011. Nuclease modulates biofilm formation in community-associated methicillin-resistant *Staphylococcus aureus*. *PLoS One* **6**:e26714.
244. Beenken KE, Spencer H, Griffin LM, Smeltzer MS. 2012. Impact of extracellular nuclease production on the biofilm phenotype of *Staphylococcus aureus* under *in vitro* and *in vivo* conditions. *Infect Immun* **80**:1634-1638.
245. Kiedrowski MR, Crosby HA, Hernandez FJ, Malone CL, McNamara JO, Horswill AR. 2014. *Staphylococcus aureus* Nuc2 Is a functional, surface-attached extracellular nuclease. *Plos One* **9**.
246. Shields RC, Mokhtar N, Ford M, Hall MJ, Burgess JG, ElBadawey MR, Jakobovics NS. 2013. Efficacy of a marine bacterial nuclease against biofilm forming microorganisms isolated from chronic rhinosinusitis. *PLoS One* **8**:e55339.
247. Cho C, Chande A, Gakhar L, Bakaletz LO, Jurcisek JA, Ketterer M, Shao J, Gotoh K, Foster E, Hunt J, O'Brien E, Apicella MA. 2014. Role of the nuclease of nontypeable *Haemophilus influenzae* in dispersal of organisms from biofilms. *Infect Immun* **83**:950-957.
248. Focareta T, Manning PA. 1991. Distinguishing between the extracellular DNases of *Vibrio cholerae* and development of a transformation system. *Mol Microbiol* **5**:2547-2555.
249. Blokesch M, Schoolnik GK. 2008. The extracellular nuclease Dns and its role in natural transformation of *Vibrio cholerae*. *J Bacteriol* **190**:7232-7240.
250. Wu SI, Lo SK, Shao CP, Tsai HW, Hor LI. 2001. Cloning and characterization of a periplasmic nuclease of *Vibrio vulnificus* and its role in preventing uptake of foreign DNA. *Appl Environ Microbiol* **67**:82-88.

251. Chang MC, Chang SY, Chen SL, Chuang SM. 1992. Cloning and expression in *Escherichia coli* of the gene encoding an extracellular deoxyribonuclease (DNase) from *Aeromonas hydrophila*. *Gene* **122**:175-180.
252. Berge M, Moscoso M, Prudhomme M, Martin B, Claverys JP. 2002. Uptake of transforming DNA in Gram-positive bacteria: a view from *Streptococcus pneumoniae*. *Mol Microbiol* **45**:411-421.
253. Brinkmann V, Reichard U, Goosmann C, Fauler B, Uhlemann Y, Weiss DS, Weinrauch Y, Zychlinsky A. 2004. Neutrophil extracellular traps kill bacteria. *Science* **303**:1532-1535.
254. Halverson TW, Wilton M, Poon KK, Petri B, Lewenza S. 2015. DNA is an antimicrobial component of neutrophil extracellular traps. *PLoS Pathog* **11**:e1004593.
255. Beiter K, Wartha F, Albiger B, Normark S, Zychlinsky A, Henriques-Normark B. 2006. An endonuclease allows *Streptococcus pneumoniae* to escape from neutrophil extracellular traps. *Curr Biol* **16**:401-407.
256. Buchanan JT, Simpson AJ, Aziz RK, Liu GY, Kristian SA, Kotb M, Feramisco J, Nizet V. 2006. DNase expression allows the pathogen group A *Streptococcus* to escape killing in neutrophil extracellular traps. *Curr Biol* **16**:396-400.
257. Berends ET, Horswill AR, Haste NM, Monestier M, Nizet V, von Kockritz-Blickwede M. 2010. Nuclease expression by *Staphylococcus aureus* facilitates escape from neutrophil extracellular traps. *J Innate Immun* **2**:576-586.
258. Seper A, Hosseinzadeh A, Gorkiewicz G, Lichtenegger S, Roier S, Leitner DR, Rohm M, Grutsch A, Reidl J, Urban CF, Schild S. 2013. *Vibrio cholerae* evades neutrophil extracellular traps by the activity of two extracellular nucleases. *PLoS Pathog* **9**:e1003614.
259. Okshevsky M, Regina VR, Meyer RL. 2014. Extracellular DNA as a target for biofilm control. *Curr Opin Biotechnol* **33C**:73-80.
260. Okumura K, Kawsar HI, Shimizu T, Ohta T, Hayashi H, Shimizu T. 2005. Identification and characterization of a cell-wall anchored DNase gene in *Clostridium perfringens*. *FEMS Microbiol Lett* **242**:281-285.
261. Wen YT, Tsou CC, Kuo HT, Wang JS, Wu JJ, Liao PC. 2011. Differential secretomics of *Streptococcus pyogenes* reveals a novel peroxide regulator (PerR)-regulated extracellular virulence factor mitogen factor 3 (MF3). *Mol Cell Proteomics* **10**:M110 007013.
262. McDowell EJ, Callegari EA, Malke H, Chaussee MS. 2012. CodY-mediated regulation of *Streptococcus pyogenes* exoproteins. *BMC Microbiol* **12**:114.
263. Myers CR, Nealson KH. 1988. Bacterial manganese reduction and growth with manganese oxide as the sole electron acceptor. *Science* **240**:1319-1321.
264. Macdonell MT, Colwell RR. 1985. Phylogeny of the Vibrionaceae, and Recommendation for 2 New Genera, *Listonella* and *Shewanella*. *Syst Appl Microbiol* **6**:171-182.
265. Fredrickson JK, Romine MF, Beliaev AS, Auchtung JM, Driscoll ME, Gardner TS, Nealson KH, Osterman AL, Pinchuk G, Reed JL, Rodionov DA, Rodrigues JL, Saffarini DA, Serres MH, Spormann AM, Zhulin IB, Tiedje JM. 2008. Towards environmental systems biology of *Shewanella*. *Nat Rev Microbiol* **6**:592-603.
266. Heidelberg JF, Paulsen IT, Nelson KE, Gaidos EJ, Nelson WC, Read TD, Eisen JA, Seshadri R, Ward N, Methe B, Clayton RA, Meyer T, Tsapin A, Scott J, Beanan M, Brinkac L, Daugherty S, DeBoy RT, Dodson RJ, Durkin AS, Haft DH, Kolonay JF, Madupu R, Peterson JD, Umayam LA, White O, Wolf AM, Vamathevan J, Weidman J, Impraim M, Lee K, Berry K, Lee C, Mueller J, Khouri H, Gill J, Utterback TR, McDonald LA, Feldblyum TV, Smith HO, Venter JC, Nealson KH, Fraser CM. 2002. Genome sequence of the dissimilatory metal ion-reducing bacterium *Shewanella oneidensis*. *Nat Biotechnol* **20**:1118-1123.
267. Hau HH, Gralnick JA. 2007. Ecology and biotechnology of the genus *Shewanella*. *Annu Rev Microbiol* **61**:237-258.
268. Nealson KH, Scott J. 2003. Ecophysiology of the genus *Shewanella*, vol. 6. Springer-NY, NY, USA.
269. Meyer TE, Tsapin AI, Vandenberghe I, de Smet L, Frishman D, Nealson KH, Cusanovich MA, van Beeumen JJ. 2004. Identification of 42 possible cytochrome C genes in the *Shewanella oneidensis* genome and characterization of six soluble cytochromes. *OMICS* **8**:57-77.
270. Marsili E, Baron DB, Shikhare ID, Coursolle D, Gralnick JA, Bond DR. 2008. *Shewanella* secretes flavins that mediate extracellular electron transfer. *Proc Natl Acad Sci U S A* **105**:3968-3973.
271. Gorby YA, Yanina S, McLean JS, Rosso KM, Moyles D, Dohnalkova A, Beveridge TJ, Chang IS, Kim BH, Kim KS, Culley DE, Reed SB, Romine MF, Saffarini DA, Hill EA, Shi L, Elias DA, Kennedy DW, Pinchuk G, Watanabe K, Ishii S, Logan B, Nealson KH, Fredrickson JK. 2006. Electrically conductive bacterial nanowires produced by *Shewanella oneidensis* strain MR-1 and other microorganisms. *Proc Natl Acad Sci U S A* **103**:11358-11363.
272. Pirbadian S, Barchinger SE, Leung KM, Byun HS, Jangir Y, Bouhenni RA, Reed SB, Romine MF, Saffarini DA, Shi L, Gorby YA, Golbeck JH, El-Naggar MY. 2014. *Shewanella oneidensis* MR-1 nanowires are outer membrane and periplasmic extensions of the extracellular electron transport components. *Proc Natl Acad Sci U S A* **111**:12883-12888.
273. Logan BE, Regan JM. 2006. Electricity-producing bacterial communities in microbial fuel cells. *Trends Microbiol* **14**:512-518.
274. Driscoll ME, Romine MF, Juhn FS, Serres MH, McCue LA, Beliaev AS, Fredrickson JK, Gardner TS. 2007. Identification of diverse carbon utilization pathways in *Shewanella oneidensis* MR-1 via expression profiling. *Genome Inform* **18**:287-298.

275. **Yang C, Rodionov DA, Li X, Laikova ON, Gelfand MS, Zagnitko OP, Romine MF, Obraztsova AY, Neilson KH, Osterman AL.** 2006. Comparative genomics and experimental characterization of N-acetylglucosamine utilization pathway of *Shewanella oneidensis*. *J Biol Chem* **281**:29872-29885.
276. **De Vriendt K, Theunissen S, Carpentier W, De Smet L, Devreese B, Van Beeumen J.** 2005. Proteomics of *Shewanella oneidensis* MR-1 biofilm reveals differentially expressed proteins, including AggA and RibB. *Proteomics* **5**:1308-1316.
277. **Lies DP, Hernandez ME, Kappler A, Mielke RE, Gralnick JA, Newman DK.** 2005. *Shewanella oneidensis* MR-1 uses overlapping pathways for iron reduction at a distance and by direct contact under conditions relevant for biofilms. *Appl Environ Microbiol* **71**:4414-4426.
278. **De Windt W, Gao H, Kromer W, Van Damme P, Dick J, Mast J, Boon N, Zhou J, Verstraete W.** 2006. AggA is required for aggregation and increased biofilm formation of a hyper-aggregating mutant of *Shewanella oneidensis* MR-1. *Microbiology* **152**:721-729.
279. **Teal TK, Lies DP, Wold BJ, Newman DK.** 2006. Spatiotemporal stratification of *Shewanella oneidensis* biofilms. *Appl Environ Microbiol* **72**:7324-7330.
280. **McLean JS, Majors PD, Reardon CL, Bilskis CL, Reed SB, Romine MF, Fredrickson JK.** 2008. Investigations of structure and metabolism within *Shewanella oneidensis* MR-1 biofilms. *J Microbiol Methods* **74**:47-56.
281. **Learman DR, Yi H, Brown SD, Martin SL, Geesey GG, Stevens AM, Hochella MF, Jr.** 2009. Involvement of *Shewanella oneidensis* MR-1 LuxS in biofilm development and sulfur metabolism. *Appl Environ Microbiol* **75**:1301-1307.
282. **Saville RM, Dieckmann N, Spormann AM.** 2010. Spatiotemporal activity of the mshA gene system in *Shewanella oneidensis* MR-1 biofilms. *FEMS Microbiol Lett* **308**:76-83.
283. **Theunissen S, De Smet L, Dansercoer A, Motte B, Coenye T, Van Beeumen JJ, Devreese B, Savvides SN, Vergauwen B.** 2010. The 285 kDa Bap/RTX hybrid cell surface protein (SO4317) of *Shewanella oneidensis* MR-1 is a key mediator of biofilm formation. *Res Microbiol* **161**:144-152.
284. **Saville RM, Rakshe S, Haagensen JAJ, Shukla S, Spormann AM.** 2011. Energy-dependent stability of *Shewanella oneidensis* MR-1 biofilms. *J Bacteriol* **193**:3257-3264.
285. **Babauta JT, Nguyen HD, Beyenal H.** 2011. Redox and pH microenvironments within *Shewanella oneidensis* MR-1 biofilms reveal an electron transfer mechanism. *Environ Sci Technol* **45**:6654-6660.
286. **Gödeke J, Binnenkade L, Thormann KM.** 2012. Transcriptome analysis of early surface-associated growth of *Shewanella oneidensis* MR-1. *PLoS One* **7**:e42160.
287. **Aldeek F, Schneider R, Fontaine-Aupart MP, Mustin C, Lecart S, Merlin C, Block JC.** 2013. Patterned hydrophobic domains in the exopolymer matrix of *Shewanella oneidensis* MR-1 biofilms. *Appl Environ Microbiol* **79**:1400-1402.
288. **Chao L, Rakshe S, Leff M, Spormann AM.** 2013. PdeB, a cyclic di-GMP-specific phosphodiesterase that regulates *Shewanella oneidensis* MR-1 motility and biofilm formation. *J Bacteriol* **195**:3827-3833.
289. **Muller J, Shukla S, Jost KA, Spormann AM.** 2013. The mxd operon in *Shewanella oneidensis* MR-1 is induced in response to starvation and regulated by ArcS/ArcA and BarA/UvrY. *BMC Microbiol* **13**.
290. **Theunissen S, Vergauwen B, De Smet L, Van Beeumen J, Van Gelder P, Savvides SN.** 2009. The agglutination protein AggA from *Shewanella oneidensis* MR-1 is a TolC-like protein and forms active channels *in vitro*. *Biochem Biophys Res Commun* **386**:380-385.
291. **Gödeke J.** 2011. Molekulare Mechanismen während der Anheftung und Biofilmbildung in *Shewanella oneidensis* MR-1. Philipps-Universität Marburg, Germany.
292. **Heun M.** 2011. Unterschiedliche Aufgaben extrazellulärer Nukleasen in *Shewanella oneidensis* MR-1. Philipps-Universität Marburg, Germany.
293. **Tang X, Yi W, Munske GR, Adhikari DP, Zakharova NL, Bruce JE.** 2007. Profiling the membrane proteome of *Shewanella oneidensis* MR-1 with new affinity labeling probes. *J Proteome Res* **6**:724-734.
294. **Brown RN, Romine MF, Schepmoes AA, Smith RD, Lipton MS.** 2010. Mapping the subcellular proteome of *Shewanella oneidensis* MR-1 using sarkosyl-based fractionation and LC-MS/MS protein identification. *J Proteome Res* **9**:4454-4463.
295. **Jekel M, Wackernagel W.** 1995. The periplasmic endonuclease I of *Escherichia coli* has amino-acid sequence homology to the extracellular DNases of *Vibrio cholerae* and *Aeromonas hydrophila*. *Gene* **154**:55-59.
296. **Teichmann L.** 2013. Die Rolle des oxidativen Stresses bei der Induktion des Lambda-Prophagen in Biofilmen von *Shewanella oneidensis* MR-1. Philipps-Universität Marburg, Germany.
297. **Zhou Y, Liang Y, Lynch KH, Dennis JJ, Wishart DS.** 2011. PHAST: a fast phage search tool. *Nucleic Acids Res* **39**:W347-352.
298. **Young I, Wang I, Roof WD.** 2000. Phages will out: strategies of host cell lysis. *Trends Microbiol* **8**:120-128.
299. **Young R.** 1992. Bacteriophage lysis: mechanism and regulation. *Microbiol Rev* **56**:430-481.
300. **Summer EJ, Berry J, Tran TA, Niu L, Struck DK, Young R.** 2007. Rz/Rz1 lysis gene equivalents in phages of Gram-negative hosts. *J Mol Biol* **373**:1098-1112.
301. **Berry J, Rajaure M, Pang T, Young R.** 2012. The spanin complex is essential for lambda lysis. *J Bacteriol* **194**:5667-5674.

302. **Ptashne M.** 2004. A genetic switch, phage lambda revisited, vol. 3. Cold Spring Harbor Laboratory Press, NY, USA.
303. **Price MN, Huang KH, Alm EJ, Arkin AP.** 2005. A novel method for accurate operon predictions in all sequenced prokaryotes. *Nucleic Acids Res* **33**:880-892.
304. **Ptashne M, Jeffrey A, Johnson AD, Maurer R, Meyer BJ, Pabo CO, Roberts TM, Sauer RT.** 1980. How the lambda repressor and cro work. *Cell* **19**:1-11.
305. **Johnson AD, Poteete AR, Lauer G, Sauer RT, Ackers GK, Ptashne M.** 1981. Lambda repressor and cro - components of an efficient molecular switch. *Nature* **294**:217-223.
306. **Svenningsen SL, Costantino N, Court DL, Adhya S.** 2005. On the role of Cro in lambda prophage induction. *Proc Natl Acad Sci U S A* **102**:4465-4469.
307. **Justice SS, Hunstad DA, Cegelski L, Hultgren SJ.** 2008. Morphological plasticity as a bacterial survival strategy. *Nat Rev Microbiol* **6**:162-168.
308. **Cox MM.** 2007. Regulation of bacterial RecA protein function. *Crit Rev Biochem Mol Biol* **42**:41-63.
309. **Kuzminov A.** 1999. Recombinational repair of DNA damage in *Escherichia coli* and bacteriophage lambda. *Microbiol Mol Biol Rev* **63**:751-813.
310. **Jiang Y, Dong Y, Luo Q, Li N, Wu G, Gao H.** 2014. Protection from oxidative stress relies mainly on derepression of OxyR-dependent KatB and Dps in *Shewanella oneidensis*. *J Bacteriol* **196**:445-458.
311. **Wan XF, Verberkmoes NC, McCue LA, Stanek D, Connelly H, Hauser LJ, Wu L, Liu X, Yan T, Leaphart A, Hettich RL, Zhou J, Thompson DK.** 2004. Transcriptomic and proteomic characterization of the Fur regulon in the metal-reducing bacterium *Shewanella oneidensis*. *J Bacteriol* **186**:8385-8400.
312. **Imhof M, Schlotterer C.** 2001. Fitness effects of advantageous mutations in evolving *Escherichia coli* populations. *Proc Natl Acad Sci U S A* **98**:1113-1117.
313. **Bus JS, Gibson JE.** 1984. Paraquat: model for oxidant-initiated toxicity. *Environ Health Perspect* **55**:37-46.
314. **Schlacher K, Goodman MF.** 2007. Lessons from 50 years of SOS DNA-damage-induced mutagenesis. *Nat Rev Mol Cell Biol* **8**:587-594.
315. **Cornelis P, Wei Q, Andrews SC, Vincx T.** 2011. Iron homeostasis and management of oxidative stress response in bacteria. *Metallomics* **3**:540-549.
316. **Imlay JA.** 2013. The molecular mechanisms and physiological consequences of oxidative stress: lessons from a model bacterium. *Nat Rev Microbiol* **11**:443-454.
317. **Goodwin JF, Whitten CF.** 1965. Chelation of ferrous sulphate solutions by desferrioxamine B. *Nature* **205**:281-283.
318. **Grant RA, Filman DJ, Finkel SE, Kolter R, Hogle JM.** 1998. The crystal structure of Dps, a ferritin homolog that binds and protects DNA. *Nat Struct Biol* **5**:294-303.
319. **Almiron M, Link AJ, Furlong D, Kolter R.** 1992. A novel DNA-binding protein with regulatory and protective roles in starved *Escherichia coli*. *Genes Dev* **6**:2646-2654.
320. **Heun M, Binnenkade L, Kreienbaum M, Thormann KM.** 2012. Functional specificity of extracellular nucleases of *Shewanella oneidensis* MR-1. *Appl Environ Microbiol* **78**:4400-4411.
321. **Kreienbaum M.** 2012. Extracellular nucleases in *Shewanella oneidensis* MR-1. Philipps-Universität Marburg, Germany.
322. **Yang W.** 2011. Nucleases: diversity of structure, function and mechanism. *Q Rev Biophys* **44**:1-93.
323. **Petersen TN, Brunak S, von Heijne G, Nielsen H.** 2011. SignalP 4.0: discriminating signal peptides from transmembrane regions. *Nat Methods* **8**:785-786.
324. **Dittmer TA, Misteli T.** 2011. The lamin protein family. *Genome Biol* **12**:222.
325. **Mans BJ, Anantharaman V, Aravind L, Koonin EV.** 2004. Comparative genomics, evolution and origins of the nuclear envelope and nuclear pore complex. *Cell Cycle* **3**:1612-1637.
326. **Dhe-Paganon S, Werner ED, Chi YI, Shoelson SE.** 2002. Structure of the globular tail of nuclear lamin. *J Biol Chem* **277**:17381-17384.
327. **Krimm I, Ostlund C, Gilquin B, Couprie J, Hossenlopp P, Mornon JP, Bonne G, Courvalin JC, Worman HJ, Zinn-Justin S.** 2002. The Ig-like structure of the C-terminal domain of lamin A/C, mutated in muscular dystrophies, cardiomyopathy, and partial lipodystrophy. *Structure* **10**:811-823.
328. **Larkin MA, Blackshields G, Brown NP, Chenna R, McGettigan PA, McWilliam H, Valentin F, Wallace IM, Wilm A, Lopez R, Thompson JD, Gibson TJ, Higgins DG.** 2007. Clustal W and Clustal X version 2.0. *Bioinformatics* **23**:2947-2948.
329. **Guindon S, Dufayard JF, Lefort V, Anisimova M, Hordijk W, Gascuel O.** 2010. New algorithms and methods to estimate maximum-likelihood phylogenies: assessing the performance of PhyML 3.0. *Syst Biol* **59**:307-321.
330. **Letunic I, Bork P.** 2007. Interactive Tree Of Life (iTOL): an online tool for phylogenetic tree display and annotation. *Bioinformatics* **23**:127-128.

331. **Oussenko IA, Sanchez R, Bechhofer DH.** 2004. *Bacillus subtilis* YhcR, a high-molecular-weight, nonspecific endonuclease with a unique domain structure. *J Bacteriol* **186**:5376-5383.
332. **Theobald DL, Mitton-Fry RM, Wuttke DS.** 2003. Nucleic acid recognition by OB-fold proteins. *Annu Rev Biophys Biomol Struct* **32**:115-133.
333. **von Heijne G.** 1992. Membrane protein structure prediction. Hydrophobicity analysis and the positive-inside rule. *J Mol Biol* **225**:487-494.
334. **Van De Vossenberg JLCM, Albers SV, Van Der Does C, Driessen AJM, Van Klompenburg W.** 1998. The positive inside rule is not determined by the polarity of the $\Delta\psi$. *Mol Microbiol* **29**:1125-1126.
335. **von Heijne G.** 1989. Control of topology and mode of assembly of a polytopic membrane protein by positively charged residues. *Nature* **341**:456-458.
336. **Haft DH, Varghese N.** 2011. GlyGly-CTERM and rhombosortase: a C-terminal protein processing signal in a many-to-one pairing with a rhomboid family intramembrane serine protease. *PLoS One* **6**:e28886.
337. **Kapust RB, Tozser J, Copeland TD, Waugh DS.** 2002. The P1' specificity of tobacco etch virus protease. *Biochem Biophys Res Commun* **294**:949-955.
338. **Diakic M.** 2000. Functionally unrelated signalling proteins contain a fold similar to Mg²⁺-dependent endonucleases. *Trends Biochem Sci* **25**:272-273.
339. **Melgar E, Goldthwait DA.** 1968. Deoxyribonucleic acid nucleases. II. The effects of metals on the mechanism of action of deoxyribonuclease I. *J Biol Chem* **243**:4409-4416.
340. **Ross DE, Ruebush SS, Brantley SL, Hartshorne RS, Clarke TA, Richardson DJ, Tien M.** 2007. Characterization of protein-protein interactions involved in iron reduction by *Shewanella oneidensis* MR-1. *Appl Environ Microbiol* **73**:5797-5808.
341. **Hoffman LR, D'Argenio DA, MacCoss MJ, Zhang Z, Jones RA, Miller SI.** 2005. Aminoglycoside antibiotics induce bacterial biofilm formation. *Nature* **436**:1171-1175.
342. **Linares JF, Gustafsson I, Baquero F, Martinez JL.** 2006. Antibiotics as intermicrobial signaling agents instead of weapons. *Proc Natl Acad Sci U S A* **103**:19484-19489.
343. **Gotoh H, Zhang Y, Dallo SF, Hong S, Kasaraneni N, Weitao T.** 2008. *Pseudomonas aeruginosa*, under DNA replication inhibition, tends to form biofilms via Arr. *Res Microbiol* **159**:294-302.
344. **Weitao T.** 2009. Multicellularity of a unicellular organism in response to DNA replication stress. *Res Microbiol* **160**:87-88.
345. **Gotoh H, Kasaraneni N, Devineni N, Dallo SF, Weitao T.** 2010. SOS involvement in stress-inducible biofilm formation. *Biofouling* **26**:603-611.
346. **Chellappa ST, Maredia R, Phipps K, Haskins WE, Weitao T.** 2013. Motility of *Pseudomonas aeruginosa* contributes to SOS-inducible biofilm formation. *Res Microbiol* **164**:1019-1027.
347. **van der Veen S, Abee T.** 2010. Dependence of continuous-flow biofilm formation by *Listeria monocytogenes* EGD-e on SOS response factor YneA. *Appl Environ Microbiol* **76**:1992-1995.
348. **Jiang SC, Kellogg CA, Paul JH.** 1998. Characterization of marine temperate phage-host systems isolated from Mamala Bay, Oahu, Hawaii. *Appl Environ Microbiol* **64**:535-542.
349. **Jiang SC, Paul JH.** 1994. Seasonal and diel abundance of viruses and occurrence of lysogeny/bacteriocinogeny in the marine-environment. *Mar Ecol Prog Ser* **104**:163-172.
350. **Stopar D, Cerne A, Zigman M, Poljsak-Prijatelj M, Turk V.** 2004. Viral abundance and a high proportion of lysogens suggest that viruses are important members of the microbial community in the Gulf of Trieste. *Microbial Ecol* **47**:1-8.
351. **Leitet C, Riemann L, Hagstrom A.** 2006. Plasmids and prophages in Baltic Sea bacterioplankton isolates. *J Mar Biol Assoc Uk* **86**:567-575.
352. **Jiang SC, Paul JH.** 1996. Occurrence of lysogenic bacteria in marine microbial communities as determined by prophage induction. *Mar Ecol Prog Ser* **142**:27-38.
353. **Roca AI, Cox MM.** 1997. RecA protein: structure, function, and role in recombinational DNA repair. *Prog Nucleic Acid Res Mol Biol* **56**:129-223.
354. **Rozanov DV, D'Ari R, Sineoky SP.** 1998. RecA-independent pathways of lambdoid prophage induction in *Escherichia coli*. *J Bacteriol* **180**:6306-6315.
355. **Ghosh D, Roy K, Williamson KE, Srinivasiah S, Wommack KE, Radosevich M.** 2009. Acyl-homoserine lactones can induce virus production in lysogenic bacteria: an alternative paradigm for prophage induction. *Appl Environ Microbiol* **75**:7142-7152.
356. **Boles BR, Singh PK.** 2008. Endogenous oxidative stress produces diversity and adaptability in biofilm communities. *Proc Natl Acad Sci U S A* **105**:12503-12508.
357. **Gates FL.** 1933. The reaction of individual bacteria to irradiation with ultraviolet light. *Science* **77**:350.
358. **Piao Z, Sze CC, Barysheva O, Iida K, Yoshida S.** 2006. Temperature-regulated formation of mycelial mat-like biofilms by *Legionella pneumophila*. *Appl Environ Microbiol* **72**:1613-1622.

359. **Ogawa M, Takade A, Miyamoto H, Taniguchi H, Yoshida S.** 2001. Morphological variety of intracellular microcolonies of *Legionella species* in Vero cells. *Microbiol Immunol* **45**:557-562.
360. **Chauhan A, Madiraju MV, Fol M, Lofton H, Maloney E, Reynolds R, Rajagopalan M.** 2006. *Mycobacterium tuberculosis* cells growing in macrophages are filamentous and deficient in FtsZ rings. *J Bacteriol* **188**:1856-1865.
361. **Rosenberger CM, Finlay BB.** 2002. Macrophages inhibit *Salmonella typhimurium* replication through MEK/ERK kinase and phagocyte NADPH oxidase activities. *J Biol Chem* **277**:18753-18762.
362. **Eriksson S, Lucchini S, Thompson A, Rhen M, Hinton JCD.** 2003. Unravelling the biology of macrophage infection by gene expression profiling of intracellular *Salmonella enterica*. *Mol Microbiol* **47**:103-118.
363. **Steinberger RE, Allen AR, Hansma HG, Holden PA.** 2002. Elongation correlates with nutrient deprivation in *Pseudomonas aeruginosa*-unsaturated biofilms. *Microbial Ecol* **43**:416-423.
364. **Yoon MY, Lee KM, Park Y, Yoon SS.** 2011. Contribution of cell elongation to the biofilm formation of *Pseudomonas aeruginosa* during anaerobic respiration. *PLoS One* **6**:e16105.
365. **van der Veen S, Abee T.** 2011. Generation of variants in *Listeria monocytogenes* continuous-flow biofilms is dependent on radical-induced DNA damage and RecA-mediated repair. *PLoS One* **6**:e28590.
366. **Ishii S, Shimoyama T, Hotta Y, Watanabe K.** 2008. Characterization of a filamentous biofilm community established in a cellulose-fed microbial fuel cell. *BMC Microbiol* **8**:6.
367. **Patil SA, Gorecki K, Hagerhall C, Gorton L.** 2013. Cisplatin-induced elongation of *Shewanella oneidensis* MR-1 cells improves microbe-electrode interactions for use in microbial fuel cells. *Energ Environ Sci* **6**:2626-2630.
368. **Qiu X, Sundin GW, Wu L, Zhou J, Tiedje JM.** 2005. Comparative analysis of differentially expressed genes in *Shewanella oneidensis* MR-1 following exposure to UVC, UVB, and UVA radiation. *J Bacteriol* **187**:3556-3564.
369. **Dunford BH, Dolphin D, Raymond KN, Sieker L.** 1982. The biological chemistry of iron, 1 ed, vol. 89. Springer, The Netherlands.
370. **Welch KD, Davis TZ, Van Eden ME, Aust SD.** 2002. Deleterious iron-mediated oxidation of biomolecules. *Free Radic Biol Med* **32**:577-583.
371. **Berlutti F, Ajello M, Bosso P, Morea C, Petrucca A, Antonini G, Valenti P.** 2004. Both lactoferrin and iron influence aggregation and biofilm formation in *Streptococcus mutans*. *Biometals* **17**:271-278.
372. **Johnson M, Cockayne A, Williams PH, Morrissey JA.** 2005. Iron-responsive regulation of biofilm formation in *Staphylococcus aureus* involves fur-dependent and fur-independent mechanisms. *J Bacteriol* **187**:8211-8215.
373. **Hindre T, Bruggemann H, Buchrieser C, Hechard Y.** 2008. Transcriptional profiling of *Legionella pneumophila* biofilm cells and the influence of iron on biofilm formation. *Microbiology* **154**:30-41.
374. **Wu Y, Outten FW.** 2009. IscR controls iron-dependent biofilm formation in *Escherichia coli* by regulating type I fimbria expression. *J Bacteriol* **191**:1248-1257.
375. **Mey AR, Craig SA, Payne SM.** 2005. Characterization of *Vibrio cholerae* RyhB: the RyhB regulon and role of ryhB in biofilm formation. *Infect Immun* **73**:5706-5719.
376. **Yang L, Barken KB, Skindersoe ME, Christensen AB, Givskov M, Tolker-Nielsen T.** 2007. Effects of iron on DNA release and biofilm development by *Pseudomonas aeruginosa*. *Microbiology* **153**:1318-1328.
377. **Banin E, Vasil ML, Greenberg EP.** 2005. Iron and *Pseudomonas aeruginosa* biofilm formation. *Proc Natl Acad Sci U S A* **102**:11076-11081.
378. **Banin E, Brady KM, Greenberg EP.** 2006. Chelator-induced dispersal and killing of *Pseudomonas aeruginosa* cells in a biofilm. *Appl Environ Microbiol* **72**:2064-2069.
379. **Daly MJ, Gaidamakova EK, Matrosova VY, Vasilenko A, Zhai M, Venkateswaran A, Hess M, Omelchenko MV, Kostandarithes HM, Makarova KS, Wackett LP, Fredrickson JK, Ghosal D.** 2004. Accumulation of Mn(II) in *Deinococcus radiodurans* facilitates gamma-radiation resistance. *Science* **306**:1025-1028.
380. **Rolfe MD, Rice CJ, Lucchini S, Pin C, Thompson A, Cameron ADS, Alston M, Stringer MF, Betts RP, Baranyi J, Peck MW, Hinton JCD.** 2012. Lag phase is a distinct growth phase that prepares bacteria for exponential growth and involves transient metal accumulation. *J Bacteriol* **194**:686-701.
381. **Lattner D, Flemming HC, Mayer C.** 2003. 13C-NMR study of the interaction of bacterial alginate with bivalent cations. *Int J Biol Macromol* **33**:81-88.
382. **Yuan J, Chen Y, Zhou G, Chen H, Gao H.** 2013. Investigation of roles of divalent cations in *Shewanella oneidensis* pellicle formation reveals unique impacts of insoluble iron. *Biochim Biophys Acta* **1830**:5248-5257.
383. **Lovley DR, Holmes DE, Nevin KP.** 2004. Dissimilatory Fe(III) and Mn(IV) reduction. *Adv Microb Physiol* **49**:219-286.
384. **Xu S, Liu H, Fan Y, Schaller R, Jiao J, Chaplen F.** 2012. Enhanced performance and mechanism study of microbial electrolysis cells using Fe nanoparticle-decorated anodes. *Appl Microbiol Biotechnol* **93**:871-880.
385. **Jang S, Imlay JA.** 2007. Micromolar intracellular hydrogen peroxide disrupts metabolism by damaging iron-sulfur enzymes. *J Biol Chem* **282**:929-937.

386. **Liang Y, Gao H, Guo X, Chen J, Qiu G, He Z, Zhou J, Liu X.** 2012. Transcriptome analysis of pellicle formation of *Shewanella oneidensis*. *Arch Microbiol* **194**:473-482.
387. **Fenton HJH.** 1894. Oxidation of tartaric acid in presence of iron. *Chem Sci* **65**:899-910.
388. **Haber F, Weiss JJ.** 1934. The catalytic decomposition of hydrogen peroxide by iron salts. *Proc R Soc London Ser* **147**:332-351.
389. **Imlay JA, Linn S.** 1988. DNA damage and oxygen radical toxicity. *Science* **240**:1302-1309.
390. **Loeb LA, James EA, Waltersdorph AM, Klebanoff SJ.** 1988. Mutagenesis by the autoxidation of iron with isolated DNA. *Proc Natl Acad Sci U S A* **85**:3918-3922.
391. **McCord JM, Keele BB, Jr., Fridovich I.** 1971. An enzyme-based theory of obligate anaerobiosis: the physiological function of superoxide dismutase. *Proc Natl Acad Sci U S A* **68**:1024-1027.
392. **Barbusinski K.** 2009. Fenton reaction - controversy concerning the chemistry. *Ecological Chemistry and Engineering S* **16**:347-358.
393. **Kelley LA, Sternberg MJE.** 2009. Protein structure prediction on the Web: a case study using the Phyre server. *Nat Protoc* **4**:363-371.
394. **Qian SY, Buettner GR.** 1999. Iron and dioxygen chemistry is an important route to initiation of biological free radical oxidations: An electron paramagnetic resonance spin trapping study. *Free Radical Bio Med* **26**:1447-1456.
395. **Saran M, Michel C, Stettmaier K, Bors W.** 2000. Arguments against the significance of the Fenton reaction contributing to signal pathways under *in vivo* conditions. *Free Radic Res* **33**:567-579.
396. **Flemmig J, Arnhold J.** 2007. Ferrous ion-induced strand breaks in the DNA plasmid pBR322 are not mediated by hydrogen peroxide. *Eur Biophys J* **36**:377-384.
397. **Imlay JA.** 2008. Cellular defenses against superoxide and hydrogen peroxide. *Annu Rev Biochem* **77**:755-776.
398. **Deguillaume L, Leriche M, Chaurnerliac N.** 2005. Impact of radical versus non-radical pathway in the Fenton chemistry on the iron redox cycle in clouds. *Chemosphere* **60**:718-724.
399. **Ryder VJ, Chopra I, O'Neill AJ.** 2012. Increased mutability of Staphylococci in biofilms as a consequence of oxidative stress. *PLoS One* **7**:e47695.
400. **Driffeld K, Miller K, Bostock JM, O'Neill AJ, Chopra I.** 2008. Increased mutability of *Pseudomonas aeruginosa* in biofilms. *J Antimicrob Chemother* **61**:1053-1056.
401. **Li CL, Hor LI, Chang ZF, Tsai LC, Yang WZ, Yuan HS.** 2003. DNA binding and cleavage by the periplasmic nuclease Vvn: a novel structure with a known active site. *EMBO J* **22**:4014-4025.
402. **Focareta T, Manning PA.** 1987. Extracellular proteins of *Vibrio cholerae*: molecular cloning, nucleotide sequence and characterization of the deoxyribonuclease (DNase) together with its periplasmic localization in *Escherichia coli* K-12. *Gene* **53**:31-40.
403. **Gorby Y, McLean J, Korenevsky A, Rosso K, El-Naggar MY, Beveridge TJ.** 2008. Redox-reactive membrane vesicles produced by *Shewanella*. *Geobiology* **6**:232-241.
404. **Papanikou E, Karamanou S, Economou A.** 2007. Bacterial protein secretion through the translocase nanomachine. *Nat Rev Microbiol* **5**:839-851.
405. **Trun NJ, Stader J, Lupas A, Kumamoto C, Silhavy TJ.** 1988. Two cellular components, PrlA and SecB, that recognize different sequence determinants are required for efficient protein export. *J Bacteriol* **170**:5928-5930.
406. **Marchler-Bauer A, Derbyshire MK, Gonzales NR, Lu S, Chitsaz F, Geer LY, Geer RC, He J, Gwadz M, Hurwitz DI, Lanczycki CJ, Lu F, Marchler GH, Song JS, Thanki N, Wang Z, Yamashita RA, Zhang D, Zheng C, Bryant SH.** 2015. CDD: NCBI's conserved domain database. *Nucleic Acids Res* **43**:D222-226.
407. **Hem JD.** 1989. Study and interpretation of the chemical characteristics of natural water, vol. 2254. U.S. Geological Survey, Water Supply Paper, USA.
408. **Venter JC, Remington K, Heidelberg JF, Halpern AL, Rusch D, Eisen JA, Wu D, Paulsen I, Nelson KE, Nelson W, Fouts DE, Levy S, Knap AH, Lomas MW, Nealson K, White O, Peterson J, Hoffman J, Parsons R, Baden-Tillson H, Pfannkoch C, Rogers YH, Smith HO.** 2004. Environmental genome shotgun sequencing of the Sargasso Sea. *Science* **304**:66-74.
409. **Dikow RB.** 2011. Genome-level homology and phylogeny of *Shewanella* (Gammaproteobacteria: Iteromonadales: Shewanellaceae). *BMC Genomics* **12**:237.
410. **Drever J.** 1997. The geochemistry of natural waters: surface and groundwater environments, 3 ed, vol. 3. Prentice Hall, Englewood Cliffs, NJ, USA.
411. **Cowan JA.** 1995. The Biological Chemistry of Magnesium. Wiley-VCH, Cambridge, UK.
412. **Kamitani S, Akiyama Y, Ito K.** 1992. Identification and characterization of an *Escherichia coli* gene required for the formation of correctly folded alkaline phosphatase, a periplasmic enzyme. *EMBO J* **11**:57-62.
413. **Bardwell JC, McGovern K, Beckwith J.** 1991. Identification of a protein required for disulfide bond formation *in vivo*. *Cell* **67**:581-589.

References

414. **Dinh T, Bernhardt TG.** 2011. Using superfolder green fluorescent protein for periplasmic protein localization studies. *J Bacteriol* **193**:4984-4987.
415. **Shi L, Deng S, Marshall MJ, Wang Z, Kennedy DW, Dohnalkova AC, Mottaz HM, Hill EA, Gorby YA, Beliaev AS, Richardson DJ, Zachara JM, Fredrickson JK.** 2008. Direct involvement of type II secretion system in extracellular translocation of *Shewanella oneidensis* outer membrane cytochromes MtrC and OmcA. *J Bacteriol* **190**:5512-5516.
416. **Green MR, J S.** 2012. Molecular cloning: a laboratory manual, 4 ed. Cold Spring Harbor Laboratory Press, Cold Spring Harbor, NY, USA.
417. **Bertani G.** 1951. Studies on lysogenesis. I. The mode of phage liberation by lysogenic *Escherichia coli*. *J Bacteriol* **62**:293-300.
418. **Hanahan D.** 1983. Studies on transformation of *Escherichia coli* with plasmids. *J Mol Biol* **166**:557-580.
419. **Paulick A, Koerdt A, Lassak J, Huntley S, Wilms I, Narberhaus F, Thormann KM.** 2009. Two different stator systems drive a single polar flagellum in *Shewanella oneidensis* MR-1. *Mol Microbiol* **71**:836-850.
420. **Kibbe WA.** 2007. OligoCalc: an online oligonucleotide properties calculator. *Nucleic Acids Res* **35**:W43-46.
421. **Venkateswaran K, Moser DP, Dollhopf ME, Lies DP, Saffarini DA, MacGregor BJ, Ringelberg DB, White DC, Nishijima M, Sano H, Burghardt J, Stackebrandt E, Nealson KH.** 1999. Polyphasic taxonomy of the genus *Shewanella* and description of *Shewanella oneidensis* sp. nov. *Int J Syst Bacteriol* **49 Pt 2**:705-724.
422. **Miller VL, Mekalanos JJ.** 1988. A novel suicide vector and its use in construction of insertion mutations: osmoregulation of outer membrane proteins and virulence determinants in *Vibrio cholerae* requires *toxR*. *J Bacteriol* **170**:2575-2583.
423. **Lassak J, Henche AL, Binnenkade L, Thormann KM.** 2010. ArcS, the cognate sensor kinase in an atypical Arc system of *Shewanella oneidensis* MR-1. *Appl Environ Microbiol* **76**:3263-3274.
424. **Weiss Nielsen M, Sternberg C, Molin S, Regenber B.** 2011. *Pseudomonas aeruginosa* and *Saccharomyces cerevisiae* biofilm in flow cells. *J Vis Exp*.
425. **Miller JH.** 1972. Experiments in molecular genetics, 3 ed. Cold Spring Harbor Laboratory Press, Cold Spring Harbor Press, NY, USA.
426. **Fuangthong M, Mongkolsuk S.** 1997. Isolation and characterization of a multiple peroxide resistant mutant from *Xanthomonas campestris* pv. *phaseoli*. *FEMS Microbiol Lett* **152**:189-194.
427. **Mongkolsuk S, Whangsuk W, Fuangthong M, Loprasert S.** 2000. Mutations in *oxyR* resulting in peroxide resistance in *Xanthomonas campestris*. *J Bacteriol* **182**:3846-3849.
428. **Pospiech A, Neumann B.** 1995. A versatile quick-prep of genomic DNA from gram-positive bacteria. *Trends Genet* **11**:217-218.
429. **Sanger F, Coulson AR.** 1975. A rapid method for determining sequences in DNA by primed synthesis with DNA polymerase. *J Mol Biol* **94**:441-448.
430. **de Boer HA, Comstock LJ, Vasser M.** 1983. The *tac* promoter: a functional hybrid derived from the *trp* and *lac* promoters. *Proc Natl Acad Sci U S A* **80**:21-25.
431. **Inoue H, Nojima H, Okayama H.** 1990. High-efficiency transformation of *Escherichia coli* with plasmids. *Gene* **96**:23-28.
432. **Aiba H, Adhya S, de Crombrughe B.** 1981. Evidence for two functional *gal* promoters in intact *Escherichia coli* cells. *J Biol Chem* **256**:11905-11910.
433. **Pfaffl MW.** 2001. A new mathematical model for relative quantification in real-time RT-PCR. *Nucleic Acids Res* **29**:e45.
434. **Laemmli UK.** 1970. Cleavage of structural proteins during the assembly of the head of bacteriophage T4. *Nature* **227**:680-685.